Post-translational modifications of BRAF and MITF

Submitted in partial fulfillment of the

requirements for the degree of

Doctor of Philosophy in Clinical Medicine

University of Oxford

Trinity Term 2015

Supervised by

Professor Colin Goding

Ludwig Institute for Cancer Research

Nuffield Department of Clinical Medicine

University of Oxford

Kao Chin Ngeow

St Anne's College, Oxford, OX2 6HS

Disclaimer

I declare that this submission is my own written work. To the best of my knowledge, it contains no material that has been written by another or previously submitted in the same or a different form as academic work, to this or any other university.

The results presented herein derive from my own experiments, with the exception of Figures 3.4, 3.5, 3.9 and part of Figure 3.8 (work performed by Robert Siddaway), as well as Figure 4.24 (work performed by Zhiqiang Zeng).

Kao Chin Ngeow

Trinity Term 2015

Abstract

Post-translational modifications of BRAF and MITF

Kao Chin Ngeow, St Anne's College

D.Phil. Clinical Medicine, Trinity Term 2015

Malignant melanoma is the deadliest and most aggressive form of skin cancer. Despite the development of targeted molecular therapies which specifically target oncogenic pathways in melanoma, melanoma remains highly refractory to treatment and prone to relapse. In order to develop more effective therapies, there is a need to investigate additional ways of manipulating aberrant molecular pathways in melanoma. To this end, we have identified novel sites of post-translational modifications in two oncogenic proteins that are known to play pivotal roles in driving melanoma tumorigenesis. We showed that BRAF, the most commonly mutated oncoprotein in melanoma, can be acetylated at K473 and K475 by the p300/CBP acetyltransferases. Importantly, acetylation of BRAF reduced its activity regardless of its mutational status at the commonly mutated V600 residue. We also identified a novel phosphorylation site targeted by GSK3 in microphthalmia-associated transcription factor (MITF), the melanocyte master regulator. GSK3 phosphorylation of S69, together with ERK-mediated phosphorylation of the nearby S73 residue, was found to promote MITF nuclear export via a previously undescribed nuclear export signal comprising of the S69, S73, M75, L78 and L80 residues. Importantly, phosphorylation-induced nuclear export was associated with reduced MITF activity, which may have important functional implications for melanocyte development and melanoma oncogenesis. In addition, we showed that the cyclin-dependent kinases CDK1 and CDK2 can also phosphorylate MITF at S73.

Acknowledgements

I am extremely grateful to my supervisor Professor Colin Goding for being an invaluable source of advice, encouragement and support over the past four years. I would also like to thank past and present members of the Goding lab whom I have had the pleasure of working with, particularly Hans Friedrichsen, Luis Sanchez and Paola Falletta for their help, feedback and scientific discussions. I am also grateful for the assistance rendered by the support staff in the Ludwig Institute, particularly Mark Shipman, whose technical expertise with the microscopes was invaluable.

I would like to specially thank Robert Siddaway, a former student in the lab who made the initial findings in the BRAF acetylation project. Thanks also go to Rebecca Konietzny and Benedikt Kessler (TDI, Oxford) for mass spectrometry analysis. I would also like to thank Zhiqiang Zeng and Elizabeth Patton (University of Edinburgh, Edinburgh) for their help in conducting the zebrafish assay in the MITF phosphorylation project. Thanks also go to Apirat Chaikuad and Stefan Knapp (SGC, Oxford) for providing purified MEK2 protein and the GSK Published Kinase Inhibitor Set used in the small molecule library screen, as well as Sarah Picaud and Panagis Filippakopoulos (SGC, Oxford) for their help in synthesising the peptide SPOT arrays.

I am grateful to A*STAR, Singapore, for funding my D.Phil. studies, and to Professor Birgit Lane, my mentor at A*STAR, for being a valuable source of advice.

I am also thankful for the support and company provided by friends and family, particularly my parents, over the past four years. Finally, I would like to thank my wife Huijia for her unconditional love and support, and for always being there for me throughout this journey.

Table of Contents

List of abbreviations

α-MSH	α-melanocyte stimulating hormone
AKT	RAC-alpha serine/threonine-protein kinase
APS	ammonium persulphate
AS	activation segment
ATP	adenosine triphosphate
BAD	Bcl2-associated agonist of cell death
BCA	bicinchoninic acid
BCL2	B-cell lymphoma 2
bHLH-LZ	basic helix-loop-helix leucine zipper
BHLHE40	class E basic helix-loop-helix protein 40
bp	base pair
BSA	bovine serum albumin
C-terminal	carboxyl terminal
cAMP	cyclic adenosine monophosphate
CDK	cyclin-dependent kinase
CDKN2A	cyclin-dependent kinase inhibitor 2A
ChIP	chromatin immunoprecipitation
CIP	calf intestinal alkaline phosphatase
CK2	casein kinase 2
CMV	cytomegalovirus
COS	CV-1 origin, SV40
COSMIC	Catalogue Of Somatic Mutations In Cancer
CRD	cysteine-rich domain
CREB	cAMP responsive element-binding protein
CT	cholera toxin
CTLA-4	cytotoxic T-lymphocyte-associated antigen 4
Da	dalton
DAPI	4',6-diamidino-2-phenylindole
DCT	dopachrome tautomerase
DFG	Asp-Phe-Gly
DMBA	dimethylbenzanthracene
DMEM	Dulbecco's Modified Eagle Medium
DMSO	dimethyl sulfoxide
DNA	deoxyribonucleic acid
dNTP	deoxynucleotide
DUSPs	dual-specificity phosphatases
ECL	enhanced chemiluminescence
EDN1	endothelin 1
EDTA	ethylenediaminetetraacetic acid
EGFR	epidermal growth factor receptor
EMSA	electrophoretic mobility shift assay

ERK	extracellular signal-regulated kinase
ETS	E26 transformation-specific
FBS	foetal bovine serum
FGF	fibroblast growth factor
FRT	flp recombination target
G1	gap 1
G2	gap 2
GDP	guanosine diphosphate
GEF	guanine nucleotide exchange factor
GFP	green fluorescent protein
GLI2	glioma-associated oncogene 2
GPCR	G protein-coupled receptor
GRB2	growth factor receptor-bound 2
GSK3	glycogen synthase kinase 3
GST	Glutathione S-transferase
GTP	guanosine triphosphate
HAT	histone acetyltransferase
HDAC	histone deacetylase
HGF	hepatocyte growth factor
HIF1	hypoxia-inducible factor 1
HRP	horseradish peroxidase
hSCF	human stem cell factor
IgG	immunoglobulin G
IP	immunoprecipitation
IPTG	isopropyl-β-D-thiogalactoside
JNK	jun amino-terminal kinase
kb	kilobase
kDa	kilodalton
KSR	kinase suppressor of RAS
LB	Luria-Bertani
LMB	leptomycin B
M	mitosis
M	molar
MAPK	mitogen-activated protein kinase
MAPKK/MAP2K/MEK	MAPK kinase
MAPKKK/MAP3K	MAP2K kinase
MC1R	melanocortin 1 receptor
MDM2	minute-double-minute 2
MiT	microphthalmia-related transcription
MITF	microphthalmia-associated transcription factor
ML-IAP	melanoma inhibitor of apoptosis
MLANA	melanoma antigen recognised by T cells
mTOR	mammalian target of rapamycin

N-region	negative charge regulatory region
N-terminal	amino terminal
NES	nuclear export signal
NLK	Nemo-like kinase
NLS	nuclear localisation signal
OIS	oncogene-induced senescence
P-loop	phosphate-binding loop
PAK	p21-activated kinases
PAX3	paired box 3
PBS	phosphate-buffered saline
PBST	0.1% Tween in PBS
PCR	polymerase chain reaction
PD-1	programmed cell death protein 1
PFA	paraformaldehyde
PGC1α	peroxisome proliferator-activated receptor γ coactivator 1α
PH	pleckstrin homology
PI	propidium iodide
PI3K	phosphoinositide 3-kinase
PIAS3	protein inhibitor of activated STAT protein 3
PIP_3	phosphatidylinositol phosphate
PKA	protein kinase A
PKC	protein kinase C
PKI	protein kinase inhibitor
PMEL	premelanosome
PP1	protein phosphatase 1
PP2A	protein phosphatase 2A
PTEN	phosphatase and tensin homolog
qPCR	quantitative real-time polymerase chain reaction
RAB27A	Ras-related protein 27A
RAF	rapidly accelerated fibrosarcoma
RANKL	receptor activator of nuclear factor κB ligand
RAS	rat sarcoma
RB	retinoblastoma
RBD	RAS-binding domain
RIPA	radioimmunoprecipitation assay
RNA	ribonucleic acid
RNAi	RNA interference
RPMI	Roswell Park Memorial Institute
RSK	ribosomal S6 kinase
RTK	receptor tyrosine kinase
S	synthesis
SAHA	suberoylanilide hydroxamic acid
SCF	stem cell factor

SDS-PAGE	sodium dodecyl sulphate polyacrylamide gel electrophoresis
SEM	standard error of the mean
SH2	sequence homology 2
siRNA	small interfering RNA
SOS	son of sevenless
SOX10	sex determining region Y-box 10
SP	serine-proline
SPRED	sprouty-related, EVH1 domain-containing
SPRY	sprouty
SUMO	small ubiquitin-like modifier
SV40	simian virus 40
TBP	TATA box binding protein
TBS	Tris-buffered saline
TBST	0.1% Tween in TBS
Tcf/Lef	T-cell factor/lymphoid enhancer-binding factor
TEMED	tetramethylethylenediamine
TetR	tet repressor
TFE3	transcription factor E3
TFEB	transcription factor EB
TFEC	transcription factor EC
TPA	tetradecanoyl phorbol acetate
TRAP	tartrate-resistant acid phosphatase type 5 gene
TRPM1	transient receptor potential cation channel subfamily M member 1
TYR	tyrosinase
TYRP1	tyrosinase-related protein 1
UV	ultraviolet
Wnt	wingless-type
WT	wild-type

Chapter 1 – Introduction

1.1 Melanoma

Cancer is a debilitating disease which accounts for one in seven deaths worldwide (American Cancer Society, 2015a). With cancer incidence increasing exponentially with age (de Magalhães, 2013), it is not surprising that there will be an unprecedented increase in cancer patients and fatalities as the world's population continues to increase and age. In fact, the number of annual new cancer cases is projected to rise to 21.6 million in 2030, an increase of 53% from the 14.1 million new cases in 2012 (Ferlay et al., 2013).

Skin cancer is by far the most common malignancy, with more than 3.5 million cases diagnosed in the US annually, compared to 1.6 million for all other cancers combined (American Cancer Society, 2015b; Rogers et al., 2010). Among skin cancers, melanoma is the rarest but deadliest form. Despite the fact that it makes up less than 2% of skin cancers (American Cancer Society, 2015b), melanoma accounts for the vast majority (75%) of skin cancer-related deaths (Schadendorf et al., 2015).

There will be an estimated 73,870 new cases of melanoma in 2015 in the United States, which makes it the sixth most commonly diagnosed cancer excluding non-melanoma skin cancers (Howlader et al., 2015). At the global level, melanoma mainly occurs in white populations with fair skin, with the top 20 incidence rates being found in countries in Europe, North America and Australia (Ferlay et al., 2013). Australia and New Zealand have the highest melanoma incidence rates by far, with about 55 cases per 100,000 inhabitants (Ferlay et al., 2013).

Troublingly, melanoma incidence rates in the United States have increased 17-fold in men and 9-fold in women between 1950 and 2007 (Geller et al., 2013), a trend that is by no means unique to the United States, although the annual rate of increase has stabilised at an average 1.4% over the past ten years (Howlader et al.,

2015) (Figure 1.1). Similar increases have also been observed in Australia, central Europe and Scandinavia (Garbe and Leiter, 2009; MacKie et al., 2009). Another cause for concern is that, among the top seven most common cancers in the United States, melanoma is the only one with an increasing incidence (Howlader et al., 2015).

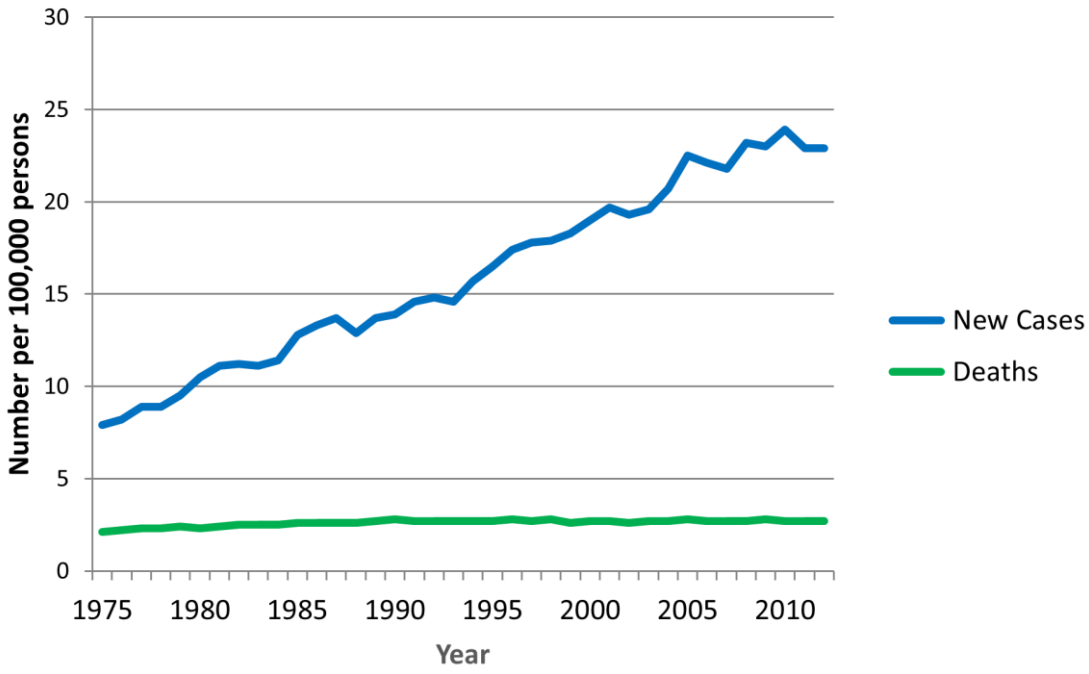

Figure 1.1 Melanoma incidence in the US has been rising over the past 40 years. Number of new cases of melanoma (blue) vs number of deaths from melanoma (green) in the US from 1975 to 2012, expressed per 100,000 persons in the population. Data represents age-adjusted rates from all races and both sexes. Data obtained from National Cancer Institute, Bethesda, MD, USA (Howlader et al., 2015).

Compared to most cancers, melanoma incidence tends to skew towards the young, with almost a third of cases in the United States occurring in people aged below 55 (Howlader et al., 2015). In fact, it is the most common cancer in the 25-29 age group (Bleyer et al., 2006). Another interesting fact is that melanoma occurs more often in people of higher socioeconomic status (Hausauer, 2011), which may be a result of increased sun exposure, a significant risk factor for melanoma (Gandini et al., 2005a).

Most melanomas (84%) are diagnosed at the local stage, which is highly curable with a 5-year survival rate of 98.3% (Howlader et al., 2015). However, 5-year survival rates drop to 16.6% for melanoma that has already metastasised at the time of diagnosis (Howlader et al., 2015). Furthermore, melanoma has a reputation for being one of the most aggressive cancers, capable of rapid metastasis even from relatively small, millimetre-sized primary tumours that are extremely difficult to detect (Braeuer et al., 2014; Chin et al., 2006; Gupta et al., 2005). Given its propensity to metastasise and the low survival rates associated with metastatic melanoma, it is not surprising that melanoma accounts for the majority of skin cancer-related deaths despite its relative rarity compared to other skin cancers like basal cell carcinoma and squamous cell carcinoma.

Mortality rates for melanoma have remained fairly constant (Howlader et al., 2015) despite the increase in incidence, reflecting the increase in survival rates. However, the rising incidence is still a cause for concern, especially since melanoma affects a disproportionate number of young adults and causes one of the highest years of life lost per patient (Burnet et al., 2005), which increases its burden on society.

Cancer is a complex group of more than 100 distinct diseases, each with its own set of risk factors and epidemiology (Stratton et al., 2009). However, most cancers are believed to share a basic model of tumorigenesis – normal cells transform into malignant cells by progressively acquiring a series of mutations that allow them to evade senescence, resulting in deregulated and limitless proliferation. Cancer cells enjoy a Darwinian selective advantage over healthy, normal cells, and their uncontrolled growth eventually manifests as tumour masses.

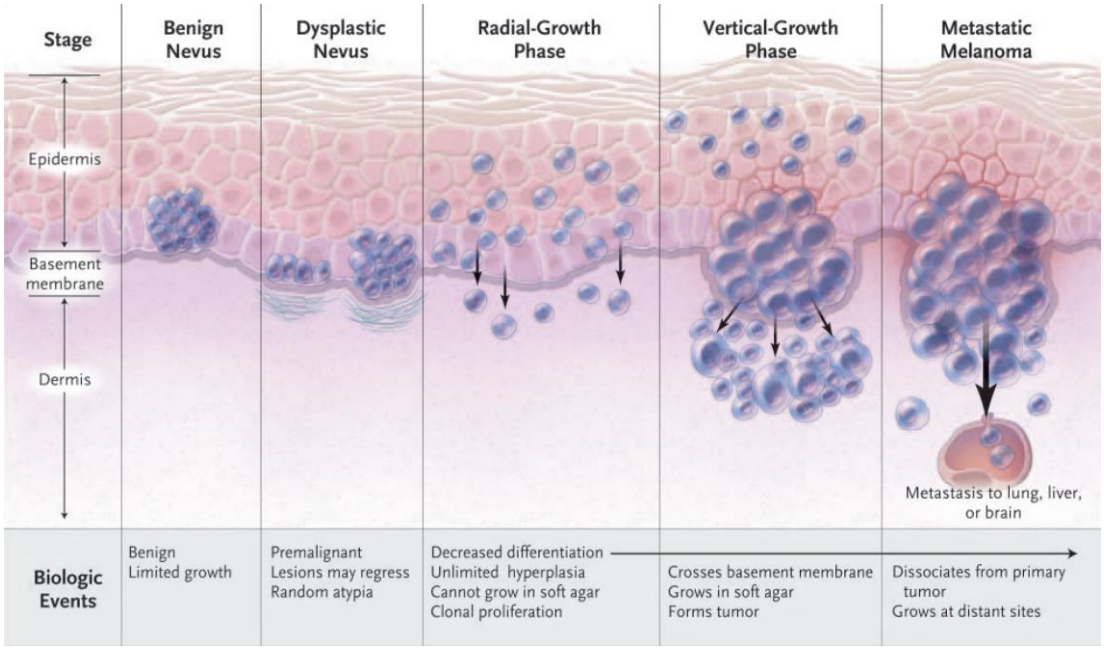

Figure 1.2 The Clark model of melanoma progression. The Clark model describes the pathophysiological changes associated with transformation of melanocytes in benign naevi into malignant melanoma. Adapted from Miller and Mihm, 2006.

With one of the highest mutation rates among cancer subtypes (Akbani et al., 2015), melanoma tumorigenesis is no different in this regard. Melanoma develops from the malignant transformation of melanocytes, which are specialised cells of neuroectodermal origin that are responsible for synthesising melanin pigment in vertebrates (Mort et al., 2015; Schadendorf et al., 2015). The pathological changes associated with the transformation of melanocytes to melanoma are described by the Clark model of melanoma progression (Clark et al., 1984; Miller and Mihm, 2006) (Figure 1.2). The first step involves the proliferation of melanocytes, which results in the formation of benign naevi. This is followed by aberrant growth that results in dysplastic lesions. In addition to developing from existing benign naevi, dysplastic naevi can also arise as lesions at new locations. The next step involves radial growth, with continued proliferation throughout the epidermis. In the subsequent vertical-growth phase, the cells become more invasive and penetrate the basement membrane

into the dermis, growing intradermally as an expansile nodule. The final step is metastasis, where tumour cells dissociate from the primary site and migrate through the surrounding tissue into the blood stream and lymphatic system. They eventually implant themselves at distant sites, resulting in the formation of metastases.

While the Clark model provides an appealing and logical step-wise description of melanoma development, it is important to note that most melanomas arise *de novo* and are not linked to pre-existing naevi (Lin et al., 2015). One plausible explanation for this observation is that different oncogenic mutations can confer a wide variety of growth advantages, such as an increase in proliferation, senescence bypass or resistance to apoptosis, depending on the genes involved. Whether melanomas arise *de novo* or from pre-existing naevi will potentially depend on the order in which these mutations occur and the phenotypes they confer (Hoek and Goding, 2010).

Although a tumour can contain as many as 50,000 mutations (Weinhold et al., 2014), only a small percentage are driver mutations which confer a selective growth advantage (Stratton et al., 2009; Vogelstein et al., 2013). Classic mathematical models have shown that 7 mutations are required to develop cancer (Fisher, 1958), although more recent studies suggest that only 3 driver mutations are necessary (Tomasetti et al., 2015). With the advent of sequencing technologies and bioinformatics, many of these driver mutations have been identified in the past decade. The most common genetic drivers of melanoma are described below.

1.2 The MAPK signalling pathway in melanoma

The mitogen-activated protein kinase (MAPK) pathway is an important, evolutionarily conserved family of proteins involved in signal transduction. As its name suggests, the MAPK pathway links extracellular signals, including mitogens and growth factors, to a vast array of cellular processes such as gene expression, proliferation, migration and apoptosis (Chang and Karin, 2001; Dhillon et al., 2007; Johnson and Lapadat, 2002). Seven distinct groups of MAP kinases have been identified in mammals so far, include extracellular signal-regulated kinase (ERK)1/2, ERK5, Jun amino-terminal kinases (JNK)1/2/3 and the p38 isoforms (α, β, γ, δ) (Johnson and Lapadat, 2002). These four groups are well-characterised and are considered to be conventional members of the family as they follow a classical three-tiered, sequential activation cascade composed of a MAPK, MAPK kinase (MAPKK or MAP2K) and a MAP2K kinase (MAPKKK or MAP3K) (Chang and Karin, 2001). Much less is known about the three remaining groups, which comprise of ERK3/4, ERK7/8 and Nemo-like kinase (NLK) and have atypical activation mechanisms compared to the conventional MAPK members (Coulombe and Meloche, 2007).

One of the principal and most well-studied MAPK pathways is the RAS/RAF/MEK/ERK signalling cascade (Figure 1.3), which also happens to be by far the most commonly mutated signal transduction pathway in melanoma. 83% of melanomas harbour a rat sarcoma (RAS) or rapidly accelerated fibrosarcoma (RAF) mutation, with the majority (52%) being a mutation in BRAF, and the second most common mutation being NRAS (28%) (Akbani et al., 2015; Cerami et al., 2012).

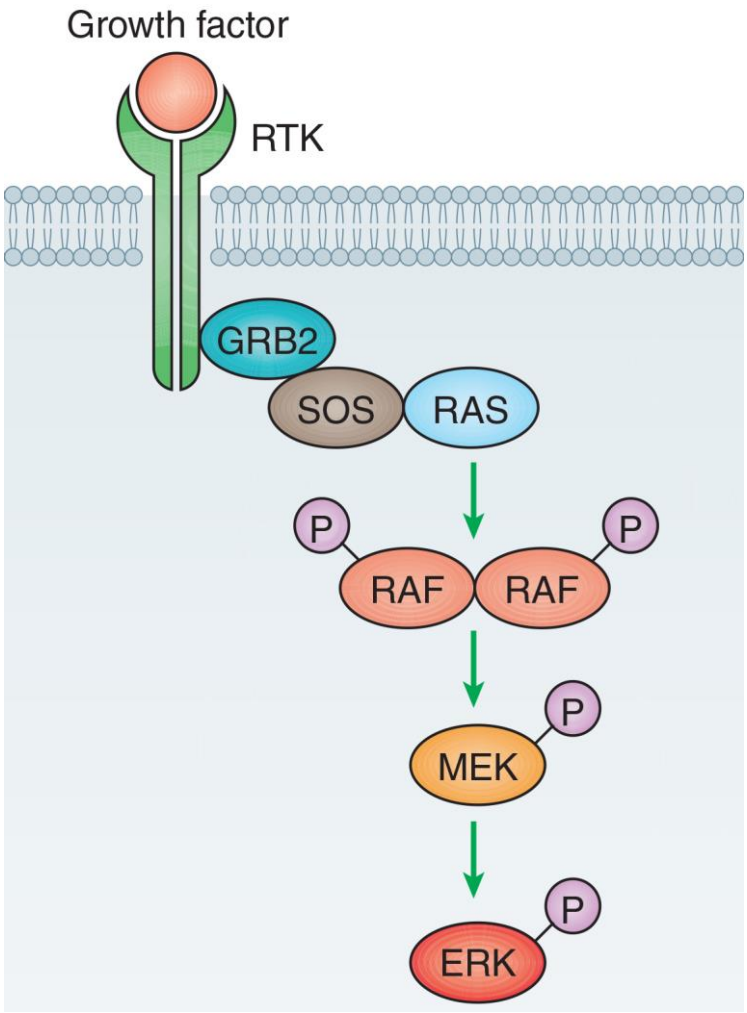

Figure 1.3 The RAS/RAF/MEK/ERK signalling cascade, downstream of RTK. The binding of growth factors triggers the activation of RTKs, which signal through the adaptor protein GRB2 and the exchange factor SOS to stimulate RAS. In turn, activated RAS recruits RAF to the plasma membrane, where RAF becomes activated following phosphorylation, conformational changes and dimerisation. Active RAF phosphorylates and activates MEK, which then phosphorylates and activates ERK. Adapted from Lito et al., 2013.

1.2.1 RAS

As the most upstream member of the RAS/RAF/MEK/ERK signalling cascade, the RAS family of guanine nucleotide-binding proteins (G proteins) is responsible for transducing signals from extracellular growth factors into the ERK pathway. In melanocytes, examples of these extracellular growth factors include stem cell factor (SCF), hepatocyte growth factor (HGF) and fibroblast growth factor (FGF) (Gray-Schopfer et al., 2007).

The tethering of growth factors to receptor tyrosine kinases (RTKs) leads to dimerisation and autophosphorylation, which triggers binding of the sequence homology 2 (SH2) domain of the growth factor receptor-bound 2 (GRB2) adaptor protein (Lodish et al., 2000). In turn, this recruits son of sevenless (SOS), a guanine nucleotide exchange factor (GEF) that facilitates nucleotide release (Boriack-Sjodin et al., 1998). SOS-mediated nucleotide release results in uptake of nucleotides from the cytosol, which culminates in guanosine triphosphate (GTP)-loading and activation of RAS since GTP is approximately ten times more common than guanosine diphosphate (GDP) in the cell (Lito et al., 2013). In addition to RTKs, ligands can also bind to G protein-coupled receptors (GPCRs), which results in RAS activation at the focal adhesion complex via heterotrimeric G proteins (Luttrell, 2005). GPCRs also transactivate RTKs to up-regulate the RAS/RAF/MEK/ERK pathway (Wetzker and Böhmer, 2003).

As a small GTPase, RAS can shuttle between a GTP-bound active state and a GDP-bound inactive state by hydrolysing GTP to GDP (Colicelli, 2004). *RAS* is one of the most frequently mutated oncogenes, with genomic alterations detected in about 30% of tumour samples across a wide range of cancers (Prior et al., 2012; Pylayeva-Gupta et al., 2011), leading to its constitutive activation. Among the three RAS isoforms, NRAS (28%) is the most commonly mutated in melanoma, while genomic alterations in HRAS (1.6%) and KRAS (1.3%) are much rarer in comparison (Akbani et al., 2015). Codon 61, which is a glutamine in the wild-type variant (Q61), is the predominant mutation hotspot, accounting for 88% of NRAS mutations in melanoma (Cerami et al., 2012). Exposure to ultraviolet (UV) light has been shown to correlate with NRAS Q61 mutations, which are preferentially found in body sites that are continuously exposed to the sun (Platz et al., 2008). Among the

NRAS Q61 mutations in melanoma, the most common variant is a Q61R substitution (44%), followed by Q61K (37%), with the rest being Q61L and Q61H substitutions (Akbani et al., 2015; Cerami et al., 2012). RAS adopts a conformation that positions Q61 in the active site following allosteric binding of Ca^{2+} (Buhrman et al., 2010). Q61 mutations impair the catalytic ability of RAS to hydrolyse GTP to GDP (Frech et al., 1994), which locks RAS in an active GTP-bound state. This results in the constitutive activation of a multitude of downstream pathways which eventually lead to tumorigenesis (Pylayeva-Gupta et al., 2011).

One of the major downstream effects of oncogenic RAS is the provision of a pro-proliferative signal, which is one of the hallmarks of cancer (Hanahan and Weinberg, 2000). Classical experiments show that microinjection of $HRAS^{G12V}$, another oncogenic variant of RAS with attenuated GTPase activity, into NIH 3T3 fibroblasts stimulated quiescent cells in the G0 phase to re-enter S phase and proliferate (Feramisco et al., 1984; Stacey and Kung, 1984). HRAS Q61 mutants were also subsequently shown to have a similar ability to transform NIH 3T3 cells (Der et al., 1986). In addition to pro-proliferative effects exerted through the RAS/RAF/MEK/ERK pathway, RAS also signals through phosphoinositide 3-kinase (PI3K) to suppress apoptosis. RAS can up-regulate the PI3K pathway by binding to and activating the p110 catalytic subunit of PI3K (Cully et al., 2006). PI3K activation results in phosphorylation of RAC-alpha serine/threonine-protein kinase (AKT), which in turn phosphorylates the pro-apoptotic protein B-cell lymphoma 2 (Bcl2)-associated agonist of cell death (BAD) (Datta et al., 1997; del Peso et al., 1997). Phosphorylated BAD is sequestered in the cytosol by 14-3-3 binding proteins, which relieves its heterodimerisation-mediated repression of BCL-2, an antagonist of apoptosis (Zha et al., 1996).

1.2.2 RAF

The RAF proteins are a family of serine/threonine kinases that form an important component of the RAS/RAF/MEK/ERK signalling cascade as the MAP3K. There are three members in the RAF family of proteins: ARAF, BRAF, and CRAF, otherwise known as RAF1. All three isoforms of RAF share a similar structure with three conserved regions: CR1, CR2 and CR3 (Figure 1.4). CR1 lies in the N-terminus of RAF and comprises a RAS-binding domain (RBD) as well as a cysteine-rich domain (CRD). CR2, also in the N-terminus, is a serine/threonine-rich region that includes a 14-3-3 binding site. CR3 is located in the C-terminus and contains the kinase domain of RAF.

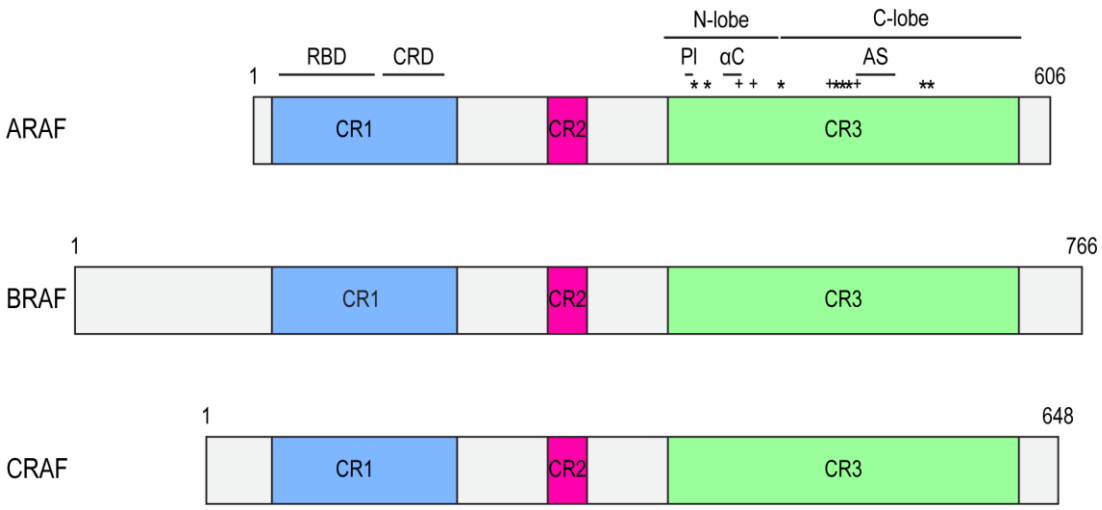

Figure 1.4 Structure of the RAF proteins. The three RAF isoforms share a similar structure with three conserved regions (CR). CR1 (blue) contains a RAS-binding domain (RBD) and a cysteine-rich domain (CRD). CR2 (red) is a domain rich in serine and threonine residues. CR3 (green) contains the kinase domain, which consists of a smaller N-terminal lobe (N-lobe) and a larger C-terminal lobe (C-lobe). Key features of the kinase domain include the P-loop (Pl), αC and the activation segment (AS). The DFG motif lies at the N-terminal end of the AS (not shown). The key residues that make up the C-spine (*) and the R-spine ($^{+}$) are indicated. Adapted from Roskoski, 2010.

1.2.2.1 RAF kinase domain structure

The crystal structure of the RAF kinase domain was first solved in 2004, when the BRAF kinase domain was crystallised in the presence of BAY43-9006 (also known as sorafenib), a small molecule inhibitor of RAF (Wan et al., 2004). The RAF kinase domain adopts a structure that is typical of most protein kinases, with a small amino terminal (N-terminal) lobe and large carboxyl terminal (C-terminal) lobe being separated by a catalytic cleft. The small N-lobe consists mainly of anti-parallel β-sheets as well as a regulatory α-helix known as the αC. Within the N-lobe lies a glycine-rich phosphate-binding loop (P-loop) that is responsible for adenosine triphosphate (ATP) anchorage and orientation. The large C-lobe comprises of α-helices and a key regulatory loop denoted as the activation segment (AS), which contains a highly conserved Asp-Phe-Gly (DFG) motif at the N-terminal side.

The relative motion and position of the two lobes determine the accessibility of the catalytic cleft to ATP, which in turn affects the kinase activity of the RAF protein (Taylor and Kornev, 2011). Another level of regulation is provided by the conformation of the AS. When RAF is inactive, the AS adopts a DFG-out conformation, whereby the aspartic acid of the DFG motif faces away from the ATP-binding pocket. In the active DFG-in conformation, the aspartic acid of the DFG motif rotates into the active site and interacts with the Mg^{2+} ions of Mg-ATP during phospho-transfer. The αC helix can also move inwards or outwards relative to the catalytic cleft. Positioning the αC helix inwards (αC-in) leads to alignment of the catalytic spine (C-spine) and regulatory spines (R-spine), resulting in an active, closed conformation of the kinase (Lavoie and Therrien, 2015).

1.2.2.2 RAF activation

In its inactive state, RAF's CR1 binds to and represses the CR3 kinase domain, resulting in its autoinhibition. This was proven by a series of studies which demonstrated that deletion of the N-terminus results in RAF activation (Heidecker et al., 1990; Stanton and Cooper, 1987). Overexpression of CR1 also results in repression of RAF catalytic activity, which is likely to be mediated in part by the physical interaction between CR1 and CR3, since CR1 also co-immunoprecipitates with CR3 (Cutler et al., 1998; Tran et al., 2005). Suppression of RAF kinase activity is also mediated by phosphorylation of S259 (relative to CRAF) in the N-terminus, which was shown to be a 14-3-3 binding site (Michaud et al., 1995; Muslin et al., 1996). Since S621 (relative to CRAF) in the C-terminus is also a 14-3-3 target (Muslin et al., 1996), 14-3-3 proteins are believed to stabilise the autoinhibitory interaction between CR1 and CR3 by binding to both the N and C-terminals of RAF (Matallanas et al., 2011; Tzivion et al., 1998).

Located downstream of RAS, RAF is recruited by GTP-bound active RAS to the cell membrane. This takes place via interactions with the RAS-binding domain (RBD) and cysteine-rich domain (CRD) in the N-terminus of RAF (Brtva et al., 1995; Vojtek et al., 1993). The RAF CRD is able to interact with farnesyl groups in the C-terminus of prenylated RAS (Fischer et al., 2007; Williams et al., 2000). Another function of the CRD is to promote translocation of RAF to the cell membrane via zinc-coordinated interactions with phosphatidylserine, a component of the cell phospholipid membrane (Ghosh et al., 1994; Strum, 1996). Binding of RAS results in displacement of 14-3-3 proteins from the N-terminus of RAF (Rommel et al., 1996), a process which is probably mediated via protein phosphatase 1 (PP1) and protein phosphatase 2A (PP2A)-catalysed dephosphorylation of S259 (relative to

CRAF) (Jaumot and Hancock, 2001). Disruption of the binding with 14-3-3 relieves N-terminal autoinhibition of the C-terminal kinase domain, and frees the N-terminus of RAF for interaction with RAS, hence promoting RAF's association and accumulation at the cell membrane (Kubicek et al., 2002; Lavoie and Therrien, 2015).

Another key event in the activation of RAF is dimerisation, which occurs via a side-to-side dimerisation interface centred around R509 (relative to BRAF) (Rajakulendran et al., 2009). Studies have shown that RAF exists predominantly as a monomer in the cytosol in the resting state (Nan et al., 2013). In the presence of active RAS, RAF is recruited to the membrane where it forms BRAF-CRAF heterodimers (Weber et al., 2001). The precise underlying mechanism is unclear, but it has been proposed that the interaction between RAS and the N-terminus of RAF relieves N-terminal repression of the C-terminus. This exposes the C-terminal 14-3-3 binding site (S621 in CRAF, S729 in BRAF), thus allowing 14-3-3 to bind to and stabilise the heterodimers (Rajakulendran et al., 2009; Weber et al., 2001). In addition, the rate of BRAF-CRAF heterodimerisation can also be enhanced by an increase in the local concentration of RAF molecules following RAS-mediated recruitment of RAF to the cell membrane (Lavoie and Therrien, 2015).

RAF dimerisation results in elevated kinase activity and stimulation of the MAPK cascade (Farrar et al., 1996; Luo et al., 1996). Another observation is that although RAF is able to form both homodimers and heterodimers, heterodimers of BRAF and CRAF possess higher kinase activity compared to their respective homodimers (Rushworth et al., 2006). The kinase activity of BRAF does not appear to affect its ability to heterodimerise with and activate CRAF, as shown in experiments involving kinase-impaired and even kinase-dead variants of BRAF (Garnett et al., 2005; Heidorn et al., 2010).

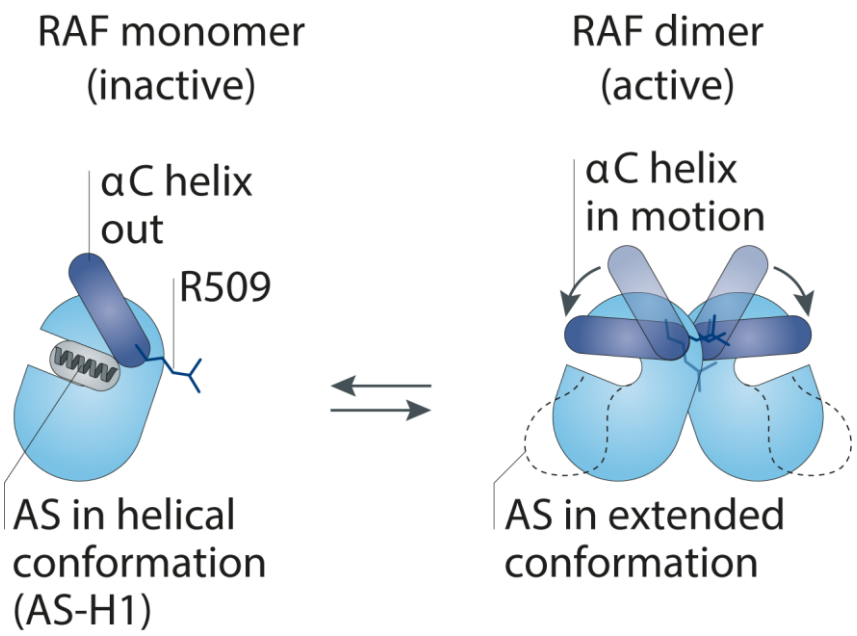

Figure 1.5 Dimerisation is a key event in the catalytic activation of RAF. In RAF's monomeric form, the activation segment (AS) in RAF adopts helical conformation (AS-H1), which stabilises the αC in its 'out' conformation in which RAF is inactive. Upon dimerisation involving the R509 residue in BRAF, the AS-H1 unravels and the αC moves inwards, which results in alignment of the residues involved in catalysis and thus activates its kinase function. Adapted from Lavoie and Therrien, 2015.

Dimerisation-driven activation of RAF is believed to be facilitated by allosteric stabilisation of the catalytic cleft, which favours the adoption of an active, closed conformation (Lavoie and Therrien, 2015; Lavoie et al., 2013) (Figure 1.5). Given that the regulatory αC helix overlaps with the side-to-side dimerisation interface, it has been postulated that the αC helix adopts an active αC-in conformation upon dimerisation (Rajakulendran et al., 2009). Indeed, the recent elucidation of the crystal structure of the BRAF kinase domain monomer showed that the inactive αC-out conformation, which is incompetent for phospho-transfer, is stabilised in its monomeric form by a short helix (AS-H1) within the AS that unravels upon dimerisation (Thevakumaran et al., 2014).

Another interaction partner of RAF is kinase suppressor of RAS (KSR), a close relative that shares a significant amount of sequence homology and domain architecture with the RAF family of proteins (Sundaram and Han, 1995; Therrien et

al., 1995). KSR interacts with RAF via the side-to-side dimerisation interface centred at R509 (relative to BRAF) that is also conserved in KSR (Rajakulendran et al., 2009). Since KSR can also bind to MEK constitutively (McKay et al., 2009), KSR functions as a scaffold that brings RAF and MEK together in close proximity to form a complex (Roy et al., 2002; Stewart et al., 1999). This facilitates phosphorylation of MEK by RAF, hence activating the MAPK pathway.

1.2.2.3 BRAF

Among the three isoforms of RAF, BRAF is the most commonly mutated in cancer, with ~8% of human cancer tumours possessing a BRAF mutation (Davies et al., 2002). In contrast, genetic alterations of ARAF and CRAF are much rarer – CRAF mutations were found in just 0.7% of cancer cell lines, while ARAF mutations were not even detected (Emuss et al., 2005).

In melanoma, *BRAF* is the most commonly mutated gene, with genetic alterations observed in 40-60% of melanoma (Akbani et al., 2015; Cerami et al., 2012; Davies et al., 2002; Forbes et al., 2015; Hodis et al., 2012; Platz et al., 2008). BRAF is also a mutational hotspot in thyroid carcinomas and colorectal cancers, with mutational frequencies of 50-60% (Agrawal et al., 2014; Cerami et al., 2012; Forbes et al., 2015) and 10-11% respectively (Cerami et al., 2012; Forbes et al., 2015; Muzny et al., 2012). Importantly, although *BRAF* and *NRAS* are two of the most commonly mutated genes in melanoma, they tend to be mutually exclusive ($p < 0.001$, Fisher's exact test) in patient-derived melanoma samples (Akbani et al., 2015; Cerami et al., 2012).

According to the COSMIC (Catalogue Of Somatic Mutations In Cancer) database of tumour samples and cancer cell lines, 345 distinct missense mutations

have been detected in the *BRAF* gene to date, encompassing 168 of 766 amino acids in the BRAF protein (Forbes et al., 2015). The vast majority of BRAF mutations in cancer occur in the kinase domain and are predominantly clustered around the glycine-rich P-loop and the activation segment (Forbes et al., 2015; Lavoie and Therrien, 2015). With regards to melanoma, an overwhelming proportion of BRAF mutations occur at codon 600, which possesses a mutational frequency of 87% (Akbani et al., 2015). A valine to glutamic acid substitution at codon 600 (V600E) in BRAF is the most common mutation in melanoma. V600E substitutions account for 86% of V600 mutations in melanoma, while the next most common alteration is the V600K mutation that is found in 12% of cases involving the V600 locus (Akbani et al., 2015).

$BRAF^{V600E}$ is 478 times more active than wild-type BRAF, as measured by an *in vitro* kinase assay with MEK as the substrate (Wan et al., 2004). However, this only translates to a 4.6-fold increase in ERK activation over wild-type BRAF when the $BRAF^{V600E}$ variant was expressed in COS (CV-1 origin, SV40) cells (Wan et al., 2004). Mechanistically, the increase in activity of the $BRAF^{V600E}$ mutant is mediated by a conformational change. In wild-type BRAF, the glycine rich P-loop interacts with the activation segment via hydrophobic interactions, hence stabilising the inactive DFG-out conformation that is inaccessible to ATP (Wan et al., 2004). There is a specific hydrophobic interaction between F468 of the P-loop and V600 of the activation segment, which would be disrupted by a mutation of V600 from valine (a medium-sized hydrophobic amino acid) to glutamic acid (a large, bulky charged residue) (Wan et al., 2004). The $BRAF^{V600E}$ mutant is phosphomimetic and analogous to RAS-mediated phosphorylation of T599 and S602 (Zhang and Guan, 2000), which disrupts the interaction between the P-loop and activation segment,

resulting in the adoption of an active DFG-in conformation. Other common mutants of BRAF at codon 600 (V600K, V600R, V600D) are believed to act in a similar fashion since they also involve bulky and charged residues (Wan et al., 2004).

P-loop mutants, which represent about 6% of BRAF mutations in melanoma (Akbani et al., 2015; Cerami et al., 2012), can also act in a similar manner to disrupt the P-loop and activation segment interaction. However, the final activity of the P-loop mutant is determined by the precise identity and nature of the substitution, since the P-loop is responsible for binding ATP. For example, the *in vitro* activity of the $BRAF^{G469A}$ mutant is 266-fold over that of the wild-type, while the $BRAF^{G469E}$ mutant is only a modest 1.3 times as active as the wild-type, even though both mutants are able to destabilise the inactive DFG-out conformation. The difference in activity between the two G469 mutants can be explained by the fact that the bulky and charged glutamic acid residue will interfere with the interactions between the P-loop and ATP. In contrast, the smaller alanine residue is more similar to the glycine residue that it replaces and hence does not adversely affect P-loop's affinity for ATP (Wan et al., 2004).

The acidic E600 residue in the $BRAF^{V600E}$ mutant may also form an electrostatic interaction with the basic K507 residue of the αC helix to stabilise the active conformation (Wan et al., 2004). Since K507 forms part of the side-to-side dimerisation interface, it has been postulated that E600-K507 interaction can potentially recapitulate the allosteric stabilisation of the catalytic cleft observed upon dimerisation (Lavoie and Therrien, 2015). Indeed, the $BRAF^{V600E}$ mutant's ability to activate the MAPK pathway appears to be independent of its ability to dimerise, as demonstrated by the observation that the $BRAF^{V600E/R509H}$ double mutant, which is incapable of forming dimers, can phosphorylate MEK to a similar extent as the

V600E single mutant (Poulikakos et al., 2011; Röring et al., 2012; Yao et al., 2015). Consistent with this observation is the fact that the activity of the $BRAF^{V600E/K507E}$ double mutant, which is no longer able to form a stabilising salt bridge between codons 507 and 600, becomes dependent on R509-mediated dimerisation (Haling et al., 2014).

Interestingly, BRAF mutations associated with cancer do not always possess high levels of intrinsic kinase activity. These kinase-impaired variants of BRAF usually involve substitutions at key residues of the catalytic site that are required for optimal kinase activity (Wan et al., 2004). For example, the $BRAF^{G466V}$ mutation possesses 35% less *in vitro* kinase activity compared to the wild-type variant. Yet, $BRAF^{G466V}$ was still able to stimulate ERK activity 1.9-fold versus the wild-type in COS cells (Wan et al., 2004). These paradoxical observations can be reconciled by studies which showed that the oncogenic potential of kinase-impaired and even kinase-dead versions of BRAF derives from their ability to promote the formation of BRAF-CRAF heterodimers, resulting in subsequent activation of downstream ERK signalling and ultimately, tumorigenesis (Garnett et al., 2005; Heidorn et al., 2010).

The elevated kinase activity of the $BRAF^{V600E}$ mutant results in its increased ability to stimulate constitutive, RAS-independent ERK signalling and proliferation in both melanocytes and melanoma cell lines (Davies et al., 2002; Wellbrock et al., 2004). In line with this, ribonucleic acid interference (RNAi)-mediated depletion of $BRAF^{V600E}$ reduced ERK phosphorylation, slowed down proliferation rates and increased apoptosis in melanocytes (Wellbrock et al., 2004) and melanoma cell lines (Karasarides et al., 2004; Wellbrock et al., 2004), as well as in mouse xenograft models of melanoma (Hoeflich et al., 2006; Karasarides et al., 2004). Notably, mutations in *NRAS* and *BRAF* tend towards mutual exclusivity ($p < 0.001$, Fisher's

exact test) in melanoma tumour samples included in the Cancer Genome Atlas (TCGA) study (Akbani et al., 2015; Cerami et al., 2012), suggesting that pathway hyperactivation may be paradoxically detrimental towards tumour progression (Gray-Schopfer et al., 2007).

The $BRAF^{V600E}$ substitution is also found in 82% of naevi (Pollock et al., 2002). However, most naevi are benign and do not proliferate (Bennett, 2003) despite the abundance of pro-proliferative oncogenic BRAF mutations. This can be explained by the onset of oncogene-induced senescence, a mechanism in which cells respond to pro-proliferative oncogenic signals by going into irreversible cell cycle arrest, thus restricting the progression of benign lesions into cancer (Courtois-Cox et al., 2008). When overexpressed in primary human melanocytes, $BRAF^{V600E}$ caused cell cycle arrest, increased senescence-associated β-galactosidase activity and up-regulated $p16^{INK4a}$ expression (Michaloglou et al., 2005).

Due to its ability to induce senescence, BRAF activation appears to be insufficient for tumorigenesis on its own without the development of additional mutations in other cancer-related pathways such as tumour suppressors. In animal models, expression of $BRAF^{V600E}$ in zebrafish led to the proliferation of melanocytes and the subsequent formation of naevi-like melanocyte clusters, but they also failed to develop melanoma unless the *tp53* tumour suppressor gene was first inactivated (Patton et al., 2005). Similarly, when $BRAF^{V600E}$ was conditionally expressed in melanocytes in mouse models, the mice developed benign melanocytic hyperplasias that did not progress to melanoma (Dankort et al., 2009). The mice only developed metastatic tumours when $BRAF^{V600E}$ expression was coupled with deletion of the *Pten* tumour suppressor gene (Dankort et al., 2009). Cooperation between BRAF mutations and PTEN loss has also been observed in human melanoma cell lines

(Tsao et al., 2004), as well as in patient-derived tumour samples (Akbani et al., 2015; Cerami et al., 2012; Curtin et al., 2005).

1.2.3 MEK and ERK

Compared to RAS and RAF, genetic alterations of MEK and ERK in melanoma are much less common. 9% of melanoma patients possess alterations in the *MAP2K1* and *MAP2K2* genes, which encode the MEK1 and MEK2 proteins respectively (Akbani et al., 2015; Cerami et al., 2012). A mere 5% of cases have alterations in the *MAPK1* and *MAPK3* genes, which code for ERK2 and ERK1 kinases respectively (Akbani et al., 2015; Cerami et al., 2012).

Although mutations of MEK and ERK are rare in melanoma, it is still informative to examine the contributions of these downstream components of the MAPK signalling cascade towards tumorigenesis. MEK is activated by RAF via phosphorylations of S218 and S222 of the activation loop (Alessil et al., 1994). As a dual-specificity kinase that is able to phosphorylate tyrosine, serine or threonine residues, activated MEK phosphorylates ERK on T202 and Y204 of the activation segment (Payne et al., 1991). Once activated, ERK acts on a multitude of more than 160 substrates with a diverse range of functions, including transcription factors, cytoskeletal proteins, kinases, phosphatases, signalling proteins and apoptotic proteins (Yoon and Seger, 2006).

Many of these downstream effects of activated ERK signalling lead to tumorigenesis. ERK signalling can contribute to evasion of apoptosis, one of the hallmarks of cancer (Hanahan and Weinberg, 2000), by inactivating BAD. ERK phosphorylates and activates ribosomal S6 kinase (RSK), which in turn

phosphorylates the pro-apoptotic protein BAD on S75 and results in its sequestration in the cytosol by 14-3-3 proteins (She et al., 2002; Zha et al., 1996).

Yet another classical feature of tumorigenesis is limitless replicative potential (Hanahan and Weinberg, 2000). Following activation, ERK is able to translocate to the nucleus (Chen et al., 1992; Chuderland et al., 2008), where it can enable replicative immortality via phosphorylation of the E26 transformation-specific (ETS) transcription factor ER81 (Janknecht, 1996). ER81 is known to up-regulate hTERT transcriptionally (Goueli and Janknecht, 2004), which results in increased telomerase activity, thus preventing the onset of replicative senescence induced by telomere shortening.

1.3 Other pathways in melanoma

1.3.1 PTEN and the PI3K-AKT pathway

Genetic alterations in the *PTEN* tumour suppressor gene are also relatively common in melanoma, with deletions or mutations of *PTEN* observed in 14% of melanoma patients (Akbani et al., 2015; Cerami et al., 2012). The *PTEN* gene encodes the phosphatase and tensin homolog (PTEN) protein, a phosphatase that dephosphorylates phosphatidylinositol phosphate (PIP_3) (Maehama and Dixon, 1998). PIP_3 is a lipid second messenger that is generated by activated PI3K at the plasma membrane upon the binding of growth factors to receptors such as RTKs and GPCRs. AKT binds to PIP_3 via its pleckstrin homology (PH) domain, resulting in translocation of AKT to the cell membrane where it is phosphorylated and activated (Liu et al., 2009). Since PTEN decreases levels of PIP_3 via dephosphorylation, it functions as a negative regulator of the PI3K-AKT pathway. Loss of PTEN leads to de-repression of the PI3K-AKT pathway, which promotes cell cycle progression as well as cell survival via decreased apoptosis in mouse embryonic fibroblasts (Stambolic et al., 1998; Sun et al., 1999). Ectopic restoration of PTEN expression in PTEN-deficient melanoma cell lines suppressed proliferation (Robertson et al., 1998), reduced tumorigenicity and inhibited metastasis in mouse models (Hwang et al., 2001; Stahl et al., 2003).

As mentioned previously, PTEN and BRAF display cooperativity in melanomas, with *PTEN* deletions and mutations possessing a significant tendency towards co-occurrence ($p = 0.021$, Fisher's exact test) with *BRAF* mutations in patient-derived tumour samples from the TCGA melanoma study (Akbani et al., 2015; Cerami et al., 2012). This relationship was also observed in melanoma cell lines (Tsao et al., 2004), as well as in a $BRAF^{V600E}$ mouse model of melanoma where

the mice developed metastatic tumours only in the context of both BRAF activation and *Pten* deletion (Dankort et al., 2009).

On the other hand, *PTEN* and *NRAS* alterations are mutually exclusive ($p = 0.027$, Fisher's exact test) in melanoma cell lines (Tsao et al., 2000). This observation may be analogous to the mutual exclusivity and functional redundancy between NRAS and BRAF mutations. Since NRAS already activates the PI3K pathway downstream (Cully et al., 2006), further loss of PTEN is not necessary for tumorigenesis, and may even be disadvantageous to tumour progression due to pathway hyperactivation (Gray-Schopfer et al., 2007).

1.3.2 CDKN2A

The cyclin-dependent kinase inhibitor 2A (*CDKN2A*) genomic locus is also frequently altered in melanoma, with deletions and mutations of *CDKN2A* observed in 44% of cases in the TCGA melanoma data set (Akbani et al., 2015; Cerami et al., 2012). Approximately 10% of melanoma cases present with a family history of melanoma (Tsao et al., 2012), which confers a 1.74-fold of risk of developing the disease (Gandini et al., 2005b). Notably, germline mutations in the *CDKN2A* gene are associated with melanoma susceptibility in 25-40% of familial melanoma cases (Hayward, 2003).

The *CDKN2A* gene codes for two distinct tumour suppressor proteins, $p16^{INK4a}$ and $p14^{ARF}$, via the use of different promoters and alternate reading frames. $p16^{INK4a}$ functions as a tumour suppressor due to its effects in impeding cell cycle progression. $p16^{INK4a}$ inhibits the cyclin-dependent kinases (CDKs) CDK4 and CDK6, thus preventing CDK phosphorylation of the retinoblastoma (RB) protein (Koh et al., 1995). Unphosphorylated RB binds to and inhibits E2F1 (Nevins et al., 1991), a

transcription factor that activates genes facilitating G1/S transition. Loss of $p16^{INK4a}$ results in increased CDK4 and CDK6 activity, hyperphosphorylated RB and de-repression of E2F1, which culminates in G1/S progression and re-entry into the cell cycle.

$p14^{ARF}$, the alternately spliced product of *CDKN2A*, is transcribed from an alternative first exon. Though $p14^{ARF}$ utilises the same second and third exons, it shares no amino acid homology with $p16^{INK4a}$ due to the use of an alternate reading frame. $p14^{ARF}$ exerts its tumour suppressor effects via p53. $p14^{ARF}$ regulates levels of p53 by binding to the E3 ubiquitin ligase minute-double-minute 2 (MDM2) and inhibiting its activity (Honda and Yasuda, 1999; Pomerantz et al., 1998). Since MDM2 ubiquitinates p53 and mediates its destruction by the proteasome (Honda and Yasuda, 1999), $p14^{ARF}$ ablation leads to destabilisation of p53. This culminates in the down-regulation of key p53 functions in the cell, such as apoptosis, deoxyribonucleic acid (DNA) damage repair and cell cycle arrest (Harris and Levine, 2005; Pomerantz et al., 1998).

The mutational hotspot status of *CDKN2A* might derive from the fact *CDKN2A* lesions can potentially eliminate two tumour suppressor proteins, resulting in the inactivation of both RB and p53 tumour suppressor pathways. Indeed, the ability of activated RAS to induce melanoma tumour formation in mice is increased dramatically in the context of both $p16^{INK4a}$ and $p14^{ARF}$ ablation (Chin et al., 1997; VanBrocklin et al., 2010). On the other hand, loss of $p16^{INK4a}$ alone appears to be insufficient for RAS-mediated transformation in mouse embryonic fibroblasts (MEFs) (Krimpenfort et al., 2001; Sharpless et al., 2001). In the context of $p14^{ARF}$ haploinsufficiency, $p16^{INK4a}$-null mice metastatic melanoma developed metastatic melanoma with high penetrance following treatment with the carcinogen

dimethylbenzanthracene (DMBA) (Krimpenfort et al., 2001). This suggests that melanoma carcinogenesis, in the context of *CDKN2A* alterations, arises from cooperation between both the $p16^{INK4a}$ and $p14^{ARF}$ pathways.

1.3.3 MITF

The microphthalmia-associated transcription factor (MITF) is the 'master regulator' of the melanocyte lineage, and plays an essential role in melanocyte development, survival and differentiation (Opdecamp et al., 1997). The *MITF* gene possesses a complex structure, with at least 11 different isoforms being expressed under multiple promoters (Levy et al., 2006; Li et al., 2010; Shiohara et al., 2009). Exons 2-9 are shared by all the different isoforms of MITF, with the only difference between the isoforms occurring in the first exon. The MITF-M isoform is expressed exclusively in melanocytes and melanoma cells under the control of the melanocyte-specific M promoter (Fuse et al., 1996; Vachtenheim and Novotná, 1999; Yasumoto et al., 1998). Since MITF-M is the dominant form of MITF in cells of the melanocyte lineage (Yasumoto et al., 1998), all discussions pertaining to MITF henceforth shall be in reference to the MITF-M isoform, unless otherwise specified.

MITF belongs to the basic helix-loop-helix leucine zipper (bHLH-LZ) family of transcription factors, which share a common basic helix-loop-helix structure as well as a leucine zipper region that are both involved in DNA binding and dimerisation (Hemesath et al., 1994; Hodgkinson et al., 1993). MITF is able to both homodimerise with itself, and heterodimerise with other microphthalmia-related transcription (MiT) factors such as transcription factor EB (TFEB), transcription factor E3 (TFE3) and transcription factor EC (TFEC) (Hemesath et al., 1994). Like other members of this family, MITF binds to the E-box (CANNTG, in particular

CA[C/T]GTG) DNA motifs in promoters and enhancers to initiate transcription (Cheli et al., 2010; Levy et al., 2006). In the case of MITF, the addition of a flanking T to the 5' end of the core CATGTG E-box motif is necessary for binding, whereas no such requirement was observed for the CACGTG variant of the E-box motif (Aksan and Goding, 1998). This TCATGTG motif was termed the M-box since it is highly conserved in melanocyte-specific promoters across various species.

MITF regulates melanocyte differentiation by initiating transcription after binding to M-box motifs in the promoters of the pigmentation-related genes *TYR* (Bentley et al., 1994; Galibert et al., 2001), *TYRP1* (Bertolotto et al., 1998a; De La Serna et al., 2006) and *DCT* (Lang et al., 2005; Yavuzer et al., 1995). These genes encode tyrosinase (TYR), tyrosinase-related protein 1 (TYRP1), and dopachrome tautomerase (DCT) respectively, all of which are enzymes involved in the synthesis of the melanin pigment. Indeed, it is possible to induce expression of all three melanogenic marker proteins by ectopically expressing MITF in fibroblasts (Tachibana et al., 1996). In addition to genes involved in the melanogenesis pathway, other transcriptional targets of MITF include genes such as premelanosome (*PMEL*) (Baxter and Pavan, 2003), melanoma antigen recognised by T cells (*MLANA*) (Du et al., 2003) and Ras-related protein 27A (*RAB27A*) (Chiaverini et al., 2008), which encode proteins responsible for melanosome biogenesis and trafficking.

Due to MITF's role as the master regulator of the melanocyte lineage, the loss of MITF is commonly associated with defects in pigmentation. In animal models, MITF-deficient mice fail to develop melanocytes, resulting in a loss of hair pigmentation, hearing impairment and small eyes (microphthalmia) (Moore, 1995; Steingrímsson et al., 1994). A null mutation in the *mitfa* gene, the zebrafish-specific homologue of *MITF*, results in a lack of melanophores in zebrafish (Lister et al.,

1999). In humans, MITF dysfunction is associated with Waardenburg syndrome type 2A, a condition characterised by hearing loss and hair pigmentary abnormalities such as a white forelock and premature greying (Hughes et al., 1994; Tassabehji et al., 1994). MITF mutations have also been implicated in Tietz syndrome, which causes deafness and hypopigmentation-induced albinism in patients (Amiel et al., 1998; Smith et al., 2000).

MITF mutations have also been implicated in cancer. Unlike the mutations involved in pigment deficiency syndromes, which tend to involve the DNA binding domain, MITF mutations in melanoma usually affect MITF's transcriptional activity as opposed to its ability to bind DNA (Grill et al., 2013). A glutamic acid to lysine substitution at codon 318 (E318K) in MITF was identified in patients with familial melanoma, where it was found to confer a significantly higher risk of developing melanoma (Bertolotto et al., 2011; Yokoyama et al., 2011). $MITF^{E318K}$ was shown to be transcriptionally more active than wild-type MITF, implicating its role as an oncogene that mediates an increase in invasion, migration and clonogenicity in melanoma cells (Bertolotto et al., 2011). The increase in transcriptional activity of the $MITF^{E318K}$ mutant is believed to a result of the abrogation of the sumoylation post-translational modification on the nearby K316 residue (Bertolotto et al., 2011; Yokoyama et al., 2011), since sumoylation has been previously shown to repress MITF-mediated transcription (Miller et al., 2005; Murakami and Arnheiter, 2005).

In addition to mutations, other genetic alterations of MITF have also been found in association with non-familial melanoma. The link between MITF and melanoma was first uncovered in 2005, when *MITF* was identified as a lineage addiction oncogene amplified in 10-20% of melanoma samples (Garraway et al., 2005). A corollary of oncogene addiction, lineage addiction refers to the lineage-

specific survival mechanisms that become deregulated and persist even after normal development, ultimately culminating in carcinogenesis by promoting tumour survival (Garraway and Sellers, 2006). Compared to primary tumours, metastatic tumours had more frequent instances of *MITF* amplification, while *MITF* copy number increments were not detected in benign naevi (Garraway et al., 2005). In addition, *MITF* amplification correlated with reduced survival in metastatic melanoma (Garraway et al., 2005). Functional assays revealed the cooperativity between MITF and BRAF, with ectopic co-expression of MITF and activated $BRAF^{V600E}$ causing transformation of immortalised human melanocytes and neural crest progenitor cells (Garraway et al., 2005; Kumar et al., 2014). In line with this, alterations in the *MITF* gene were found to co-occur together with *BRAF* mutations ($p = 0.006$, Fisher's exact test) in patient-derived melanoma tumour samples (Akbani et al., 2015; Cerami et al., 2012).

The oncogenic potential of MITF has also been elegantly demonstrated in zebrafish models of melanoma, via the use of a temperature-sensitive *mitfa* mutant to conditionally manipulate endogenous levels of Mitfa activity (Lister et al., 2014). Low levels of Mitfa activity were found to promote melanoma formation in conjunction with activated human $BRAF^{V600E}$ (Lister et al., 2014). Importantly, these melanomas regressed upon ablation of Mitfa activity, demonstrating the critical role played by MITF in $BRAF^{V600E}$-mediated oncogenesis (Lister et al., 2014).

MITF's oncogenic effect can potentially be explained by the fact that transcriptional targets of MITF include genes that mediate pro-survival functions. For example, MITF was found to directly up-regulate the expression of the anti-apoptotic proteins BCL2 and BCL2A1 by binding to their respective promoters (Haq et al., 2013a; McGill et al., 2002). In the case of BCL2, the expression of dominant-

negative MITF in melanocytes and melanoma cells resulted in cell death that could be rescued by constitutive BCL2 overexpression (McGill et al., 2002). BCL2A1 was specifically up-regulated in melanomas compared to other cancers, and knockdown of *BCL2A1* led to an increase in apoptosis upon BRAF inhibition (Haq et al., 2013a). Another transcriptional target of MITF is the melanoma inhibitor of apoptosis (*ML-IAP*), an anti-apoptotic protein which is highly expressed in melanomas (Dynek et al., 2008).

In addition to anti-apoptotic pathways, MITF also regulates cell-cycle progression by controlling the transcription of cyclin-dependent kinase 2 (*CDK2*) (Du et al., 2004). Quantitative real-time polymerase chain reaction (qPCR) analysis of primary melanoma samples revealed that mRNA levels of *MITF* and *CDK2* were significantly correlated in melanoma, but not in other tumour types (Du et al., 2004). In addition, overexpression of CDK2 could rescue the suppression of melanoma colony formation by dominant-negative MITF in a colony growth assay (Du et al., 2004).

Another transcriptional target of MITF is the *MET* proto-oncogene, which encodes the c-MET protein that is believed to play an important role in metastasis and is also highly expressed in melanomas (McGill et al., 2006). In line with c-MET's ability to up-regulate invasive potential after hepatocyte growth factor (HGF) stimulation, HGF-mediated invasion in primary human melanocytes and melanoma cells was dramatically increased in the presence of ectopic MITF (McGill et al., 2006).

Deregulated cellular energetics has been identified as an emerging hallmark of cancer, reflecting the large amount of evidence for reprogrammed cellular metabolism in cancer cells (Hanahan and Weinberg, 2011). MITF also has an effect

on cellular metabolism in melanoma cells, where it up-regulates expression of oxidative phosphorylation genes (Haq et al., 2013b). In particular, the peroxisome proliferator-activated receptor γ coactivator 1α (PGC1α), a transcriptional coactivator which drives mitochondrial biogenesis and energy metabolism, was shown to be up-regulated transcriptionally by MITF in primary human melanocytes and melanoma cells, but not in non-melanoma cancers (Haq et al., 2013b; Vazquez et al., 2013).

Sustained proliferative signalling is arguably the most fundamental hallmark of cancer (Hanahan and Weinberg, 2000, 2011). The role of MITF in melanoma proliferation is complex. Despite being classified as a lineage addiction oncogene, MITF was found to have anti-proliferative effects, with an ability to induce cell cycle arrest via up-regulation of the *CDKN1A* and *CDKN2A* genes encoding the $p21^{Cip1}$ and $p16^{INK4a}$ cyclin-dependent kinase inhibitors respectively (Carreira et al., 2005; Loercher et al., 2005). MITF could also exert an anti-proliferative role in melanocytes and melanoma cell lines by negating $BRAF^{V600E}$-stimulated proliferation (Wellbrock and Marais, 2005). Furthermore, expression of MITF in MITF-negative melanocytes and melanoma cell lines was shown to inhibit tumour growth in mouse xenograft models (Selzer et al., 2002).

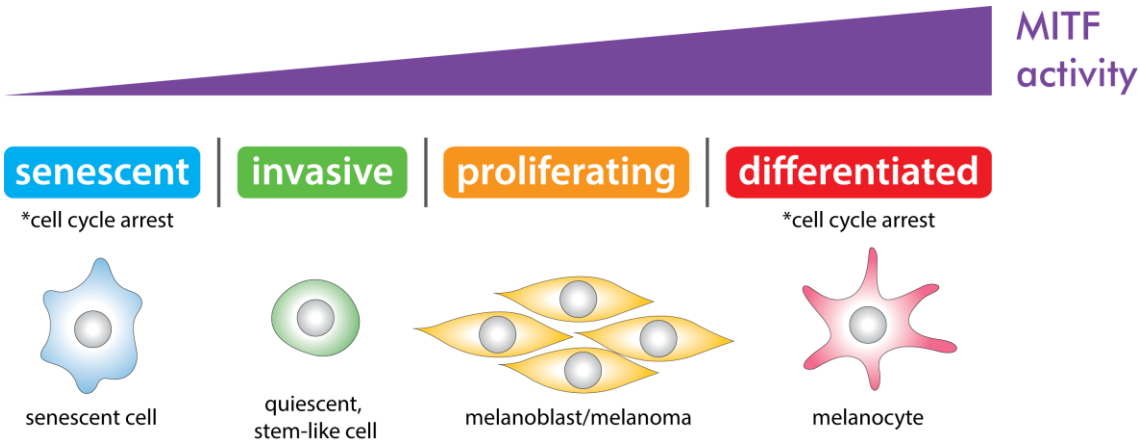

Figure 1.6 The MITF rheostat model. MITF plays a key role in determining sub-population identity of melanoma cells. Low MITF levels result in invasive and stem-like cells that are arrested in G1 via $p27^{Kip1}$. However, high MITF levels lead to differentiation and G1 arrest via $p16^{INK4a}$ and $p21^{Cip1}$. Maximum proliferation occurs at an intermediate level of MITF. Adapted from Carreira et al., 2006; Goding, 2011; Hoek and Goding, 2010.

However, MITF is also capable of exerting pro-proliferative effects in melanoma, as is evident in the fact that small interfering RNA (siRNA)-mediated depletion of MITF in melanoma cells results in $p27^{Kip1}$-mediated G1 cell cycle arrest (Carreira et al., 2006), and ultimately leads to senescence (Giuliano et al., 2010; Strub et al., 2011). MITF knockdown is also accompanied by DNA damage (Giuliano et al., 2010; Strub et al., 2011), mitotic aberrations (Strub et al., 2011), as well as increased invasiveness (Carreira et al., 2006). The seemingly paradoxical anti and pro-proliferative roles of MITF can be reconciled by the rheostat model (Carreira et al., 2006; Goding, 2011; Hoek and Goding, 2010) (Figure 1.6). In this model, the level of MITF activity determines the sub-population identity and phenotype of the melanoma cells. Low levels of MITF activity are associated with stemness (Cheli et al., 2011), tumorigenic potential (Cheli et al., 2011), invasiveness and G1 arrest via $p27^{Kip1}$ (Carreira et al., 2006). As the level of MITF activity increases, cells become more proliferative and lose their stem-like characteristics. In accordance to its role in regulating differentiation-associated genes, high levels of MITF activity lead to $p16^{INK4a}$, $p21^{Cip1}$-dependent G1 cell cycle arrest, a prerequisite for differentiation

(Carreira et al., 2005; Loercher et al., 2005). In support of the rheostat model, melanoma cells were found to switch between invasive and proliferative states *in vivo*, with MITF expression levels being a key determinant of the phenotypic state (Hoek et al., 2008). In addition, both depletion and overexpression of MITF resulted in significant inhibition of proliferation in three different melanoma cell lines (Kido et al., 2009), highlighting the existence of a threshold range of MITF levels within which maximum cell proliferation occurs.

1.4 Melanoma therapy

1.4.1 Therapeutic options

For patients with localised melanoma, surgical removal of tumours is the gold standard for treatment (Schadendorf et al., 2015). However, surgery is rarely curative for metastatic malignant melanoma (Schadendorf et al., 2015). For the past 40 years until 2011, the standard treatment option for patients whose melanoma had metastasised was dacarbazine, a chemotherapy drug with a paltry response rate of 10% (Eggermont and Robert, 2012).

The identification of BRAF as the dominant oncogene in melanoma (Karasarides et al., 2004) was a significant milestone which spurred intensive drug development efforts to devise ATP-competitive RAF inhibitors, particularly ones that could selectively target the most common mutation, $BRAF^{V600E}$. Sorafenib was the first RAF inhibitor to be investigated across extensive clinical trials in melanoma. Despite being a potent multi-kinase inhibitor with activity against CRAF, wild-type BRAF, $BRAF^{V600E}$ as well as several RTKs (Wilhelm et al., 2004), sorafenib unfortunately did not display any efficacy either as a single agent or in combination

with the chemotherapeutic agents carboplatin and paclitaxel (Eisen et al., 2006; Flaherty et al., 2013; Hauschild et al., 2009).

In contrast, the BRAF inhibitor vemurafenib, which specifically targets the $BRAF^{V600E}$ mutant protein, fared much better in clinical trials. Vemurafenib treatment elicited a response rate of 57% in patients with metastatic melanoma bearing $BRAF^{V600E}$ or $BRAF^{V600K}$ mutations, compared to 9% for dacarbazine (Chapman et al., 2011; McArthur et al., 2014). Median progression-free survival was 6.9 months for the vemurafenib treatment group, which is significantly longer than the 1.6 months observed with the dacarbazine group (McArthur et al., 2014). Median overall survival was 13.6 months with vemurafenib treatment, versus 9.7 months in the case of dacarbazine. Dabrafenib, another $BRAF^{V600E}$-specific inhibitor, elicited similar improvements in response rates and progression-free survival compared to dacarbazine in patients with $BRAF^{V600}$ mutations (Hauschild et al., 2012).

In addition to targeted therapies against members of the MAPK pathway, immunotherapy has emerged as another promising avenue for the treatment of advanced melanoma. So far, immunotherapy for melanoma treatment mainly involves circumventing immunoinhibitory pathways in order to promote an antitumour response. This can be achieved via immune checkpoint blockade, using monoclonal antibodies that block immune checkpoint receptors and thus activate tumour-specific T cells (Mahoney et al., 2015). Ipilimumab, a monoclonal antibody that targets the cytotoxic T-lymphocyte-associated antigen 4 (CTLA-4), was first approved for use in the treatment of advanced melanoma in 2011 following promising phase 3 clinical trials, where patients treated with ipilimumab and dacarbazine demonstrated significantly better response rates and overall survival compared to patients treated with dacarbazine alone (Robert et al., 2011). More

recently, pembrolizumab and nivolumab were also approved for use in the treatment of advanced melanoma which were unresponsive to ipilimumab and BRAF inhibition. Both pembrolizumab and nivolumab are monoclonal antibodies which target another immune checkpoint receptor known as programmed cell death protein 1 (PD-1). Combinatorial immunotherapies have also shown very promising results in patients with advanced melanoma, with the combination of ipilimumab and nivolumab proving to be significantly more effective than either agent alone (Larkin et al., 2015; Postow et al., 2015).

1.4.2 Resistance to therapy

Despite bearing $BRAF^{V600}$ mutations, approximately half of the patients who are treated with BRAF inhibitors do not respond to therapy (Hauschild et al., 2012; McArthur et al., 2014; Sosman et al., 2012). Not much is known about why some BRAF-mutated melanomas are intrinsically more resistant to BRAF inhibition than others, although adaptive resistance might play a role in this. Adaptive resistance refers to the attenuation of therapeutic response within a short period, on the order of hours, following initiation of drug treatment (Lito et al., 2013). Treatment with selective inhibitors of a specific pathway relieves negative feedback inhibition, resulting in the reactivation of other mitogenic signalling pathways, which ultimately diminishes therapeutic effectiveness. For example, it has been demonstrated that BRAF inhibition leads to RAS activation by relieving ERK-dependent negative feedback of RAS (Lito et al., 2012). In another example, vemurafenib therapy is far less effective in colorectal cancer than in melanoma (Kopetz et al., 2010). This can be explained by the loss of feedback from ERK culminating in activation of

epidermal growth factor receptor (EGFR), which is highly expressed in colon cancer but not in melanoma (Prahallad et al., 2012).

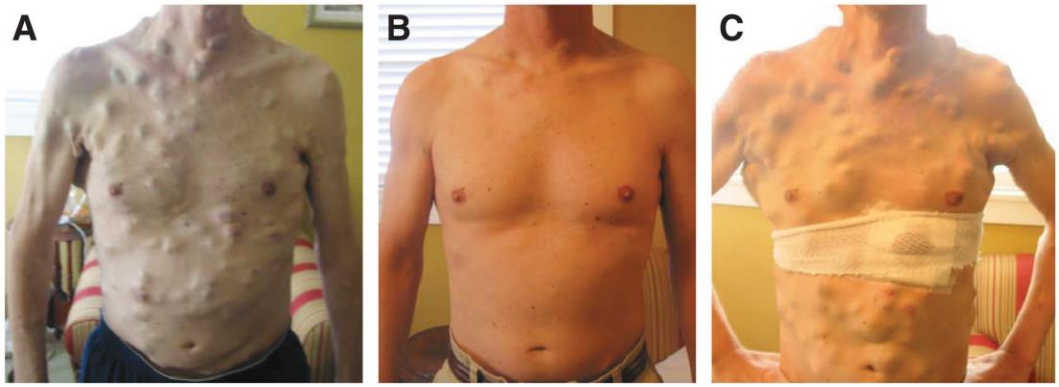

Figure 1.7 An example of a patient who developed resistance to BRAF inhibitor therapy and relapsed after an initial period of tumour regression. A 38-year-old man with metastatic, $BRAF^{V600E}$ melanoma was treated with vemurafenib. Photographs were taken **(a)** before initiation of vemurafenib therapy, **(b)** after 15 weeks of vemurafenib therapy and **(c)** after 23 weeks of vemurafenib therapy. From Wagle et al., 2011.

For the other half of BRAF-mutated melanoma patients in which therapeutic benefit is observed, most of them eventually suffer a relapse of the disease due to acquired resistance to BRAF inhibitor therapy (Hauschild et al., 2012; McArthur et al., 2014; Sosman et al., 2012) (Figure 1.7). Acquired resistance to BRAF inhibitors is mediated via several different mechanisms, but most of them appear to converge on a common, central theme – reactivation of the RAS/RAF/MEK/ERK pathway. For example, *BRAF* copy number amplification has been identified as a resistance mechanism in some patients (Shi et al., 2012, 2014). Aberrantly spliced variants of $BRAF^{V600E}$ have also been detected in some patients with acquired resistance to BRAF inhibition (Poulikakos et al., 2011; Shi et al., 2014). These splice isoforms, which lack the RAS-binding domain, demonstrate enhanced RAS-independent dimerisation (Poulikakos et al., 2011). Dimerisation confers increased kinase activity and resistance to BRAF inhibition due to negative cooperativity, whereby the binding of an inhibitor to one protomer of the dimer significantly inhibits the affinity

of the drug for the other protomer (Yao et al., 2015). Increased expression of CRAF has also been demonstrated as a resistance mechanism in cell culture models, although this has yet to be detected in actual patient samples (Johannessen et al., 2010; Montagut et al., 2008; Su et al., 2012a).

Such reactivation is not limited to the RAF level, but instead can occur at multiple points along the RAS/RAF/MEK/ERK pathway. Upstream of RAF, up-regulation of RTKs and activating secondary mutations of NRAS and KRAS have been detected in patient-derived, BRAF therapy-resistant tumours (Nazarian et al., 2010; Shi et al., 2014). Similarly, a loss of expression of neurofibromin **(**NF1), a negative regulator of RAS, has also been linked to BRAF inhibitor resistance in patients (Maertens et al., 2013; Whittaker et al., 2013). Interestingly, BRAF inhibitors are also known to induce the formation of cutaneous squamous cell carcinomas and keratoacanthomas (Oberholzer et al., 2012; Su et al., 2012b). These secondary lesions are believed to arise as a result of paradoxical CRAF-mediated activation of the ERK pathway in cells with wild-type BRAF (Hatzivassiliou et al., 2010; Heidorn et al., 2010; Holderfield et al., 2013; Poulikakos et al., 2010) .

Downstream of RAF, the acquisition of activating secondary mutations in MEK can lead to BRAF inhibitor resistance as well, as shown in both cell culture models and patient tumour samples (Van Allen et al., 2014; Emery et al., 2009; Shi et al., 2014). Another resistance mechanism is RAF-independent activation of MEK via up-regulation of COT, a MAP3K (Johannessen et al., 2010).

A significant proportion of resistance to BRAF inhibition is also mediated through pro-survival signalling pathways that do not involve MAPK (Van Allen et al., 2014; Shi et al., 2014). The PTEN/PI3K/AKT axis is one such pathway. PTEN deletions and inactivating mutations, as well as activating mutations in PI3K and

AKT, all contribute to enhanced AKT phosphorylation and thus increased cell survival upon BRAF inhibition (Van Allen et al., 2014; Shi et al., 2014; Villanueva et al., 2010). MITF has also been identified as a mediator of resistance to BRAF inhibitors (Johannessen et al., 2013). Patient-derived tumour samples were found to contain *MITF* amplifications, which can promote resistance by up-regulating the anti-apoptotic protein BCL2A1 (Van Allen et al., 2014; Haq et al., 2013a; Smith et al., 2013). Interestingly, MITF-low cells also demonstrated resistance to BRAF inhibitor therapy, although part of the resistance appeared to be mediated by concurrent elevated expression of the receptor tyrosine kinase AXL (Konieczkowski et al., 2014; Müller et al., 2014).

1.5 Summary and Aims

In terms of therapy, melanoma has indeed come a long way from its former reputation of being the "graveyard of pharmaceutical development" (Schadendorf et al., 2015) to being the new "poster child for personalised medicine" (Smalley and Sondak, 2010). However, despite major advances in our understanding of melanoma biology, a cure for melanoma is still elusive. Even with the development of drugs targeted against specific mutations, disease relapse is a frustratingly common problem. A large proportion of the research has, with good reasons thus far, been concentrated on the most common $BRAF^{V600E}$ mutation since it accounts for almost half of all melanoma cases. This has born fruit in the form of clinically effective small molecule inhibitors that confer therapeutic benefits on patients with BRAF-mutated melanomas. In fact, BRAF-mutated melanoma patients, after treatment with BRAF inhibitors, can now survive longer than melanoma patients with wild-type BRAF (Long et al., 2011). More recent clinical trials have utilised combinatorial

therapies with both BRAF and MEK inhibitors in a bid to overcome BRAF inhibitor resistance. Indeed, combined BRAF and MEK inhibition demonstrated increased efficacy compared to treatment with BRAF inhibitors alone (Flaherty et al., 2012; Larkin et al., 2014; Long et al., 2014; Robert et al., 2015). However, viable therapeutic options also need to be developed for the other 50% of patients who do not possess $BRAF^{V600}$ mutations. To do so, we would need to further our understanding of BRAF regulation by investigating novel pathways that regulate BRAF function.

The innate heterogeneity (Gillies et al., 2012; Marusyk et al., 2012; Meacham and Morrison, 2013; Yates and Campbell, 2012) of cancer tumours also presents a substantial challenge to effective therapy. Phenotypic heterogeneity confers innate resistance to conventional chemotherapy, since quiescent cancer cells can survive treatments that target dividing cells (Dean et al., 2005). The diverse genetic background of cancer cells means that since there will almost always be some cells that are resistant to molecular therapies target specific pathways (Turner and Reis-Filho, 2012). Consequently, a reduction of heterogeneity will be beneficial in conjunction with any targeted therapy. In this regard, MITF presents an attractive target since it plays a key role in defining sub-population identity of melanoma cells (Hoek and Goding, 2010). Furthermore, both elevated and decreased levels of MITF have been shown to mediate resistance to BRAF inhibition (Müller et al., 2014), demonstrating the complex role played by the MITF rheostat in melanoma. By broadening our knowledge of MITF regulation, we could potentially find effective ways of manipulating MITF activity in order to drive melanoma cells towards therapeutically sensitive phenotypes.

Chapter 2 – Materials and Methods

2.1 Bacterial methods

2.1.1 Growth media and conditions

Liquid bacterial cultures were grown at a temperature of 37°C in a shaking incubator set at 225 rpm. The growth media was the Lennox formulation (1% w/v tryptone, 0.5% w/v yeast extract, 0.5% w/v NaCl) of Luria-Bertani (LB) broth (Invitrogen, Waltham, MA, USA), which was autoclaved before use. LB agar plates were made by autoclaving LB agar powder (1% w/v tryptone, 0.5% w/v yeast extract, 0.5% w/v NaCl, 1.2% w/v agar) from Invitrogen with the appropriate volume of deionised water, after which it was poured into individual petri dishes (Sterilin, Newport, UK) and then allowed to cool to room temperature before storing at 4°C. To isolate individual bacterial colonies, bacteria were streaked on pre-warmed LB agar plates, before being incubated upside down at 37°C to allow colony formation overnight. Where necessary, LB was supplemented with the appropriate antibiotics, at a concentration of 100 μg/ml for ampicillin (Fisher Scientific, Waltham, MA, USA) or 50 μg/ml for kanamycin (Fisher Scientific).

2.1.2 Bacterial strains

Chemically competent subcloning efficiency DH5α (Invitrogen), which had a transformation efficiency of 1 x 10^6 colony forming units (cfu) per μg DNA, was used for general cloning. The genotype of the DH5α strain of *E. Coli* is F^- Φ80*lac*ZΔM15 Δ(*lac*ZYA-*arg*F)U169 *rec*A1 *end*A1 *hsd*R17(r_k^-,m_k^+) *pho*A *sup*E44 *thi*-1 *gyr*A96 *rel*A1 λ^-. One Shot TOP10 chemically competent *E. coli* (Invitrogen), which had a transformation efficiency of 1 x 10^9 cfu/μg DNA, was employed when higher transformation efficiencies were required. The genotype of the TOP10 strain

of *E. coli* is F^- *mcrA* Δ(*mrr-hsd*RMS-*mcr*BC) Φ80*lacZ*ΔM15 Δ*lac*X74 *rec*A1 *ara*D139 Δ(*araleu*)7697 *gal*U *gal*K *rps*L (Str^R) *end*A1 *nup*G λ-.

For site-directed mutagenesis, XL10-Gold ultracompetent cells (Agilent, Santa Clara, CA, USA), which possessed a transformation efficiency of 5 x 10^9 cfu/µg DNA, were used. The genotype of the XL10-Gold strain of *E. coli* is Tet^r Δ(*mcrA*)183 Δ(*mcrCB-hsdSMR-mrr*)173 *end*A1 *sup*E44 *thi-1 rec*A1 *gyr*A96 *rel*A1 *lac* Hte [F' *pro*AB *lacI*^{q}*Z* Δ*M15* Tn*10* (Tet^r) Amy Cam^r].

BL21(DE3) (Invitrogen) was used for the production of recombinant protein. The genotype of the BL21(DE3) strain of *E. coli* is F^- *ompT hsdS*$_B$ ($r_B^-m_B^-$) *gal dcm* (DE3).

2.1.3 Transformation of competent bacteria

For transformation of chemically competent bacteria, cells were thawed on ice and aliquoted into pre-chilled 14 ml polypropylene round-bottom tubes (BD Biosciences, San Jose, CA, USA). Plasmid DNA was added to the bacteria to a maximum of 10% v/v, followed by a 30-minute incubation on ice. To stimulate uptake of DNA, the cells were subjected to heat shock at 42°C for 30 seconds, after which they were placed on ice for 2 minutes. This was followed by the addition of 250 µl of S.O.C medium (2% tryptone, 0.5% yeast extract, 10 mM NaCl, 2.5 mM KCl, 10 mM $MgCl_2$, 10 mM $MgSO_4$, and 20 mM glucose) that was sourced from Invitrogen. The cells were then allowed to recover in a shaking incubator at 37°C and 225 rpm, before being spread on pre-warmed LB agar plates containing the appropriate antibiotics.

2.1.4 Expression of recombinant protein

Following transformation with the plasmid with the gene encoding the protein of interest, BL21(DE3) cells were allowed to grow overnight on LB agar plates containing the appropriate antibiotics. A single colony was picked and grown overnight in 5 ml of LB medium, containing the same antibiotics, in a shaking incubator set at 37°C and 225 rpm. The next day, the overnight culture was diluted 1:100 into 500 ml of fresh LB medium, again containing the same antibiotics. The cells were then grown at 37°C and 225 rpm until mid-log phase (OD_{600} = 0.6-1.0), after which isopropyl-β-D-thiogalactoside (IPTG) (Sigma-Aldrich, St. Louis, MO, USA) was added to a final concentration of 250 μM to induce protein expression. The cells were allowed to grow for an additional 3 hours at 37°C and 225 rpm, after which they were harvested via centrifugation at 6000x g for 15 minutes at 4°C. The bacterial pellet was then subjected to lysis and purification procedures or stored at 80°C.

2.2 Mammalian cell methods

2.2.1 Cell culture

Human melanoma cell lines, including 501mel and SK-MEL-28, were grown in Roswell Park Memorial Institute (RPMI) 1640 media (Invitrogen), supplemented with 10% foetal bovine serum (FBS) (PAA Laboratories, Pasching, Austria) and 50 units/ml penicillin, 50 μg/ml streptomycin (Invitrogen). The HERMES immortalised human melanocyte cell line was cultured in RPMI 1640 supplemented with 10% FBS, 50 units/ml penicillin, 50 μg/ml streptomycin, 200 nM tetradecanoyl phorbol acetate (TPA) (Sigma-Aldrich), 200 pM cholera toxin (CT) (Sigma-Aldrich), 10 ng/ml human stem cell factor (hSCF) (Invitrogen) and 10 nM endothelin 1 (EDN1)

(Sigma-Aldrich). Cell lines of non-melanocytic origin, including HeLa and Phoenix-AMPHO, were grown in Dulbecco's Modified Eagle Medium (DMEM), supplemented with 10% foetal bovine serum and 50 units/ml penicillin, 50 μg/ml streptomycin.

Unless otherwise stated, cells were grown in culture vessels (Corning, Corning, New York, USA) kept in humidified incubators at 37°C with 10% CO_2. For general maintenance, cells were allowed to grow in a monolayer until 80-90% confluence, after which they were detached from the growth surface via trypsinisation. Trypsinisation was carried out by first aspirating the medium from the culture vessel, followed by washing with phosphate-buffered saline (PBS) (137 mM NaCl, 2.7 mM KCl, 10 mM Na_2HPO_4, 1.8 mM KH_2PO_4, pH 7.4), which was obtained from Fisher Scientific and autoclaved before use. Next, sufficient 0.05% trypsin-EDTA (Invitrogen) was added to cover the entire growth surface. The cells were then incubated at 37°C for two minutes to initiate detachment, after which trypsin was inactivated with one volume of complete medium. The detached cells were harvested by centrifugation at 200x g, after which the pellet was resuspended in complete medium and inoculated into a fresh culture vessel at an appropriate density (typically 1:6).

For medium-term storage, cells were resuspended in complete medium containing 10% dimethyl sulfoxide (DMSO) (Sigma-Aldrich) before being aliquoted into a cryo tube (Thermo Scientific, Waltham, MA, USA), which was then placed in a Mr Frosty freezing container (Thermo Scientific) and stored at -80°C. For long-term storage, cells were transferred from -80°C to liquid nitrogen storage. To revive frozen cells, the cryo tubes were thawed at room temperature, after which the

freezing medium was removed via centrifugation at 200x g. The cell pellet was then resuspended in complete medium before being inoculated into a fresh culture vessel.

2.2.2 Transient transfection of DNA

Transient transfection of DNA was carried out using the FuGENE 6 (Promega, Madison, WI, USA), a non-liposomal transfection reagent, according to the manufacturer's instructions. Briefly, cells were inoculated into a 6-well plate and grown to 50% confluence overnight. The following day, 1 μg of DNA was mixed with 3 μl of FuGENE 6 in 100 μl of Opti-MEM (Invitrogen), and incubated at room temperature for 15 minutes. The transfection mix was then added drop-wise to a single well of a 6-well plate. The amount of transfection mix can be scaled up or down depending on the number and size of the culture vessels. Cells were then incubated for 48 hours before being processed.

2.2.3 Stable transfection of DNA

Inducible, stable cell lines exhibiting tetracycline-inducible expression of a gene of interest were generated using the Flp-In T-REx system from Invitrogen. The host cell line was HeLa Flp-In T-REx, a gift from Skirmantas Kriaucionis (Ludwig Institute for Cancer Research, Oxford, UK). HeLa Flp-In T-REx are HeLa cells which contain a stably integrated Flp Recombination Target (FRT) site and also express the Tet repressor (TetR) under a constitutive cytomegalovirus (CMV) promoter. HeLa Flp-In T-REx cells were maintained as per wild-type HeLa cells, but with a further supplement of 4 μg/ml blasticidin to maintain TetR expression and 50 μg/ml zeocin to ensure that the FRT sites were retained.

HeLa Flp-In T-REx cells were seeded on a 6 cm dish (Corning) and grown to 50% confluence overnight. They were then co-transfected with two plasmids as per the transient transfection protocol. The first plasmid was the pcDNA5/FRT/TO plasmid expressing the gene of interest under the control of a tetracycline-regulated CMV/TetO_2 promoter, while the second was the pOG44 plasmid that expresses the Flp recombinase under a constitutive CMV promoter. The two plasmids were co-transfected at a ratio of 3 pcDNA5/FRT/TO : 1 pOG44.

The cells were allowed to take up the DNA over 48 hours, after which they were trypsinised. 50% of the cells were frozen down for storage, while the other 50% were seeded onto a 15 cm dish (Corning). The Flp recombinase mediates recombination at the FRT sites, resulting in specific integration of the pcDNA5/FRT/TO plasmid into the pre-existing FRT site in the host cell line. Recombination results in the replacement of the zeocin resistance gene in the host cell line with the hygromycin resistance gene in the pcDNA5/FRT/TO plasmid, hence the transfected cells were selected with 200 μg/ml hygromycin and 4 μg/ml blasticidin. Stable polyclonals were observed after two weeks of antibiotic selection, upon which they were assayed for expression of the gene of interest and frozen down for storage.

2.2.4 Transient transfection of siRNA

Transient transfection of small interfering RNA (siRNA) was carried out using the Lipofectamine 2000 (Invitrogen), a lipid-based reagent, according to the manufacturer's protocol. Briefly, cells were grown without antibiotics to 50% confluence in a 6-well plate overnight. The following day, 10 μl of Lipofectamine 2000 was mixed with 190 μl of Opti-MEM, and incubated for 5 minutes at room

temperature. In a separate tube, 166 pmol of siRNA was diluted in Opti-MEM to give a total volume of 200 µl. The diluted Lipofectamine 2000 was then mixed with the diluted siRNA to encourage the formation of a transfection complex. After a 20-minute incubation at room temperature, the transfection complex was then added drop-wise to a single well of a 6-well plate. The amount of transfection mix can be scaled up or down depending on the number and size of the culture vessels. Cells were then incubated for 48 hours before being processed.

siRNA against p300 was obtained from Santa Cruz Biotechnology (Santa Cruz, CA, USA). AllStars Negative Control siRNA (Qiagen) was used as the negative control.

2.3 Nucleic acid methods

2.3.1 Plasmid purification

For small-scale plasmid production, individual bacteria colonies, obtained following transformation with the plasmid of interest, were inoculated into 3 ml of LB containing the appropriate antibiotics in a 14 ml polypropylene round-bottom tube. The bacteria were allowed to grow overnight at 37°C and 225 rpm. The following day, the bacteria were centrifuged at 6800x g, and the pellet processed with a QIAprep Spin Miniprep Kit (QIAGEN, Hilden, Germany) according to the manufacturer's instructions. Purified plasmid DNA was subsequently eluted in buffer EB (10 mM Tris-Cl, pH 8.5) and its concentration was measured with a NanoDrop 2000 spectrophotometer (Thermo Scientific).

For large-scale plasmid production, individual bacteria colonies were inoculated into 3 ml of LB containing the appropriate antibiotics in a 14 ml polypropylene round-bottom tube and grown for 8 hours at 37°C and 225 rpm. This

starter culture was then inoculated 1:500 into 100 ml of LB containing the appropriate antibiotics in the case of high-copy plasmids. For low-copy plasmids, the culture volume was scaled up to 500 ml. The bacteria were then allowed to grow overnight at 37°C and 225 rpm, after which they were pelleted at 6000x g. The pellet was processed with a Plasmid Maxi Kit (QIAGEN) according to the instructions provided by the manufacturer. Purified plasmid DNA was subsequently resuspended in buffer EB, after which its concentration was ascertained with a NanoDrop 2000 spectrophotometer.

2.3.2 Agarose gel electrophoresis

Agarose gels were used to resolve DNA fragments by size. With the help of a microwave, agarose gels were prepared by heating and dissolving agarose (Web Scientific, Crewe, UK) in TBE buffer (100 mM Tris, 90 mM boric acid, 1 mM EDTA) sourced from Invitrogen. peqGREEN (PEQLAB, Erlangen, Germany) intercalating dye was added to the agarose gel at a concentration of 1:20000. DNA samples were mixed with 0.2 volumes of 6x purple gel loading dye (New England Biolabs, Ipswich, MA, USA) before being loaded into the wells of the agarose gel. HyperLadder 1kb and HyperLadder 50bp (Bioline, London, UK) were used as molecular weight markers. Electrophoresis was carried out at 120 V in TBE buffer. The DNA was visualised under ultraviolet (UV) light in an UVIdoc (UVItec, Cambridge, UK). Where necessary, DNA fragments were excised with a scalpel and purified using the QIAquick Gel Extraction Kit (QIAGEN) in line with the manufacturer's instructions.

2.3.3 Polymerase chain reaction

Polymerase chain reaction (PCR) was employed to amplify DNA. MyTaq Red Mix (Bioline), a ready-to-use mix of *Taq* polymerase, was used for situations where detection was the main purpose and DNA fidelity was not important, such as colony PCR. For each reaction, 2 ng of template DNA was mixed with 4 pmol of each primer, 5 µl of 2x MyTaq Red Mix and deionised water to give a final volume of 10 µl. Reactions were carried out in a T100 Thermal Cycler (Bio-Rad, Hercules, CA, USA) with an initial denaturation step at 95°C for 3 minutes, followed by 35 cycles of denaturation (95°C, 15 s), annealing (primer melting temperature - 5°C, 15 s) and extension (72°C, 10 s). This was then finished with a final extension step at 72°C for 5 minutes, after which the PCR products were visualised on an agarose gel.

In cases where DNA fidelity was important, such as cloning, Phusion High-Fidelity DNA polymerase (Thermo Scientific) was employed. For each reaction, 10 ng template DNA was mixed with 25 pmol of each oligonucleotide primer, 10 µl 5x Phusion HF buffer, 10 nmol dATP, 10 nmol dTTP, 10 nmol dCTP, 10 nmol dGTP, 1 unit Phusion DNA polymerase and deionised water to give a final volume of 50 µl. Reactions were carried out in a T100 Thermal Cycler with an initial denaturation step at 98°C for 30 s, followed by 35 cycles of denaturation (98°C, 10 s), annealing (primer melting temperature, 15 s) and extension (72°C, 30 s/kb of product). This was then finished with a final extension step at 72°C for 5 minutes, after which the PCR products were visualised on an agarose gel and purified with the QIAquick Gel Extraction Kit.

Oligonucleotides were synthesised by Integrated DNA Technologies (Leuven, Belgium). The melting temperature of the oligonucleotide primers were determined with the Tm calculator at https://www.thermofisher.com/uk/en/home/brands/thermo-scientific/molecular-biology/molecular-biology-learning-center/molecular-biology-resource-library/thermo-scientific-web-tools/tm-calculator.html.

2.3.4 Restriction enzyme digestion

Restriction digests were carried out using the appropriate restriction enzyme (New England Biolabs). Briefly, 1 µg of DNA was mixed with 10 units of enzyme, 5 µl of the appropriate 10x reaction buffer and deionised water to give a total volume of 50 µl. The digest reaction was incubated at 37°C for 2 hours. The restriction enzyme was then heat inactivated if possible. If the restriction enzyme could not be heat inactivated, it was subsequently removed by the QIAquick PCR Purification Kit (QIAGEN) according to the manufacturer's recommendations.

2.3.5 Dephosphorylation of DNA

To prevent re-ligation of the vector DNA following restriction digest, the vector DNA can be dephosphorylated with calf intestinal alkaline phosphatase (CIP) (New England Biolabs). 2 units of CIP were added directly to the restriction enzyme mix and incubated at 37°C for 1 hour. The reaction mix was then purified with the QIAquick PCR Purification Kit (QIAGEN) according to the manufacturer's recommendations.

2.3.6 Ligation

Following digestion and purification, the insert DNA is mixed with 75 ng of vector DNA, at a molar ratio of 10 insert : 1 vector. 2 µl of 10x T4 DNA Ligase Buffer, 400 units of T4 DNA ligase (New England Biolabs) and deionised water are also added to give a final volume of 20 µl. The ligation reaction was incubated at room temperature for 10 minutes, after which it was transformed into chemically competent bacteria. Successful integration of the insert was verified via colony PCR and Sanger sequencing.

2.3.7 Site-directed mutagenesis

The QuikChange Lightning Site-Directed Mutagenesis (SDM) Kit (Agilent) was employed to introduce point mutations at specific loci in genes of interest. Mutagenic primers were designed with the help of the QuikChange Primer Design Program available at http://www.genomics.agilent.com/primerDesignProgram.jsp. For each reaction, 10 ng template plasmid DNA was mixed with 125 ng of each primer, 1 µl 10x reaction buffer, 0.2 µl dNTP mix, 0.3 µl QuikSolution reagent, 1 µl Quikchange Lightning Enzyme and deionised water to give a final reaction volume of 10 µl. The reactions were cycled in a T100 Thermal Cycler with an initial denaturation step at 95°C for 2 minutes, followed by 25 cycles of denaturation (95°C, 20 s), annealing (60°C, 10 s) and extension (68°C, 30 s/kb of product). This was then finished with a final extension step at 68°C for 5 minutes. The dam-methylated parental template was then digested by adding 0.4 µl DpnI to the reaction mix and incubating at 37°C for 1 hour. Finally, the reaction mix was transformed into XL10-Gold ultracompetent cells, and the resultant colonies were screened for mutations with Sanger sequencing. With the exception of the template DNA and primers, all

other reagents were proprietary formulations that were included in the QuikChange Lightning Site-Directed Mutagenesis Kit.

2.3.8 qPCR

The RNeasy Mini Kit (QIAGEN) was used to extract and purify RNA from cells in accordance with the manufacturer's instructions. Upon elution with RNase-free water, the RNA concentration was determined with a Nanodrop 2000 spectrophotometer. To generate cDNA, 1 μg of RNA was processed using the QuantiTect Reverse Transcription Kit (QIAGEN) according to the manufacturer's recommendations. Briefly, contaminating genomic DNA is removed from the template RNA, after which Quantiscript Reverse Transcriptase generates cDNA via reverse transcription. Quantiscript Reverse Transcriptase also possesses Rnase H activity, which results in degradation of template RNA after reverse transcription.

Next, qPCR was used to quantify relative gene expression levels. qPCR primers were designed to amplify a 100-150 bp-long target region and to span exon-exon junctions where possible. Reactions were performed in triplicates, with each replicate containing 30 ng of cDNA mixed with 4.5 pmol of each primer, 7.5 μl of 2x SensiMix SYBR (Bioline) and deionised water to give a total volume of 15 μl. Thermocycling and analysis was carried out in a Rotor-Gene 6000 (Corbett Life Science, Sydney, Australia) real-time analyser. The reactions were cycled with an initial step at 95°C for 10 minutes, followed by 55 cycles of 96°C for 5 s, 61°C for 10 s and 72°C for 5 s. Lastly, the temperature was raised from 72°C to 96°C at a rate of 1°C every 5 seconds to generate melt-curves.

Expression of the gene of interest was normalised relative to a housekeeping gene according to the $2^{-\Delta\Delta CT}$ method (Livak and Schmittgen, 2001), which states that:

Relative fold change of target gene in treated vs untreated sample = $2^{-\Delta\Delta CT}$

where $\Delta\Delta C_T = \Delta C_T$[treated sample] – ΔC_T[untreated sample] and

$\Delta C_T = C_T$[target gene] - C_T[housekeeping gene]

2.4 Protein methods

2.4.1 Cell Extracts

2.4.1.1 Whole cell extracts

Cell lysis was typically carried out by adding 1x Laemmli sample buffer (62.5 mM Tris-Cl pH 6.8, 2% SDS, 0.1 M DTT, 0.01% bromophenol blue, 10% glycerol) directly to the culture vessel. The cells were scraped with a cell scraper (TPP, Trasadingen, Switzerland), after which the lysate was collected and sonicated for 3 seconds with a probe sonicator (Sonics, Newton, CT, USA). Extracts were boiled at 95°C for 5 minutes before being cooled to room temperature and stored at -20°C.

If quantification of protein concentration was required, then cells were trypsinised and solubilised in cold radioimmunoprecipitation assay (RIPA) lysis buffer (50 mM Tris-Cl pH 8.0, 150 mM NaCl, 0.5% sodium deoxycholate, 0.1% SDS, 1% NP-40) supplemented with 1x Complete Protease Inhibitor (Roche, Basel, Switzerland) and 1x PhosSTOP Phosphatase Inhibitor (Roche). After a 20-minute incubation on ice, the cell lysate was spun at 16000x g and 4°C in a bench-top centrifuge for 15 minutes. The supernatant was saved as the lysate while the pellet was discarded. Bicinchoninic acid (BCA) protein assay (Thermo Scientific) was used to quantify the protein concentration according to manufacturer's instructions, after

which a suitable amount of RIPA buffer was added to each sample to equilibrate protein concentrations. Samples were subsequently stored at -20°C.

2.4.1.2 Sub-cellular fractionation

To separate out the cytosolic components of the cell from the nuclear fraction, trypsinised cells were lysed in cold Triton X lysis buffer (50 mM Tris-Cl pH 7.5, 137.5 mM NaCl, 0.5% Triton X-100, 10% glycerol) supplemented with 1x Complete Protease Inhibitor and 1x PhosSTOP Phosphatase Inhibitor. The cell lysate was incubated on ice for 20 minutes, then centrifuged at 16000x g and 4°C in a bench-top centrifuge for 15 minutes. The supernatant was the cytoplasmic fraction while the pellet was resuspended in 1x Laemmli sample buffer and taken to be the nuclear fraction. Both fractions were stored at -20°C.

2.4.2 Protein purification

2.4.2.1 Immunoprecipitation

For typical immunoprecipitations, adherent cells were detached via trypsinisation before being lysed in 1 ml of cold IP lysis buffer (50 mM Tris-Cl pH 8.0, 150 mM NaCl, 1 mM EDTA, 1% Triton X-100) supplemented with 1x Complete Protease Inhibitor and 1x PhosSTOP Phosphatase Inhibitor. When studying acetylated proteins, IP lysis buffer was supplemented with an additional amount of histone deacetylase inhibitors (10 mM sodium butyrate and 10 mM nicotinamide). Following a 20-minute incubation on ice, the cell lysate was spun at 16000x g and 4°C in a bench-top centrifuge for 15 minutes. After discarding the cell pellet, 5% of the supernatant was saved as input, while the remainder was incubated with 1 μg of antibody overnight on a rotating platform at 4°C. The next day, 20 μl of

Dynabeads Protein G (Invitrogen) was added to the samples, assuming that a mouse antibody had been used. If the antibody had been raised in a rabbit, then 20 µl of Dynabeads Protein A (Invitrogen) was added instead. After a further 2-hour incubation on a rotating platform at 4°C, the beads were washed 3 times with cold IP lysis buffer for 10 minutes each time, then stored at -20°C.

In the case of immunoprecipitations involving a FLAG tag, we used anti-FLAG antibody that had already been directly conjugated to agarose beads. The cell lysate was incubated with 20 µl of ANTI-FLAG M2 Affinity Gel (Sigma-Aldrich) overnight on a rotating platform at 4°C. The following day, the beads were washed 3 times with cold IP lysis buffer for 10 minutes each time, after which they were stored at -20°C. Where necessary, the bound proteins were eluted off the beads by incubating with 150 ng/ml of 3x FLAG peptide (Sigma-Aldrich) in 100 ml of Tris-buffered saline (TBS) (50 mM Tris, 150 mM NaCl, pH 7.6) for 30 minutes at 4°C with gentle shaking. After a 30-second centrifugation at 5000x g, the supernatant was saved and stored at 4°C. For long-term storage, the samples were kept at -20°C after the addition of glycerol (Fisher Scientific) to a final concentration of 50% v/v.

2.4.2.2 GST-tagged protein purification

Bacterial cell pellets were resuspended in 10 ml of cold PBS lysis buffer (1% Triton-X in PBS) that had been supplemented with 1x Complete Protease Inhibitor. The cells were lysed on ice with the help of mild sonication. Sonication was carried out using a probe sonicator, with a 10-second burst of power alternating with a 10-second recovery on ice, for a total of 6 cycles. The lysate was then centrifuged at 15000x g, 4°C for 15 minutes. The supernatant was kept while the pellet was discarded. Next, 1 ml of a 50:50 slurry of Glutathione Sepharose 4B (GE Healthcare

Life Sciences, Uppsala, Sweden) in PBS lysis buffer was added to the supernatant. After 1 hour-long incubation on a rotating platform at 4°C, the beads were washed 3 times with cold PBS lysis buffer for 10 minutes each time, then stored at 4°C.

2.4.3 SDS-PAGE

Proteins were resolved according to their molecular weight by sodium dodecyl sulphate polyacrylamide gel electrophoresis (SDS-PAGE). The system comprises of 2 acrylamide gels with different concentrations of acrylamide. The resolving gel, which resolves proteins according to their molecular weight, is cast first. An appropriate amount of 30% acrylamide solution (37.5 acrylamide : 1 bis-acrylamide) (Severn Biotech, Kidderminster, UK) and deionised water is added to 4x resolving buffer (1.5 M Tris, 0.4% SDS, pH 8.8) to obtain a final solution of 12% acrylamide, 375 mM Tris, 0.1% SDS, pH 8.8. The acrylamide concentration of the resolving gel can be adjusted depending on the size of the protein of interest. Next, ammonium persulphate (APS) and tetramethylethylenediamine (TEMED) were added to a final concentration of 0.1% to catalyse acrylamide polymerisation. After pipetting the solution into the gel casting apparatus, the resolving gel was then overlaid with a 50:50 mixture of butanol and deionised water. For MITF immunoblots, samples were separated on a 12% acrylamide resolving gel made from 45% acrylamide solution (200 acrylamide : 1 bis-acrylamide) (Severn Biotech). The increased ratio of acrylamide to bis-acrylamide enables better resolution of MITF phospho-variants.

Following polymerisation of the resolving gel, the 50:50 mixture of butanol and deionised water was decanted away. The resolving gel was then overlaid with a stacking gel comprising of 3.75% acrylamide, 125 mM Tris, 0.1% SDS, pH 6.8.

Polymerisation was initiated by the addition of APS and TEMED to a final concentration of 0.17% and 0.083% respectively.

To denature protein samples, 0.33 volumes of 4x Laemmli sample buffer (250 mM Tris-Cl pH 6.8, 8% SDS, 0.4 M DTT, 0.04% bromophenol blue, 40% glycerol) were added to each sample, unless the proteins were already solubilised in Laemmli sample buffer. Samples were then boiled at 95°C for 5 minutes before being cooled to room temperature. Denatured samples were loaded onto the gel, upon which proteins were electrophoretically separated at 150 V in running buffer (25 mM Tris, 192 mM glycine, 0.1% SDS) for approximately 90 minutes until the dye front had just travelled off the bottom of the gel. Precision Plus Protein Unstained Protein Standards (Bio-Rad), a protein ladder, was also included in one of the lanes as an indicator of molecular weight.

2.4.4 Coomassie staining

To directly visualise proteins on acrylamide gels following SDS-PAGE, gels were placed in Coomassie staining solution (0.03% Coomassie Brilliant Blue R-250, 50% methanol, 10% glacial acetic acid) and heated in a microwave for 20 s until boiling. The gels were then incubated in the same Coomassie staining solution on a rocker for 15 minutes at room temperature. The Coomassie staining solution was subsequently exchanged for destaining solution (25% methanol, 10% glacial acetic acid) after 3 washes with deionised water. Gels were destained on a rocker for 1 hour at room temperature. Where necessary, stained gels were dried in a gel dryer at 80°C for 40 minutes.

2.4.5 Western blotting

Following SDS-PAGE, the gel was transferred onto a Protran nitrocellulose membrane (Whatman, Kent, UK) via electroblotting. The transfer took place in transfer buffer (25 mM Tris, 192 mM glycine, 20% methanol) at 70 V for 90 minutes. The integrity of the transfer reaction was ascertained by incubating the nitrocellulose membrane for 1 minute at room temperature with Ponceau solution (0.1% Ponceau S, 5% acetic acid), which stained proteins on the membrane for visualisation. The Ponceau stain was then removed by washing with deionised water. The membrane was blocked with 5% skimmed milk in 0.1% Tween in PBS (PBST) for 1 hour at room temperature, after which it was incubated with the primary antibody (typically diluted 1:2000 in 5% milk in PBST unless otherwise stated) at 4°C overnight with gentle agitation on a rocking platform. In the case of phospho-specific and pan-acetyl-lysine antibodies, the blocking and staining solutions were replaced with 5% bovine serum albumin (BSA) (Sigma-Aldrich) dissolved in 0.1% Tween in TBS (TBST). The next day, the membrane was washed 3 times with PBST for 5 minutes each time. Depending on the host species that the primary antibody was raised in, the membrane was then incubated with the corresponding horseradish peroxidase (HRP)-conjugated secondary antibody (Bio-Rad) (typically diluted 1:5000 in 5% milk in PBST unless otherwise stated) for 1 hour at room temperature, before another 3x 5-minute wash in PBST. Finally, enhanced chemiluminescence (ECL) reagent (Amersham, Uppsala, Sweden) was added and the signal was detected with X-ray film (Fujifilm, Tokyo, Japan).

2.4.6 In vitro kinase assay

For radioactive *in vitro* kinase assays, 1 µg of bacterially expressed recombinant protein (either on glutathione beads or already eluted) was mixed with 50 ng of kinase in 1x NEBuffer for Protein Kinases (50 mM Tris-HCl, 10 mM $MgCl_2$, 0.1 mM EDTA, 2 mM DTT, 0.01% Brij 35, pH 7.5) (New England Biolabs), supplemented with adenosine triphosphate (ATP) (Sigma-Aldrich) to a final concentration of 200 µM and 2.5 µCi [γ-^{32}P]-ATP (Perkin Elmer), in a total volume of 20 µl. The reaction was incubated at 30°C for 1 hour, after which the samples were denatured by boiling in Laemmli sample buffer. The denatured samples were then resolved by SDS-PAGE and the proteins visualised with Coomassie stain. After drying, the gel was incubated at -80°C overnight with X-ray film, which was developed the following day.

Reaction conditions for non-radioactive *in vitro* kinase assays were similar to that of radioactive *in vitro* kinase assays, except [γ-^{32}P]-ATP was omitted from the reaction mix. Following incubation and SDS-PAGE, the proteins were then transferred onto a nitrocellulose membrane, after which they were immunoblotted with phospho-specific antibodies against the phosphorylated form of the recombinant protein. The signals were then detected via chemiluminescence as per a typical western blot.

2.4.7 Peptide SPOT kinase assay

Short peptides, comprising of 21 amino acids with the desired post-translational modifications, were directly synthesised on cellulose membranes by Sarah Picaud (Structural Genomics Consortium, Oxford, UK) using SPOT technology (Winkler et al., 2009). The membrane was first rinsed with 95% ethanol, then washed 3 times

with TBST. Next, reaction mix was prepared by mixing 100 ng of kinase in 1x NEBuffer for Protein Kinases, supplemented with adenosine triphosphate (ATP) (Sigma-Aldrich) to a final concentration of 200 μM and 5 μCi [γ-^{32}P]-ATP (Perkin Elmer), in a final volume that is sufficient to cover the entire surface of the membrane. The membrane was incubated with the reaction mix at 30°C for 30 minutes, after which the reaction mix was discarded. The membrane was then washed 3 times with stripping buffer A (1% SDS, 8 M urea, 0.5% β-mercaptoethanol) for 5 minutes each time. This was followed by another 3x 5-minute wash with stripping buffer B (50% ethanol, 10% glacial acetic acid). A final 3x 5-minute wash with 95% ethanol was also included. After drying for 10 minutes in a fume hood, the membrane was then wrapped in cling film and exposed to a blank phosphor screen in an autoradiography cassette overnight at -80°C. The next day, the phosphor screen was scanned using a PMI phosphorimager system (Bio-Rad).

2.4.8 Mass spectrometry

The protein of interest was immunoprecipitated, using ANTI-FLAG M2 Affinity Gel, from Phoenix-AMPHO cells that had been transfected with plasmids expressing the FLAG-tagged protein of interest. The immunoprecipitated protein sample was boiled in 1x Laemmli sample buffer and resolved using SDS-PAGE. Following electrophoresis, the acrylamide gel was stained using Coomassie to visualise the protein of interest. The band corresponding to the protein of interest was excised from the gel using a scalpel, after which it was submitted to the Mass Spectrometry Laboratory (Target Discovery Institute, Oxford, UK) for mass spectrometry analysis.

2.5 Cell biology methods

2.5.1 Immunofluorescence

Cells were typically grown to 80% confluence on round, 13 mm-diameter, 0.16 mm-thick, glass coverslips (VWR, Radnor, PA, USA). Cells were fixed with 3.7% paraformaldehyde (PFA) (Sigma-Aldrich), which was dissolved in PBS and adjusted to pH 7.4, for 15 minutes. This was followed by 30 minutes of blocking and permeabilisation with 0.1% Triton-X and 1% BSA in PBS. The cells were incubated with primary antibody (typically diluted 1:500 in 1% BSA in PBST unless otherwise stated) at 4°C overnight with gentle agitation on a rocking platform. After washing 3 times with PBST for 5 minutes each time, the cells were incubated with the appropriate Alexa Fluor-conjugated secondary antibody (Invitrogen) (typically diluted 1:1000 in 1% BSA in PBST unless otherwise stated) for 1 hour, before another 3x 5-minute wash in PBST. Next, nuclear DNA in the cells was stained with 300 nM 4',6-diamidino-2-phenylindole (DAPI) (Invitrogen) in PBS for 15 minutes, before another 3x 5-minute wash in PBST. For cells grown on glass coverslips, the coverslips were mounted on microscope glass slides (VWR) with Vectashield Mounting Medium (Vector Laboratories, Burlingame, CA, USA) before being sealed with nail polish around the edges. Images were acquired using a LSM710 confocal microscope (Carl-Zeiss, Jena, Germany).

In cases where cells were expressing fluorescent proteins of interest, the cells were stained with DAPI after PFA fixation. Blocking, permeabilisation and antibody staining steps were omitted unless detection of non-fluorescent proteins were required. The coverslips were then mounted and imaged as above.

2.5.2 Small molecule library screen

For the small molecule library screen, approximately 5000 SK-MEL-28 melanoma cells were seeded into each well of 96-well black CellCarrier plates (PerkinElmer, Waltham, MA, USA) with optically clear plastic bottoms. Cells were grown to 80% confluence overnight, upon which they were treated for 6 hours with 2.5 μM of each compound from a small molecule inhibitor library (GSK GlaxoSmithKline [GSK] Published Kinase Inhibitor Set, a gift from Stefan Knapp, SGC). The cells were then fixed, blocked and permeabilised as described in the immunofluorescence protocol above. Next, the cells were incubated with mouse anti-BRN2 antibody and rabbit anti-MITF antibody (both generated in-house and diluted 1:500 in 1% BSA in PBST) at 4°C overnight with gentle agitation on a rocking platform. After washing 3 times with PBST for 5 minutes each time, the cells were incubated with Alexa Fluor 488 donkey anti-mouse antibody and Alexa Fluor 546 donkey anti-rabbit antibody (both sourced from Invitrogen and diluted 1:1000 in 1% BSA in PBST) for 1 hour. Next, they were subjected to a 3x 5-minute wash in PBST, after which the nuclear DNA in the cells was stained with 300 nM DAPI in PBS for 15 minutes, before another 3x 5-minute wash in PBST.

Images were acquired using a LSM710 confocal microscope using an automated routine on the ZEN software (Carl-Zeiss), with automated focusing based on DAPI staining. The CellProfiler (Carpenter et al., 2006; Kamentsky et al., 2011) image analysis software was used to quantify and analyse the signals in the images.

2.5.3 Flow cytometry

Flow cytometry was performed on a BD FACSCanto flow cytometer (BD Biosciences). Briefly, cells were detached via trypsinisation, then fixed in 70%

ethanol overnight at -20°C. To measure the cell cycle profile, cells were incubated with 50 μg/ml propidium iodide (PI) (Invitrogen) and 0.1 mg/ml RNAse A (Invitrogen) in PBS at 37°C for 40 minutes. Finally, cells were resuspended in PBS and fed into the BD FACSCanto flow cytometer. A minimum of 5000 events was collected per sample, with subsequent analysis being carried out using the BD FACSDiva version 6 software (BS Biosciences).

To measure MITF intensity across the cell cycle, ethanol-fixed cells were incubated for 1 hour on ice with mouse anti-MITF primary antibody (As9), washed 3x in PBST for 5 minutes each. This was followed by another hour-long incubation on ice with the secondary antibody (Alexa Fluor 488 goat anti-mouse, Invitrogen) and another 3x 5-minute wash in PBST. Cells were then incubated with 10 nm TO-PRO-3 (Invitrogen) and 0.1 mg/ml RNAse A in PBS at 37°C for 40 minutes, after which they were processed by the flow cytometer as above.

2.5.4 Cell cycle synchronisation via mitotic shake-off

Adherent cells were synchronised using the mitotic shake-off method, which isolates mitotic cells via mechanical agitation. Cells were grown in T175 flasks (Corning) till they were 80% confluent. Next, mitotic cells were detached and harvested by tapping the sides of the flasks once on each side and collecting the media for centrifugation. The flasks were then topped up with fresh media. Additional cells can be collected from the flasks as frequently as every 2 hours.

Following centrifugation, the pellet of mitotic cells was resuspended in fresh media and plated into a well of a 6-well plate. Cells were collected and processed after an appropriate amount of time, depending on which stage of the cell cycle was required.

2.5.5 Luciferase reporter assays

Luciferase reporter assays were utilised to study the transcriptional activity of MITF towards the *TYR* promoter that was driving expression of luciferase. Cells were plated overnight in 24-well plates (Corning) until 50% confluent, then transfected with 2 plasmids in a 1:1 ratio – a plasmid encoding *MITF* and a plasmid encoding the firefly luciferase gene under the control of the *TYR* promoter. Cells were harvested 48 hours post-transfection by incubating with 100 µl Passive Lysis Buffer (Promega) for 30 minutes at 4°C on a rocking platform. 20 µl of the lysate was mixed with 50 µl of Luciferase Assay Reagent (Promega) in a white 96-well plate (Corning), after which luminescence was detected with a GloMax-Multi Microplate Multimode Reader (Promega) luminometer.

2.6 Reagents

2.6.1 Chemicals

Deionised, type 1+ 18.2 MΩ-cm water from a PURELAB Ultra system (ELGA LabWater, Albania) was used to prepare all buffers and solutions unless otherwise stated. Dimethyl sulfoxide (DMSO), methanol, ethanol, isopropanol, butanol and other common laboratory solvents were obtained from Sigma-Aldrich unless otherwise specified. Glycerol was sourced from Fisher Scientific.

Tris and glycine were obtained from Fisher Scientific. Other chemical salts, such as NaCl, were obtained from Sigma-Aldrich unless otherwise specified. Acetic acid was sourced from Fisher Scientific, while hydrochloric acid and sodium hydroxide were obtained from Sigma-Aldrich.

The detergents SDS and Tween were obtained from Fisher Scientific. NP-40 was a product of Sigma-Aldrich, while Triton-X was sourced from Merck (Darmstadt, Germany).

The antibiotics ampicillin and kanamycin were sourced from Fisher Scientific. Doxycycline was bought from Sigma-Aldrich.

In the case of active compounds, TPA, leptomycin B, thymidine and nocodazole were bought from Sigma-Aldrich. The small molecule inhibitors C646, BIO and CVT-313 were obtained from Merck. U0126 and Torin 1 were sourced from Cell Signaling Technology (Danvers, MA, USA). PLX4720 was a gift from Richard Marais (CRUK, Manchester, UK). SAHA was a gift from Nicholas La Thangue (University of Oxford, Oxford, UK).

2.6.2 Purified kinases

Purified glycogen synthase kinase 3 (GSK3) was sourced from New England Biolabs. CDK1/cyclin B was and CDK2/cyclin A were obtained from EMD Millipore (Billerica, MA, USA).

2.6.3 Oligonucleotides

Category	Sequence	Comments
Cloning	ATGATTATCGATGGCGGCGCTG AGCGGTGGC	Forward. To clone BRAF into p3xFLAG-CMV-14. ClaI site underlined.
Cloning	AGACCTCTAGAGTGGACAGGAA ACGCACCAT	Reverse. To clone BRAF into p3xFLAG-CMV-14. XbaI site underlined.
Cloning	AGTATAGATATCGCCACCATGG CGGCGCTGAGCGGT	Forward. To clone BRAF-3xFLAG into pcDNA5/FRT/TO. EcoRV site underlined.
Cloning	TGCTATGCGGCCGCTACTTGTCA TCGTCATCCTTGTAGTCGATG	Reverse. To clone BRAF-3xFLAG into pcDNA5/FRT/TO. NotI site underlined.

Cloning	AGTATTAAGCTTCGCATGCCATGCCACCAGTGCC	Forward. To clone MITF residues 60-99 into pEGFP-C1. HindIII site underlined.
Cloning	TGCTATGTCGACTACTCTGCCCTGCTCTGCTCCTCAAAC	Reverse. To clone MITF residues 60-99 into pEGFP-C1. SalI site underlined.
Cloning	TGCTATAAGCTTCAATGGCCAAGTTACCTATACTAGG	Forward. To clone GST into pEGFP-C1 and pEGFP-C1-MITF.60-99. HindIII site underlined.
Cloning	AGTATTAAGCTTGATCCGATTTTGGAGGAT	Reverse. To clone GST and NLS-GST into pEGFP-C1 and pEGFP-C1-MITF.60-99. HindIII site underlined.
Cloning	TGCTATAAGCTTCACCTAAAAAGAAACGTAAAGTTATGGCCAAGTTACCTATACTAGG	Forward. To clone NLS-GST and NLS-GST-NES into pEGFP-C1 and pEGFP-C1-MITF.60-99. HindIII site underlined.
Cloning	AGTATTAAGCTTGGATATCAAGACCTGCTAATTTCAAGGCTAAATCCGATTTTGGAGGAT	Reverse. To clone NLS-GST-NES into pEGFP-C1 and pEGFP-C1-MITF.60-99. HindIII site underlined.
Cloning	CTGATGAATTCTCATGCTGGAAATGCTAGAATAC	Forward. To clone MITF residues 1-203 into pGEX-2TK. EcoRI site underlined.
Cloning	GACTAGAATTCCCTCTCTTTAGCCAATGC	Reverse. To clone MITF residues 1-203 into pGEX-2TK. EcoRI site underlined.
SDM	GGAACAGTCTACCAGGGAAAGTGGCATGG	Forward. BRAF.K473Q mutagenesis.
SDM	CCATGCCACTTTCCCTGGTAGACTGTTCC	Reverse. BRAF.K473Q mutagenesis.
SDM	GGAACAGTCTACAGGGGAAAGTGGCATGG	Forward. BRAF.K473R mutagenesis.
SDM	CCATGCCACTTTCCCCTGTAGACTGTTCC	Reverse. BRAF.K473R mutagenesis.
SDM	ATTTGGAACAGTCTACAAGGGACAGTGGCATGGTG	Forward. BRAF.K475Q mutagenesis.
SDM	CACCATGCCACTGTCCCTTGTAGACTGTTCCAAAT	Reverse. BRAF.K475Q mutagenesis.
SDM	TTTGGAACAGTCTACAAGGGAAGGTGGCATGGTGA	Forward. BRAF.K475R mutagenesis.
SDM	TCACCATGCCACCTTCCCTTGTAGACTGTTCCAAA	Reverse. BRAF.K475R mutagenesis.
SDM	CATTTGGAACAGTCTACCAGGGACAGTGGCATGGT	Forward. BRAF.K473Q.K475Q mutagenesis.
SDM	ACCATGCCACTGTCCCTGGTAGACTGTTCCAAATG	Reverse. BRAF.K473Q.K475Q mutagenesis.

SDM	GGAACAGTCTACAGGGGAAGGTGGCATGG	Forward. BRAF.K473R.K475R mutagenesis.
SDM	CCATGCCACCTTCCCCTGTAGACTGTTCC	Reverse. BRAF.K473R.K475R mutagenesis.
SDM	AAGCTTCGCATGCCGCGCCACCAGTGCCGG	Forward. GFP-NLS-GST-MITF.60-99.M62A mutagenesis.
SDM	CCGGCACTGGTGGCGCGGCATGCGAAGCTT	Reverse. GFP-NLS-GST-MITF.60-99.M62A mutagenesis.
SDM	CCATGCCACCAGCGCCGGGGAGCAG	Forward. MITF.V65A mutagenesis.
SDM	CTGCTCCCCGGCGCTGGTGGCATGG	Reverse. MITF.V65A mutagenesis.
SDM	AGTGCCGGGGAGCGCCGCACCCAACAGC	Forward. MITF.S69A mutagenesis.
SDM	GCTGTTGGGTGCGGCGCTCCCCGGCACT	Reverse. MITF.S69A mutagenesis.
SDM	CAGTGCCGGGGAGCGAGGCACCCAACAGCCC	Forward. MITF.S69E mutagenesis.
SDM	GGGCTGTTGGGTGCCTCGCTCCCCGGCACTG	Reverse. MITF.S69E mutagenesis.
SDM	GCAGCGCACCCAACGCCCCTATGGCTATGC	Forward. MITF.S73A mutagenesis.
SDM	GCATAGCCATAGGGGCGTTGGGTGCGCTGC	Reverse. MITF.S73A mutagenesis.
SDM	GGAGCAGCGCACCCAACGAGCCTATGGCTATGCTCAC	Forward. MITF.S73E mutagenesis.
SDM	GTGAGCATAGCCATAGGCTCGTTGGGTGCGCTGCTCC	Reverse. MITF.S73E mutagenesis.
SDM	GCGCACCCAACAGCCCTGCGGCTATGCTCAC	Forward. MITF.M75A mutagenesis.
SDM	GTGAGCATAGCCGCAGGGCTGTTGGGTGCGC	Reverse. MITF.M75A mutagenesis.
SDM	ACCCAACAGCCCTATGGCTGCGCTCACTCTTAACTCC	Forward. MITF.M77A mutagenesis.
SDM	GGAGTTAAGAGTGAGCGCAGCCATAGGGCTGTTGGGT	Reverse. MITF.M77A mutagenesis.
SDM	CAACAGCCCTATGGCTATGGCCACTCTTAACTCCAACTGT	Forward. MITF.L78A mutagenesis.
SDM	ACAGTTGGAGTTAAGAGTGGCCATAGCCATAGGGCTGTTG	Reverse. MITF.L78A mutagenesis.
SDM	GCCCTATGGCTATGCTCACTGCTAACTCCAACTGTGAAAAAG	Forward. MITF.L80A mutagenesis.
SDM	CTTTTTCACAGTTGGAGTTAGCAGTGAGCATAGCCATAGGGC	Reverse. MITF.L80A mutagenesis.
SDM	CTTACCATCAGCAACGCCTGTCCAGCCAACC	Forward. MITF.S173A mutagenesis.
SDM	GGTTGGCTGGACAGGCGTTGCTGATGGTAAG	Reverse. MITF.S173A mutagenesis.

SDM	GGCTAGAGCGCATGGACTTGCC CTTATCCCATC	Forward. MITF.S298A mutagenesis.
SDM	GATGGGATAAGGGCAAGTCCAT GCGCTCTAGCC	Reverse. MITF.S298A mutagenesis.
SDM	CCAGGAGCTGCAAAAACAAGCG CCCGGAGGAGCAGTATGAGCGC AG	Forward. MITF.S397A.S401A.S405A mutagenesis.
SDM	GCTTGTTTTTGCAGCTCCTGGCG CCACTGATGACAGCAGTGGGTC	Reverse. MITF S397A.S401A.S405A mutagenesis.
SDM	CCAGGAGCTGAAAAAACAAGCG AGCGGAGGAGCAGTATGAGCGC AG	Forward. MITF.S397E.S401E.S405E mutagenesis.
SDM	GCTTGTTTTTTCAGCTCCTGGCT CCACTGATGACAGCAGTGGGTC	Reverse. MITF.S397E.S401E.S405E mutagenesis.
SDM	GGGACCCGGAGCCGCCGCTCCC AACAGC	Forward. Mitfa.S69A mutagenesis.
SDM	GCTGTTGGGAGCGGCGGCTCCG GGTCCC	Reverse. Mitfa.S69A mutagenesis.
SDM	CGGGACCCGGAGCCGAGGCTCC CAACAGCCC	Forward. Mitfa.S69E mutagenesis.
SDM	GGGCTGTTGGGAGCCTCGGCTC CGGGTCCCG	Reverse. Mitfa.S69E mutagenesis.
qPCR	GGAAGTGCTGGCAACTTACTG	Forward. human *EP300*.
qPCR	CCATAAGGATTGGGGTTGTTC	Reverse. human *EP300*.
qPCR	TTGGGTTTTCCAGCTAAGTTCT	Forward. human *TBP*.
qPCR	CCAGGAAATAACTCTGGCTCA	Reverse. human *TBP*.

2.6.4 Plasmids

Construct	Comments
pEF-Myc-BRAF	available in laboratory, BRAF-Myc
pEF-Myc-BRAF.V600E	available in laboratory, BRAF-Myc.V600E
p3xFLAG-CMV-14	Sigma-Aldrich, mammalian FLAG expression vector
p3xFLAG-CMV-14-BRAF	prepared by the candidate, BRAF-3xFLAG
p3xFLAG-CMV-14-BRAF.K473Q	prepared by the candidate, BRAF-3xFLAG.K473Q
p3xFLAG-CMV-14-BRAF.K473R	prepared by the candidate, BRAF-3xFLAG.K473R
p3xFLAG-CMV-14-BRAF.K475Q	prepared by the candidate, BRAF-3xFLAG.K475Q
p3xFLAG-CMV-14-BRAF.K475R	prepared by the candidate, BRAF-3xFLAG.K475R
p3xFLAG-CMV-14-BRAF.K473Q.K475Q	prepared by the candidate, BRAF-3xFLAG.K473Q.K475Q

p3xFLAG-CMV-14-BRAF.K473R.K475R	prepared by the candidate, BRAF-3xFLAG.K473R.K475R
p3xFLAG-CMV-14-BRAF.V600E	prepared by the candidate, BRAF-3xFLAG.V600E
p3xFLAG-CMV-14-BRAF.K473Q.V600E	prepared by the candidate, BRAF-3xFLAG.K473Q.V600E
p3xFLAG-CMV-14-BRAF.K473R.V600E	prepared by the candidate, BRAF-3xFLAG.K473R.V600E
p3xFLAG-CMV-14-BRAF.K475Q.V600E	prepared by the candidate, BRAF-3xFLAG.K475Q.V600E
p3xFLAG-CMV-14-BRAF.K475R.V600E	prepared by the candidate, BRAF-3xFLAG.K475R.V600E
p3xFLAG-CMV-14-BRAF.K473Q.K475Q.V600E	prepared by the candidate, BRAF-3xFLAG.K473Q.K475Q.V600E
p3xFLAG-CMV-14-BRAF.K473R.K475R.V600E	prepared by the candidate, BRAF-3xFLAG.K473R.K475R.V600E
pcDNA5/FRT/TO	Invitrogen, mammalian expression vector used in Flp-In T-REx system
pcDNA5/FRT/TO-BRAF-3xFLAG	prepared by the candidate, BRAF-3xFLAG
pcDNA5/FRT/TO-BRAF-3xFLAG.K473Q.K475Q	prepared by the candidate, BRAF-3xFLAG.K473Q.K475Q
pcDNA5/FRT/TO-BRAF-3xFLAG.K473R.K475R	prepared by the candidate, BRAF-3xFLAG.K473R.K475R
pcDNA5/FRT/TO-BRAF-3xFLAG.V600E	prepared by the candidate, BRAF-3xFLAG.V600E
pcDNA5/FRT/TO-BRAF-3xFLAG.K473Q.K475Q.V600E	prepared by the candidate, BRAF-3xFLAG.K473Q.K475Q.V600E
pcDNA5/FRT/TO-BRAF-3xFLAG.K473R.K475R.V600E	prepared by the candidate, BRAF-3xFLAG.K473R.K475R.V600E
pcDNA3- p300-HA	available in laboratory, p300-HA
pcDNA3- CBP-HA	available in laboratory, CBP-HA
pCMV-HDAC1-FLAG	from Heinz Arnheiter (NIH), HDAC1-FLAG
pCMV-HDAC2-FLAG	from Heinz Arnheiter (NIH), HDAC2-FLAG
pCMV-HDAC3-FLAG	from Heinz Arnheiter (NIH), HDAC3-FLAG
pCMV-HDAC4-FLAG	from Heinz Arnheiter (NIH), HDAC4-FLAG
pCMV-HDAC5-FLAG	from Heinz Arnheiter (NIH), HDAC5-FLAG
p3xFLAG-CMV-14-MITF	available in laboratory, MITF-3xFLAG
p3xFLAG-CMV-14-MITF.S69A	prepared by the candidate, MITF-3xFLAG.S69A
p3xFLAG-CMV-14-MITF.S69E	prepared by the candidate, MITF-3xFLAG.S69E
p3xFLAG-CMV-14-MITF.S73A	prepared by the candidate, MITF-3xFLAG.S73A
p3xFLAG-CMV-14-MITF.S73E	prepared by the candidate MITF-3xFLAG.S73E
p3xFLAG-CMV-14-MITF.M75A	prepared by the candidate, MITF-3xFLAG.M75A

p3xFLAG-CMV-14-MITF.L78A	prepared by the candidate, MITF-3xFLAG.L78A
p3xFLAG-CMV-14-MITF.L80A	prepared by the candidate, MITF-3xFLAG.L80A
p3xFLAG-CMV-14-MITF.S298A	prepared by the candidate, MITF-3xFLAG.S298A
p3xFLAG-CMV-14-MITF.S397A.S401A.S405A	prepared by the candidate, MITF-3xFLAG.S397A.S401A.S405A
p3xFLAG-CMV-14-MITF.S397E.S401E.S405E	prepared by the candidate, MITF-3xFLAG.S397E.S401E.S405E
p3xFLAG-CMV-14-MITF.1-180	available in laboratory, MITF.1-180-3xFLAG
p3xFLAG-CMV-14-MITF.20-419	available in laboratory, MITF.20-419-3xFLAG
p3xFLAG-CMV-14-MITF.40-419	available in laboratory, MITF.40-419-3xFLAG
p3xFLAG-CMV-14-MITF.60-419	available in laboratory, MITF.60-419-3xFLAG
p3xFLAG-CMV-14-MITF.100-419	available in laboratory, MITF.100-419-3xFLAG
pDestTol2CG2-Mitfa	from Elizabeth Patton (University of Edinburgh), zebrafish expression vector with Mitfa under *mitfa* promoter
pDestTol2CG2-Mitfa.S69A	prepared by the candidate, Mitfa.S69A
pDestTol2CG2-Mitfa.S69E	prepared by the candidate, Mitfa.S69E
pEGFP-C1	Clontech, mammalian GFP expression vector
pEGFP-C1-MITF	available in laboratory, GFP-MITF
pEGFP-C1-MITF.S69A	prepared by the candidate, GFP-MITF.S69A
pEGFP-C1-MITF.S69E	prepared by the candidate, GFP-MITF.S69E
pEGFP-C1-MITF.S73A	prepared by the candidate, GFP-MITF.S73A
pEGFP-C1-MITF.S73E	prepared by the candidate, GFP-MITF.S73E
pEGFP-C1-MITF.M75A	prepared by the candidate, GFP-MITF.M75A
pEGFP-C1-MITF.L78A	prepared by the candidate, GFP-MITF.L78A
pEGFP-C1-MITF.L80A	prepared by the candidate, GFP-MITF.L80A
pEGFP-C1-MITF.S173A	prepared by the candidate, GFP-MITF.S173A
pEGFP-C1-MITF.S298A	prepared by the candidate, GFP-MITF.S298A
pEGFP-C1-MITF.S397A.S401A.S405A	prepared by the candidate, GFP-MITF.S397A.S401A.S405A
pEGFP-C1-MITF.S397E.S401E.S405E	prepared by the candidate, GFP-MITF.S397E.S401E.S405E
pEGFP-C1-MITF.60-99	prepared by the candidate, GFP-MITF.60-99
pEGFP-C1-GST	prepared by the candidate, GFP-GST
pEGFP-C1-NLS-GST	prepared by the candidate, GFP-NLS-GST
pEGFP-C1-NLS-GST-NES	prepared by the candidate, GFP-NLS-GST-NES
pEGFP-C1-NLS-GST-MITF.60-99	prepared by the candidate, GFP-NLS-GST-MITF.60-99
pEGFP-C1-NLS-GST-MITF.60-99.M62A	prepared by the candidate, GFP-NLS-GST-MITF.60-99.M62A
pEGFP-C1-NLS-GST-MITF.60-99.V65A	prepared by the candidate, GFP-NLS-GST-MITF.60-99.V65A
pEGFP-C1-NLS-GST-MITF.60-99.S69A	prepared by the candidate, GFP-NLS-GST-MITF.60-99.S69A

pEGFP-C1-NLS-GST-MITF.60-99.S73A	prepared by the candidate, GFP-NLS-GST-MITF.60-99.S73A
pEGFP-C1-NLS-GST-MITF.60-99.M75A	prepared by the candidate, GFP-NLS-GST-MITF.60-99.M75A
pEGFP-C1-NLS-GST-MITF.60-99.M77A	prepared by the candidate, GFP-NLS-GST-MITF.60-99.M77A
pEGFP-C1-NLS-GST-MITF.60-99.L78A	prepared by the candidate, GFP-NLS-GST-MITF.60-99.L78A
pEGFP-C1-NLS-GST-MITF.60-99.L80A	prepared by the candidate, GFP-NLS-GST-MITF.60-99.L80A
pEGFP-N1-TFEB	available in laboratory, TFEB-GFP
pGEX-2TK	GE Healthcare Life Sciences, bacterial GST expression vector
pGEX-2TK-MITF.1-203	prepared by the candidate, GST-MITF.1-203
pGEX-2TK-MITF.1-203.S73A	prepared by the candidate, GST-MITF.1-203.S73A
pGL3-basic	Promega, mammalian expression vector for firefly luciferase, lacks promoter
pGL3-TYR	available in laboratory, -300/+80 bp human TYR promoter driving luciferase expression

2.6.5 Antibodies

Antibody	Type	Immunogen	Supplier	Dilution	
				WB	IF
α-acetylated Lysine (#9441)	rabbit polyclonal	acetylated lysine	Cell Signaling	1:1000	–
α-Actin (AC-40)	mouse monoclonal	SGPSIVHRKCF	Sigma-Aldrich	1:10000	–
α-BRAF (F-7)	mouse monoclonal	amino acids 12-156	Santa Cruz	1:2000	–
α-BRAF (H-145)	rabbit polyclonal	amino acids 12-156	Santa Cruz	1:2000	–
α-BRN2	mouse monoclonal	unknown	Generated in-house	1:1000	1:500
α-β-catenin (ab2365)	rabbit polyclonal	amino acids 768-781	Abcam	1:2000	–
α-Cyclin B1 (H-433)	rabbit polyclonal	full-length protein	Santa Cruz	1:1000	–
α-ERK2 (C-14)	rabbit polyclonal	C-terminus	Santa Cruz	1:10000	–
α-phospho-ERK1/2 (T202/Y204) (197G2)	rabbit polyclonal	phospho-T202/Y204	Cell Signaling	1:2000	1:500
α-FLAG (M2)	mouse monoclonal	DYKDDDDK	Sigma-Aldrich	1:10000	1:1000

α-FLAG	rabbit polyclonal	DYKDDDDK	Sigma-Aldrich	1:10000	–
α-HA (HA-7)	mouse monoclonal	YPYDVPDYA	Sigma-Aldrich	1:2000	–
α-HA (Y-11)	rabbit polyclonal	YPYDVPDYA	Santa Cruz	1:2000	–
α-Lamin B (C-20)	goat polyclonal	C-terminus	Santa Cruz	1:1000	–
α-MEK1/2 (#9122)	rabbit polyclonal	unknown	Cell Signaling	1:1000	–
α-phospho-MEK1/2 (S217/S221) (#9121)	rabbit polyclonal	phospho-S217/S221	Cell Signaling	1:2000	–
α-MITF (As9)	mouse monoclonal	C-terminus	Generated in-house	1:5000	1:1000
α-MITF	rabbit polyclonal	C-terminus	Generated in-house	1:5000	1:1000
α-c-Myc (9E10)	mouse monoclonal	EQKLISEEDL	Sigma-Aldrich	1:2000	–
α-Myc tag (ab9106)	rabbit polyclonal	EQKLISEEDL	Abcam	1:2000	–
α-S6 ribosomal protein (5G10)	rabbit monoclonal	unknown	Cell Signaling	1:1000	
α-phospho-S6 (S235/S236)	rabbit polyclonal	phospho-S235/S236	Cell Signaling	1:1000	
α-β-tubulin (H-235)	rabbit polyclonal	amino acids 210-444	Santa Cruz	1:2000	–
α-acetylated tubulin (K40) (6-11B-1)	mouse monoclonal	acetyl-K40	Sigma-Aldrich	1:1000	

Chapter 3 – Acetylation of BRAF affects its kinase activity

3.1 Introduction

3.1.1 Feedback loops in ERK signalling

In most biological systems, including signal transduction pathways, negative feedback loops provide an opportunity to modulate output. In the case of the MAPK pathway, activation of ERK signalling is similarly limited by a complex network of negative feedback interactions (Avraham and Yarden, 2011; Lito et al., 2013).

As shown in experiments involving RAF and MEK inhibition in cancer cells, a change in ERK signalling output causes alterations in the transcriptional profile of a certain subset of genes, including several that act on the MAPK pathway (Joseph et al., 2010; Pratilas et al., 2009). Some of the negative feedback loops involved in modulating ERK output are mediated by ERK-driven transcriptional up-regulation of genes that have inhibitory effects on the signalling cascade. For example, activated ERK signalling induces the transcription of dual-specificity phosphatases (DUSPs) (Amit et al., 2007; Blüthgen et al., 2009; Brondello et al., 1997), which directly attenuate ERK signalling output by dephosphorylating ERK. An additional level of reciprocal regulation is provided by ERK phosphorylation of DUSP1. ERK phosphorylates DUSP1 on two C-terminal serine residues S359 and S364, which leads to stabilisation of DUSP1 via a reduction in ubiquitin-dependent degradation, but does not affect its ability to dephosphorylate ERK (Brondello et al., 1999). Interestingly, another group has reported that ERK phosphorylation of DUSP1 on S296 and S323 triggers the ubiquitination and degradation of DUSP1 (Lin and Yang, 2006; Lin et al., 2003).

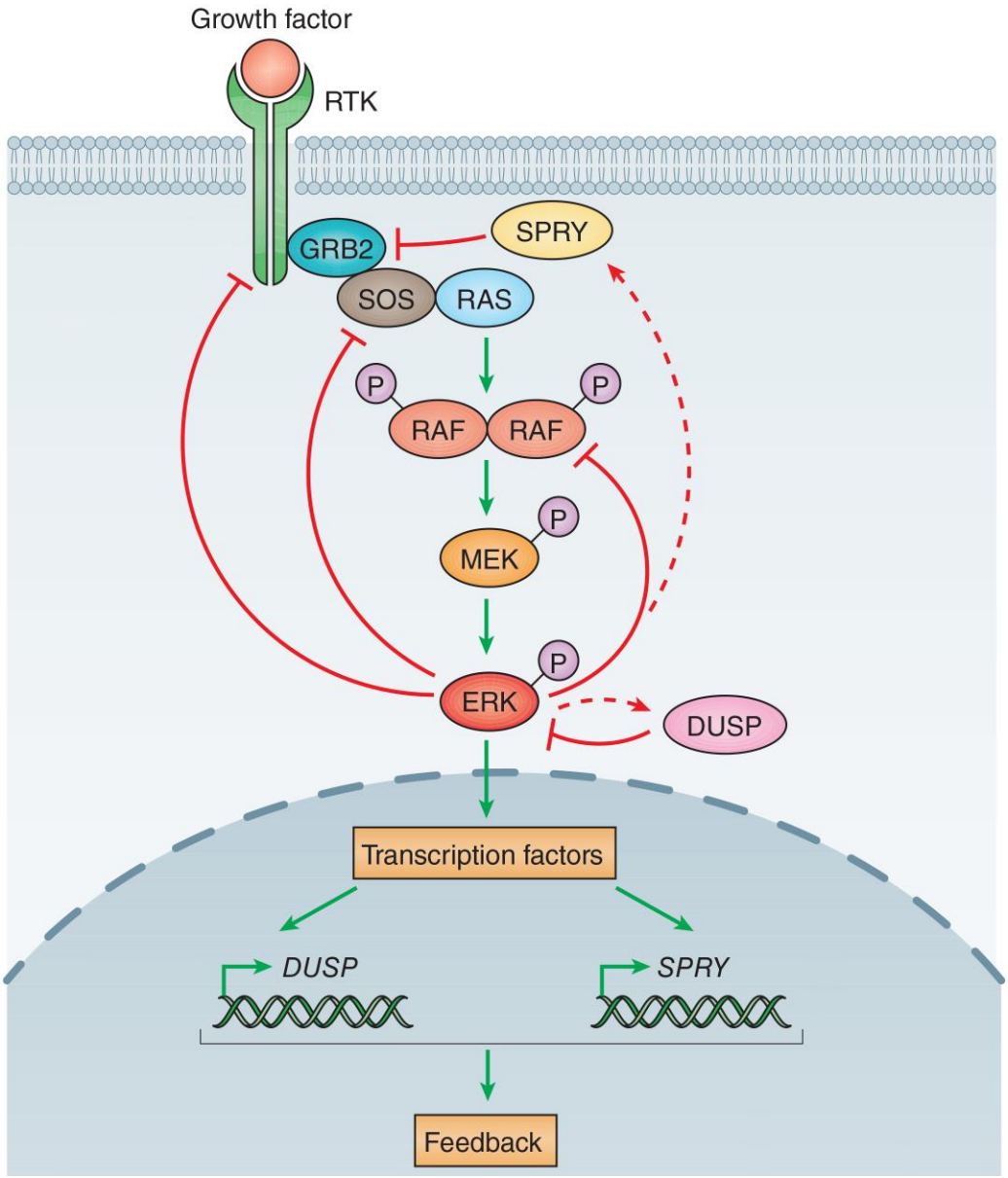

Figure 3.1 ERK signalling output is modulated by multiple negative feedback mechanisms. Direct negative feedback (solid lines) occurs when ERK phosphorylates and inhibits the activity of upstream components, such as RTK, SOS and CRAF. Indirect negative feedback (dotted lines) takes place via ERK-driven transcriptional up-regulation of genes encoding DUSP and SPRY proteins, which have inhibitory effects on the pathway. Adapted from Lito et al., 2013.

Other than DUSPs, ERK-driven transcriptional activation of the Sprouty (SPRY) family of proteins (Ozaki et al., 2001) also contributes to negative feedback regulation of ERK signalling. SPRYs function as adaptor proteins that affect protein-protein interactions at the level of RTKs and RAS, which allows them to modulate

RTK signalling in a context-dependent manner (Kim and Bar-Sagi, 2004). Mechanistically, the phosphorylation of SPRY on a conserved tyrosine residue (Y55 in SPRY2) in response to growth factor stimulation enables it to bind to the SH2 domain of the GRB2 adaptor protein (Hanafusa et al., 2002). In turn, this sequesters GRB2 away from SOS, thus inhibiting RTK-mediated activation of RAS. SPRY4 has also been shown to bind to CRAF via the cysteine-rich domain in the C-terminus of SPRY4, which results in inhibition of ERK signalling (Sasaki et al., 2003). Sprouty-related, EVH1 domain-containing protein (SPRED), another member of the SPRY family, is also transcriptionally up-regulated by ERK (Joseph et al., 2010; Pratilas et al., 2009). SPRED1 has been shown to inhibit the MAPK pathway by inducing the recruitment of NF1, a negative regulator of RAS, to the plasma membrane (Stowe et al., 2012).

In addition to transcription, negative feedback modulation of ERK signalling is also mediated by ERK phosphorylation of other upstream components of the pathway. ERK phosphorylates the RTK epidermal growth factor receptor (EGFR) at T669 (Takishima et al., 1991), which results in inhibition of EGFR's kinase activity (Li et al., 2008). ERK also phosphorylates SOS in conjunction with RSK, another downstream target of ERK (Corbalan-Garcia et al., 1996; Douville and Downward, 1997). Phosphorylation of SOS reduces its binding affinity towards GRB2 and leads to the dissociation of the GRB2-SOS complex, thus inhibiting RAS activation (Chen et al., 1996; Corbalan-Garcia et al., 1996). Downstream of RAS, CRAF is another target of ERK, which phosphorylates CRAF on S29, S43, S289, S296, S301 and S642 (Dougherty et al., 2005). Mutation of all six serine residues to alanine, which cannot be phosphorylated, resulted in an increase in CRAF activity (Dougherty et al., 2005). In addition, hyperphosphorylation of CRAF by ERK also impeded CRAF's

ability to interact with RAS, thus providing yet another avenue for negative feedback regulation (Dougherty et al., 2005).

ERK phosphorylation is also involved in regulating positive feedback interactions in addition to negative feedback. Interestingly, in apparent contradiction of the study mentioned above, phosphorylation of the constitutively active $CRAF^{S259A}$ mutant at S289, S296 and S301 by ERK increased CRAF's kinase activity (Balan et al., 2005), resulting in a positive feedback loop. Another target of ERK phosphorylation is NF1 (von Kriegsheim et al., 2009). Growth factor-stimulation of the ERK pathway caused the dissociation of NF1 from RAS (von Kriegsheim et al., 2009), resulting in a positive feedback loop from ERK to RAS.

3.1.2 Regulation of RAF by phosphorylation

Phosphorylation plays an important role in the regulation of RAF (ARAF, BRAF, CRAF) activation and function. Phosphorylation-mediated regulation of RAF predominantly occurs at four main areas within RAF – the negative charge regulatory region (N-region), the activation segment, and the two 14-3-3 binding sites at CR2 and the C-terminus.

The N-region comprises of a stretch of four residues located just outside the N-terminal end of the RAF kinase domain. In CRAF, this corresponds to a SSYY motif (residues 338-341), compared to SGYY in ARAF (residues 299-302) and SSDD (residues 446-449) in BRAF. Phosphorylation of the serine and tyrosine residues in the N-region of CRAF, in particular S338 and Y341, provides the negative charges required for kinase activity (Diaz et al., 1997; Fabian et al., 1993; Mason et al., 1999). Mechanistically, the exact role played by these phosphorylation events is not yet fully understood, although some believe that they affect dimerisation and

transactivation of RAFs (Hu et al., 2013). Phosphorylation of the tyrosine residues Y340 and Y341 on CRAF appear to be mediated by the Src family of non-receptor tyrosine kinases (Fabian et al., 1993; Marais et al., 1995; Tilbrook et al., 2001). As for S338 of CRAF, it is able to be phosphorylated by p21-activated kinases (PAK) *in vitro* (Chaudhary et al., 2000; King et al., 1998). However, the actual *in vivo* significance of this finding has been disputed (Chiloeches et al., 2001). More recently, casein kinase 2 (CK2) has been reported to phosphorylate S338 in CRAF, as well as the homologous S446 in BRAF (Ritt et al., 2007).

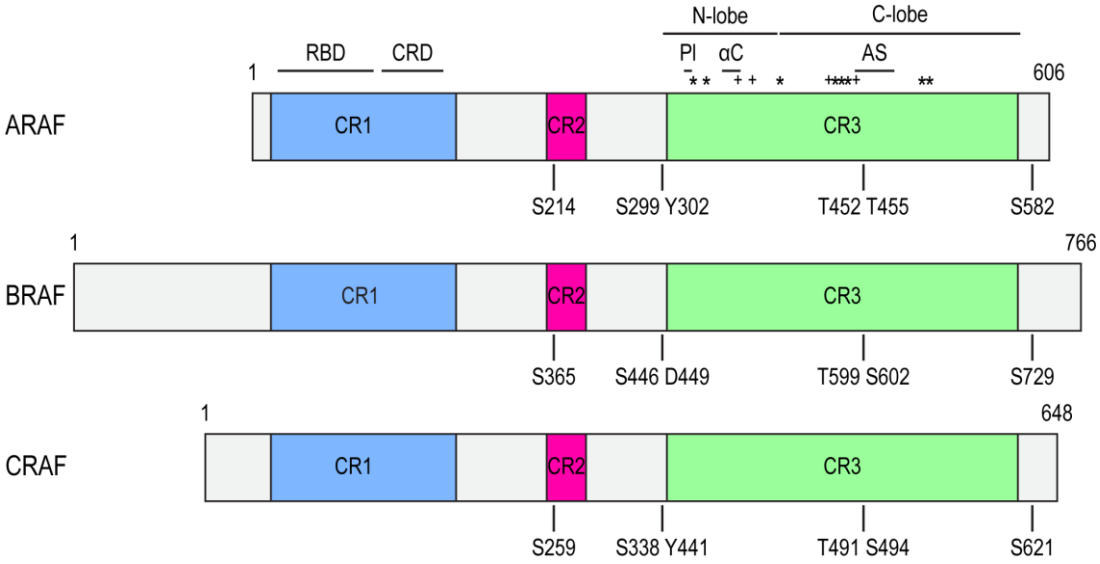

Figure 3.2 Major phosphorylation sites in all three RAF isoforms. The 14-3-3 binding sites (S259 and S621), N-region phosphorylation sites (S338 and Y441) and activation segment phosphorylation sites (T491 and S494) are indicated in CRAF. The equivalent residues in ARAF and BRAF are also marked. The relative positions of the P-loop (Pl), αC and the activation segment (AS) are indicated. The key residues that make up the C-spine (*) and the R-spine ($^{+}$) are also marked. Adapted from Roskoski, 2010.

Like CRAF, ARAF contains tyrosine residues in its homologous N-region. In contrast, the tyrosine residues in the N-region of CRAF have been replaced by phosphomimetic aspartic acid residues in the homologous region in BRAF. The consensus recognition motif of CK2 is **S/T**-X-X-E/D (Marin et al., 1986), where E/D in the +3 position can also be replaced with a phosphorylated residue. This means

that both ARAF and CRAF require priming phosphorylations on their N-region tyrosine residues before they can be phosphorylated by CK2 on S299 in ARAF and S338 in CRAF. On the other hand, BRAF can already be phosphorylated by CK2 on S446 without the need for priming phosphorylation. As a result, ARAF and CRAF behave similarly in terms of their activation by SRC tyrosine kinases, while BRAF is not responsive to SRC (Marais et al., 1997). The presence of two aspartic acids in the N-region of BRAF provides negative charges and enables the constitutive phosphorylation of S446 in BRAF (Mason et al., 1999) that is necessary for kinase activity, which allows BRAF to have a much higher basal kinase activity than CRAF.

The activation segment, which lies in the kinase domain, also contains phosphorylation sites that are important for RAF activation. It has been shown in a number of studies that phosphorylation of two residues in the activation segment – T452 and T455 in ARAF (Baljuls et al., 2008), T599 and S602 in BRAF (Zhang and Guan, 2000), and T491 and S494 in CRAF (Chong et al., 2001), is required for their respective kinase activities. Based on insights gained from the crystal structure of BRAF, activation segment phosphorylation events are believed to increase RAF kinase activity by disrupting inhibitory hydrophobic interactions between the P-loop and activation segment of RAF, thus allowing it to fold into an active conformation (Wan et al., 2004). Not much is known about the kinase(s) that are involved in phosphorylating the activation segment, although a recent study proposed that the two residues may be phosphorylated via *cis* autophosphorylation (Hu et al., 2013).

As discussed in Chapter 1, S259 in CR2 and S621 in the C-terminus of CRAF are 14-3-3 binding sites (Michaud et al., 1995; Muslin et al., 1996). S259 is phosphorylated by protein kinase A (PKA) (Dhillon et al., 2002; Dumaz and Marais, 2003), as well as AKT (Zimmermann and Moelling, 1999). AKT was also shown to

phosphorylate the homologous S365 residue in BRAF (Guan et al., 2000). Phosphorylation of S259 in CRAF and S365 in BRAF is inhibitory towards RAF activity (Dhillon et al., 2002; Dumaz and Marais, 2003; Guan et al., 2000; Morrison et al., 1993; Zimmermann and Moelling, 1999) as it promotes binding of 14-3-3 proteins, which are thought to stabilise the N-terminal autoinhibition of the C-terminal kinase domain (Matallanas et al., 2011; Tzivion et al., 1998) and prevent its interaction with RAS (Dumaz and Marais, 2003).

While S259 phosphorylation is clearly inhibitory, the role of S621 phosphorylation in CRAF is more complex. Phosphorylation at S621 in CRAF leads to a decrease in kinase activity *in vitro* (Dhillon et al., 2009; Mischak et al., 1996), which may be caused by disruption of its interaction with the scaffolding protein KSR (Shen et al., 2013). However, other studies indicate that the binding of 14-3-3 proteins to S621 in CRAF and the homologous S729 residue in BRAF is essential for RAF activation (MacNicol et al., 2000; Tzivion et al., 1998; Yip-Schneider et al., 2000). The exact underlying mechanism behind CRAF S621 phosphorylation-mediated activation is not known, but C-terminal 14-3-3 interactions are believed to stabilise heterodimerisation and transactivation between CRAF and BRAF protomers (Rajakulendran et al., 2009; Weber et al., 2001). In addition to stabilising RAF heterodimerisation, the C-terminal binding of 14-3-3 proteins can also increase RAF kinase activity by increasing its affinity for ATP (Dhillon et al., 2009). As for the identity of kinase, both AMP-activated kinase (AMPK) (Shen et al., 2013; Sprenkle et al., 1997) and PKA (Mischak et al., 1996) have been linked with phosphorylation of CRAF S621, although autophosphorylation of this site has been reported as well (Noble et al., 2008).

3.1.3 MAPK feedback loops are mediated by post-translational modifications

In cancers where downstream MAPK effectors are constitutively activated, such as in $BRAF^{V600E}$ melanoma, negative feedback is impaired since the dependence of the MAPK pathway on a number of upstream components is bypassed (Yao et al., 2015). Although there would still be negative feedback in the form of ERK-mediated transcriptional up-regulation of DUSPs, we reasoned that negative feedback mediated by a transcription response would be relatively slow, and that additional non-transcription-dependent feedback mechanisms would be necessary to facilitate short-term flexibility in MAPK output.

In contrast to transcription, post-translational modifications occur on a much shorter time scale, often in a matter of minutes (Ahmed et al., 2014). As outlined above, a sizeable number of feedback loops are regulated via phosphorylation, particularly with regards to RAF. In considering possible alternative mechanisms, we wondered if other types of post-translational modifications, such as acetylation, could affect RAF activity. Acetylation is a reversible post-translational modification which typically involves the transfer of an acetyl group from acetyl-CoA to the ε-amino group of a lysine residue (Choudhary et al., 2009), thus neutralising its positive charge (Figure 3.3). In addition to lysine, acetylation of serine and threonine residues has been reported as well (Mukherjee et al., 2007). Acetylation is catalysed by a group of enzymes known as histone acetyltransferases (HATs), such as p300 and PCAF. Conversely, deacetylation is carried out by the family of histone deacetylases (HDACs), which includes sirtuins.

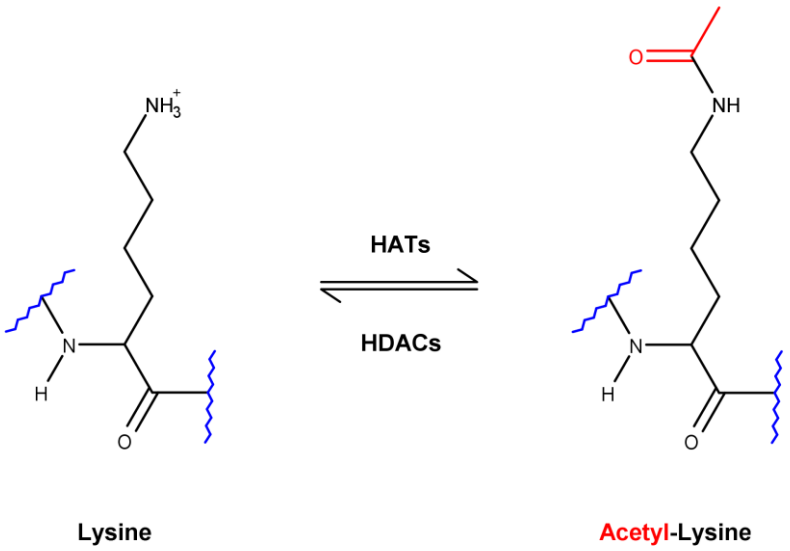

Figure 3.3 Lysine acetylation. Acetylation of lysine residues is characterised by the transfer of an acetyl group (red) from acetyl-CoA (not shown) to the ε-amino group of lysine. Acetylation is carried out by HATs, while deacetylation is catalysed by HDACs.

Protein acetylation has historically been studied and described in the context of epigenetics and chromatin remodelling (Allfrey et al., 1964; Grunstein, 1997). Acetylation of histones neutralises the positive charges on their lysine residues, which decreases their affinity for DNA by reducing their interaction with the negatively-charged phosphate groups in DNA. This results in relaxation of the chromatin structure, thus allowing access to transcription factors and increasing transcription (Grunstein, 1997). In addition to histones, any other non-histone proteins are also known to be acetylated (Glozak et al., 2005; Norris et al., 2009). For example, acetylation of the p53 tumour suppressor protein is known to be required for its activity (Gu and Roeder, 1997; Tang et al., 2008). The importance of acetylation as a post-translational modification was underlined when a study to elucidate the lysine acetylome revealed the existence of over 3600 lysine acetylation sites on 1750 proteins (Choudhary et al., 2009), which is of a comparable scale to

phosphorylation with 6600 phosphorylation sites detected in 2244 proteins (Olsen et al., 2006).

We noted that ERK can phosphorylate the HATs p300 and the closely related CREB-binding protein (CBP) at their respective C-terminals (Ait-Si-Ali et al., 1999; Chen et al., 2007; Sang et al., 2003). Both p300 and CBP are well-known transcriptional co-activators which can also function as acetyltransferases and catalyse the acetylation of proteins (Ogryzko et al., 1996). ERK phosphorylation of CBP increased its HAT activity *in vitro* (Ait-Si-Ali et al., 1999) and enhanced its transactivation potential (Janknecht and Nordheim, 1996). Similarly, MAPK signalling also stimulated the HAT activity of p300, which subsequently plays a major role in inducing keratin 16 expression (Chen et al., 2007). Acetylation was also involved in regulating kinases such as MEK (Mittal et al., 2006; Mukherjee et al., 2006; Trosky et al., 2007) and CDK9 (Fu et al., 2007; Sabo et al., 2008), whose activities were inhibited via acetylation of critical residues in their active site. Another study reported acetylation at two lysine residues in MEK1 which increased its activity (Yeung et al., 2015). With this in mind, we wondered if there could be a feedback loop between the MAPK pathway and p300/CBP, especially since MAPK signalling affects p300/CBP activity.

3.2 Results

3.2.1 Inhibition of p300/CBP activates MAPK signalling

To test whether acetylation could regulate MAPK output, we used C646 (Bowers et al., 2010), a sensitive and selective (K_i = 400 nM) small molecule inhibitor of p300 and CBP, to treat 501mel melanoma cells bearing a $BRAF^{V600E}$ mutation and western blotted for phosphorylated ERK (Figure 3.4; data from Robert

Siddaway). Since C646 can induce a G1/S cell cycle arrest in melanoma cells (Bowers et al., 2010), and we were interested in effects mediated by acetylation, we initially limited treatment time to 1 hour in order to prevent cell cycle-related effects from confounding our results. The results were striking (Figure 3.4), with C646 inducing an increase in the amount of phospho-ERK, as detected by an antibody that recognises phosphorylated T202/Y204 in ERK1 and T185/Y187 in ERK2, in the 501mel human melanoma cell line.

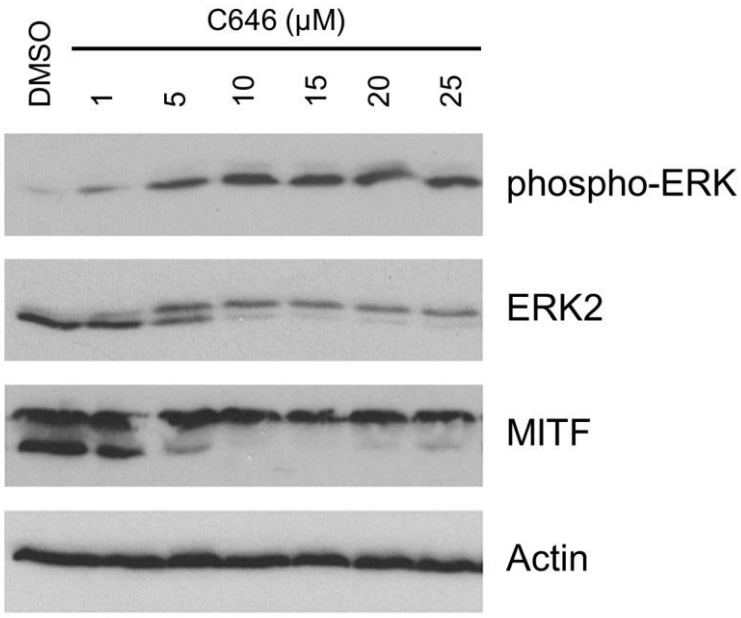

Figure 3.4 Short-term inhibition of p300/CBP induced MAPK pathway activation. Western blot of 501mel cells following treatment with C646. 501mel cells were grown to 80% confluence and treated with various concentrations of C646 or an equivalent volume of DMSO for 1 hour. Data from Robert Siddaway.

As little as 5 μM of C646 led to elevated ERK phosphorylation 1 hour after treatment (Figure 3.4). The increase in the amount of phosphorylated ERK was also reflected in the blot for ERK2, which demonstrated a mobility shift after C646 treatment. This was accompanied by a decrease in the electrophoretic mobility of MITF, which is consistent with the well-characterised ERK-dependent

phosphorylation at S73 in MITF (Hemesath et al., 1998). This result suggests that C646 treatment leads to activation of the MAPK pathway.

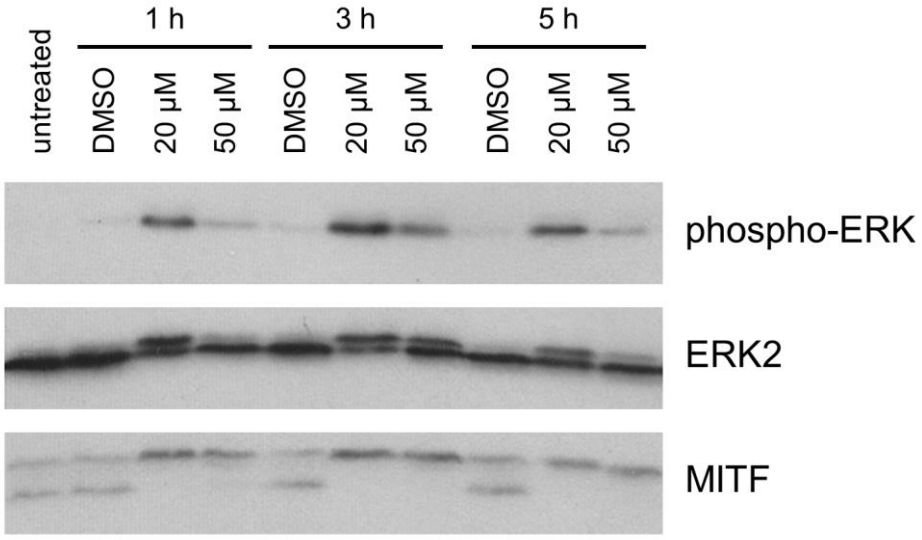

Figure 3.5 C646-induced MAPK pathway activation could be sustained for at least 5 hours. Western blot of 501mel cells following treatment with C646. Cells were grown to 80% confluence and treated with two different concentrations of C646 or an equivalent volume of DMSO for up to 5 hours. Lower concentrations of C646 were also tested but they were not as effective in activating the MAPK pathway (data not shown). Data from Robert Siddaway.

To further investigate the response to C646, 501mel cells were treated with two concentrations of C646 over a period of up to 5 hours (Figure 3.5; data from Robert Siddaway). With 20 µM of C646, an increase in phospho-ERK was observed as before, along with a shift in MITF mobility. This effect was sustained for at least 5 hours, with the maximum amount of phospho-ERK observed at the 3-hour mark. Although the 50 µM C646 treatment also elicited an increase in ERK phosphorylation, this magnitude of this increase was less than that observed with the lower 20 µM concentration. However, there was still a similar shift in MITF mobility as was observed with the lower C646 concentration. Based on the above, we decided to restrict C646 treatment in further experiments to a maximum concentration of 20 µM since this was sufficient to induce a sizeable increase in ERK phosphorylation.

To confirm that the increase in ERK phosphorylation following C646 treatment is mediated through p300, we did an siRNA knockdown of p300 in 501mel cells and harvested them after 48 hours (Figure 3.6).

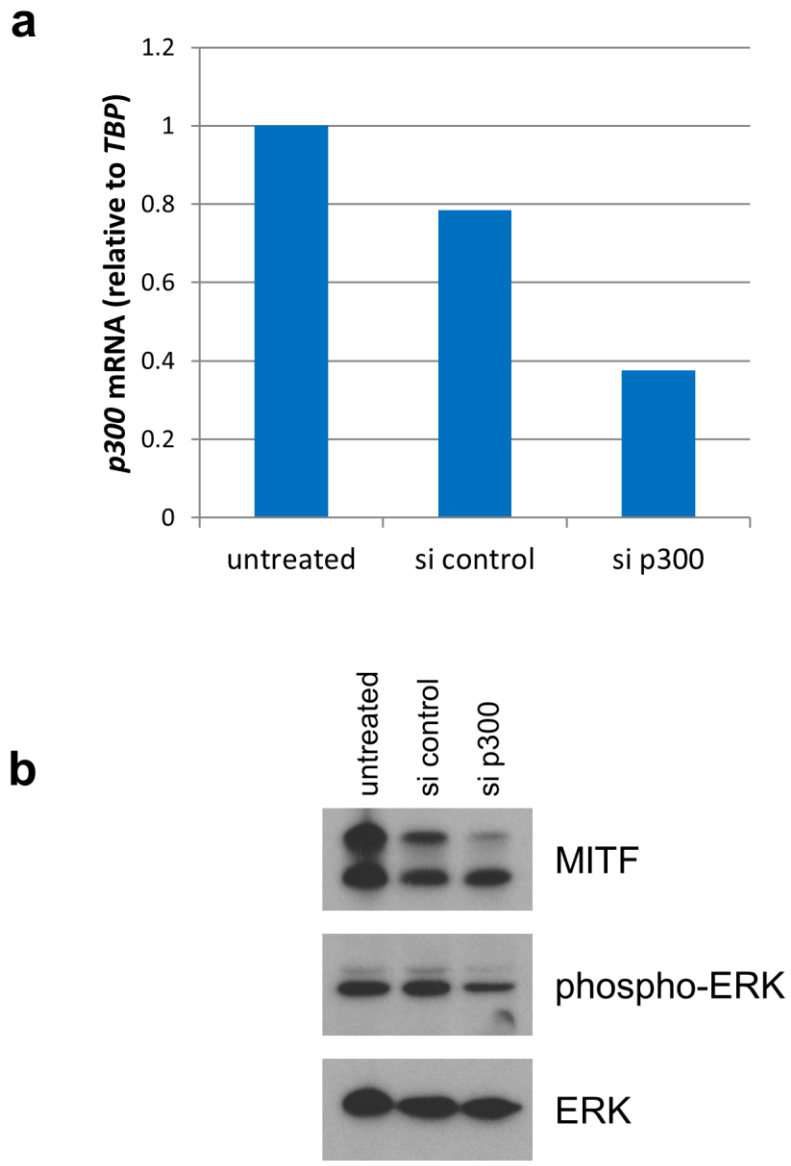

Figure 3.6 siRNA knockdown of p300 failed to activate the MAPK pathway in 501mel cells. (a) qPCR analysis of *p300* mRNA levels in 501mel cells after siRNA knockdown of p300, using *TBP* as the reference gene. Cells were grown to 50% confluence and transfected with siRNA against p300 or scrambled control siRNA. After 48 hours, cells were harvested and their RNA was extracted. **(b)** Western blot of 501mel cells after after siRNA knockdown of p300. Cells were treated as in (a), then harvested for western blotting.

As shown in Figure 3.6a, we confirmed that the knockdown of p300 was successful by qPCR, using TATA box binding protein (*TBP*) as the reference gene. However, we were unable to detect any increases in ERK phosphorylation by western blot following p300 knockdown; in fact phospho-ERK levels appeared to have decreased slightly relative to the control (Figure 3.6b). We postulate that the disparity in ERK phosphorylation in response to p300 inactivation might possibly be explained by the difference in time scales between C646 treatment and siRNA knockdown of p300. Another plausible reason for the discrepancy would be that while C646 inhibits both p300 and CBP acetyltransferases, CBP is not targeted by p300 siRNA.

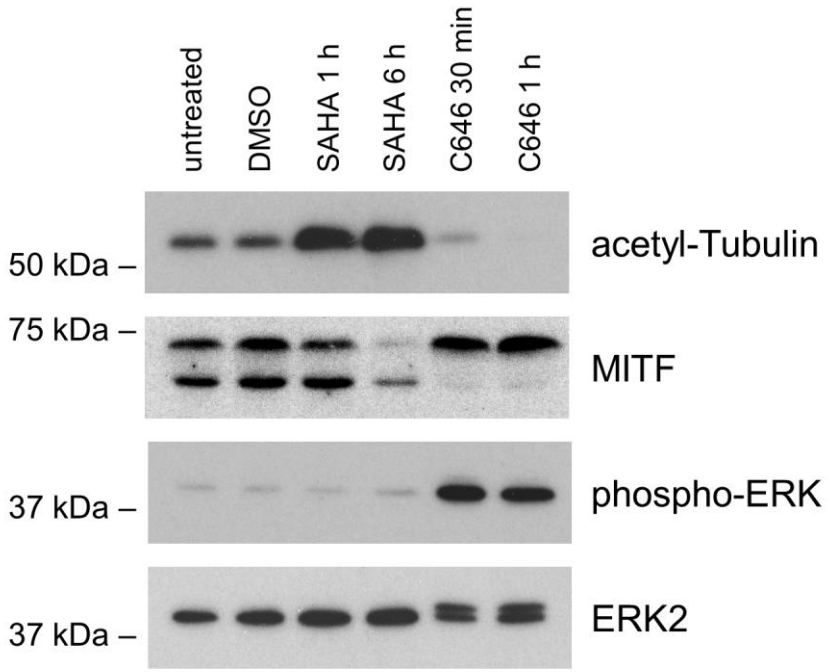

Figure 3.7 HDAC inhibition resulted in reduced ERK-phosphorylation of MITF in 501mel cells. Western blot of 501mel cells following treatment with SAHA and C646. Cells were grown to 80% confluence and treated with 2.5 µM SAHA, 20 µM C646 or an equivalent volume of DMSO for up to 6 hours.

Since the inhibition of p300/CBP acetyltransferases caused an up-regulation of the MAPK pathway, we wanted to determine if we could decrease MAPK signalling

by increasing the amount of acetylation. To investigate this, we treated 50mel cells with suberoylanilide hydroxamic acid (SAHA) (Richon et al., 1998), a pan-HDAC inhibitor (IC_{50} < 86 nM) (Figure 3.7).

Treatment with 2.5 μM of SAHA led to diminished MITF expression, as reported previously (Yokoyama et al., 2008), but also decreased the proportion of ERK-phosphorylated MITF (Figure 3.7). However, we did not detect any changes in ERK phosphorylation levels following SAHA treatment. In addition, we also sought to verify the effects of C646 and SAHA on acetylation by checking the levels of acetylated α-tubulin, as detected by an antibody recognising acetylated K40 on α-tubulin. In line with inhibition of HDACs, SAHA treatment increased the amount of acetyl-tubulin. On the other hand, treatment with C646 led to a decrease in acetyl-tubulin levels, which is in line with p300/CBP inhibition. The results demonstrate that C646 treatment inhibits acetylation and increases ERK-mediated MITF phosphorylation. In contrast, SAHA treatment increases acetylation and inhibits ERK phosphorylation of MITF.

Cancer cell lines often harbour mutations in multiple signalling pathways, resulting in the misregulation of these pathways. To verify if C646 treatment was having a bona fide effect on the MAPK pathway, or whether it was a phenomenon specific to the 501mel cell line, we examined a panel of cell lines from melanoma and melanocytes, as well as those from non-melanocytic origins (Figure 3.8; data from Robert Siddaway).

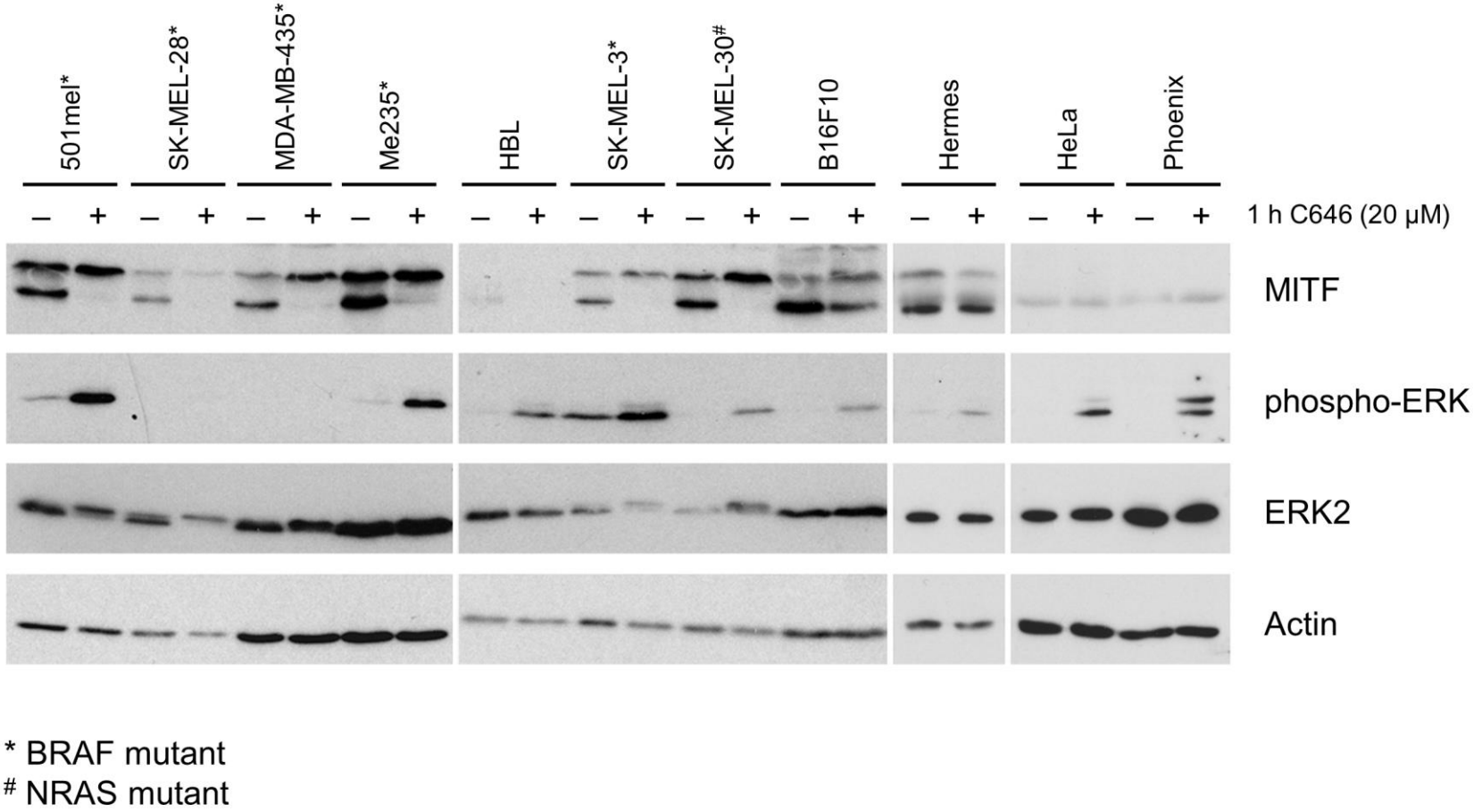

Figure 3.8 p300/CBP inhibition activated the MAPK pathway in melanoma, melanocyte and non-melanocyte cell lines, regardless of BRAF/NRAS mutational status. Western blot of different cell lines following treatment with C646. Cells were grown to 80% confluence and treated with 20 μM C646 or an equivalent volume of DMSO for 1 hour. Data from Robert Siddaway.

Following an hour-long treatment with 20 μM of C646, MAPK signalling was up-regulated in human melanoma cell lines bearing activating BRAF or NRAS mutations, as indicated by the increase in phospho-ERK staining (Figure 3.8). Even in cell lines such as SK-MEL-28 and MDA-MB-435, where the levels of phospho-ERK were not readily detectable, we were able to use ERK-mediated phosphorylation of MITF as a sensitive marker for ERK activation induced by C646 treatment. A similar pattern of increase in phospho-ERK was observed in murine B16F10 and human HBL melanoma cells, both of which do not possess mutations in BRAF or NRAS. However, MITF expression was not detected in HBL cells in this experiment. Hermes cells, which are immortalised human melanocytes, also exhibited increased phospho-ERK levels following treatment with C646, although there were no apparent changes in MITF mobility.

C646-mediated activation of the MAPK pathway was also observed in cells of non-melanocytic origin, including HeLa, a human cervical cancer cell line, and Phoenix, a derivative of the HEK293T human embryonic kidney cell line (Figure 3.8). Both HeLa and Phoenix cells exhibited a discernable increase in phospho-ERK levels in response to C646 treatment. The results indicate that C646 is able to up-regulate MAPK signalling in a number of cell lines of melanoma, melanocytic and non-melanocytic origin, regardless of BRAF and NRAS mutational statuses.

3.2.2 BRAF is acetylated by p300/CBP

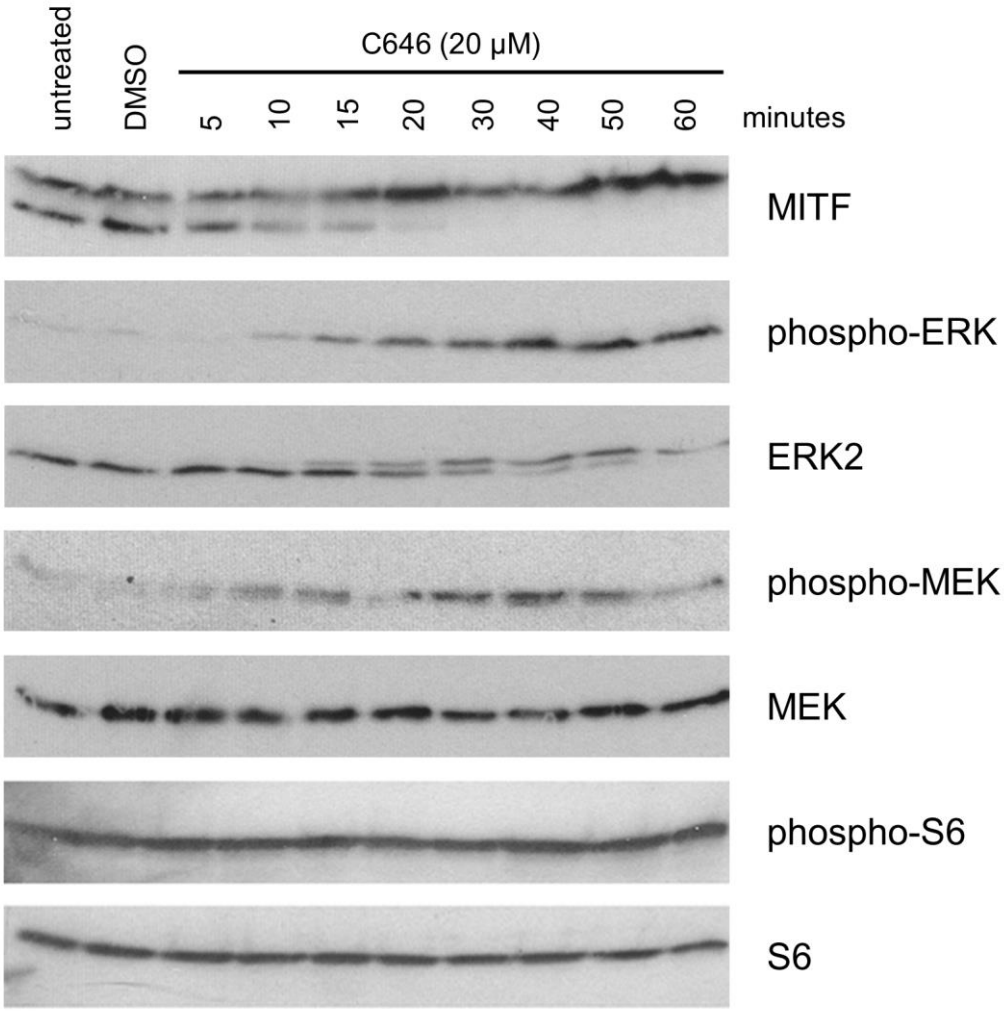

Figure 3.9 p300/CBP inhibition resulted in rapid induction of MEK phosphorylation. Western blot of 501mel cells following treatment with C646. Cells were grown to 80% confluence and treated with 20 μM C646 or an equivalent volume of DMSO for various periods of time up to 1 hour. Data from Robert Siddaway.

We sought to further understand the kinetics of MAPK activation induced by C646 treatment. We treated 501mel cells with 20 μM of C646 for various time intervals up to an hour (Figure 3.9; data from Robert Siddaway), since we already knew that phospho-ERK was up-regulated following 1 hour of C646 treatment. A rapid increase in phospho-ERK and ERK-mediated MITF phosphorylation was observed after just 15 minutes of treatment with C646. The levels of phospho-ERK

continued increasing, with maximum phospho-ERK levels observed at 40 minutes of C646 treatment, after which it remained high until at least 60 minutes.

We were conscious that the C646-mediated ERK activation could potentially occur via the crosstalk with the PI3K pathway. Hence, we also blotted for phosphorylated S6 ribosomal protein, as detected by an antibody that recognises phosphorylated S235/S236 in S6 (Figure 3.9). S6 is phosphorylated by S6K (S6 kinase), which is itself phosphorylated by mammalian target of rapamycin (mTOR), downstream of the PI3K-AKT pathway. No change was observed on S6 phosphorylation or total S6 levels upon C646 treatment, indicating that the effects of C646 on ERK were not mediated through PI3K signalling.

To identify the potential target for C646 in the MAPK pathway, we also examined MEK phosphorylation, as detected by an antibody that recognises phosphorylated S217/S221 in MEK1 and MEK2, over time following addition of C646 (Figure 3.9). The results revealed increased phosphorylation of MEK occurring after 10 minutes of C646 treatment, prior to activation of ERK. The levels of phospho-MEK continued increasing until it reached a maximum at 40 minutes of C646 treatment, after which it appeared to decrease till the 60-minute time point. No change was observed in the levels of total MEK. This suggests that C646 was acting on a component of the MAPK pathway that was upstream of MEK.

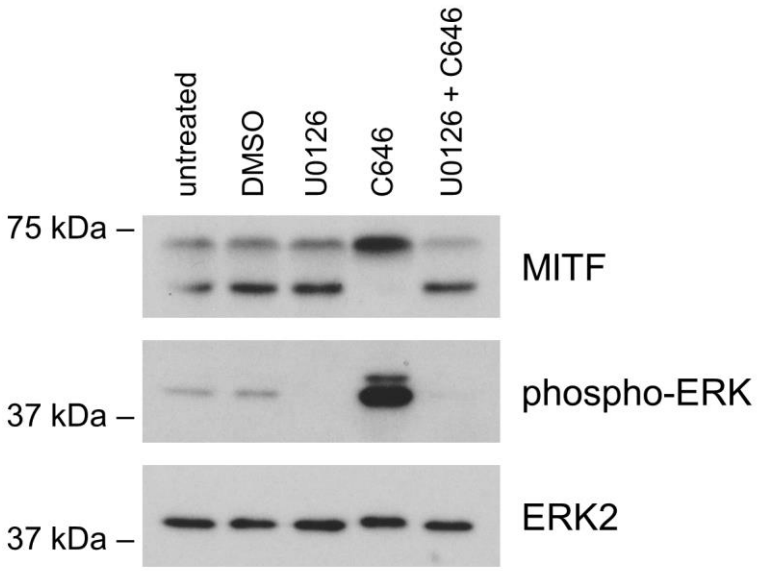

Figure 3.10 MEK inhibition prevented C646-induced activation of MAPK. Western blot of 501mel cells following treatment with C646 and/or the MEK inhibitor U0126. Cells were grown to 80% confluence and treated with 20 μM C646 for 1 hour and/or 10 μM of U0126 for 3 hours.

Consistent with this, treatment of 501mel cells with the MEK inhibitor U0126 (Favata et al., 1998) (IC_{50} < 72 nM), either on its own or in conjunction with C646, led to an almost complete abrogation of phospho-ERK levels as detected by western blot (Figure 3.10). Not only was U0126 pre-treatment able to prevent the effects of C646 on ERK phosphorylation, it could also decrease the amount of phospho-ERK below basal levels even in the presence of C646. In fact, the phospho-ERK levels observed with U0126 and C646 co-treatment were similar to that with U0126 alone. U0126 was also able to reverse ERK phosphorylation of MITF that was induced by C646.

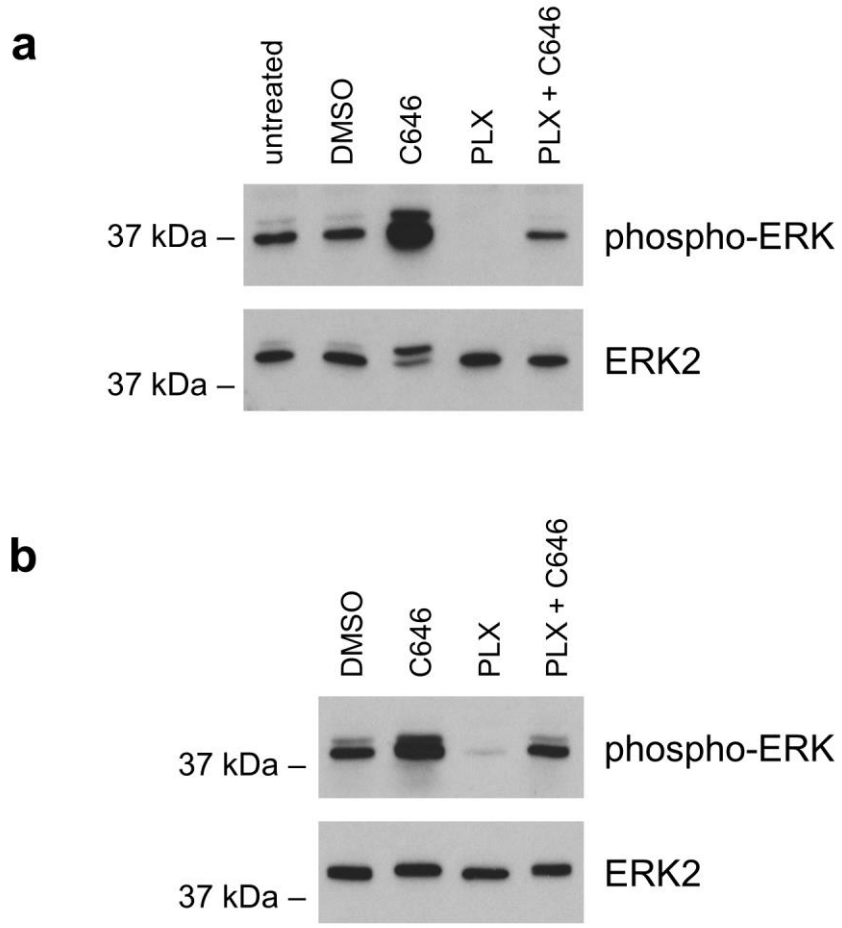

Figure 3.11 BRAF inhibition could only partially abrogate C646-induced activation of MAPK. (a) Western blot of 501mel cells following treatment with C646 and/or the BRAF inhibitor PLX4720 (abbreviated as PLX). Cells were grown to 80% confluence and treated with 20 µM C646 for 1 hour and/or 5 µM of PLX4720 for 3 hours. **(b)** Western blot of SK-MEL-28 cells following treatment with C646 and/or PLX4720. Cells were treated as in (a).

Since BRAF lies upstream of MEK, we wondered if C646 was acting on BRAF. To investigate this, we applied 5 µM of PLX4720 (Tsai et al., 2008), a small molecule inhibitor of BRAF that is the preclinical analogue of vemurafenib and exhibits ten-fold selectivity for $BRAF^{V600E}$ (IC_{50} = 13 nM) over wild-type BRAF (IC_{50} = 160 nM), to human melanoma cell lines for 3 hours. 501mel (Figure 3.11a) and SK-MEL-28 (Figure 3.11b) cells, both of which contain activating $BRAF^{V600E}$ mutations, demonstrated similar responses to C646 and PLX4720 single treatments and co-treatments. Pre-treatment with PLX4720 was sufficient to reverse the increase in ERK phosphorylation induced by C646 and return phospho-ERK to

DMSO-treated basal levels. On the other hand, if we compared co-treatment of PLX4720 and C646 to C646 treatment alone, we see that C646 was still able to induce an increase in ERK phosphorylation even in the presence of the BRAF inhibitor PLX4720, which was not the case with the MEK inhibitor U0126 (Figure 3.10). Hence, we theorised that C646 could be acting on the MAPK pathway by inducing a change in BRAF acetylation status, and possibly in other RAF isoforms as well.

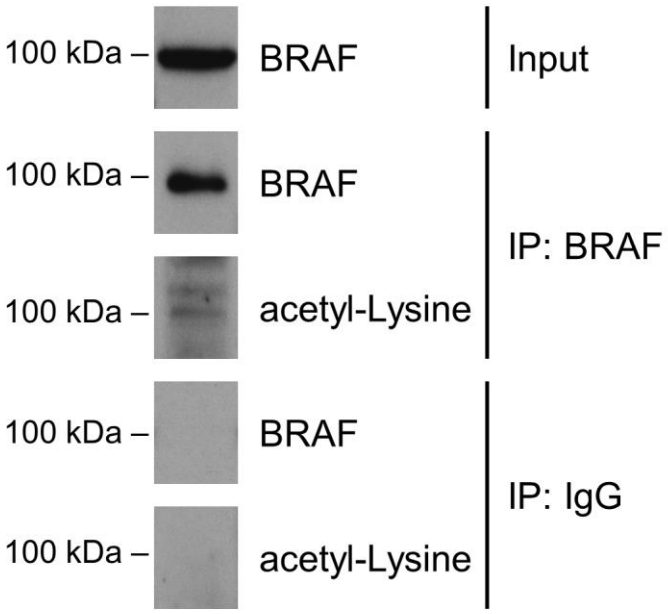

Figure 3.12 Endogenous BRAF was acetylated in melanoma cells. Western blot of SK-MEL-28 cells following immunoprecipitation of endogenous BRAF. Cells were grown to 80% confluence, then lysed and incubated overnight with an antibody recognising BRAF or mouse IgG, which acted as the negative control.

Subsequently, we sought to examine whether BRAF was acetylated in melanoma cells by immunoprecipitating endogenous BRAF protein, using an antibody that recognises BRAF, from SK-MEL-28 cells and probing its western blot with a pan-acetyl-lysine antibody that could detect acetylated lysine residues. As Figure 3.12 indicates, endogenous BRAF appears to be acetylated on at least one of its lysine residues. Acetylated lysine was not detected in the negative control, in

which immunoprecipitation was carried out with mouse IgG instead of the anti-BRAF antibody.

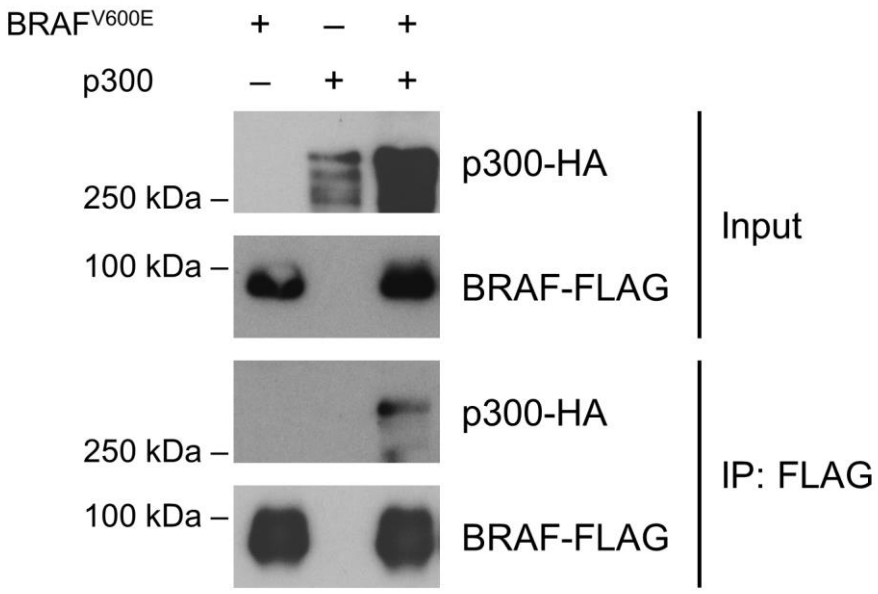

Figure 3.13 p300 co-immunoprecipitated with BRAF^{V600E}. Western blot of Phoenix cells following co-immunoprecipitation of ectopic FLAG-tagged BRAF^{V600E} and ectopic HA-tagged p300. Cells were grown to 50% confluence before being transfected using Fugene 6. After 48 hours, cells were lysed and incubated overnight with an antibody against FLAG.

To investigate if BRAF could interact with p300, we over-expressed FLAG-tagged BRAF^{V600E} together with HA-tagged p300 in Phoenix cells and did a pull-down with anti-FLAG antibody (Figure 3.13). Consistent with acetylation of BRAF being mediated by p300, p300-HA co-immunoprecipitated with BRAF-FLAG. However, expression levels of p300-HA were consistently elevated in the presence of overexpressed BRAF-FLAG versus the negative control lacking BRAF-FLAG, across multiple experimental repeats. The presence of disproportionate levels of p300-HA in the input means that it may be inappropriate to draw conclusions from the negative control. That said, we were unable to detect any traces of p300-HA in the negative control immunoprecipitation of BRAF-FLAG even after pro-longed overexposure of the blots (data not shown). Since we were interested in the presence

or absence of p300-HA in the pull-down, rather than its relative levels, we felt quite confident that p300-HA was not pulled down in the absence of BRAF-FLAG, which suggests that there is a specific interaction between p300 and BRAF.

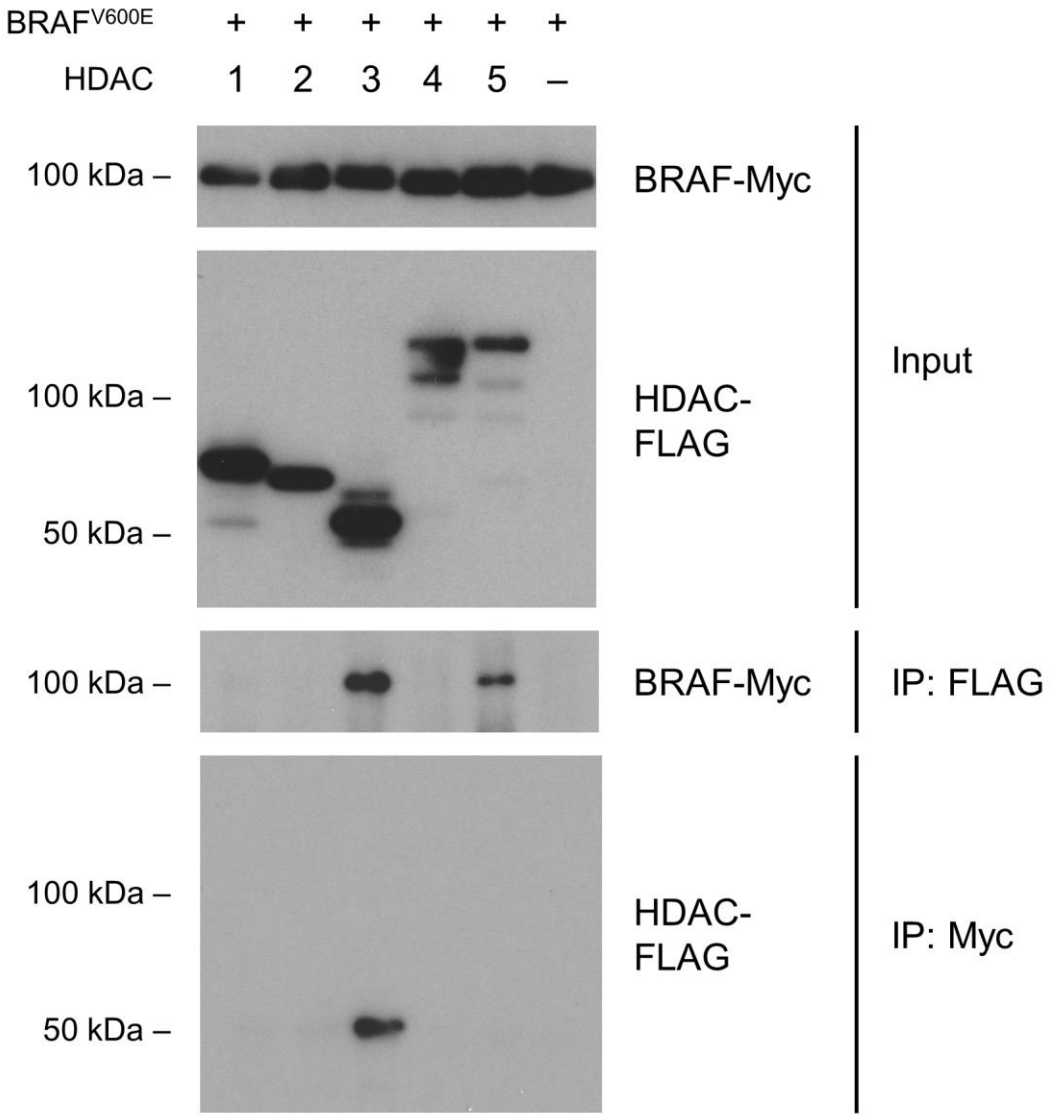

Figure 3.14 HDAC3 co-immunoprecipitated with BRAF^{V600E}. Western blot of Phoenix cells following co-immunoprecipitation of ectopic Myc-tagged BRAF^{V600E} and various FLAG-tagged HDACs. Cells were grown to 50% confluence, then transfected using Fugene 6. After 48 hours, cells were lysed and incubated overnight with an antibody against FLAG or an antibody against Myc.

We were also interested in finding out if BRAF could interact with histone deacetylases (HDACs). We over-expressed Myc-tagged BRAF^{V600E} together with FLAG-tagged HDAC1, HDAC2, HDAC3, HDAC4 or HDAC5 in Phoenix cells and

did a pull-down with both anti-FLAG antibody and anti-Myc antibody (Figure 3.14). $BRAF^{V600E}$ was pulled down with both HDAC3 and HDAC5. However, HDAC3 was the only one which co-immunoprecipitated with $BRAF^{V600E}$. These results show that $BRAF^{V600E}$ can interact with HDAC3 specifically.

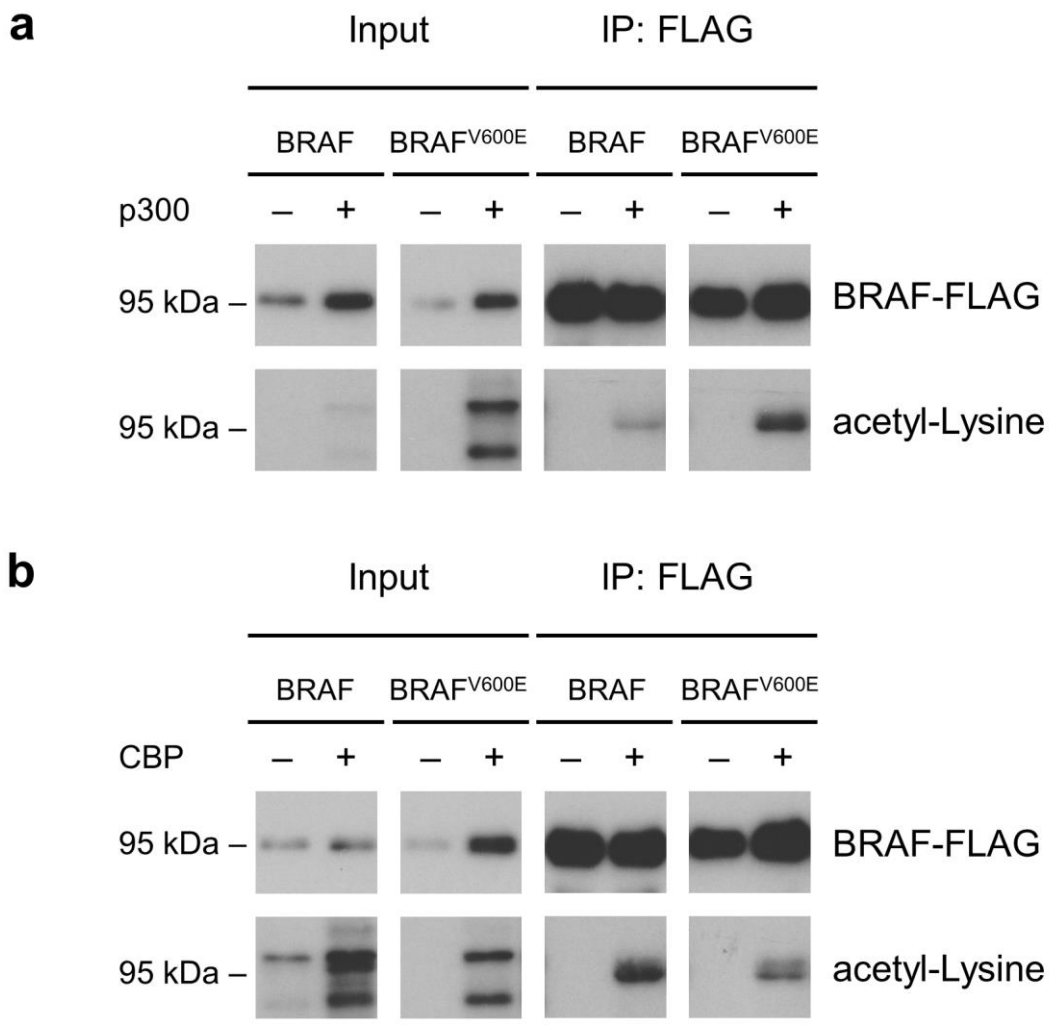

Figure 3.15 BRAF could be acetylated by both p300 and CBP. (a) Western blot of Phoenix cells following immunoprecipitation of ectopic FLAG-tagged $BRAF^{V600E}$ in the presence of ectopic HA-tagged p300. Cells were grown to 50% confluence before being transfected using Fugene 6. After 48 hours, cells were lysed and incubated overnight with an antibody against FLAG. **(b)** Western blot of Phoenix cells following immunoprecipitation of ectopic FLAG-tagged $BRAF^{V600E}$ in the presence of ectopic HA-tagged CBP. Cells were prepared as in (a), with HA-tagged CBP being used in place of HA-tagged p300.

Next, we asked whether BRAF could be acetylated by p300 or its close relative CBP. We co-expressed HA-tagged p300 with FLAG-tagged wild-type BRAF or

FLAG-tagged $BRAF^{V600E}$ in Phoenix cells (Figure 3.15a). We also did the same with HA-tagged CBP replacing HA-tagged p300 (Figure 3.15b). We then immunoprecipitated BRAF-FLAG with an anti-FLAG antibody conjugated to agarose beads. Acetylation of both wild-type BRAF and the $BRAF^{V600E}$ mutant was substantially increased by co-expression with either p300 or CBP, as revealed by western blotting of immunoprecipitated BRAF with the pan-acetyl-lysine antibody. On the other hand, in the absence of ectopically expressed p300 or CBP, acetylated lysines were not detected on either wild-type BRAF or $BRAF^{V600E}$. However, this might be an artefact arising from the BRAF overexpression. In terms of relative abundance, ectopically expressed BRAF might be present in so much excess that endogenous p300/CBP was unable to acetylate the vast majority of it, and so the proportion of BRAF that got acetylated was too low to be detected.

3.2.3 BRAF is acetylated at K473 and K475

Mass spectrometry of immunoprecipitated BRAF revealed 4 acetylation sites on K150, K418, K473 and K475 (Figure 3.16). The K473 and K475 residues were of particular interest to us as they lay inside the kinase domain of BRAF. Importantly, rare K475 mutations are found in colorectal cancer (K475R) as well as melanoma (K475M) in the absence of other activating BRAF mutations, according to the COSMIC database (Forbes et al., 2015). Both K473 and K475 are also highly evolutionarily conserved across multiple species (Figure 3.16). Another significant observation is that both residues are also found in human CRAF, but are substituted in ARAF by arginine, which functions as a mimic of non-acetylated lysine since it shares a similar positive charge but cannot be acetylated.

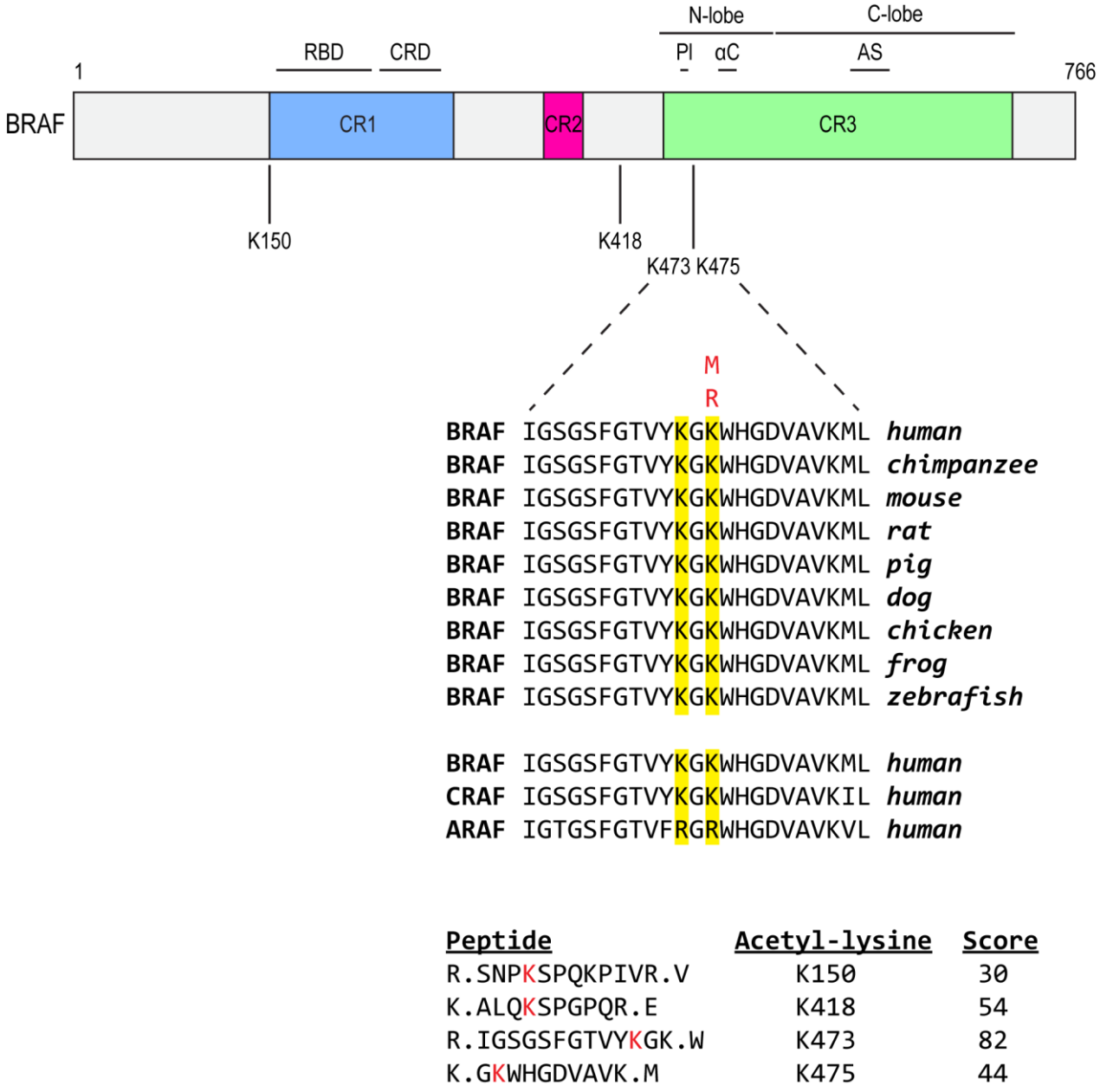

Peptide	Acetyl-lysine	Score
R.SNPKSPQKPIVR.V	K150	30
K.ALQKSPGPQR.E	K418	54
R.IGSGSFGTVYKGK.W	K473	82
K.GKWHGDVAVK.M	K475	44

Figure 3.16 BRAF was acetylated by p300 at the highly conserved K473 and K475 residues. Top: Relative positions of the four acetylated lysine residues in BRAF identified by mass spectrometry. The key features of BRAF are indicated, including conserved regions (CR) 1, 2 and 3, as well as the RAS-binding domain (RBD), cysteine-rich domain (CRD), N-terminal lobe (N-lobe), C-terminal lobe (C-lobe), P-loop (Pl), αC and activation segment (AS). Middle: K473 and K475 are evolutionarily conserved in BRAF across species, as well as in the CRAF isoform. Mutations (in red) at K475 in BRAF were also found in melanoma and colorectal patient samples in the COSMIC database. Bottom: Four acetylated lysine residues were detected in BRAF via mass spectrometry. Phoenix cells were grown to 50% confluence, then transfected via Fugene 6 with plasmids encoding FLAG-tagged $BRAF^{V600E}$ and HA-tagged p300. After 48 hours, cells were lysed and incubated overnight with an antibody against FLAG. Immunoprecipitated $BRAF^{V600E}$-FLAG was then resolved by SDS-PAGE and processed for mass spectrometry. Acetylated residues are marked in red on their respective peptide fragments. The ion score for each peptide is also indicated, with a score ≥20 considered statistically significant.

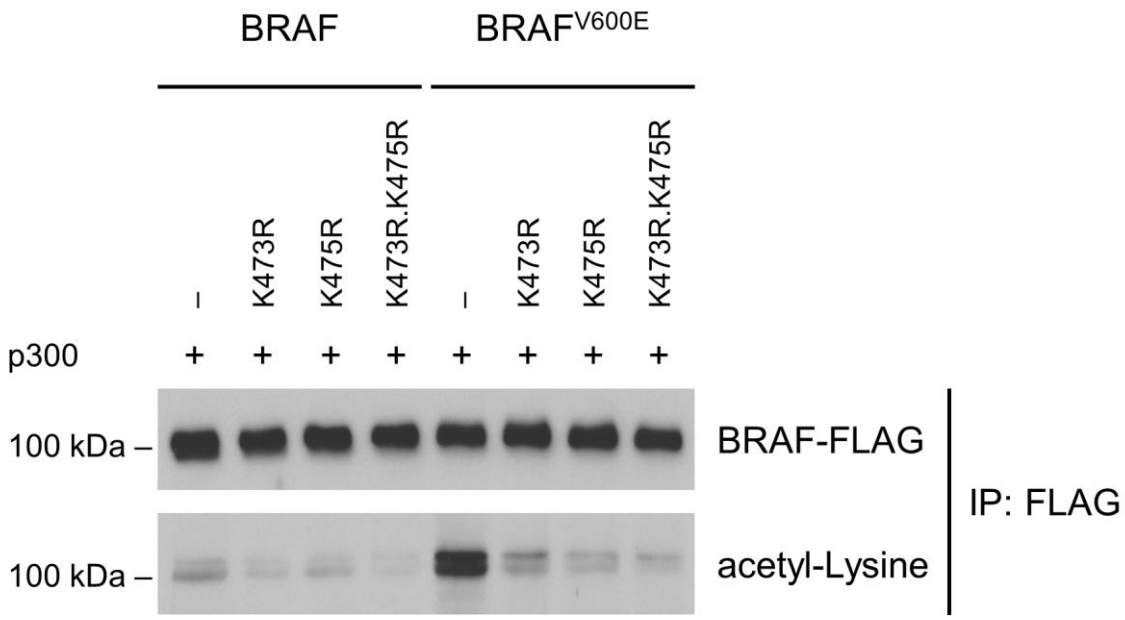

Figure 3.17 p300-mediated acetylation was abrogated with single and double mutations of the K473 and K475 residues in BRAF. Western blot of Phoenix cells following immunoprecipitation of various ectopic FLAG-tagged BRAF mutants in the presence of ectopic HA-tagged p300. Cells were grown to 50% confluence before being transfected using Fugene 6. After 48 hours, cells were lysed and incubated overnight with an antibody against FLAG.

To verify that the BRAF K473 and K475 residues were indeed acetylated, we mutated the lysine residues at K473 and K475 to arginine residues, which cannot be acetylated, in both FLAG-tagged wild-type BRAF and FLAG-tagged $BRAF^{V600E}$. We then overexpressed these BRAF-FLAG mutants together with p300-HA in Phoenix cells. Following immunoprecipitation, wild-type BRAF and $BRAF^{V600E}$ bearing mutations in K473 and/or K475 were probed with pan-acetyl-lysine antibodies on a western blot (Figure 3.17). For wild-type BRAF, the single K473R and K475R mutants both exhibited reduced acetylation, while the double K473R.K475R mutant was more severely affected. The effect on $BRAF^{V600E}$ was even more dramatic, with basal acetylation being higher than wild-type BRAF, most likely because increased MAPK signalling downstream from this mutant effectively increases global acetylation by p300 (unpublished data, Robert Siddaway).

Consistent with BRAF^{V600E} K473 and K475 being acetylated, mutation of either or both residues to arginine led to a substantial loss of acetylation, with the residual acetylation observed presumably reflecting modification of K150 and K418.

3.2.4 K473/K475 acetylation inhibits BRAF kinase activity in vitro

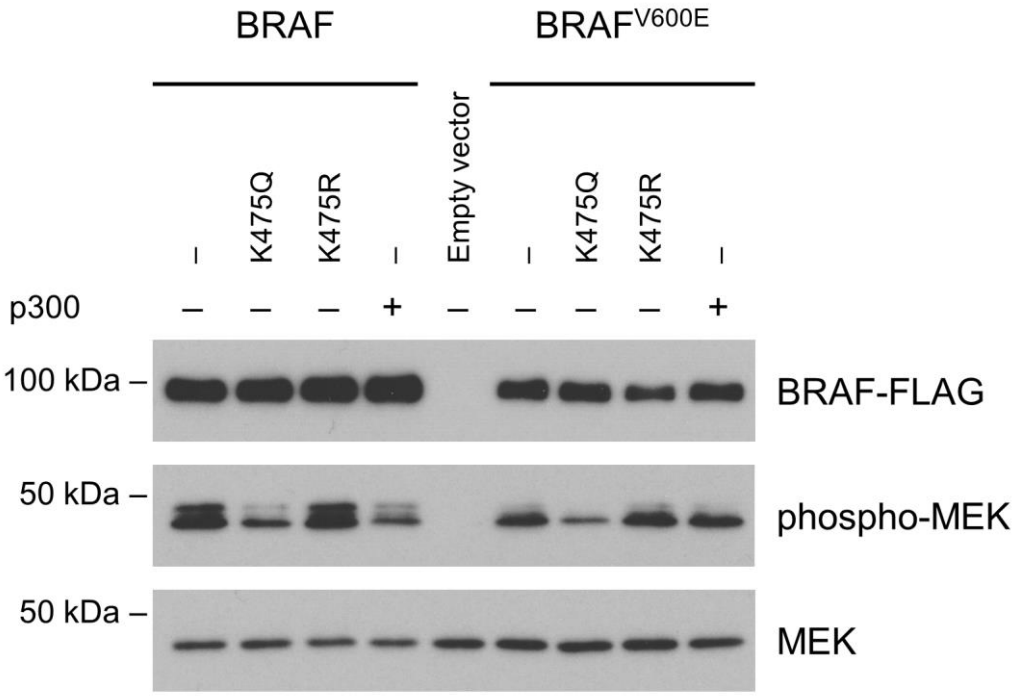

Figure 3.18 BRAF kinase activity was inhibited by acetylation at K475. *In vitro* kinase assay with immunoprecipitated FLAG-tagged BRAF mutants and purified MEK2. Phoenix cells were grown to 50% confluence before being transfected via Fugene 6 with plasmids encoding BRAF-FLAG mutants and p300-HA. After 48 hours, cells were lysed and incubated overnight with an antibody against FLAG. Immunoprecipitated BRAF-FLAG mutants were incubated with 1 µg of MEK2 and 200 µM ATP at 30°C for 15 minutes. The amount of MEK2 phosphorylation was subsequently determined by immunoblotting with phospho-MEK antibody.

To examine the consequences of BRAF acetylation, we initially mutated the BRAF K475 residue to a non-acetylatable arginine residue, as found in colon cancer and in ARAF, or to glutamine, which mimics the acetylated form of lysine that has its positive charge neutralised. We then examined the capacity of the wild-type and

mutant BRAF proteins to phosphorylate MEK2 *in vitro*, as detected by western blotting with a phospho-specific antibody that recognises phosphorylated S217 and S221 in MEK (Figure 3.18). Immunoprecipitated FLAG-tagged BRAF was able to efficiently phosphorylate bacterially-expressed and purified MEK2 protein, with phosphorylation being reduced by the acetyl-lysine-mimicking K475Q mutation, but not the non-acetylatable K475R substitution. In line with acetylation having an inhibitory effect on BRAF kinase activity, co-expression of ectopic p300 reduced the capacity of BRAF to phosphorylate MEK. Similar results were obtained in the $BRAF^{V600E}$ variant background, though ectopic p300 had a much smaller effect on MEK phosphorylation in this case. The results suggest that acetylation at K475 inhibits the ability of BRAF to phosphorylate MEK, independent of its mutational status at the V600 residue.

We were also interested in the effects of acetylation at the K473 residue due to its proximity to the K475 residue, which we already demonstrated to be a key residue affecting on BRAF activity. We next compared the effects of the single mutations to double mutations at the K473 and K475 residues, based on their ability to phosphorylate MEK in an *in vitro* kinase assay (Figure 3.19). Consistent with the results of the BRAF acetylation at both residues, the K473Q.K475Q double mutation blocked the ability of BRAF to phosphorylate MEK, while the K473R.K475R double mutant decreased MEK phosphorylation slightly (Figure 3.19a). Both the K473Q and K475Q single mutants impaired MEK phosphorylation, though a slightly greater effect was observed with the K473Q mutant. The single lysine to glutamine mutations were less effective than the double glutamine substitutions in disrupting MEK phosphorylation. Again, the single lysine to arginine mutations had no major effect on BRAF kinase activity *in vitro*, inducing only slight decreases in MEK

phosphorylation. Similar results were obtained with these mutations in the $BRAF^{V600E}$ background (Figure 3.19b). Thus, surprisingly, the results are consistent with acetylation-mediated inhibition of BRAF being dominant over the activating $BRAF^{V600E}$ mutation, at least in the *in vitro* context.

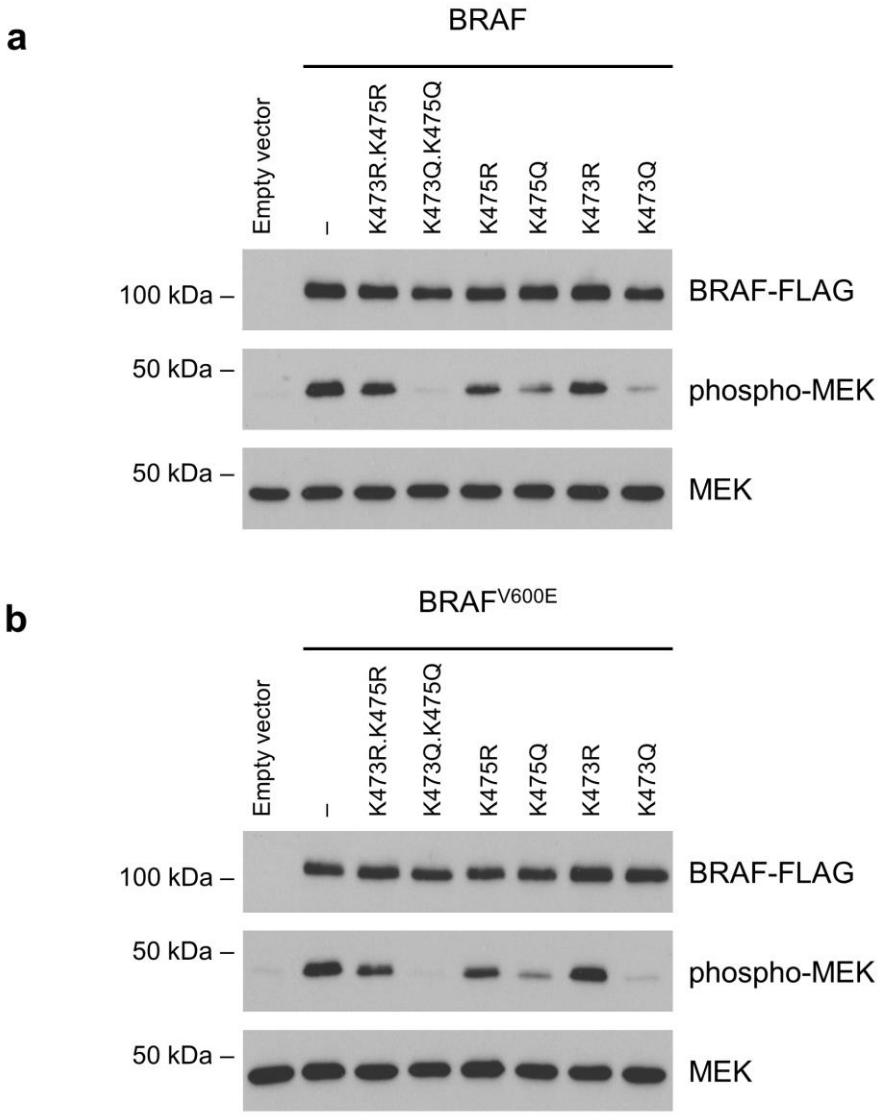

Figure 3.19 BRAF kinase activity was inhibited by acetyl-mimicking glutamine substitutions at K473 and K475. (a) *In vitro* kinase assay with purified MEK2 in the presence of K473 and K475 mutants of FLAG-tagged BRAF. Phoenix cells were grown to 50% confluence before being transfected via Fugene 6 with plasmids encoding BRAF-FLAG mutants and p300-HA. After 48 hours, cells were lysed and incubated overnight with an antibody against FLAG. Immunoprecipitated BRAF-FLAG mutants were incubated with 1 μg of MEK2 and 200 μM ATP at 30°C for 15 minutes. The amount of MEK2 phosphorylation was subsequently determined by immunoblotting with phospho-MEK antibody. **(b)** *In vitro* kinase assay with purified MEK2 in the presence of K473 and K475 mutants of FLAG-tagged $BRAF^{V600E}$. Reaction conditions were similar to that in (a).

3.2.5 K473/K475 acetylation inhibits BRAF kinase activity in cells

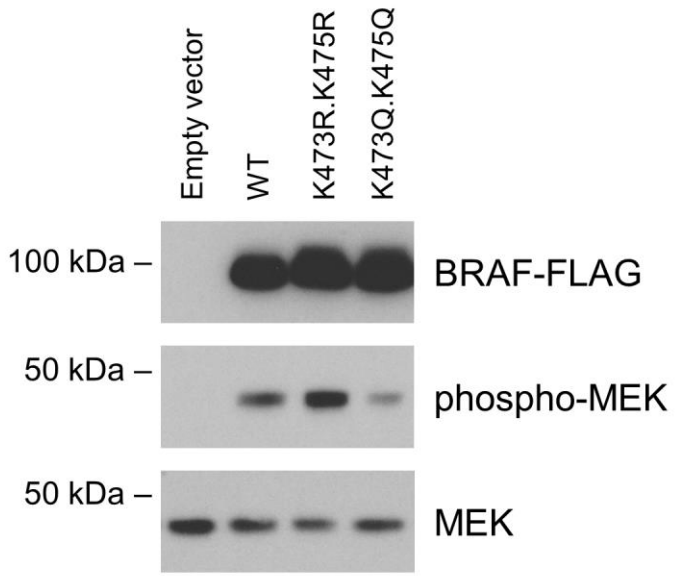

Figure 3.20 The acetyl-mimicking K473Q.K475Q double mutation in BRAF reduced its kinase activity in Phoenix cells. Western blot of Phoenix cells expressing ectopic K473 and K475 mutants of BRAF-FLAG. Cells were grown to 50% confluence before being transfected using Fugene 6. After 48 hours, cells were lysed and processed for western blotting.

These conclusions were reinforced by examining the phosphorylation of MEK in cell culture models following transient transfection of Phoenix cells with FLAG-tagged wild-type BRAF, as well as the K473Q.K475Q and K473R.K475R double mutants. Western blotting with a phospho-specific antibody revealed reduced phosphorylation of MEK in the presence of the K473Q.K475Q acetyl-mimic compared to wild-type BRAF (Figure 3.20). In contrast, phospho-MEK levels were elevated with the non-acetylatable K473R.K475R mutant relative to the wild-type protein, although this might be due to the K473R.K475R mutant being expressed in slightly greater amounts. The results obtained with the K473Q.K475Q mutant in the stable cell line were consistent with the observations from the *in vitro* kinase assay described previously, once again highlighting the inhibitory effect of K473 and K475 acetylation on BRAF kinase activity.

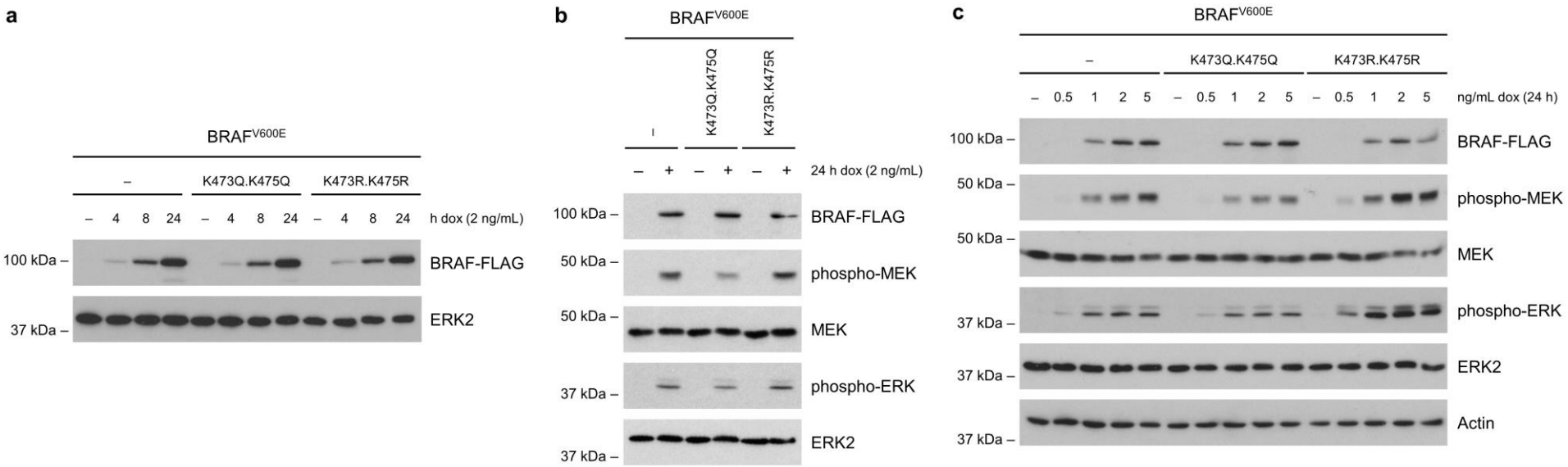

Figure 3.21 Stable polyclonal HeLa Flp-In T-rex cell lines expressing tetracycline-inducible BRAF^{V600E}-FLAG mutants. (a) Induction of BRAF^{V600E}-FLAG expression, as determined by western blot, over a period of up to 24 hours with 2 ng/mL doxycycline. Each cell line expresses a different mutant, but to similar levels. **(b)** Western blot of HeLa Flp-In T-rex cells after 24-hour induction of BRAF^{V600E}-FLAG expression with 2 ng/mL doxycycline. **(c)** Western blot of HeLa Flp-In T-rex cells after 24-hour induction of BRAF^{V600E}-FLAG expression with various concentrations of doxycycline.

We were also curious about the effects of K473 and K475 mutations on the kinase activity of $BRAF^{V600E}$, the most common BRAF mutation in melanoma, in a cell culture model. To investigate, we made use of the Flp-In T-rex system from Invitrogen to generate stable, tetracycline-responsive HeLa cell lines expressing FLAG-tagged $BRAF^{V600E}$ as well as its respective K473Q.K475Q and K473R.K475R double mutants. The HeLa Flp-In T-rex cell line also constitutively expressed the Tet repressor, which bound to Tet operator sequences in the promoter driving expression of BRAF and thus repressed BRAF expression in the absence of tetracycline. In the presence of tetracycline, the Tet repressor is unable to bind to the promoter driving BRAF expression, thus resulting in derepression and induction of BRAF expression.

To induce expression of BRAF, we treated the three stable cell lines with 2 ng/mL of doxycycline, a tetracycline analogue that possesses a longer half-life, and followed BRAF-FLAG levels over a period of 24 hours as detected by western blotting (Figure 3.21a). Following the addition of doxycycline, BRAF-FLAG levels increased over time and reached a maximum at 24 hours, the endpoint of the experiment. This was true for all three cell lines, which were expressing either $BRAF^{V600E}$-FLAG or its respective K473Q.K475Q and K473R.K475R double mutants but at very similar levels to each other. In the absence of doxycycline, expression of BRAF-FLAG was not detected, demonstrating that BRAF expression was tightly controlled by doxycycline.

Subsequently, we treated the stable cell lines with 2 ng/mL of doxycycline for 24 hours and determined MEK and ERK phosphorylation levels by western blot. As shown in Figure 3.21b, BRAF-FLAG expression was induced to a similar level in all three cell lines. In line with previous results, expression of the K473Q.K475Q double

mutant gave the lowest amount of phospho-MEK among the three cell lines, while the K473R.K475R double mutant induced the largest increase in MEK phosphorylation. This trend was also true for ERK phosphorylation, although the differences in phospho-ERK levels were less stark compared to the contrast observed with phospho-MEK. No differences were observed in both total MEK and ERK2 levels. In addition, phospho-MEK and phospho-ERK levels were also too low to be detected in the absence of BRAF-FLAG induction by doxycycline, suggesting that the observed disparities in MEK and ERK phosphorylation were due to differences in BRAF kinase activity between the mutants.

We also wanted to see whether the inhibitory effect of the K473Q.K475Q mutation on BRAF kinase activity would hold true regardless of the absolute amount of BRAF. To investigate this, we treated the three HeLa stable cell lines with varying concentrations of doxycycline ranging from 0 to 5 ng/mL for a total of 24 hours. As shown in Figure 3.21c, BRAF-FLAG expression increased as doxycycline concentration was raised from 0 to 2 ng/mL. However, there was little to no increase between 2 and 5 ng/mL of doxycycline, which suggested that 2 ng/mL of doxycycline was sufficient to induce maximum expression of BRAF-FLAG in these cell lines. In terms of MEK phosphorylation, phospho-MEK levels were closely correlated to BRAF expression levels, with higher BRAF-FLAG expression inducing an increase in MEK phosphorylation for all three BRAF mutants. However, despite expression levels of BRAF-FLAG being uniform across all three cell lines, the K473Q.K475Q double mutant had consistently lower amounts of MEK phosphorylation compared to the unmutated one and the K473R.K475R double mutant, at any given concentration of doxycycline. In contrast, the K473R.K475R double mutant had consistently higher amounts of MEK phosphorylation at any

given concentration of doxycycline. As before, these observations also held true for phospho-ERK levels although differences in ERK phosphorylation were again slightly less apparent compared to the contrast in the MEK phosphorylation results. In line with the *in vitro* data presented previously, the data from the stable cell lines suggests that BRAF acetylation at K473 and K475 had an inhibitory effect on BRAF kinase activity regardless of V600 mutational status.

3.2.6 BRAF acetylation inhibits its interaction with MEK

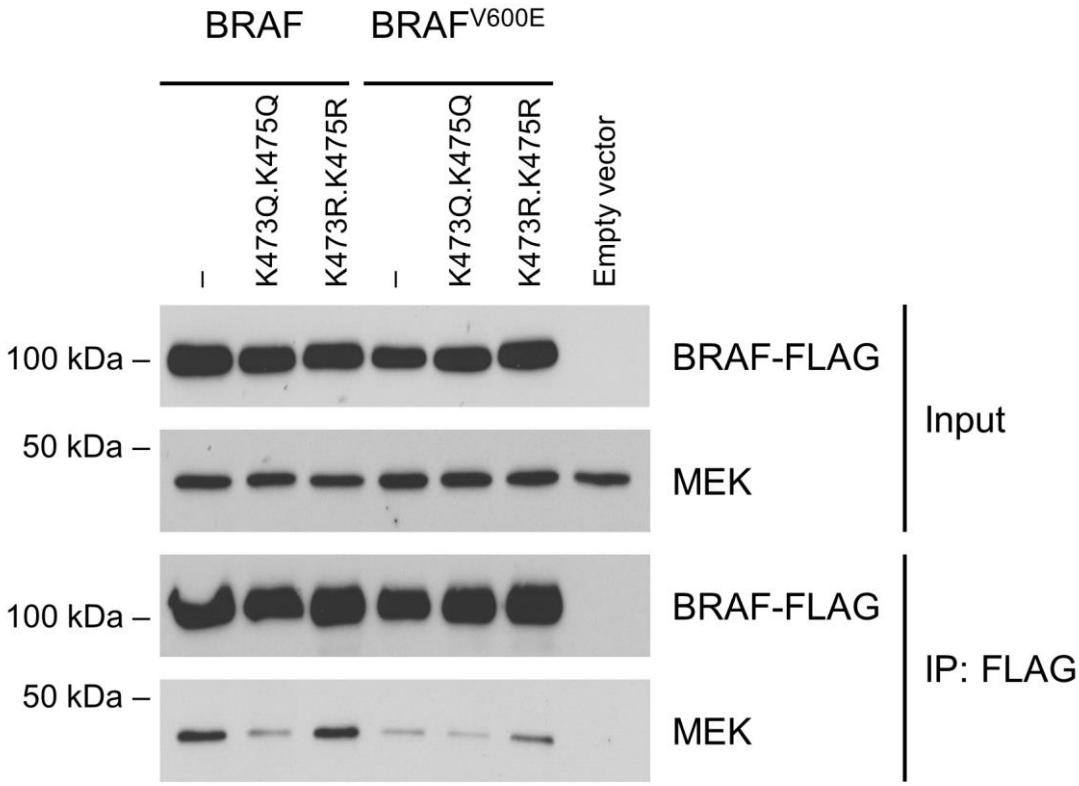

Figure 3.22 MEK2 co-immunoprecipitated less efficiently with the K473Q.K475Q mutant of BRAF-FLAG. Western blot of Phoenix cells following co-immunoprecipitation of purified MEK2 with ectopic K473 and K475 mutants of BRAF-FLAG. Cells were grown to 50% confluence before being transfected via Fugene 6 with plasmids encoding BRAF-FLAG mutants. After 48 hours, cells were lysed and incubated overnight with 1 μg of purified MEK2 and an antibody against FLAG.

Although our data is consistent with BRAF acetylation affecting its kinase activity, the results thus far were devoid of any mechanistic insights. We postulated that acetylation of BRAF might be affecting its interaction with MEK. To investigate this theory, we overexpressed FLAG-tagged BRAF and $BRAF^{V600E}$, along with their respective K473Q.K475Q and K473R.K475R double mutants, in Phoenix cells. After lysing the cells, we incubated the lysate with bacterially-expressed MEK2 protein, before doing a pull-down with anti-FLAG antibody. As shown in Figure 3.22, MEK was able to co-immunoprecipitate with all of the BRAF variants tested, but did so poorly with the K473Q.K475Q double mutant compared to the wild-type or the K473R.K475R mutant. The acetyl mutants in the $BRAF^{V600E}$ background exhibited a similar trend, with the K473R.K475R mutant co-immunoprecipitating MEK more efficiently than the K473Q.K475Q mutant. There was a smaller difference between the $BRAF^{V600E}$ K473Q.K475Q mutant and $BRAF^{V600E}$ in terms of the amount of MEK that was co-immunoprecipitated, but this might have been a result of there being less $BRAF^{V600E}$ pulled down. In the absence of BRAF-FLAG, we were unable to detect any co-immunoprecipitation of MEK, indicating that this interaction was specific to BRAF and MEK. The results demonstrate that acetylation of BRAF inhibited its ability to bind to MEK, thus providing a mechanism for the inability of acetylated BRAF to phosphorylate MEK.

3.3 Discussion

The MAPK pathway is traditionally portrayed as a unidirectional pathway in which extracellular stimuli, such as growth factors, bind to membrane receptors and induce the activation of downstream effectors of cellular processes via the RAS/RAF/MEK/ERK signalling cascade. It may be tempting to think of the MAPK

pathway as a simple, linear pathway, especially since RAF and MEK are generally considered to have only one substrate each. However, the existence of various isoforms at each tier of the signalling cascade lends complexity to the pathway. For example, there are three RAS isoforms (HRAS, KRAS, NRAS), three RAF isoforms (ARAF, BRAF, CRAF), two MEK isoforms (MEK1, MEK2) and two ERK isoforms (ERK1, ERK2). Since RAF signals as a dimer, each of the three RAF isoforms can form homo- and heterodimers with one another, which makes for a total of six unique dimeric combinations. The presence of these various isoforms makes the MAPK cascade a highly branched pathway.

In addition, the MAPK pathway is by no means unidirectional, due to the existence of numerous regulatory feedback loops along the RAS/RAF/MEK/ERK signalling cascade that serve to modulate MAPK output in a spatiotemporal manner. The importance of temporal dynamics in MAPK signalling was underlined by classical studies demonstrating the link between the duration of ERK activation and cell fate decisions (Marshall, 1995). For example, transient activation of ERK by epidermal growth factor (EGF) stimulated proliferation in rat pheochromocytoma PC-12 cells (Huff et al., 1981; Nguyen et al., 1993). On the other hand, sustained ERK signalling, which was induced by nerve growth factor (NGF), triggered neuronal differentiation in the same cell type (Cowley et al., 1994; Nguyen et al., 1993; Traverse et al., 1994). However, the converse may apply in other cell types, such as in mouse NIH 3T3 fibroblasts where sustained ERK activation is correlated with proliferation (Cowley et al., 1994; Mansour et al., 1994). This adds a further layer of complexity to the MAPK pathway.

The great versatility in the magnitude and dynamics of MAPK output derives from the aggregate effect of regulation at each tier of the signalling cascade by

multiple mechanisms (Kholodenko, 2006; Kholodenko et al., 2010; von Kriegsheim et al., 2009; Santos et al., 2007). As outlined in Chapter 3.1, a substantial portion of their regulation is mediated by post-translational modifications, particularly in the case of RAF. So far, the regulation of RAF by post-translational modifications have been mainly described in the context of phosphorylation. Our data suggests that BRAF is acetylated, and that its acetylation plays an important role in regulating MAPK output.

We showed by mass spectrometry that BRAF can be acetylated by the p300 acetyltransferase on at least four separate lysine residues – K150, K418, K473 and K475. In line with this finding, acetylation at K418 was also previously described in a landmark study of the acetylome (Choudhary et al., 2009), which provided the first proteome-wide survey of lysine acetylation in human cells. Although the other three lysine residues were not picked up as acetylation sites in the previous study, we were not alarmed as this might have been due to the transient nature of the modification, or technical reasons such as poor antibody specificity resulting in the lack of sensitivity for low abundance sites.

Our investigations were mainly focussed on the K473 and K475 residues due to their location in the kinase domain of BRAF. As shown in Figure 3.16, the sequence at residues 473-475 of BRAF is KGK. This sequence fits the GK recognition motif that was previously identified as a target of p300/CBP acetylation in a separate study (Bannister et al., 2000). Notably, BRAF mutations at K475 have been detected in cancer, although these are extremely rare events. For example, according to the COSMIC database, there have been three individual cases of $BRAF^{K475R}$ mutations detected in colon cancer, and a single case of $BRAF^{K475M}$ in melanoma (Forbes et al., 2015). The K475R mutation in colon cancer was of

particular interest to us because the lysine at residue 475 has been substituted for an arginine, which has similar characteristics as lysine but cannot be acetylated. BRAF mutations are also known to be drivers of tumorigenesis in colon cancer (Muzny et al., 2012), and this K475R was the only BRAF mutation found in the three cases. Both K473 and K475 residues in BRAF are also conserved evolutionarily across multiple species, as well as in CRAF, another isoform of RAF. Interestingly, K473 and K475 are not conserved in the ARAF isoform, but are instead substituted for the non-acetylatable arginine residue. Arginine residues are also found at the equivalent positions in the KSR scaffold protein, which is capable of dimerising with RAF.

Our data shows that by introducing a lysine to glutamine substitution at both K473 and K475 in BRAF, we can abrogate the ability of BRAF to phosphorylate MEK both *in vitro* and in cell culture models. Glutamine is commonly used as a mimic of acetylated lysine due to their similarities in charge and chemical structure (Li et al., 2002). Glutamine substitution at either of these residues in BRAF was sufficient to reduce MEK phosphorylation, while mutating both sites to glutamine led to an additive effect in terms of even greater inhibition of BRAF kinase activity. The importance of the K473 and K475 sites has also been highlighted in previous studies of CRAF (Lu et al., 1998), where kinase activity was completely abrogated when the equivalent residues in CRAF was mutated to alanine, which can also potentially mimic acetylated lysine through neutralisation of the positive charge. However, the reason behind CRAF activity being affected by mutation of these residues was not determined. Our results would suggest that CRAF, like BRAF, is also acetylated on these sites and that the presence of a basic residue is critical for MEK phosphorylation.

In contrast, an arginine substitution, which mimics the positive charge of lysine while blocking acetylation, at either one of these sites had little effect on BRAF kinase activity. Perplexingly, the K473R.K475R double mutants had slightly reduced kinase activity *in vitro* compared to the unmutated form, while it exhibited increased kinase activity in cell lines. However, this may also be a result of there being different starting levels of BRAF acetylation across the two assays. In the *in vitro* assay, BRAF-expressing cells were first lysed before immunoprecipitating BRAF overnight, during which time a proportion of inhibitory endogenous acetylation might have been lost.

Downstream of MEK, ERK phosphorylation was also reduced with the K473Q.K475Q double mutant and elevated with the K473R.K475R double mutant. However, the differences in ERK phosphorylation were less stark compared to those observed with MEK phosphorylation. This may be mediated by negative feedback mechanisms that act directly on ERK to modulate ERK phosphorylation, such as DUSPs.

Mechanistically, our data suggests that acetylation-mediated inhibition of BRAF kinase activity was caused by interference of the interaction between BRAF and MEK, as indicated by results of co-immunoprecipitation experiments. However, based on the recently elucidated co-crystal structure of the BRAF-MEK1 complex (Haling et al., 2014), the K473 and K475 residues in BRAF do not appear to be part of the BRAF-MEK interaction interface. Interestingly, the RAF proteins can dimerise with each other via a side-to-side interface involving the N-lobe of their kinase domains, and residues W476 to G478 (in BRAF) form an integral part of this dimerisation interface (Rajakulendran et al., 2009). The equivalent residues are also conserved in the KSR organising scaffold protein and participate in the dimerisation

between KSR and RAF (Rajakulendran et al., 2009). Since RAF dimerisation with itself and KSR is an important step in MEK phosphorylation (Brennan et al., 2011), we postulate that lysine acetylation at K473 and K475 may possibly inhibit BRAF kinase activity by affecting its dimerisation, given the close proximity of the two lysine residues to W476 in the side-to-side dimerisation interface. Another possibility is that K473 and K475 acetylation affects the nearby glycine rich P-loop (G464 – V471 in BRAF), which plays a key role in ATP anchorage and orientation.

Importantly, acetylation of BRAF affects its kinase activity regardless of V600 mutational status. This raises the possibility that altering BRAF acetylation status may be of therapeutic benefit to patients who possess activating BRAF V600 mutations, as well patients who have mutations in other BRAF residues or even other members of the MAPK pathway such as NRAS. In line with BRAF acetylation having an inhibitory effect on MAPK output, p300 expression levels have been shown to correlate positively with survival in melanoma patients (Bhandaru et al., 2014). Another study showed that co-treatment with the pan-HDAC inhibitor SAHA and the $BRAF^{V600E}$ inhibitor PLX4720 resulted in synergistic killing of $BRAF^{V600E}$-positive melanoma cells, but not melanocytes (Lai et al., 2013). However, similar to what we observed in our own experiments, phospho-ERK levels did not appear to be affected by SAHA (Lai et al., 2013).

Although BRAF inhibition has been a significant development in the terms of melanoma therapy, it is rarely curative, with a common occurrence being an initial dramatic remission of the disease, followed by an equally spectacular relapse in virtually identical tumour locations (Wagle et al., 2011) (Figure 1.7). The durability of the response to BRAF inhibition is limited by the acquisition of resistance mechanisms, often via mutations in other members of the MAPK pathway. In a bid

to forestall tumour relapse mediated by acquired resistance to BRAF inhibition, researchers have increasingly turned to combinatorial therapies, such as co-treatment with both BRAF inhibitors and MEK inhibitors, being employed in many recent clinical trials (Schadendorf et al., 2015).

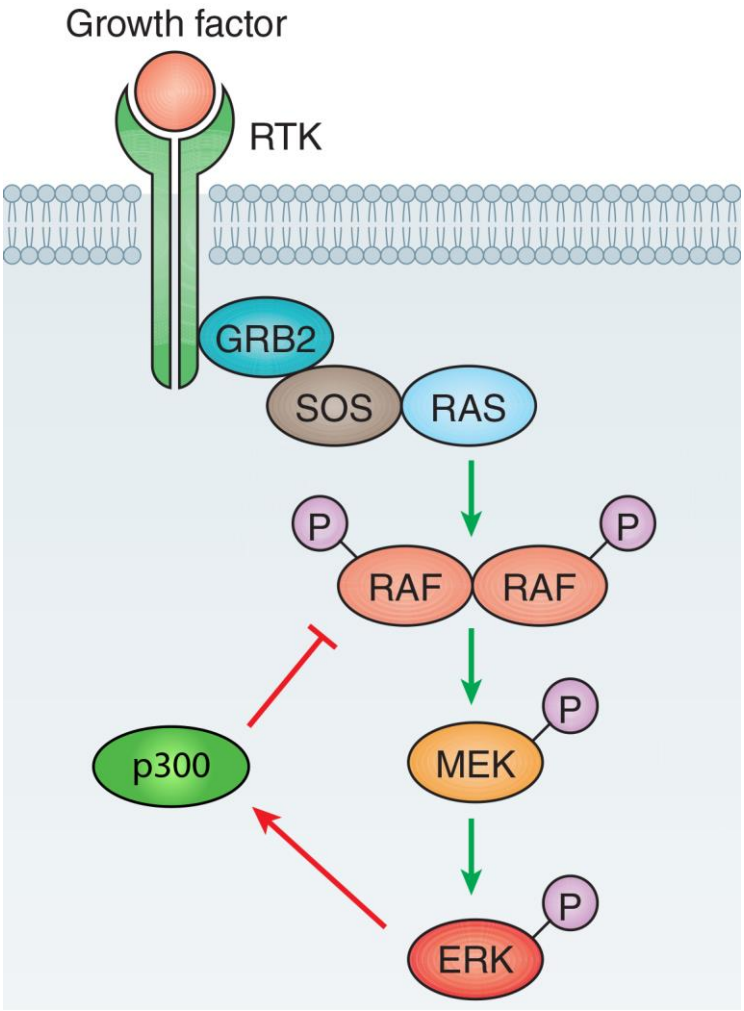

Figure 3.23 Proposed negative feedback loop between p300 and the MAPK pathway. ERK phosphorylates p300, activating its acetyltransferase activity. This results in increased acetylation of BRAF and/or CRAF, which inhibits their ability to bind to MEK and thus reduces further ERK phosphorylation of p300.

BRAF acetylation by the p300/CBP acetyltransferases appears to be part of a negative feedback loop, with ERK phosphorylation of p300/CBP activating their HAT activity (Ait-Si-Ali et al., 1999; Chen et al., 2007). This in turn leads to the inhibition of BRAF activity via increased acetylation, thus dampening further ERK

phosphorylation of p300/CBP (Figure 3.23). Although p300-mediated acetylation of MEK1 has been reported to increase its activity in another study (Yeung et al., 2015), we believe that the inhibitory effect of BRAF acetylation is dominant, since p300 inhibition with C646 caused demonstrable up-regulation of MAPK output in a multitude of different cell lines.

With further research to elucidate specific pathways pertaining to BRAF acetylation, especially with regards to its activators and inhibitors, we think that BRAF acetylation has the potential to complement existing mechanisms of controlling MAPK output. For example, since BRAF acetylation results in the attenuation of its kinase activity, drugs that increase BRAF acetylation can potentially be used in combinatorial therapies with existing BRAF inhibitors. Since the BRAF K473 and K475 residues are also conserved in CRAF, BRAF acetylation-promoting drugs are likely to affect CRAF in a similar manner, and thus may be useful in circumventing acquired resistance mechanisms to BRAF inhibition that are mediated via CRAF hyperactivation. With regards to the third RAF isoform, ARAF, it is unlikely that these drugs would have an effect on its kinase activity, since the two lysine residues are not conserved in ARAF. However, ARAF has a much lower basal level of kinase activity compared to BRAF and CRAF (Marais et al., 1997), due to differences in its RAS-binding domain (Weber et al., 2000) and N-region (Baljuls et al., 2007). In fact, siRNA-mediated depletion of ARAF did not even affect ERK phosphorylation in melanoma cell lines bearing NRAS or BRAF mutations (Rebocho and Marais, 2013). Thus, we believe that the theoretical inability of ARAF to respond to BRAF acetylation-promoting drugs would not significantly hamper drug efficacy, since the role played by ARAF in melanoma MAPK

signalling appears to pertain to scaffolding and is largely independent of its kinase activity (Rebocho and Marais, 2013).

On the opposite end of the spectrum, drugs that inhibit BRAF acetylation and promote BRAF kinase activity can also be useful therapeutically. Studies involving patient-derived xenograft models of melanoma have shown drug-resistant tumour cells becoming addicted to the BRAF inhibitor vemurafenib, such that tumour regression was observed upon withdrawal of the drug (Das Thakur et al., 2013). The dependency of these drug-resistant cells on BRAF inhibition for peak proliferation has led to intermittent dosing being proposed as a way to circumvent tumour relapse caused by acquired drug resistance (Deuker and McMahon, 2014; Holderfield et al., 2014). Indeed, a clinical trial investigating the utility of intermittent dosing is already underway (Deuker and McMahon, 2014). As such, drugs that inhibit BRAF acetylation and elevate BRAF kinase activity can be potentially employed to kill drug-resistant tumour cells, particularly in light of studies demonstrating antiproliferative and cytotoxic effects caused by hyperactivation of the MAPK pathway in melanoma cells (Petti et al., 2006). The potentially deleterious effects of MAPK hyperactivation is also reflected by the fact that BRAF and NRAS mutations tend to be mutually exclusive in patient-derived melanoma samples (Akbani et al., 2015). By cycling drugs on and off and in combination with each other, we can potentially manipulate MAPK output such that the bulk of the tumour population will always remain sensitive to BRAF inhibition.

In conclusion, our results describe a novel post-translational modification of BRAF that has a demonstrable effect on its kinase activity both *in vitro* and in cell culture models. We believe that BRAF acetylation by p300/CBP constitutes a bona fide negative feedback loop that can potentially be exploited for melanoma therapy, pending the outcome of further investigations.

Chapter 4 – Phosphorylation of MITF affects its nuclear export

4.1 Introduction

4.1.1 Regulation of MITF by transcription

As noted in Chapter 1, MITF is the master regulator of the melanocyte lineage as well as a major melanoma oncogene. Importantly, the level of MITF activity is a crucial determinant of the sub-population identity and phenotype in melanoma cells, as outlined in the rheostat model (Carreira et al., 2006; Goding, 2011; Hoek and Goding, 2010).

One of the ways in which MITF activity is regulated is at the level of transcription. The M promoter, which is melanocyte-specific and controls expression of the dominant isoform of MITF (MITF-M) in cells of melanocytic origin (Fuse et al., 1996; Vachtenheim and Novotná, 1999; Yasumoto et al., 1998), is subject to complex transcriptional regulation through a multitude of different pathways.

Studies have shown that the Wnt (wingless-type) signalling pathway plays a vital role in pigment cell development in zebrafish (Dorsky et al., 1998) and mice (Hari et al., 2002; Ikeya et al., 1997). Subsequently, the promoter for *nacre*, the zebrafish homolog of the *MITF* gene, was found to contain three binding sites for the Tcf/Lef (T-cell factor/lymphoid enhancer-binding factor) family of transcription factors that form part of the Wnt signalling pathway (Dorsky et al., 2000). TCF/LEF binding sites were also identified in the M promoter of the *MITF* gene in humans, and shown to be necessary for MITF expression via the recruitment of the LEF1 transcription factor, in complex with its coactivator β-catenin, to these sites (Widlund et al., 2002). MITF can also directly interact with LEF1 to transactivate its own M promoter (Saito et al., 2002), as well as MITF target genes such as *DCT* (Yasumoto et al., 2002). β-catenin can also interact with MITF at its helix domain to drive expression of MITF target genes such as *TYR* and *TYRP1* (Schepsky et al., 2006),

providing yet another level of crosstalk between MITF and the Wnt signalling pathway.

The PAX3 (paired box 3) transcription factor plays an important role in melanocyte differentiation (Lang et al., 2005), a large part of which is mediated through its ability to activate *MITF* expression. Mechanistically, PAX3 up-regulates *MITF* expression by binding the M promoter of the *MITF* gene at two recognition sites that are conserved in both humans and mice, which results in transactivation of the promoter (Bondurand et al., 2000; Potterf et al., 2000; Watanabe et al., 1998).

PAX3 can also cooperate with sex determining region Y-box 10 (SOX10) to activate *MITF* expression in a synergistic fashion (Bondurand et al., 2000; Potterf et al., 2000). SOX10 is another transcription factor that is capable of inducing MITF expression in various human and mouse cell lines (Bondurand et al., 2000; Lee et al., 2000; Potterf et al., 2000; Verastegui et al., 2000). In another indirect piece of evidence for SOX10 regulation of *MITF* expression, the tyrosine-protein kinase receptor TYRO3 was shown to induce *MITF* expression by promoting nuclear localisation of SOX10 (Zhu et al., 2009). SOX10-mediated *MITF* expression has also been validated in animal models. For example, mice bearing *Sox10* mutations fail to express *Mitf* transcripts (Bondurand et al., 2000). In *sox10*-mutant zebrafish, which are also negative for *mitfa* transcripts, *mitfa* transcription can be rescued by microinjecting *sox10* RNA (Elworthy et al., 2003). In terms of the mechanism, several putative SOX10 binding sites have been identified in the M promoter of the *MITF* gene (Bondurand et al., 2000; Lee et al., 2000; Potterf et al., 2000), as well as in a distal enhancer located 14.5 kb upstream of the start codon of MITF-M (Watanabe et al., 2002). The SOX10 binding sites in the M promoter exhibit functional redundancy, in the sense that SOX10-mediated transcription was affected

with mutation of multiple SOX10 binding sites in parallel, but not with independent mutations of single sites (Lee et al., 2000).

Another important pathway involved in transcription regulation of MITF is the α-melanocyte stimulating hormone (α-MSH) and the cyclic adenosine monophosphate (cAMP) pathway. Binding of α-MSH to the melanocortin 1 receptor (MC1R) induces activation of adenylyl cyclase, which in turn catalyses the conversion of adenosine triphosphate (ATP) to cAMP. cAMP stimulates PKA phosphorylation of the CREB (cAMP responsive element-binding protein) transcription factor. Phosphorylated CREB binds to a CRE (cAMP responsive element) motif located in the M promoter of the *MITF* gene, which results in transcriptional activation of *MITF* expression (Bertolotto et al., 1998b; Price et al., 1998). This is accompanied by the up-regulation of MITF target genes including *TYR*, *TYRP1* and *DCT* (Bertolotto et al., 1998a, 1998b; Price et al., 1998). In addition, phosphorylation of CREB by the stress-responsive p38 MAPK can also result in up-regulation of *MITF* and *TYR* (Saha et al., 2006). However, despite the cAMP pathway being ubiquitous in many cell types, cAMP-mediated activation of *MITF* was observed in B16 mouse melanoma cells but not in NIH 3T3 mouse fibroblasts (Bertolotto et al., 1998b). Further research showed that the melanocyte-specific context of cAMP-mediated *MITF* activation can be explained by the obligate cooperativity between CREB and SOX10, the expression of which is restricted to cells of neural crest origin, at the M promoter that drives MITF expression in melanocytes (Huber et al., 2003).

α-MSH can also induce the expression of the transcriptional coactivator PGC-1α (peroxisome proliferator-activated receptor γ coactivator 1α) via canonical CRE motifs in the *PGC-1α* promoter (Shoag et al., 2013). PGC-1α then stimulates MITF

expression and ultimately melanogenesis by binding to and coactivating SOX10 on the M promoter (Shoag et al., 2013). In turn, MITF can also up-regulate PGC-1α expression by binding to E-box motifs in the *PGC-1α* promoter (Haq et al., 2013b), which adds an additional level of complexity to the relationship between MITF and PGC-1α.

MITF expression can also be induced by the transcription factor ONECUT-2, which can bind to ONECUT-2 recognition sites on the M promoter of the *MITF* gene (Jacquemin et al., 2001).

In addition to the activators described above, several transcriptional repressors of MITF have also been identified. For example, MITF levels were found to be inversely correlated to expression of the GLI2 (glioma-associated oncogene 2) transcription factor, a critical mediator of the Hedgehog signalling pathway (Javelaud et al., 2011). GLI2 repression of *MITF* was subsequently confirmed by the identification of a GLI2 binding site, within the M promoter of the *MITF* gene, which was responsible for reduced transcription of *MITF* (Pierrat et al., 2012). Another transcription factor involved in transcriptional regulation of *MITF* is HIF1 (hypoxia-inducible factor 1), which can down-regulate MITF levels in response to hypoxia by inducing expression of BHLHE40 (class E basic helix-loop-helix protein 40) (Cheli et al., 2012; Feige et al., 2011). BHLHE40 is then recruited to a consensus recognition site in the M promoter where it acts as a transcriptional repressor (Feige et al., 2011).

MITF repression is also mediated by the POU domain transcription factor BRN2, which can bind directly to a recognition site in the M promoter of the *MITF* gene, as shown by electrophoretic mobility shift assay (EMSA) and chromatin immunoprecipitation (ChIP) (Goodall et al., 2008). Binding of BRN2 results in

repression of *MITF* transcription, which manifests as inverse expression of BRN2 and MITF in melanoma spheres and xenograft tumours (Thurber et al., 2011), as well as in patient tumour samples (Goodall et al., 2008). However, co-expression of BRN2 and MITF is observed in melanoma cell lines (Thurber et al., 2011; Wellbrock et al., 2008). A further layer of complexity is provided by microRNA miR-211 which is transcriptionally induced by MITF (Levy et al., 2010; Mazar et al., 2010), and silences BRN2 expression (Boyle et al., 2011), thus forming a positive feedback loop which can potentially account for the inverse expression states of BRN2 and MITF in melanoma samples *in vivo*.

4.1.2 Regulation of MITF by post-translational modifications

In addition to transcriptional regulation, MITF activity is also extensively regulated at the post-translational level (Figure 4.1). An important post-translational modification of MITF is the phosphorylation of S73 by the kinase ERK (Hemesath et al., 1998), which is induced in response to treatment with stem cell factor (SCF). SCF, a ligand that activates the c-KIT receptor, also induces phosphorylation of MITF at S409 by the kinase RSK1 (Wu et al., 2000). Phosphorylation at both S73 and S409 is believed to be responsible for increased proteosomal degradation of the MITF protein following c-KIT stimulation (Wu et al., 2000). A separate study showed that the mutation of S73 to a non-phosphorylatable alanine residue almost completely abrogated ubiquitination of MITF (Xu et al., 2000). K201 was identified as a potential ubiquitination site in MITF in the same study (Xu et al., 2000).

Furthermore, the mutation of S73 to a non-phosphorylatable alanine residue reduced the ability of MITF to transactivate the *TYR* promoter in mammalian cells (Hemesath et al., 1998; Wu et al., 2000). However, in spite of the *in vitro* data,

mouse models with the Mitf^{S73A} mutant had normal eye development and coat pigmentation (Bauer et al., 2009; Bismuth et al., 2008), although this might have been caused by aberrant splicing following mutation of S73, which is part of a splice enhancer sequence (Debbache et al., 2012). The S409A mutation and S73A.S409A double mutation did not result in any abnormal pigmentation phenotypes *in vivo* either (Bauer et al., 2009).

RSK1-mediated S409 phosphorylation has also been reported to relieve the inhibition of MITF transcriptional activity by the E3 SUMO-protein ligase PIAS3 (protein inhibitor of activated STAT protein 3). PIAS3 represses MITF's transcriptional activity by binding to its leucine zipper domain (Levy et al., 2003). RSK1 phosphorylation at MITF S409 interferes with this interaction, thus relieving PIAS-mediated repression (Levy et al., 2003).

The S298 residue in MITF is another site where phosphorylation reportedly occurs (Takeda et al., 2000a). This phosphorylation event is believed to be mediated by glycogen synthase kinase 3 (GSK3) (Takeda et al., 2000a). Phosphorylation by GSK3 increased the DNA-binding ability of MITF, while an S298A substitution inhibited its affinity for DNA and reduced its ability to transactivate the *TYR* promoter (Takeda et al., 2000a). However, in apparent contradiction to this finding, a separate study showed that the S298A mutation did not have any significant effects on MITF's ability to transactivate the *TYR* promoter, as well as other downstream targets such as the *TYRP1* and *DCT* promoters (Grill et al., 2013).

Recently, three additional GSK3 phosphorylation sites (S397, S401 and S405) were identified on MITF (Ploper et al., 2015). Similar to the well-known GSK3 substrates glycogen synthase and β-catenin, these are consecutive GSK3 phosphorylation sites that are phosphorylated sequentially (Fiol et al., 1990)

following an initial priming phosphorylation by another kinase. In MITF's case, the priming phosphorylation event occurs on S409 and is mediated by RSK1, as described above. Wnt signalling led to the inhibition of GSK3 activity, which resulted in stabilisation of the MITF protein (Ploper et al., 2015).

MITF also plays an important role in osteoclast differentiation (Hershey and Fisher, 2004), although this would presumably involve the MITF-A and MITF-E isoforms that are abundantly found in osteoclasts (Lu et al., 2010), and not the melanocyte-specific MITF-M isoform. In committed myeloid precursors, which are osteoclast progenitors, MITF is phosphorylated on S173 (relative to MITF-M), probably by C-TAK1 (Cdc25C-associated protein kinase 1) (Bronisz et al., 2006). Phosphorylation on S173 promotes MITF's association with 14-3-3 proteins, which sequesters it in the cytosol and suppresses its ability to transactivate the osteoclast-specific *TRAP* (tartrate-resistant acid phosphatase type 5) promoter (Bronisz et al., 2006). In osteoclasts, MITF is also phosphorylated on S307 by p38 MAPK in response to stimulation by the RANKL (receptor activator of nuclear factor κB ligand) cytokine, which increases its ability to transactivate the *TRAP* promoter (Mansky et al., 2002). However, both S173 and S307 phosphorylation events have yet to be demonstrated in the melanocyte context to date.

Other than phosphorylation, MITF is also post-translationally modified by the addition of SUMO (small ubiquitin-like modifier) on the lysine residues K182 and K316, an event which is mediated by the SUMO-activating enzyme SAE1/2 and the SUMO-conjugating enzyme ubiquitin carrier protein 9 (UBC9) (Miller et al., 2005; Murakami and Arnheiter, 2005). Sumoylation of these residues resulted in the repression of MITF's transcriptional activity towards target genes such as *TYR*, *DCT* and transient receptor potential cation channel subfamily M member 1 (*TRPM1*)

(Miller et al., 2005; Murakami and Arnheiter, 2005). An E318K mutation in MITF, which disrupts K316 sumoylation, has been linked to familial melanoma (Bertolotto et al., 2011; Yokoyama et al., 2011).

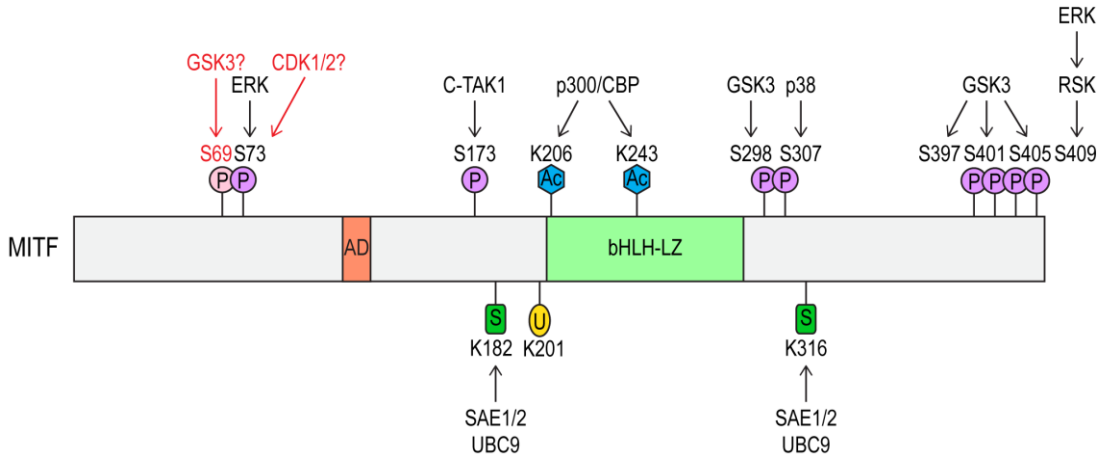

Figure 4.1 Map of MITF post-translational modifications. AD – transcription activation domain, bHLH-LZ – basic helix-loop-helix leucine zipper domain. P – phosphorylation, Ac – acetylation, S – sumoylation, U – ubiquitination. GSK3 phosphorylation of S69 and CDK1/2 phosphorylation of S73 (highlighted in red) are described in Chapters 4 and 5 respectively.

4.1.3 MITF's role in melanoma

Like many cancers, melanoma cells exist as a heterogeneous population (Akbani et al., 2015; Quintana et al., 2010; Roesch, 2015), which presents a significant barrier to targeted therapy. As outlined in the rheostat model described in Chapter 1, MITF activity plays an important role in determining the sub-population identity of melanoma cells (Hoek and Goding, 2010). Changes in the level of MITF activity can potentially sensitise cells to therapeutic treatment by reducing phenotypic heterogeneity and driving heterogeneous melanoma cells towards certain therapeutically sensitive phenotypes. In order for that to happen, we must first find effective ways of manipulating MITF activity, which remains a challenge since transcription factors such as MITF lack ligand dependency and hence do not present readily druggable targets. We believe that post-translational modifications represent

a promising avenue to control MITF activity, since years of research have culminated in a number of different post-translational modifications being identified in MITF. However, in spite of MITF's importance in melanocyte development and melanoma, there is a significant lack of information on the functional significance of many of these post-translational modifications and their effects on MITF activity.

We were particularly interested in the potential interplay between MITF and the MAPK pathway, since MAPK pathway activation is frequently observed in melanoma, particularly in the context of BRAF or NRAS mutations (Akbani et al., 2015). While activation of the MAPK pathway would presumably increase ERK-phosphorylation of MITF at S73, the exact effects appear to be complex, with S73 phosphorylation inducing an increase in MITF activity while promoting its degradation (Wu et al., 2000). Furthermore, activated $BRAF^{V600E}$ appears to be capable of both inducing and repressing MITF expression levels (Wellbrock and Marais, 2005; Wellbrock et al., 2008). To add a further level of complexity to the relationship between MITF and the MAPK pathway, both high (Van Allen et al., 2014; Haq et al., 2013a; Johannessen et al., 2013; Müller et al., 2014; Smith et al., 2013) and low (Konieczkowski et al., 2014; Müller et al., 2014) MITF levels have been shown to mediate resistance to MAPK inhibition in melanoma. With all this in mind, we set out to investigate novel ways of regulating MITF activity via post-translational modifications, by first characterising the effects mediated by the MAPK pathway on MITF.

4.2 Results

4.2.1 MITF sub-cellular localisation is dependent on MAPK signalling

To test if changes in MAPK output had any effects on MITF, we treated 501mel melanoma cells with either tetradecanoyl phorbol acetate (TPA) and/or U0126. TPA stimulates the MAPK pathway by binding to and activating protein kinase C (PKC) (Lee et al., 2002), while U0126 inactivates the MAPK pathway by inhibiting MEK (Favata et al., 1998). We then examined the expression and sub-cellular localisation of MITF in these cells via immunofluorescence using an anti-MITF antibody raised against the C-terminus of MITF (Figure 4.2a). In line with MAPK activation, TPA caused an increase in the amount of phospho-ERK (Figure 4.2a, c), as detected by an antibody that recognises phosphorylated T202/Y204 in ERK1 and T185/Y187 in ERK2. In conjunction with MAPK activation, TPA treatment also caused a fraction of MITF, which is typically a nuclear protein, to translocate to the cytoplasm, with a significant corresponding drop in the proportion of MITF in the nucleus compared to the DMSO-treated cells (Figure 4.2b).

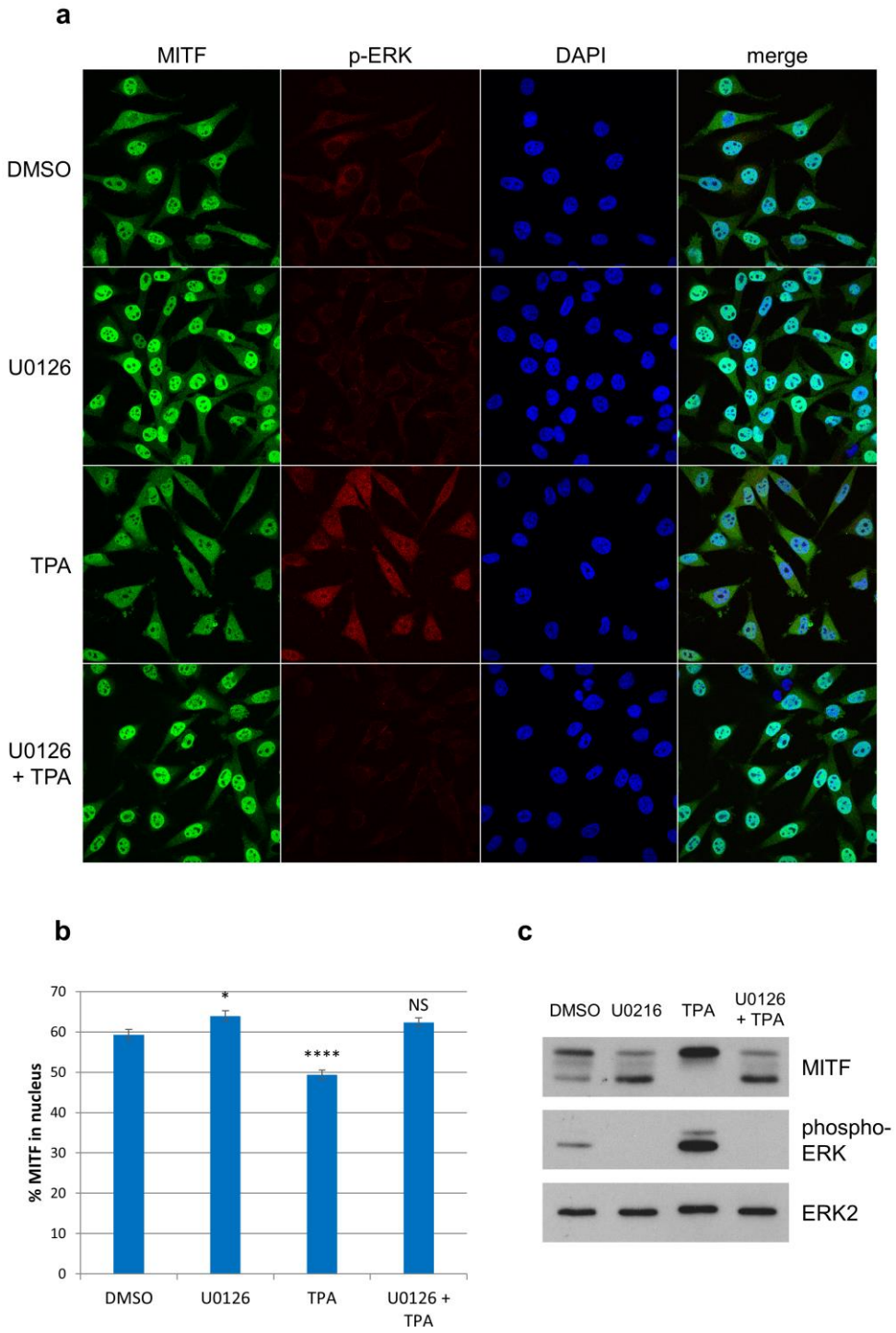

Figure 4.2 MITF translocated to the cytoplasm following TPA-mediated MAPK activation, and was preferentially localised to the nucleus following U0126-mediated MAPK inhibition. (a) Immunofluorescence images of 501mel cells following MAPK activation/inhibition. Cells were grown on glass coverslips to 80% confluence and treated with 200 nM TPA for 1 hour and/or 10 μM of U0126 for 3 hours. After fixation and permeabilisation, the cells were stained with the nucleic acid stain DAPI (blue) and antibodies against MITF (green) and phospho-ERK (red). Images were acquired by confocal microscopy. **(b)** Quantification of MITF sub-cellular localisation in 501mel cells following MAPK activation/inhibition. Cells were treated and processed as in (a). A minimum of 100 cells were quantified per condition. Error bars represent standard error of the mean (SEM). 2-tailed t-test: * $p<0.05$, **** $p<0.0001$. **(c)** Western blot of 501mel cells following MAPK activation/inhibition. Cells were treated as in (a).

In contrast, treatment with the MEK inhibitor U0126 resulted in a significant increase in MITF nuclear localisation relative to the DMSO-treated control (Figure 4.2a, b). When cells were co-treated with both TPA and U0126, U0126 was able to block TPA-mediated ERK phosphorylation (Figure 4.2a, c), and prevent translocation of MITF to the cytoplasm (Figure 4.2a, b).

In addition, western blotting revealed that MITF phosphorylation status was altered according to changes in MAPK output (Figure 4.2c). MITF typically appears as a doublet on western blots, with the upper band corresponding to a species that is phosphorylated by ERK on S73 (Hemesath et al., 1998). MAPK inhibition with U0126 resulted in a reduction in the proportion of the upper band, consistent with MITF dephosphorylation. In contrast, MAPK activation with TPA caused virtually all of MITF to appear as the upper band, which indicated hyperphosphorylation of MITF on S73. In co-treatments, U0126 was able to block TPA-mediated MITF hyperphosphorylation, which could be attributed to the lack of phospho-ERK induction.

4.2.2 S73 phosphorylation causes MITF to translocate to the cytoplasm

Since MAPK output appeared to affect both sub-cellular localisation and phosphorylation status of MITF, we wanted to see if the changes in its localisation were mediated by a change in phosphorylation at S73. To investigate this, we mutated the serine residue at S73 in MITF to an alanine residue, which cannot be phosphorylated, and fused MITF to an N-terminal green fluorescent protein (GFP) tag. We were aware that MITF was capable of homodimerising with itself (Hemesath et al., 1994; Pogenberg et al., 2012); thus the presence of endogenous MITF might confound the results pertaining to the localisation of the ectopic MITF mutant. Hence

we decided to transiently transfected the GFP-MITF constructs into HeLa cells, which are of non-melanocytic origin and thus lack endogenous MITF. We then treated the cells with TPA to stimulate the MAPK pathway, and examined the sub-cellular localisation of MITF via confocal microscopy (Figure 4.3).

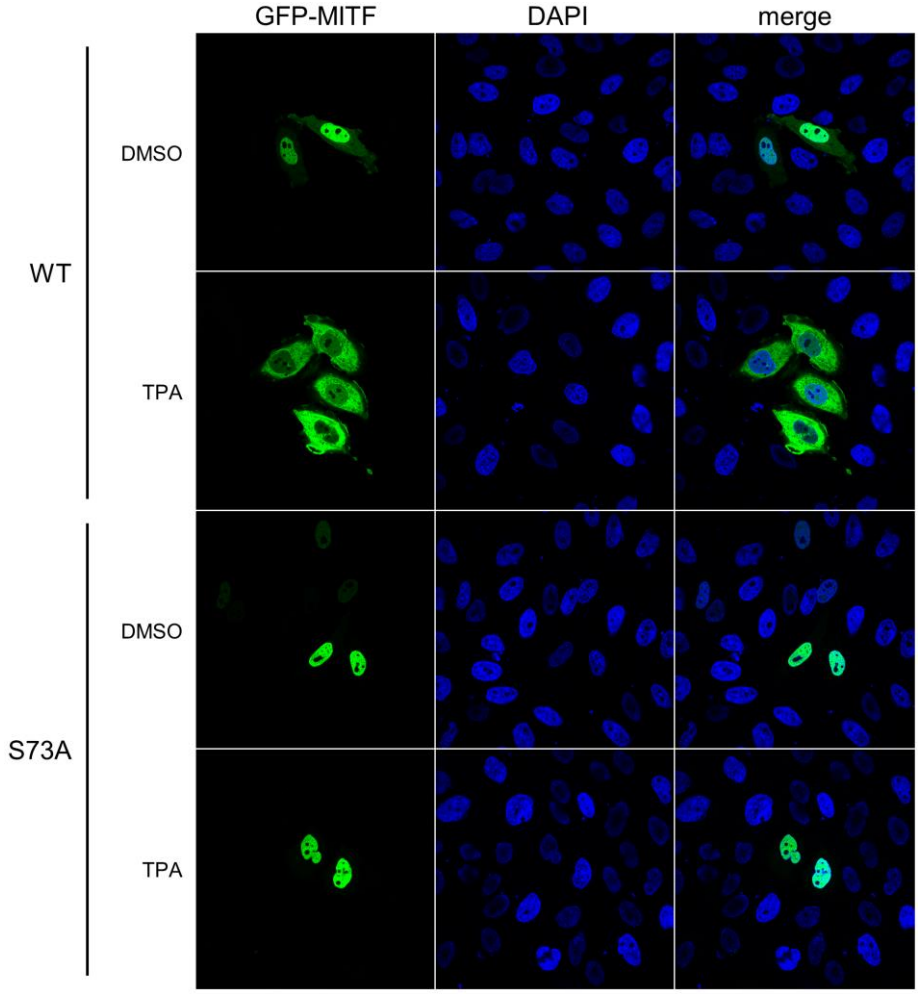

Figure 4.3 An S73A mutation in MITF prevented TPA-mediated translocation to the cytoplasm. Fluorescence images of HeLa cells ectopically expressing GFP-MITF mutants (green). Cells were grown on glass coverslips to 50% confluence before being transfected using Fugene 6. After 48 hours, cells were treated with 200 nM TPA or an equivalent volume of DMSO for 1 hour. Cells were then fixed and stained with DAPI (blue). Images were acquired by confocal microscopy.

Like endogenous MITF in 501mel cells, ectopically expressed wild-type GFP-MITF translocated to the cytoplasm upon TPA stimulation. In contrast, the S73A mutant remained in the nucleus after treatment with TPA, indicating that the TPA-

induced translocation of MITF was dependent on phosphorylation of MITF at the S73 residue.

We wanted to verify that the MITF localisation effects observed with TPA treatment was a bona fide effect of the MAPK activation, as opposed to other effects of PKC stimulation by TPA. Thus, we made use of the stable, tetracycline-responsive HeLa Flp-In T-rex $BRAF^{V600E}$-FLAG cell line, in which the expression of activated $BRAF^{V600E}$ could be induced by the addition of doxycycline, as described in Chapter 3. We expressed both wild-type and S73A GFP-MITF variants in the HeLa Flp-In T-rex $BRAF^{V600E}$-FLAG cell line, and treated them with the MEK inhibitor U0126 after doxycycline induction of $BRAF^{V600E}$ expression (Figure 4.4).

As shown in Figure 4.4, doxycycline induction of $BRAF^{V600E}$ caused wild-type GFP-MITF to translocate into the cytoplasm. $BRAF^{V600E}$-mediated cytoplasmic translocation of MITF could be blocked by treating the cells with the MEK inhibitor U0126. On the other hand, the S73A mutant, in terms of its sub-cellular localisation, was not responsive to $BRAF^{V600E}$ expression even in the absence of MEK inhibition. These results show that the change in MITF localisation was indeed being mediated via the MAPK pathway, and that S73 phosphorylation was a critical determinant.

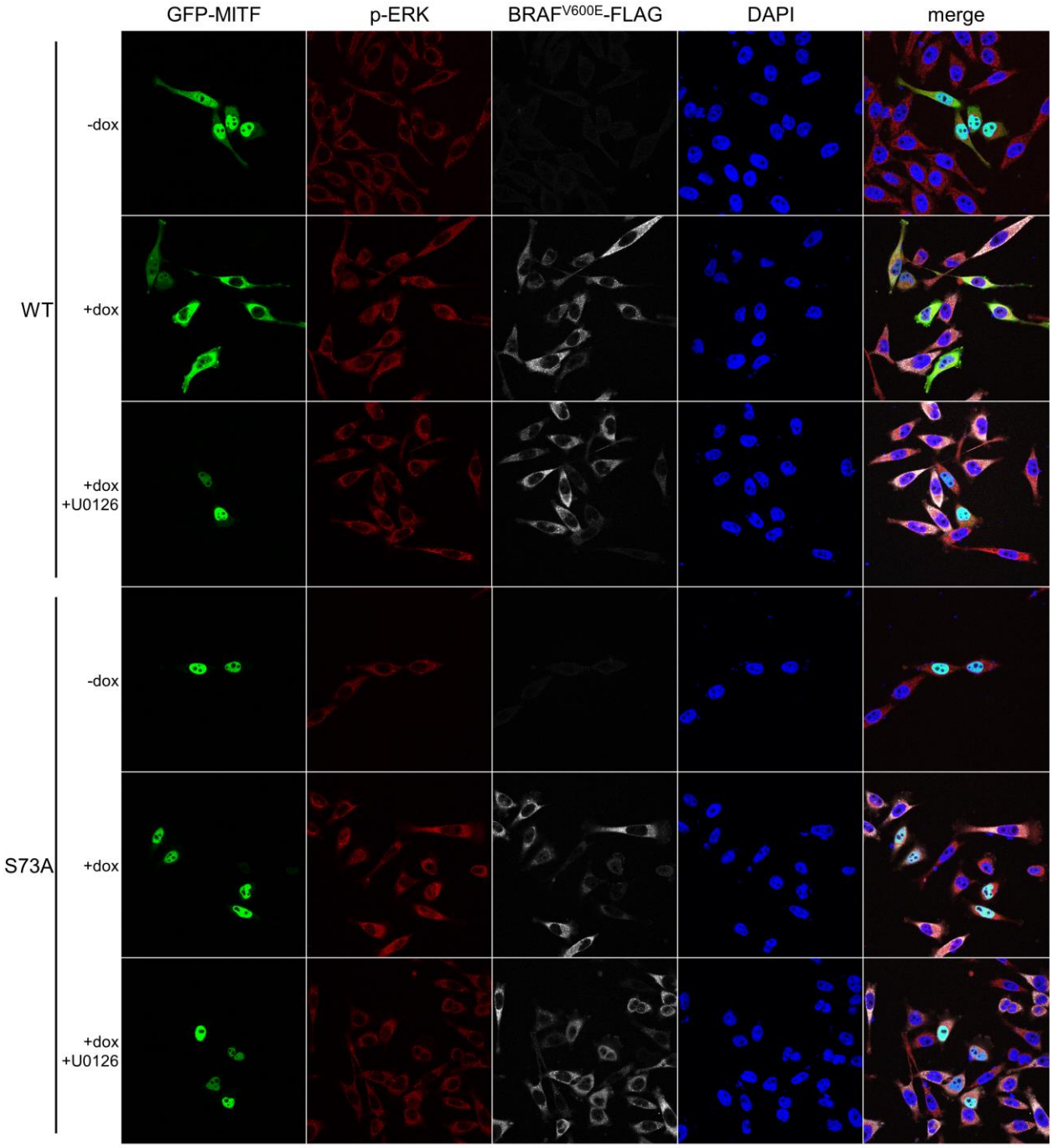

Figure 4.4 Ectopic wild-type MITF translocated to the cytoplasm following doxycycline induction of BRAF^{V600E} expression in HeLa cells, while translocation was not observed the S73A mutant. Immunofluorescence images of HeLa cells ectopically expressing GFP-MITF mutants (green). Cells were grown on glass coverslips to 50% confluence before being transfected using Fugene 6. After 24 hours, cells were treated with 2 ng/mL doxycycline for 24 hours. Cells were treated with 200 nM TPA for 1 hour and/or 10 μM of U0126 for 3 hours before fixation and permeabilisation. Cells were then stained with DAPI (blue), and antibodies against phospho-ERK (red) and FLAG (white). Images were acquired by confocal microscopy.

4.2.3 GSK3 inhibition causes translocation of MITF to the nucleus

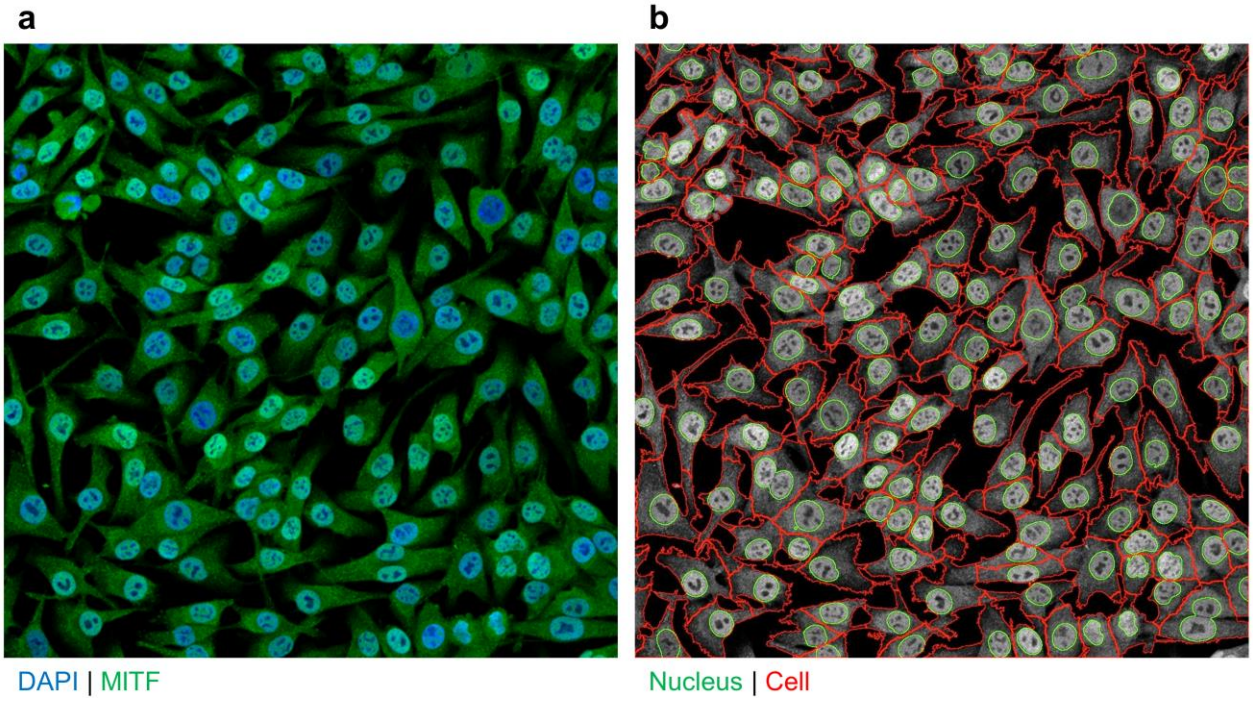

Figure 4.5 Automated immunofluorescence-based screening and quantification. (a) SK-MEL-28s were grown to 80% confluence in 96-well CellCarrier plates, then treated with 2.5 μM of each compound from the GSK Published Kinase Inhibitor Set for 6 hours. After fixation and permeabilisation, the cells were stained with DAPI (blue) and an antibody against MITF (green). Images were acquired by confocal microscopy, with automated focussing based on the DAPI signal. **(b)** Segmentation of individual cells in (a) into regions of interest using CellProfiler. Nuclear outline (green) is based on DAPI staining, cellular outline (red) is based on MITF staining.

While it was clear that the MAPK pathway was involved in translocation of MITF, we were also interested in other signalling pathways that might affect MITF's localisation, either on their own or via cross-talk with the MAPK pathway. With this in mind, we carried out a screen using a small molecule library consisting of 367 validated kinase inhibitors from the GSK Published Kinase Inhibitor Set (Drewry et al., 2014), a gift from Stefan Knapp, SGC. The primary target of the screen was to look for kinase inhibitors that had an effect on MITF localisation. The screen was based on automatically acquired immunofluorescence images of SK-MEL-28 melanoma cells following a 6-hour treatment with 2.5 μM of each compound from

the GSK Published Kinase Inhibitor Set (Figure 4.5a). Once images were acquired, we made use of the CellProfiler image analysis software (Carpenter et al., 2006; Kamentsky et al., 2011) to identify individual cells within each image and segment them into nuclear and cytoplasmic regions of interest (Figure 4.5b). Subsequently, the amount of MITF signal in each region was quantified after correcting for background fluorescence. A minimum of 280 cells were quantified per condition.

The main read-out of the assay was the mean intensity of MITF in the nucleus and the cytoplasm. To get a gauge of whether any translocation of MITF had taken place, we also calculated the ratio of the staining in the nuclear compartment to that of the cytoplasmic compartment. All calculated parameters were normalised relative to the corresponding DMSO-treated internal control located on the same physical plate.

After analysing the data, we shortlisted a list of 8 hits from the screen, all of which were inhibitors against the kinase GSK3 (Table 4.1). These 8 GSK3 inhibitors all increased the intensity of MITF staining in the nucleus while reducing MITF staining intensity in the cytoplasm, which was consistent with MITF translocation from the cytoplasm to the nucleus. It should be noted that while there were other GSK3 inhibitors in the library that did not give the same phenotype, we were not overly concerned as the screen was carried out at a single drug concentration, at only one time point.

Compound	MITF intensity (nuclear)	MITF intensity (cytoplasmic)	MITF intensity (nuclear:cytoplasmic)
SB-725317	1.17	0.61	1.92
SB-686709-A	1.28	0.61	2.11
SB-675259-M	1.33	0.69	1.93
GW814408X	1.22	0.53	2.28
GW806290X	1.22	0.74	1.66
SB-698596-AC	1.09	0.76	1.43
GW811168X	1.25	0.64	1.97
GW784752X	1.24	0.44	2.84
DMSO	1.00	1.00	1.00

Table 4.1 Shortlisted hits from the screen. List of 8 GSK3 inhibitors shortlisted from the automated screen on SK-MEL-28s, with their respective read-outs colour-coded like a heat-map (red = higher signal, green = lower signal). Mean signal intensities (total signal in region of interest/total area in region of interest) are presented, along with a ratio of nuclear to cytoplasmic intensity (mean nuclear intensity/mean cytoplasmic intensity). All readings were normalised to the DMSO control.

From the shortlist of 8 compounds, we chose compound SB-675259-M (Witherington et al., 2003) for further analysis and validation, since it gave the strongest increase in MITF intensity in the nucleus. To validate the results from the screen, SK-MEL-28 melanoma cells were again treated with SB-675259-M and analysed via immunofluorescence (Figure 4.6a). However, we had to decrease the concentration to 1 μM due to the lack of material. To compensate for the reduced concentration, we extended the treatment period to 18 hours. As shown in Figure 4.6a, our previous results obtained with the automated screen were validated, with an increase in MITF staining in the nucleus accompanied by a decrease in MITF staining in the cytoplasm.

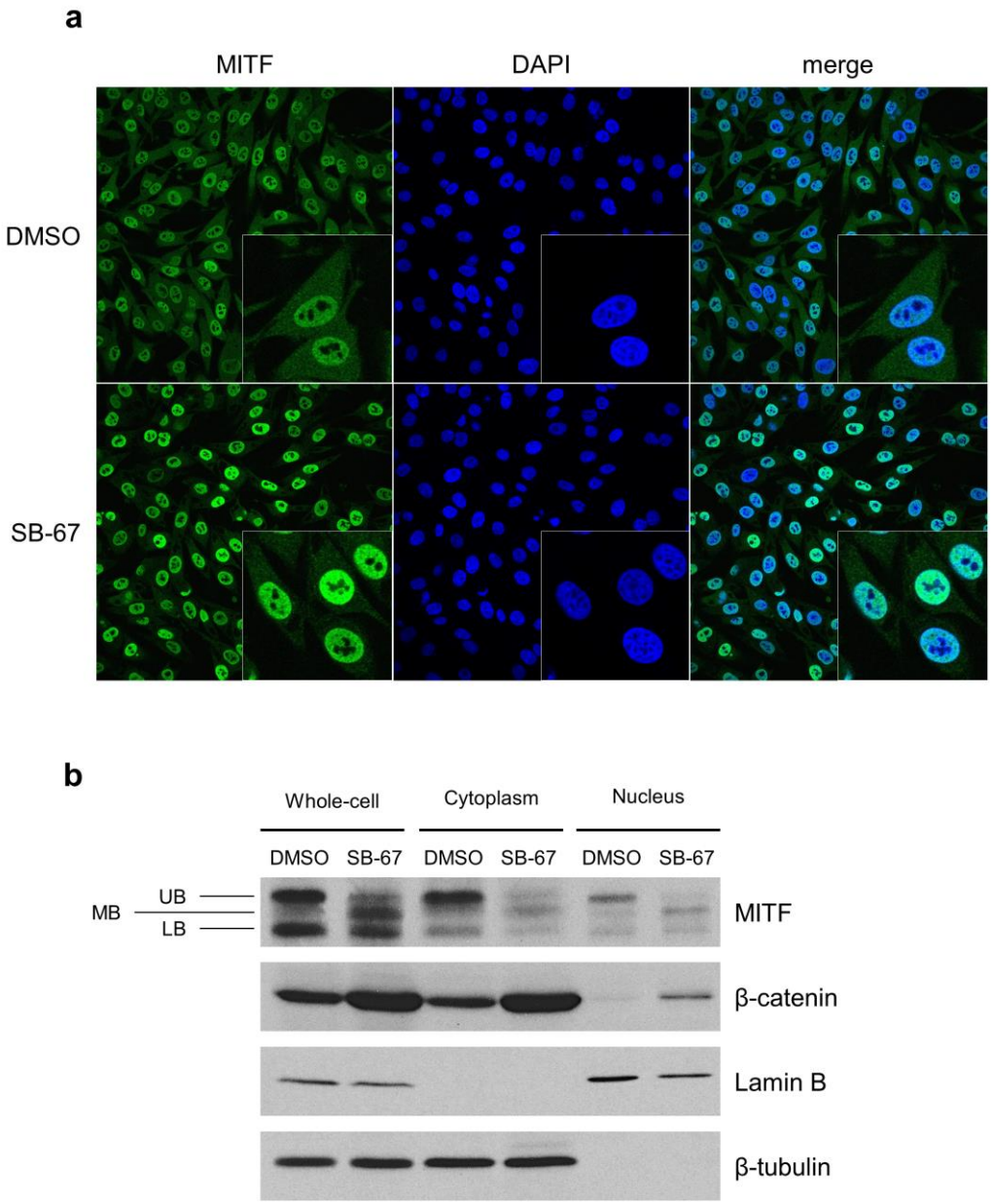

Figure 4.6 SB-675259-M caused an increase in MITF localisation in the nucleus and a decrease in MITF localisation in the cytoplasm. (a) Immunofluorescence images of SK-MEL-28 cells following treatment with SB-675259-M. SK-MEL-28 cells were grown on glass coverslips to 80% confluence and treated with 1 μM of SB-675259-M (abbreviated as SB-67) or an equivalent volume of DMSO for 18 hours. After fixation and permeabilisation, the cells were stained with DAPI (blue) and an antibody against MITF (green). **(b)** Western blot of SK-MEL-28 cells following treatment with SB-675259-M. Cells were treated as in (a), then lysed and fractionated before western blotting. UB – upper band, MB – middle band, LB – lower band.

To further corroborate our results, we also analysed MITF levels by sub-cellular fractionation and western blotting (Figure 4.6b). β-tubulin was used as a cytoplasmic marker and loading control, while Lamin B was used as a nuclear marker and loading control. Fractionation of the cells appeared to be successful, with β-tubulin only present in the cytoplasmic fraction and Lamin B only present in the nuclear fraction. MITF levels in the cytoplasmic fraction decreased upon treatment with SB-675259-M, as was observed in immunofluorescence images. However, no increase in nuclear MITF levels was observed. We also blotted for β-catenin, which accumulated in the nucleus when treated with SB-675259-M, as was expected with GSK3 inhibition.

We wanted to ensure that the MITF localisation effects we saw with SB-675259-M were indeed a result of GSK3 inhibition and not due to off-target effects. Hence, we tried to replicate the results with BIO (Meijer et al., 2003), a selective, ATP-competitive inhibitor of GSK3 (IC_{50} = 5 nM). As was the case with SB-675259-M, BIO induced an increase in MITF levels in the nucleus, as well as a corresponding decrease in MITF levels in the cytoplasm. This was true for both immunofluorescence (Figure 4.7a, b) and western blotting after sub-cellular fractionation (Figure 4.7c). Treatment with BIO also resulted in accumulation of β-catenin, consistent with GSK3 inhibition (Kimelman and Xu, 2006; Wu and Pan, 2010). These results show that the increase in nuclear localisation of MITF was probably a bona fide effect of GSK3 inhibition.

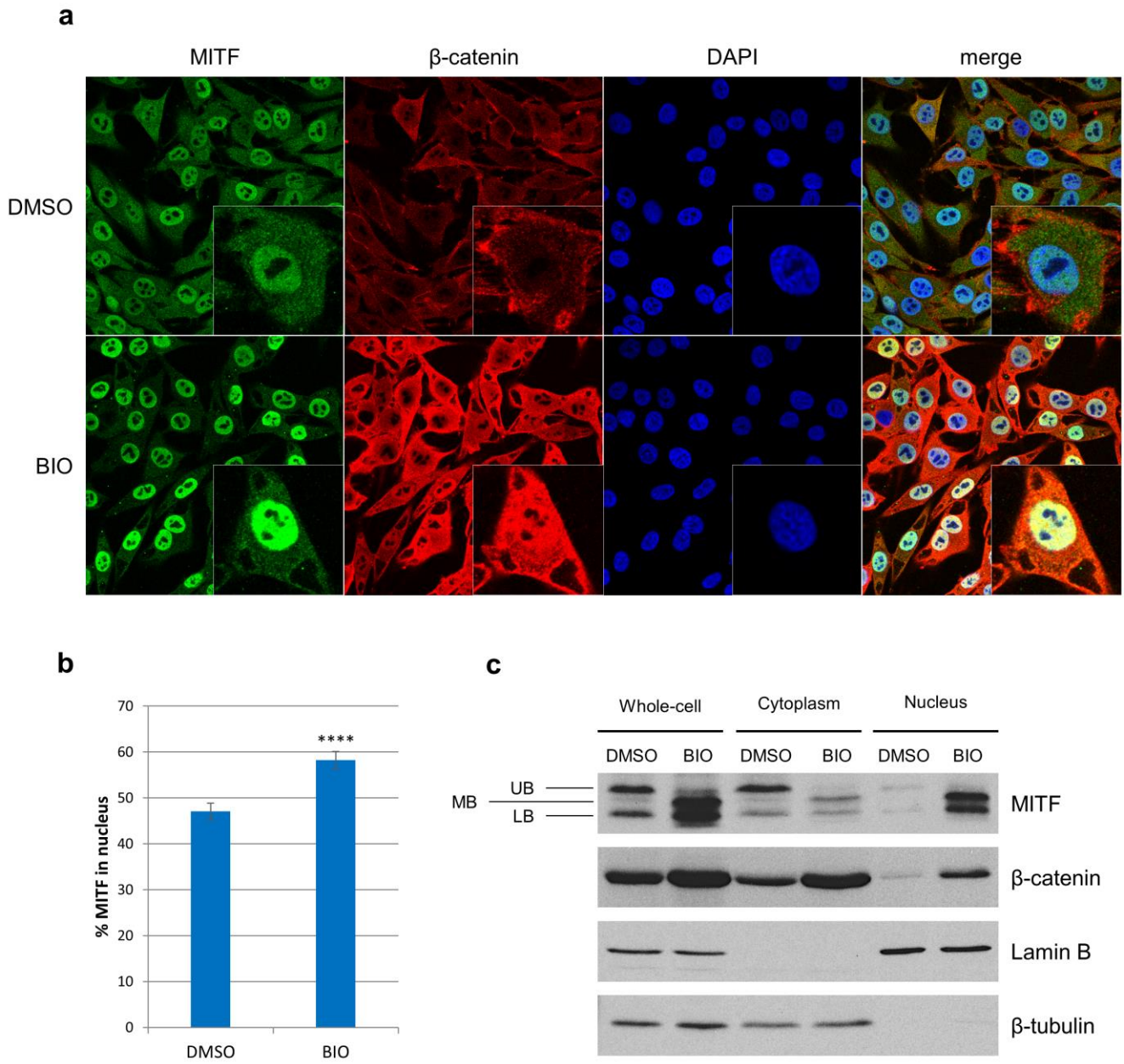

Figure 4.7 GSK3 inhibition caused an increase in MITF localisation in the nucleus and a decrease in MITF localisation in the cytoplasm. (a) Immunofluorescence images of SK-MEL-28 cells following treatment with BIO. SK-MEL-28 cells were grown on glass coverslips to 80% confluence and treated with 1 μM of BIO or an equivalent volume of DMSO for 18 hours. After fixation and permeabilisation, the cells were stained with DAPI (blue) and antibodies against MITF (green) and β-catenin (red). **(b)** Quantification of MITF sub-cellular localisation in SK-MEL-28 cells following treatment with BIO. Cells were treated and processed as in (a). A minimum of 70 cells were quantified per condition. Error bars represent SEM. 2-tailed t-test: **** *p<0.0001*. **(c)** Western blot of SK-MEL-28 cells following treatment with BIO. Cells were treated as in (a), then lysed and fractionated before western blotting. UB – upper band, MB – middle band, LB – lower band.

4.2.4 S69 phosphorylation by GSK3 affects MITF localisation

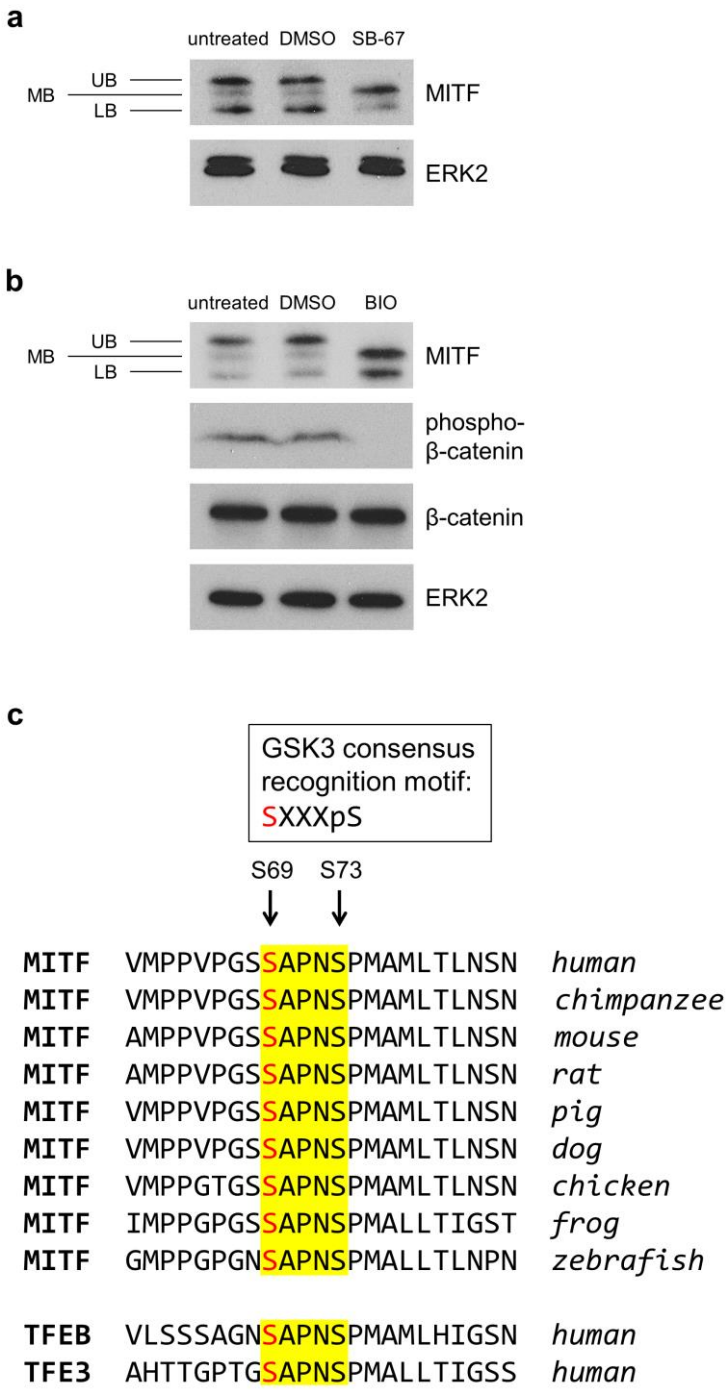

Figure 4.8 GSK3 inhibition caused a shift in MITF electrophoretic mobility. (a) Western blot of SK-MEL-28 cells following treatment with SB-675259-M. SK-MEL-28 cells were grown to 80% confluence and treated with 1 μM of SB-675259-M (abbreviated as SB-67) or an equivalent volume of DMSO for 18 hours. UB – upper band, MB – middle band, LB – lower band. **(b)** Western blot of SK-MEL-28 cells following treatment with BIO. SK-MEL-28 cells were grown to 80% confluence and treated with 1 μM of BIO or an equivalent volume of DMSO for 18 hours. **(c)** Protein sequence alignment of MITF, TFEB and TFE3. S69 (red) in MITF fits the recognition motif of GSK3, and is evolutionarily conserved across multiple species, as well as in TFEB and TFE3. X = any amino acid.

In addition to the localisation effects on MITF, we observed that treatment with SB-675259-M or BIO also caused a shift in the electrophoretic mobility of MITF as detected by western blotting (Figures 4.6b, 4.7c, 4.8a, 4.8b). BIO also caused a decrease in levels of phospho-β-catenin, as detected by an antibody that recognises phosphorylated S33/S37/T41 on β-catenin (Figure 4.8b). Since β-catenin is a direct phosphorylation target of GSK3, this further confirmed that the results obtained with BIO were a bona fide effect of GSK3 inhibition.

As noted earlier, MITF typically appears as a doublet on western blots, with the upper band (UB) corresponding to a species that is phosphorylated by ERK on S73 (Figure 4.8a, b). GSK3 inhibition with either SB-675259-M or BIO led to a downwards shift in the upper band to an intermediate position, which we have marked as the middle band (MB). This downward shift in electrophoretic mobility of the upper band was consistent with a dephosphorylation event. Interestingly, the lower band (LB), which corresponds to a species that is not phosphorylated at S73, did not exhibit the same downward electrophoretic shift upon GSK3 inhibition. This led us to theorise that GSK3 phosphorylation of MITF could be dependent on the phosphorylation status of MITF at S73.

The consensus recognition motif for GSK3 is S-X-X-X-pS, with the first serine being phosphorylated by GSK3 after a priming phosphorylation on the serine in the +4 position (Cohen and Frame, 2001; Fiol et al., 1987, 1990; ter Haar et al., 2001). Upon examining the sequence of MITF, we noticed that the region between S69 and S73 would fit the GSK3 consensus recognition motif perfectly. The pattern of phosphorylation we observed upon GSK3 inhibition was consistent with GSK3 phosphorylation of S69 in MITF, with S73 being the site of priming phosphorylation. Importantly, we also noted that S69 and S73 were highly evolutionarily conserved

across multiple species, as well as in the related members of the MiT family, TFEB and TFE3 (Figure 4.8c).

To verify if the S69 site was also involved in regulating localisation of MITF, we mutated the serine residue at S69 in MITF to a non-phosphorylatable alanine residue. We then expressed the GFP-MITF mutants in 501mel melanoma cells and determined their sub-cellular localisation via confocal microscopy (Figure 4.9a, b). Both S69A and S73A mutants were significantly more nuclear compared to wild-type MITF, with S73A having the highest proportion located in the nucleus among all the variants tested.

As described previously in Chapter 4.1.2, MITF is also known to be phosphorylated by GSK3 on S298 (Takeda et al., 2000a) and S397, S401 and S405 (Ploper et al., 2015). To determine if the MITF localisation effects we observed following GSK3 inhibition were mediated via these four reported GSK3 phosphorylation sites, we also generated alanine mutants at these residues in GFP-MITF and analysed their sub-cellular localisation by immunofluorescence. We did not observe any significant changes in localisation with either the S298A single mutant or the S397.S401A.S405A triple mutant in GFP-MITF (Figure 4.9a, b).

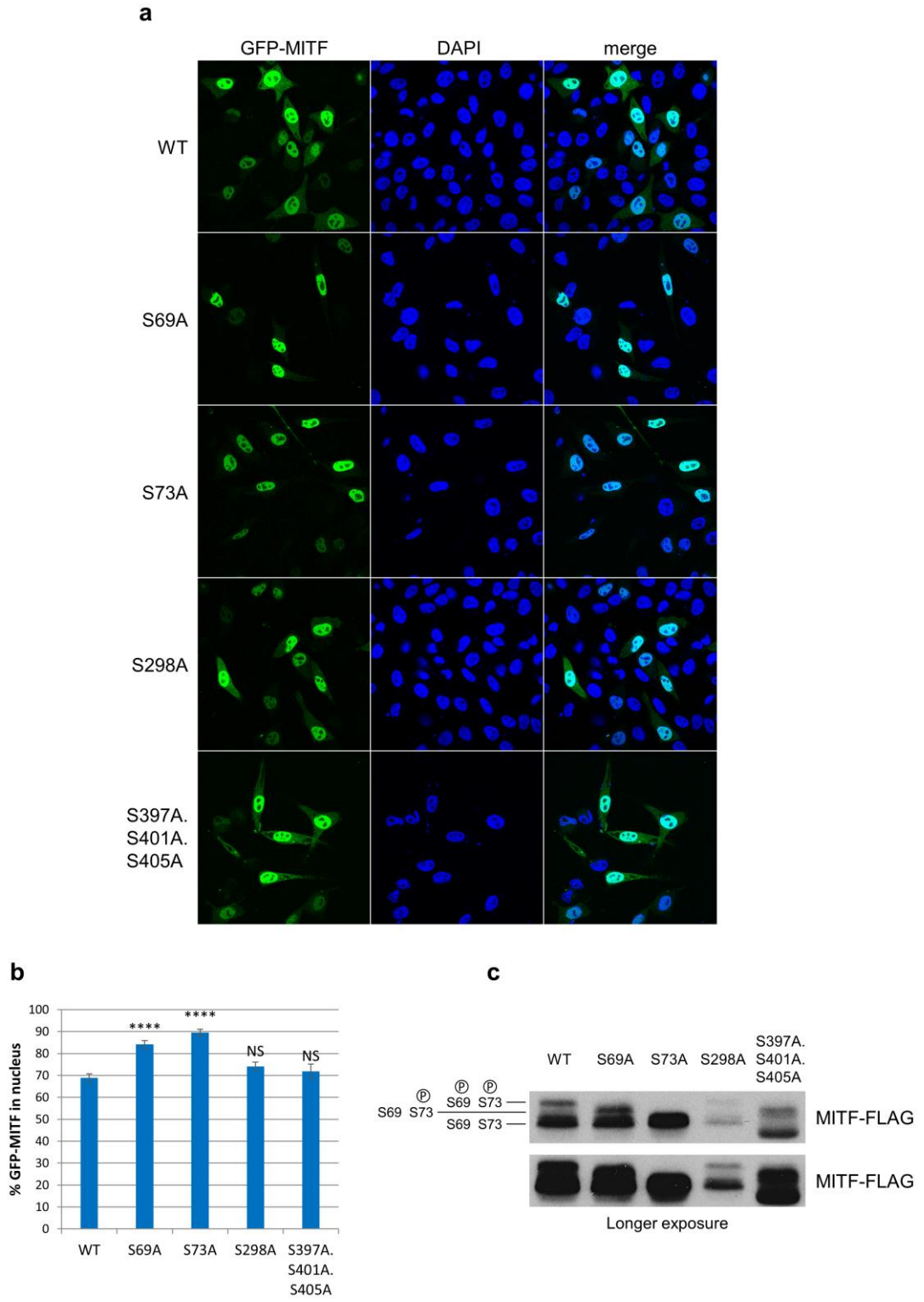

Figure 4.9 S69A mutagenesis caused an increase in GFP-MITF nuclear localisation, while S69A mutagenesis recapitulated the MITF mobility shift observed with GSK3 inhibition. (a) Fluorescence images of 501mel cells ectopically expressing GFP-MITF mutants (green). Cells were grown on glass coverslips to 50% confluence before being transfected using Fugene 6. Cells were fixed 48 hours post transfection, before being stained with DAPI (blue). Images were acquired by confocal microscopy. **(b)** Quantification of the sub-cellular localisation of GFP-MITF mutants in 501mel cells. Cells were transfected and processed as in (a). A minimum of 40 cells were quantified per mutant. Error bars represent SEM. 2-tailed t-test: **** *p<0.0001*, NS (not significant) *p>0.05*. **(c)** Western blot of 501mel cells ectopically expressing MITF-FLAG mutants. Cells were grown to 50% confluence before being transfected using Fugene 6. After 48 hours, cells were lysed and immunoblotted with an antibody against FLAG.

We also analysed the electrophoretic mobility of these mutants in MITF-FLAG via western blot (Figure 4.9c). The mobility of the S298A mutant looked very similar to that of wild-type. For the S397.S401A.S405A triple mutant, both upper and lower bands shifted downwards by a similar amount, while the separation between the two bands remained unchanged. Neither of these two mutants could recapitulate the mobility shift seen with GSK3 inhibition in Figure 4.8a, b.

On the other hand, when analysed by western blot, S69A mutagenesis in MITF-FLAG recapitulated the shift in MITF electrophoretic mobility observed with GSK3 inhibition. As shown in Figure 4.9c, the upper band in the S69A mutant had shifted downwards to an intermediate position, similar to the middle band in Figure 4.8a, b. The position of the lower band the S69A mutant remained unchanged. In comparison, the S73A mutant only had a single band at the lower position. This led us to believe that the upper, middle and lower bands represented MITF with different combinations of phosphorylation status at S69 and S73. The upper band would correspond to MITF that was phosphorylated on both S69 and S73, while the middle band was phosphorylated on S73 but not S69 (Figure 4.9c). The lower band would represent a species that was not phosphorylated at either residue. The fact that the majority of endogenous MITF typically appears as either the upper band or the lower band, but not the middle band, suggests that S73 phosphorylation is the limiting factor. Since there appears to be very little MITF that is phosphorylated on S73 but not S69, this indicates that any MITF has a priming phosphorylation on S73 will invariably also get phosphorylated by GSK3 on S69, which indicates that GSK3 activity is present in excess in the system.

We also wanted to investigate the effects of TPA treatment on the sub-cellular localisation of the S69A mutant. Unlike the S73A mutant which did not demonstrate any significant response to TPA stimulation, TPA treatment caused the both wild-type GFP-MITF and the S69A mutant to translocate significantly to the cytoplasm (Figure 4.10a, b). However, translocation occurred to a lesser extent in the case of the S69A mutant compared to wild-type GFP-MITF, with a 12% decrease in nuclear localisation of the S69A mutant after TPA treatment versus a 29% reduction in nuclear localisation in the case of wild-type GFP-MITF (Figure 4.10b). These results suggest that phosphorylation events at both S69 and S73 residues play a critical functional role in mediating MITF translocation, with two phosphorylation events having an additive effect that is stronger than one phosphorylation.

Next, we carried out an *in vitro* kinase assay in order to verify that the S69 residue in MITF was indeed being phosphorylated by GSK3. However, we were unable to utilise bacterially-expressed MITF protein as the substrate since GSK3 phosphorylation requires a priming phosphorylation on S73. To address this issue, we made use of SPOT technology (Winkler et al., 2009) to synthesise 21 residue-long peptides corresponding to the region between MITF residues 61 and 81, including ones that were phosphorylated at S73. These peptides were immobilised on a cellulose support membrane, after which they were incubated with purified GSK3 kinase and radioactive [γ-^{32}P]-ATP. We then analysed the membrane for incorporation of radioactive ATP using a phosphorimager system (Figure 4.11).

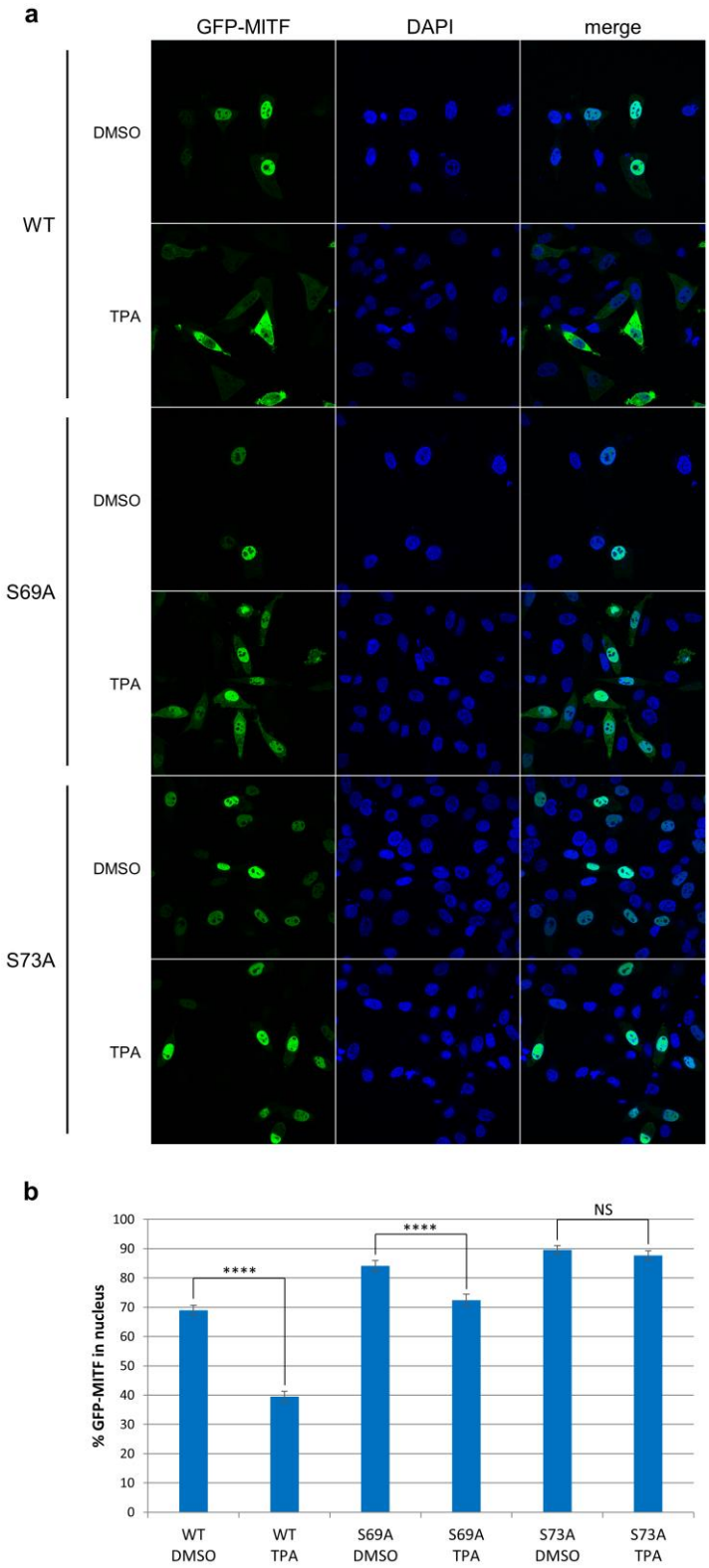

Figure 4.10 Unlike the S73A mutant, the S69A mutant responded to TPA-mediated cytoplasmic translocation, but to a lesser extent than than wild-type GFP-MITF. (a) Fluorescence images of 501mel cells ectopically expressing GFP-MITF mutants (green). Cells were grown on glass coverslips to 50% confluence before being transfected using Fugene 6. After 48 hours, cells were treated with 200 nM TPA or an equivalent volume of DMSO for 1 hour. Cells were then fixed before being stained with DAPI (blue). Images were acquired by confocal microscopy. **(b)** Quantification of the sub-cellular localisation of GFP-MITF mutants in 501mel cells. Cells were transfected and processed as in (a). A minimum of 45 cells were quantified per condition. Error bars represent SEM. 2-tailed t-test: **** $p<0.0001$, NS (not significant) $p>0.05$.

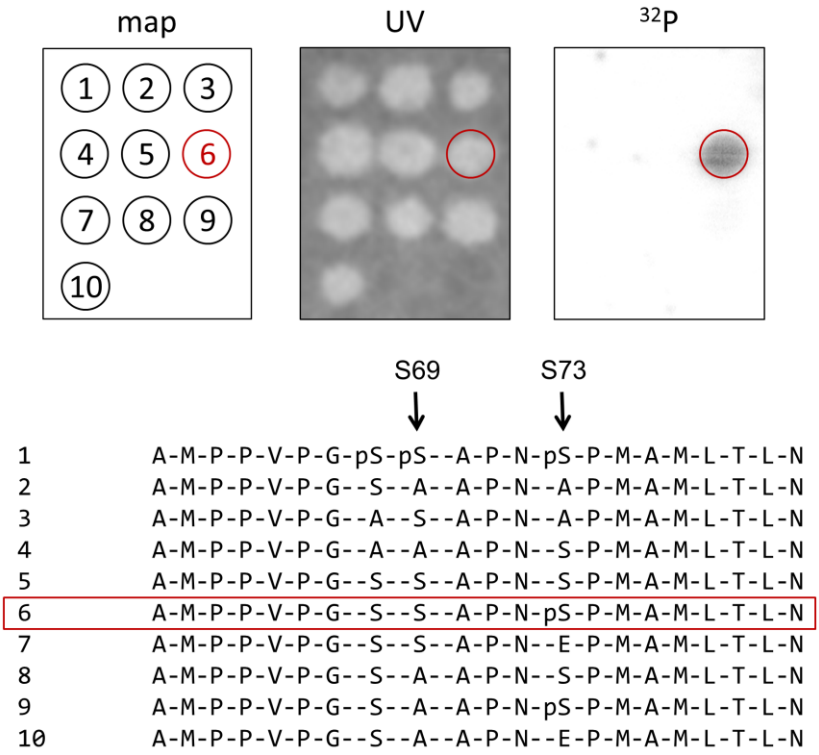

Figure 4.11 A peptide SPOT kinase assay demonstrated GSK3 phosphorylation of MITF at S69 following a priming phosphorylation at S73. 21 residue-long peptides corresponding to MITF residues 61 to 81, and incorporating various mutations and modifications, were immobilised on a cellulose support membrane. The membrane was then incubated with 100 ng of purified GSK3 kinase and 5 µCi [γ-^{32}P]-ATP at 30°C for 30 minutes. After washing, incorporation of ^{32}P was detected by phosphorimager (top, right panel). The membrane was imaged in UV light to show the relative size of the peptide spots (top, middle panel). A map showing the identity of the 10 tested peptides is also provided (top, left panel and bottom list).

As shown in Figure 4.11, we tested various mutations and modifications, including phosphorylation, at the key residues. Spot 6, highlighted in red, was the only spot that gave a positive signal demonstrating phosphorylation by GSK3. The identity of spot 6 corresponded exactly to the **S**-X-X-X-pS consensus recognition motif of GSK3, with S69 phosphorylated after a priming phosphorylation at the +4 position on S73. Comparing spots 6 and 9, we see that GSK3 phosphorylation was abrogated upon mutation of S69 to the non-phosphorylatable alanine residue, demonstrating that the positive signal observed with spot 6 was indeed due to phosphorylation at S69 and not at other residues. A comparison of spots 6 and 5 reveals that GSK3 phosphorylation at S69 was abrogated in the absence of S73

phosphorylation. Comparing spots 6 and 7, we see that a glutamic acid substitution, which is typically used as a phospho-serine mimic, at S73 was not sufficient to induce S69 phosphorylation by GSK3. The results of this *in vitro* kinase assay indicated that GSK3 can phosphorylate the S69 residue of MITF, with a priming phosphorylation at S73 being a prerequisite for this to occur.

4.2.5 TPA-mediated MITF cytoplasmic translocation is not dependent on DNA binding and 14-3-3 interaction

While we were aware that phosphorylation at S69 and S73 in MITF could affect MITF localisation, the exact mechanism of action was still unknown to us. We wondered if the localisation effects seen with TPA treatment could be mediated by a change in the ability of MITF to bind DNA. To investigate this further, we mutated E213, a key residue involved in binding M-box and E-box DNA elements (Pogenberg et al., 2012), to an alanine residue in the MITF-FLAG construct. We then expressed this mutant in 501mel melanoma cells and treated them with TPA before analysing MITF's sub-cellular localisation via immunofluorescence (Figure 4.12).

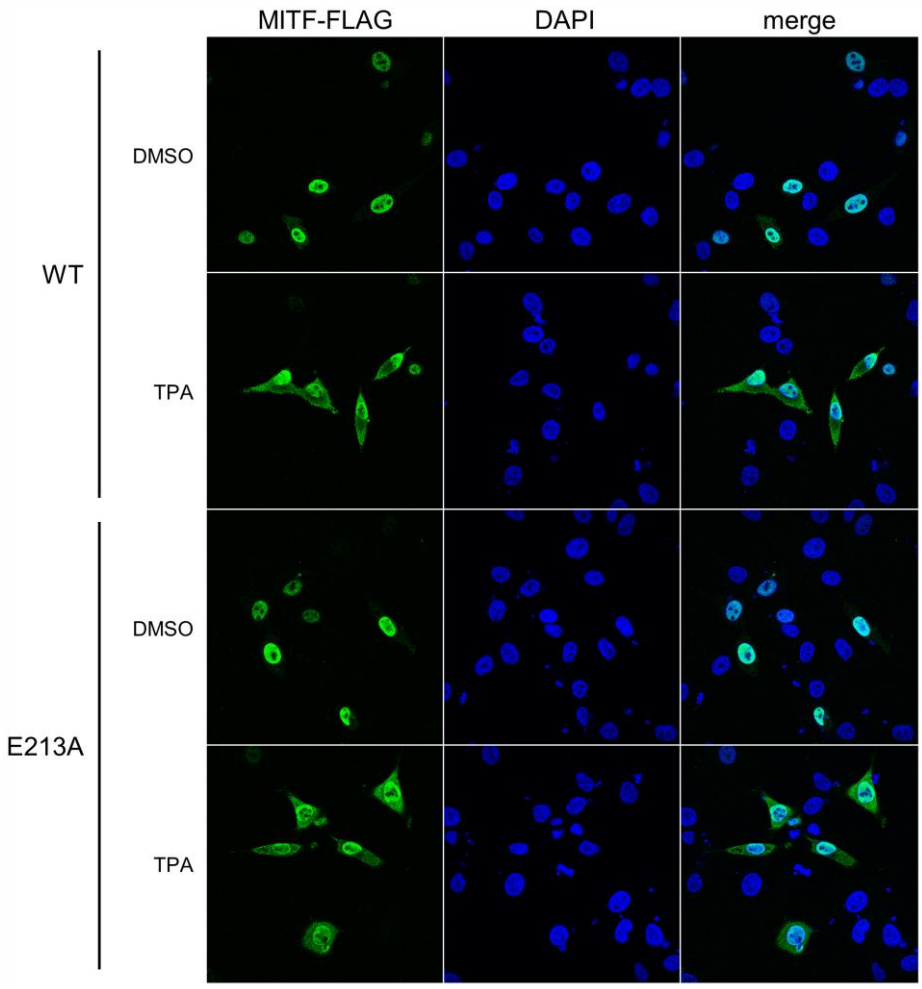

Figure 4.12 Lack of DNA binding ability did not affect localisation of MITF. Immunofluorescence images of 501mel cells ectopically expressing both wild-type MITF-FLAG and the non-DNA binding E213A mutant. Cells were grown on glass coverslips to 50% confluence before being transfected using Fugene 6. 48 hours later, cells were treated with 200 nM TPA or an equivalent volume of DMSO for 1 hour. Cells were fixed and permeabilised, before being stained with DAPI (blue) and an antibody against FLAG (green). Images were acquired by confocal microscopy.

As shown in Figure 4.12, compared to wild-type MITF-FLAG, an alanine substitution at E213 in MITF did not seem to affect its localisation with either TPA or DMSO treatment. Despite being theoretically incapable of binding DNA, the E213A MITF-FLAG mutant was still mainly nuclear in the DMSO-treated control. Following TPA stimulation, the E213A mutant also exhibited a similar amount of cytoplasmic translocation as wild-type MITF-FLAG.

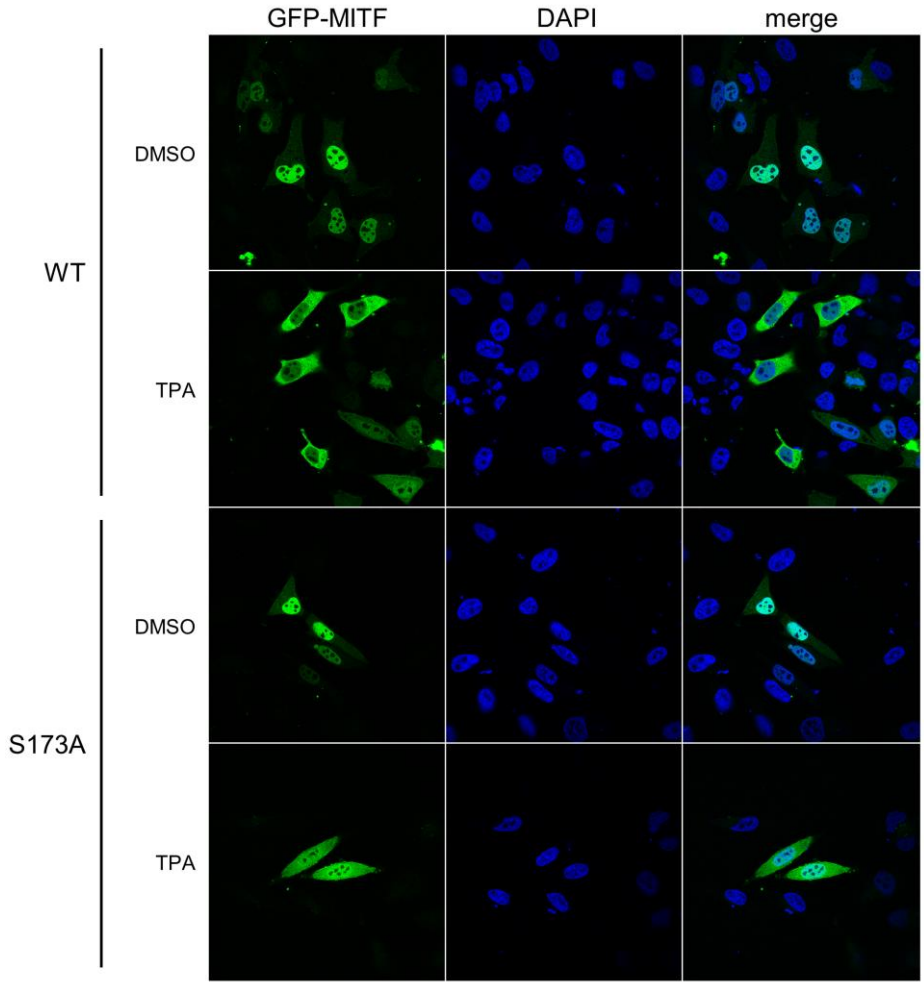

Figure 4.13 TPA-mediated cytoplasmic translocation of MITF was observed despite the lack of 14-3-3 binding. Fluorescence images of 501mel cells ectopically expressing both the S173A mutant and wild-type GFP-MITF (green). Cells were grown on glass coverslips to 50% confluence before being transfected using Fugene 6. At 48 hours post transfection, cells were treated with 200 nM TPA or an equivalent volume of DMSO for 1 hour. After fixation, cells were stained with DAPI (blue). Images were acquired by confocal microscopy.

We also suspected that MITF translocation to the cytoplasm could be mediated via interactions with 14-3-3 proteins, which are known to be molecular chaperones that can sequester their binding partners in the cytoplasm (Mhawech, 2005). As outlined previously in Chapter 4.1.2, phosphorylation at S173 in MITF is required for its interaction with 14-3-3 proteins in osteoclasts (Bronisz et al., 2006). Hence, we mutated S173 to a non-phosphorylatable alanine residue in GFP-MITF to abolish its association with 14-3-3 proteins, and analysed its localisation in 501melanoma cells via confocal microscopy (Figure 4.13). In the absence of TPA, there were no visible differences in the localisation of the wild-type GFP-MITF and the S173A

mutant. TPA treatment was still able to induce cytoplasmic translocation of the S173A mutant despite its inability to bind to 14-3-3 proteins in the cytoplasm. However, compared to wild-type GFP-MITF, there seemed to be slightly less translocation to the cytoplasm in the S173A mutant. These results were consistent with TPA-mediated MITF cytoplasmic translocation not being mediated via changes in DNA binding and interactions with 14-3-3 proteins.

4.2.6 TPA-mediated MITF cytoplasmic translocation is regulated by the region between MITF residues 60 and 99

We also wondered if intra-molecular interactions could be playing a role in TPA-mediated MITF cytoplasmic translocation, particularly in terms of nuclear import being affected by potential intra-molecular interactions between the nuclear localisation signal (NLS) located in the basic region of MITF (Takebayashi et al., 1996) and S73 in the N-terminus. To address this question, we fused the N-terminus in MITF, comprising of the first 180 amino acids, to a FLAG tag and expressed it in 501mel melanoma cells in the presence of TPA. We then analysed its sub-cellular localisation via immunofluorescence (Figure 4.14).

The MITF N-terminal fragment was responsive to TPA stimulation, with a similar degree of cytoplasmic translocation observed compared to the full-length protein. This led us to conclude that TPA-mediated cytoplasmic translocation of MITF was not being mediated via intra-molecular interactions with the NLS, nor did it require dimerization since the N-terminus appeared to be sufficient for cytoplasmic localisation on its own without the basic region.

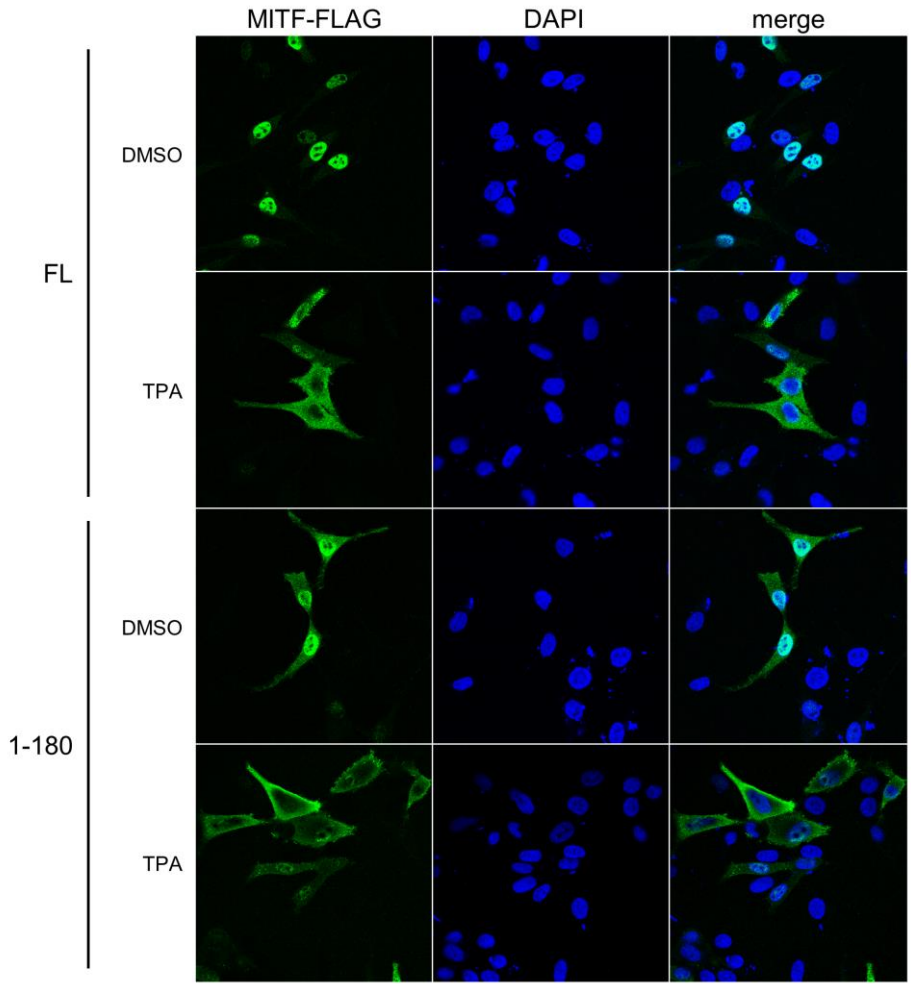

Figure 4.14 The MITF.1-180 N-terminal fragment was localised to the cytoplasm following TPA treatment. Immunofluorescence images of 501mel cells ectopically expressing both full-length (FL) MITF-FLAG and an N-terminal fragment comprising of the first 180 amino acids (1-180) in MITF. Cells were grown on glass coverslips to 50% confluence before being transfected using Fugene 6. After 48 hours, cells were treated with 200 nM TPA or an equivalent volume of DMSO for 1 hour. After fixation and permeabilisation, cells were stained with DAPI (blue) and an antibody against FLAG (green). Images were acquired by confocal microscopy.

We knew that S69 and S73 were the key residues in mediating the cytoplasmic localisation of MITF in response to TPA treatment, but we wanted to know if other regions were also required. Since the N-terminus appeared to be sufficient for cytoplasmic translocation, we made N-terminal deletion mutants to determine more precisely the region involved in MITF translocation to the cytoplasm.

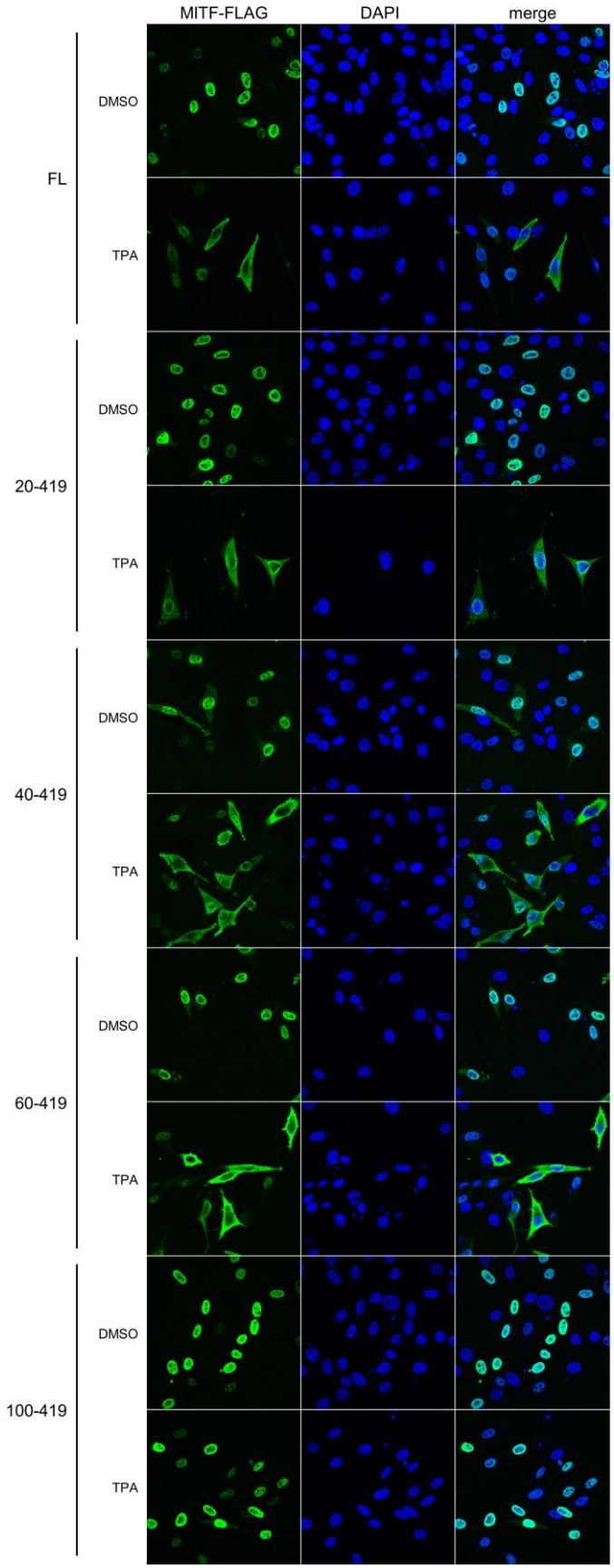

Figure 4.15 TPA-mediated MITF cytoplasmic translocation was dependent on MITF residues 60 to 99. Immunofluorescence images of 501mel cells ectopically expressing full-length (FL) MITF-FLAG as well as various N-terminal deletion mutants with up to the first 99 residues being removed. Cells were grown on glass coverslips to 50% confluence before being transfected using Fugene 6. After 48 hours, cells were treated with 200 nM TPA or an equivalent volume of DMSO for 1 hour. Following fixation and permeabilisation, cells were stained with DAPI (blue) and an antibody against FLAG (green). Images were acquired by confocal microscopy.

We generated MITF fragments encoding residues 20-419, 40-419, 60-419 and 100-419, which represented MITF lacking the first 19, 39, 59 and 99 amino acids respectively. We then appended these mutants with a C-terminal FLAG tag and analysed their sub-cellular localisation in 501mel melanoma cells in response to TPA treatment via immunofluorescence (Figure 4.15). MITF fragments lacking the first 19, 39 and 59 residues were still able to translocate to the cytoplasm following TPA treatment. However, the MITF fragment encoding residues 100-419 remained in the nucleus after TPA stimulation. These results were consistent with TPA-induced MITF cytoplasmic translocation was being mediated by the specific region between MITF residues 60 and 99.

4.2.7 MITF cytoplasmic translocation is mediated by nuclear export

Since TPA-induced cytoplasmic localisation of MITF did not appear to involve its NLS and, by extension, the process of nuclear import, we postulated that it might be a result of increased nuclear export. To investigate this theory, we expressed wild-type GFP-MITF in 501mel melanoma cells and treated them with TPA in the presence of leptomycin B (LMB), a small molecule which inhibits nuclear export by binding to exportin 1 (Fornerod et al., 1997). We then analysed the sub-cellular localisation of GFP-MITF via confocal microscopy (Figure 4.16a, b).

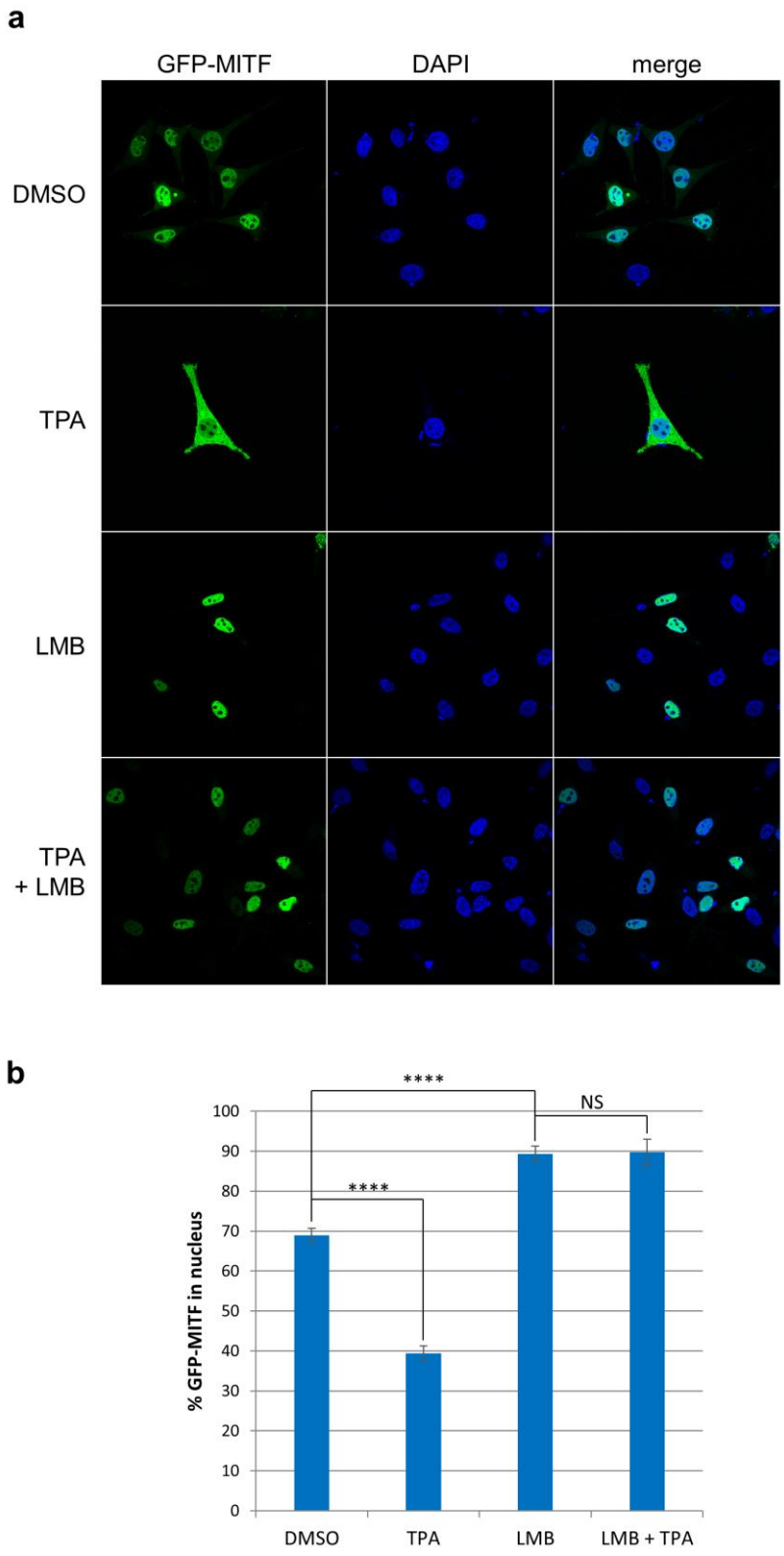

Figure 4.16 Inhibition of nuclear export with leptomycin B blocked TPA-induced cytoplasmic translocation of MITF. (a) Fluorescence images of 501mel cells ectopically expressing wild-type GFP-MITF (green). Cells were grown on glass coverslips to 50% confluence before being transfected using Fugene 6. After 48 hours, cells were treated with 200 nM TPA for 1 hour and/or 20 nM LMB for 3 hours. Cells were then fixed before being stained with DAPI (blue). Images were acquired by confocal microscopy. **(b)** Quantification of GFP-MITF sub-cellular localisation in 501mel cells. Cells were transfected and processed as in (a). A minimum of 45 cells were quantified per condition. Error bars represent SEM. 2-tailed t-test: **** $p<0.0001$, NS (not significant) $p>0.05$.

As shown in Figure 4.16b, relative to the DMSO-treated control, LMB treatment caused a significant increase in the proportion of GFP-MITF present in the nucleus. Inhibition of nuclear export with LMB also completely blocked TPA-mediated cytoplasmic translocation of GFP-MITF (Figure 4.16a), with no significant differences observed in the proportion of GFP-MITF present in the nucleus when cells were co-treated with LMB and TPA compared to treatment with LMB alone (Figure 4.16b). These results were consistent with TPA-induced MITF cytoplasmic translocation being mediated by an increase in nuclear export.

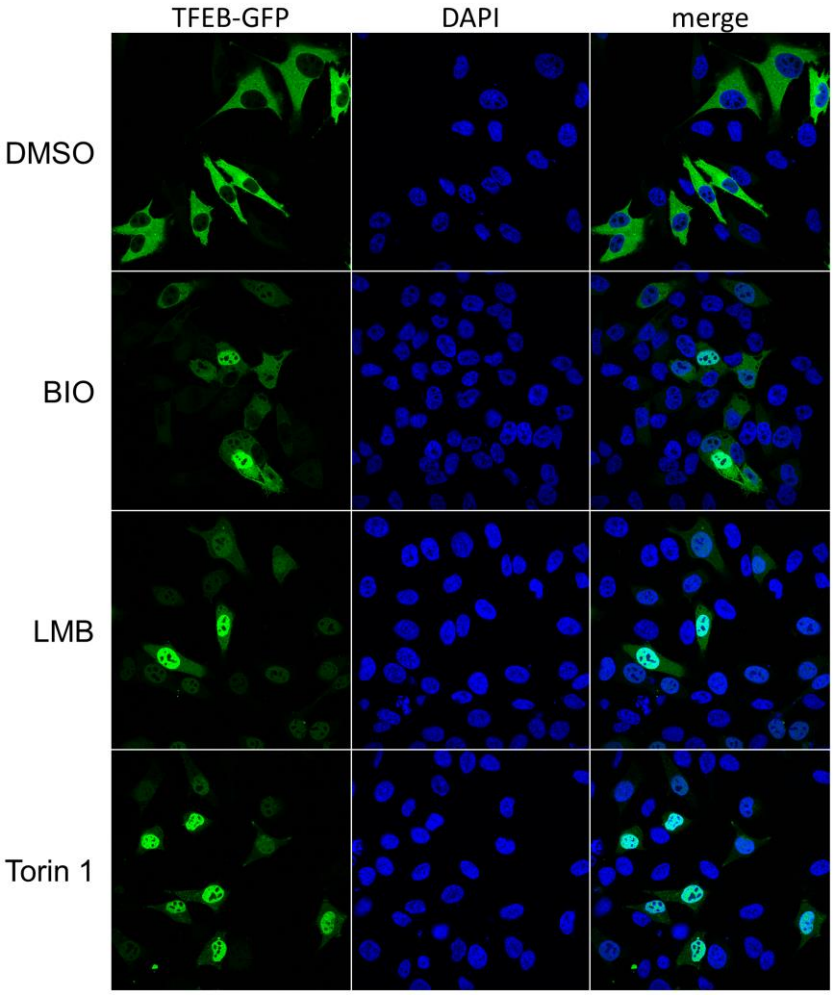

Figure 4.17 BIO and Leptomycin B caused TFEB to translocate to the nucleus. Fluorescence images of 501mel cells ectopically expressing wild-type TFEB-GFP (green). Cells were grown on glass coverslips to 50% confluence before being transfected using Fugene 6. After 48 hours, cells were treated with 1 μM BIO for 1 hour, 20 nM LMB for 3 hours or 250 nM Torin 1 for 3 hours. Cells were then fixed before being stained with DAPI (blue). Images were acquired by confocal microscopy.

We were also curious to know if the localisation of TFEB, a related member of the MiT family, could be regulated in a similar manner as that of MITF, given that the S69 and S73 residues in MITF are both conserved in TFEB (Figure 4.8). We expressed wild-type TFEB-GFP in 501mel melanoma cells and treated the cells with either BIO, LMB, or Torin 1. Torin 1 is a potent and selective inhibitor of mTOR (IC_{50} = 3 nM) (Thoreen et al., 2009). We then examined the sub-cellular localisation of GFP-MITF via confocal microscopy (Figure 4.17).

As shown in the DMSO-treated control in Figure 4.17, the majority of TFEB was typically localised in the cytoplasm. TFEB is known to be a cytoplasmic protein that translocates to the nucleus upon dephosphorylation of S142 (Settembre et al., 2012), the equivalent residue to S73 in MITF. Since S142 is phosphorylated by mTOR, treatment with the mTOR inhibitor Torin 1 causes TFEB to translocate into the nucleus (Settembre et al., 2012). Thus, we utilised Torin 1 treatment as the positive control for nuclear translocation of TFEB. Inhibiting nuclear export with LMB also resulted in TFEB being translocated into the nucleus, to a similar extent as that observed with Torin 1 treatment. GSK3 inhibition with BIO also resulted in nuclear translocation of TFEB, but to a lesser extent compared to LMB and Torin 1. These results suggest that, as is the case with MITF, the localisation of TFEB can also be affected by nuclear export as well as GSK3 phosphorylation.

4.2.8 MITF contains a functional NES between MITF residues 60 and 99

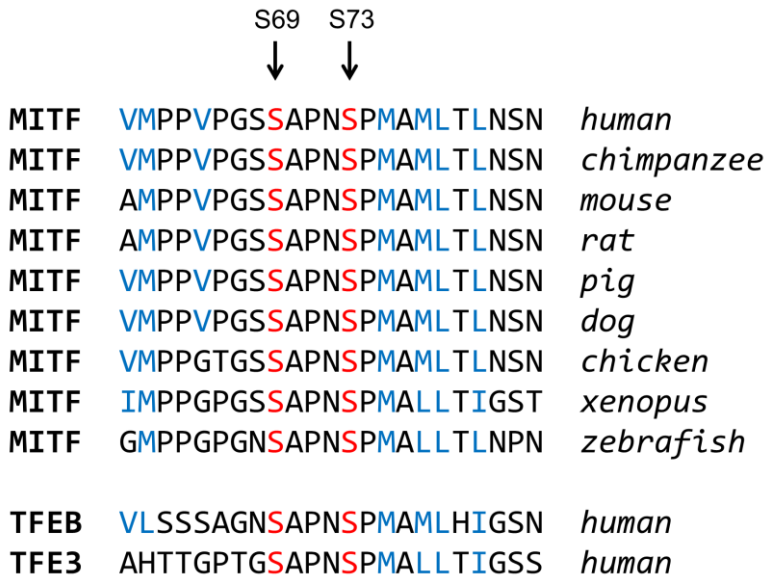

Figure 4.18 MITF contains many hydrophobic residues in the vicinity of S69 and S73. Protein sequence alignment of MITF, TFEB and TFE3. S69 and S73 in MITF highlighted in red, hydrophobic amino acids highlighted in blue.

The results obtained with LMB treatment indicated a key role for nuclear export in mediating TPA-induced cytoplasmic translocation of MITF. Together with the previous data, this suggested to us that there was a functional nuclear export signal (NES) located between MITF residues 60 and 99, probably centred around S69 and S73 residues. Thus, we took a closer look at the protein sequence around S69 and S73 in MITF (Figure 4.18). We noted the presence of multiple hydrophobic residues in this region of MITF, many of which are conserved across multiple species, and also in the related MiT family members TFEB and TFE3. Since NES motifs typically consist of a series of hydrophobic residues (Güttler et al., 2010; Kosugi et al., 2008; Kutay and Güttinger, 2005), this strengthened our suspicion that the region between MITF residues 60 and 99 contains a functional NES.

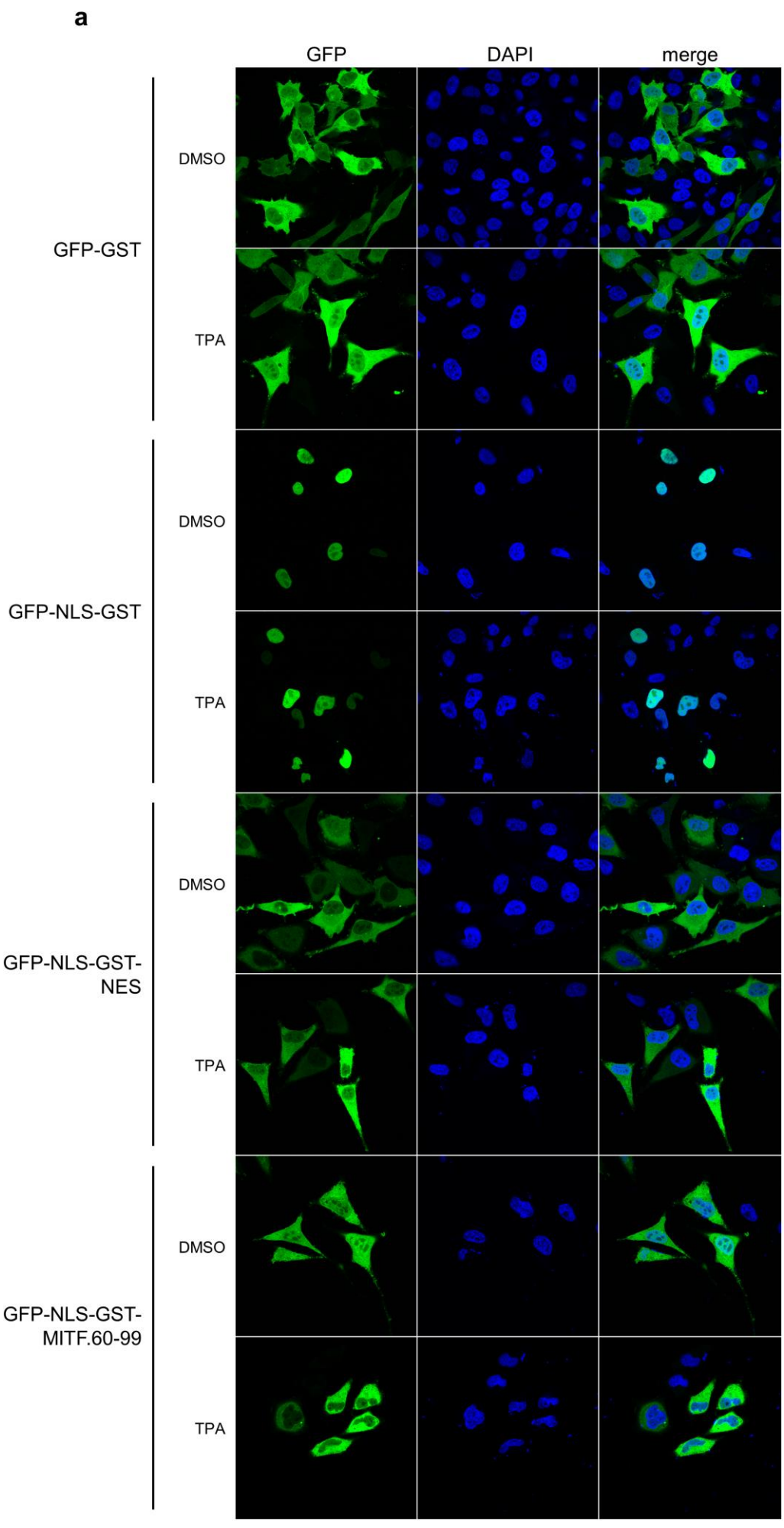
a
GFP
DAPI
merge
GFP-GST
DMSO
TPA
GFP-NLS-GST
DMSO
TPA
GFP-NLS-GST-NES
DMSO
TPA
GFP-NLS-GST-MITF.60-99
DMSO
TPA

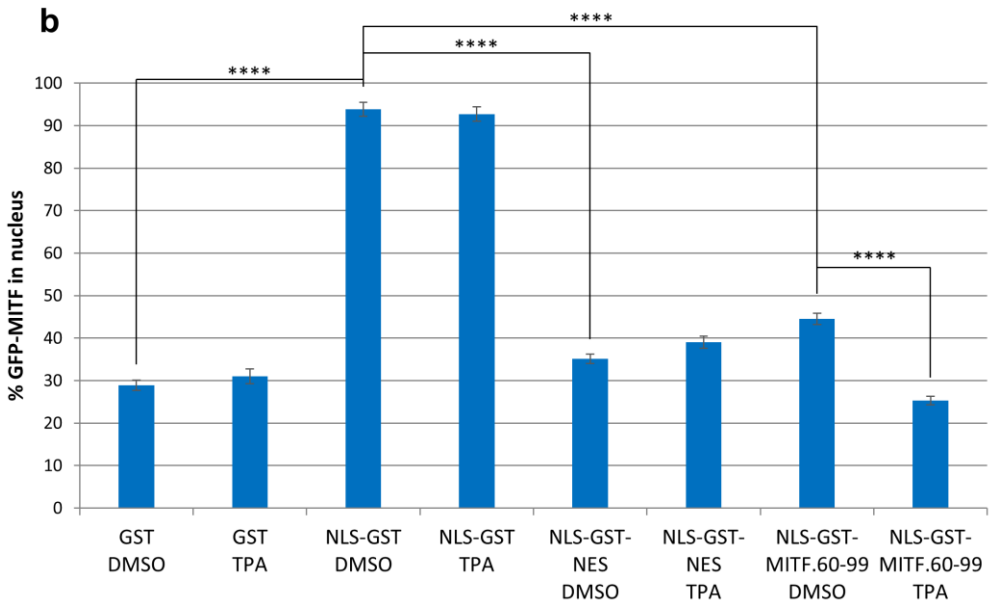

Figure 4.19 A functional NES was present in the MITF.60-99 fragment. **(a)** Fluorescence images of 501mel cells ectopically expressing fragments tagged with GFP-GST (green). Cells were grown on glass coverslips to 50% confluence before being transfected using Fugene 6. After 48 hours, cells were treated with 200 nM TPA or an equivalent volume of DMSO for 1 hour. Cells were then fixed before being stained with DAPI (blue). Images were acquired by confocal microscopy. **(b)** Quantification of the sub-cellular localisation of GFP-GST fragments in 501mel cells. Cells were transfected and processed as in (a). A minimum of 35 cells were quantified per condition. Error bars represent SEM. 2-tailed t-test: **** $p<0.0001$.

To investigate further, we cloned the region between MITF residues 60 and 99 (MITF.60-99), and tagged it with GFP for visualisation. We also added a Glutathione S-transferase (GST) tag to increase the size of the fusion protein and prevent background diffusion from affecting our results, since the size limit for passive diffusion across the nuclear pore complex is believed to be between 40 and 60 kDa (Weis, 2003). However, in order to investigate nuclear export, we needed the protein in the nucleus. Hence, we also included a classical NLS, PKKKRKV, from the simian virus 40 (SV40) T-antigen (Kalderon et al., 1984) to promote nuclear import in our fusion protein.

We expressed the fusion proteins in 501mel melanoma cells and analysed their sub-cellular localisation via confocal microscopy (Figure 4.19a, b). As expected, the GST-GFP fusion protein on its own is predominantly cytoplasmic as its size (56

kDa) is at the limit of passive diffusion across the nuclear pore complex. The addition of the SV40 NLS makes the GST-NLS-GFP fusion protein significantly more nuclear compared to GST-GFP (Figure 4.19b). As a positive control, we appended a putative NES, LALKLAGLDI, from cAMP-dependent protein kinase inhibitor (PKI) (Wen et al., 1995) to the GST-NLS-GFP fusion protein. In line with an increase in nuclear export, the addition of the putative NES makes the GST-NLS-GFP-NES fusion protein significantly more cytoplasmic compared to GST-NLS-GFP.

Results obtained with the GST-NLS-GFP-MITF.60-99 fusion protein were similar to that of the positive control, with GST-NLS-GFP-MITF.60-99 significantly more cytoplasmic compared to GST-NLS-GFP lacking the additional MITF.60-99 fragment. Importantly, treatment with TPA caused GST-NLS-GFP-MITF.60-99 to become significantly more cytoplasmic, an effect not observed with any of the other fusion proteins tested. These results were consistent with the existence of a functional NES between MITF residues 60 and 99, whose functionality was significantly enhanced by TPA stimulation.

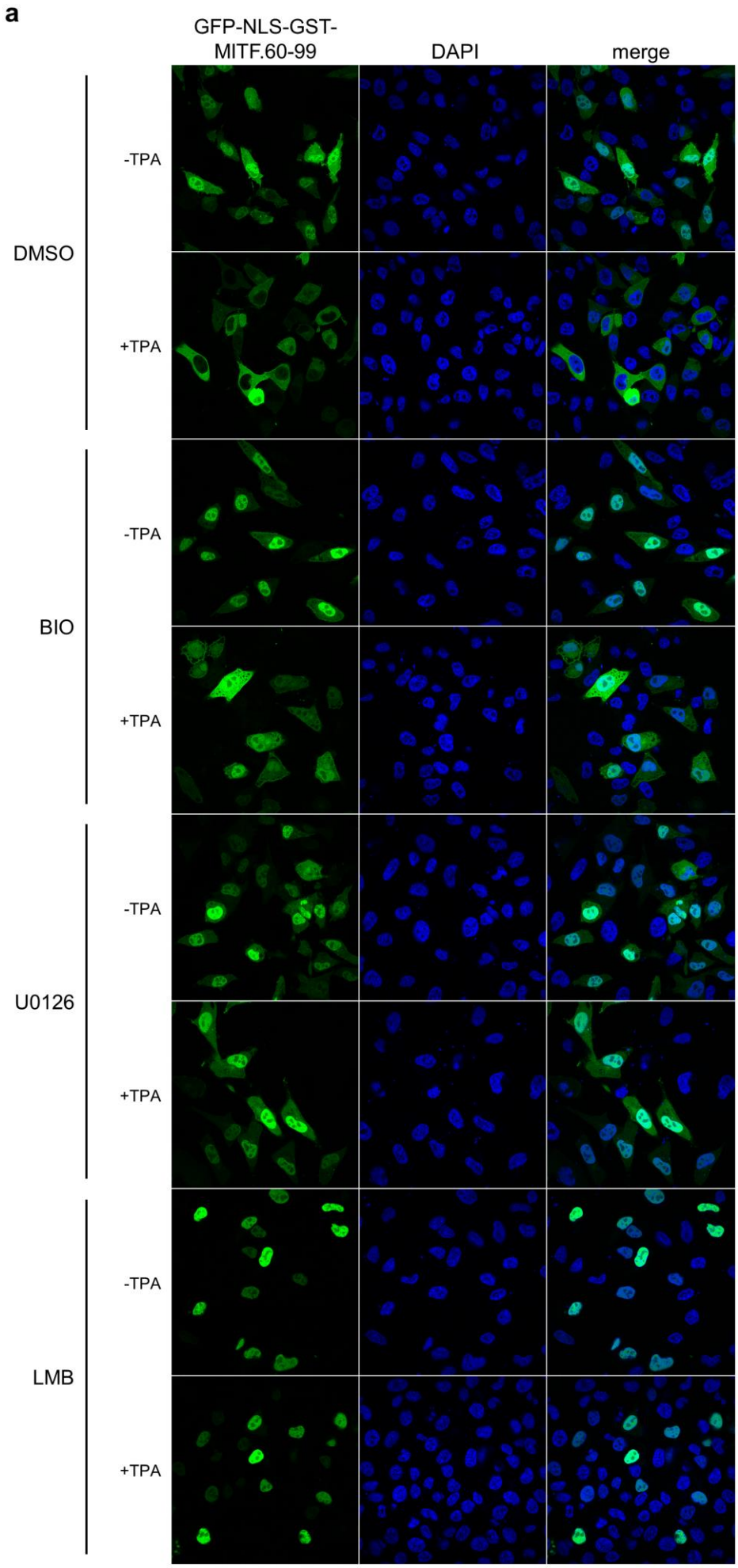
a
GFP-NLS-GST-MITF.60-99
DAPI
merge
DMSO
-TPA
+TPA
BIO
-TPA
+TPA
U0126
-TPA
+TPA
LMB
-TPA
+TPA

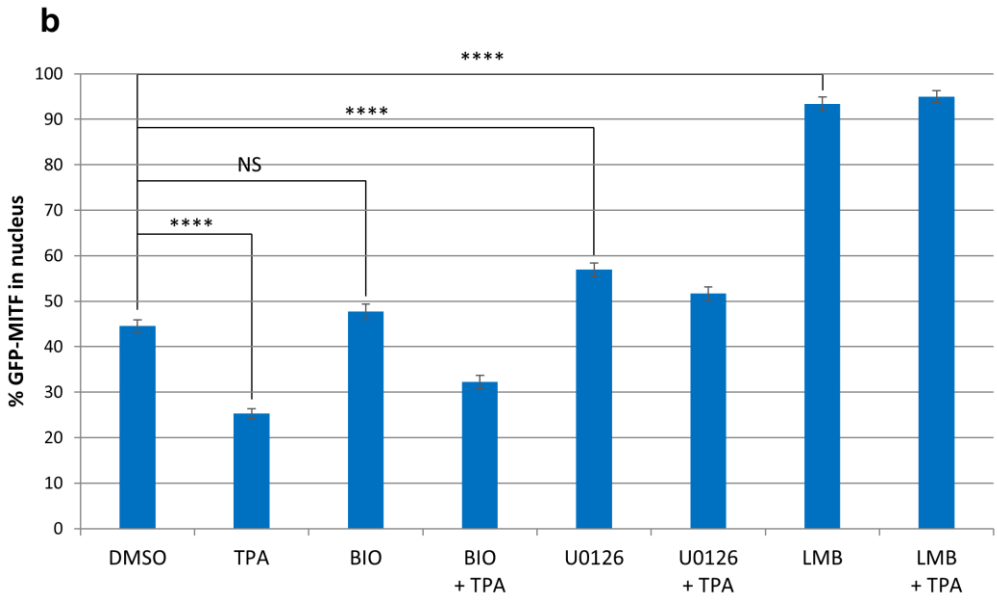

Figure 4.20 The NES within MITF.60-99 responded to GSK3 inhibition, MAPK activation/inhibition and nuclear export inhibition. (a) Fluorescence images of 501mel cells ectopically expressing GFP-NLS-GST-MITF.60-99 (green). Cells were grown on glass coverslips to 50% confluence before being transfected using Fugene 6. After 48 hours, cells were treated with 1 μM BIO for 1 hour, 10 μM of U0126 for 3 hours, 20 nM LMB for 3 hours and/or 200 nM TPA for 1 hour. Cells were then fixed before being stained with DAPI (blue). Images were acquired by confocal microscopy. **(b)** Quantification of GFP-NLS-GST-MITF.60-99 sub-cellular localisation in 501mel cells. Cells were transfected and processed as in (a). A minimum of 40 cells were quantified per condition. Error bars represent SEM. 2-tailed t-test: **** *p<0.0001*.

Next, we wanted to find out if the NES contained within MITF.60-99 was responsible for the response of full-length MITF to GSK3 inhibition, MAPK activation/inhibition and nuclear export inhibition. We expressed the GFP-NLS-GST-MITF.60-99 fusion protein in 501mel melanoma cells and treated them with BIO, U0126, LMB and/or TPA. We then analysed the sub-cellular localisation of the fusion protein via confocal microscopy (Figure 4.20a, b).

Similar to full-length MITF, MAPK activation with TPA resulted in a significant increase in cytoplasmic localisation of GFP-NLS-GST-MITF.60-99 compared to the DMSO-treated control (Figure 4.20b). In contrast, MEK inhibition with U0126 caused a significant increase in nuclear localisation of GFP-NLS-GST-MITF.60-99, while inhibition of nuclear export with LMB resulted in an even greater increase in nuclear localisation, as was the case with full-length MITF. However,

GSK3 inhibitor BIO had no significant effects on the localisation of GFP-NLS-GST-MITF.60-99. Both U0126 and LMB were able to prevent TPA-mediated cytoplasmic translocation, while BIO could only block the effects of TPA partially. These results were consistent with the NES between MITF residues 60 and 99 mediating the localisation phenotypes observed with full-length MITF in response to MAPK activation/inhibition and nuclear export inhibition.

4.2.9 S69, S73, M75, L78 and L80 are the key residues that make up the MITF NES

Since we had shown that MITF contained a functional NES between residues 60 and 99, we wanted to locate the critical residues that define this NES. To this end, we mutated S69 and S73, along with some of the hydrophobic residues in the vicinity of S69 and S73 that were outlined in Figure 4.18. In particular, we chose to mutate M62, V65, M75, M77, L78 and L80 as these residues were highly conserved. These candidate sites were mutated to alanine, a significantly less hydrophobic residue compared to leucine, methionine and valine. We incorporated these mutations into the GFP-NLS-GST-MITF.60-99 fusion protein and expressed them in 501mel melanoma cells. We then treated the cells with TPA and analysed the sub-cellular localisation of the mutants via confocal microscopy (Figure 4.21a, b, c).

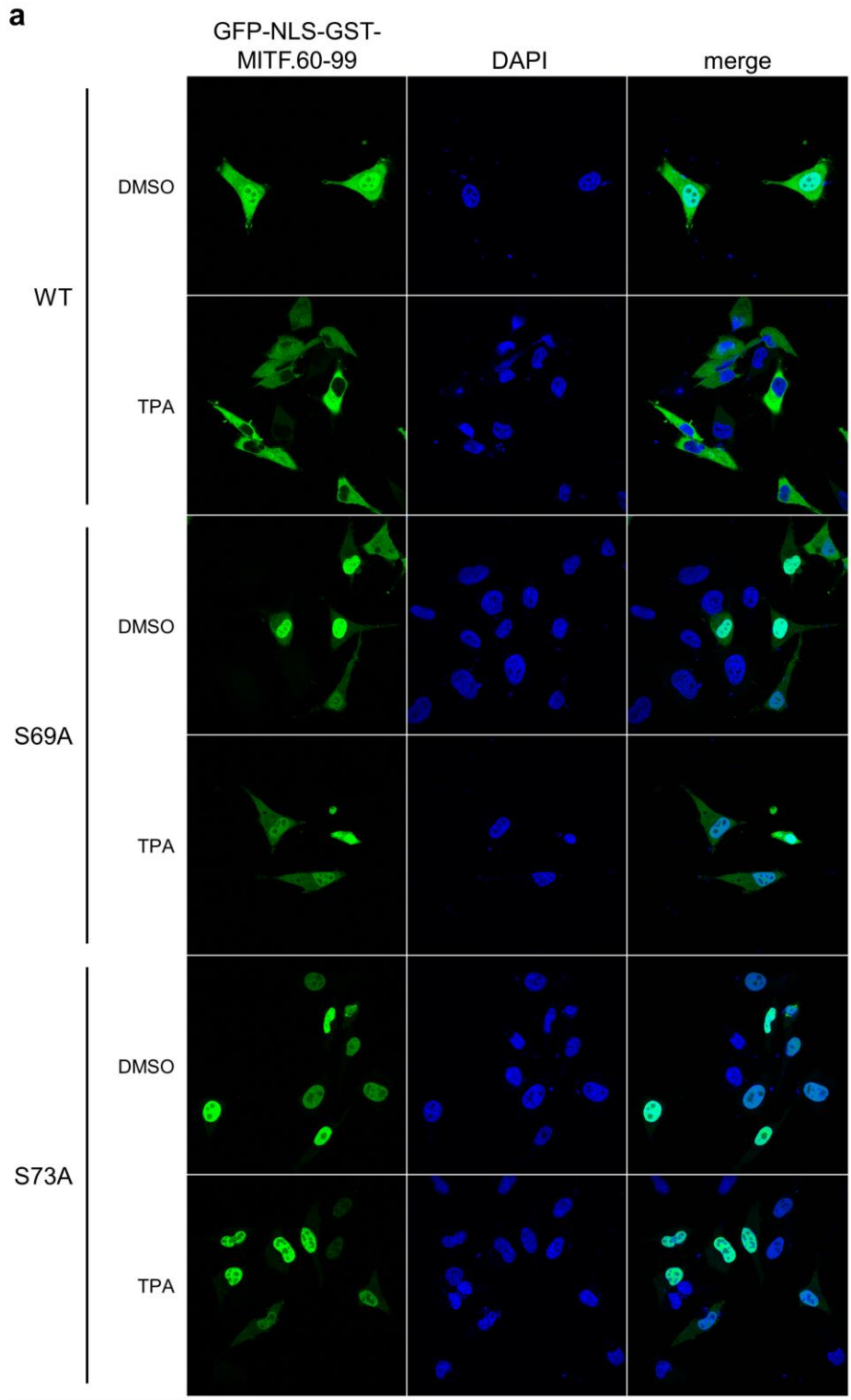

Figure 4.21 S69, S73, M75, L78 and L80 are the key residues in the MITF NES. (a) Fluorescence images of 501mel cells ectopically expressing wild-type GFP-NLS-GST-MITF.60-99 (green), as well as its S69A and S73A mutants. Cells were grown on glass coverslips to 50% confluence before being transfected using Fugene 6. After 48 hours, cells were treated with 200 nM TPA or an equivalent volume of DMSO for 1 hour. Cells were then fixed before being stained with DAPI (blue). Images were acquired by confocal microscopy.

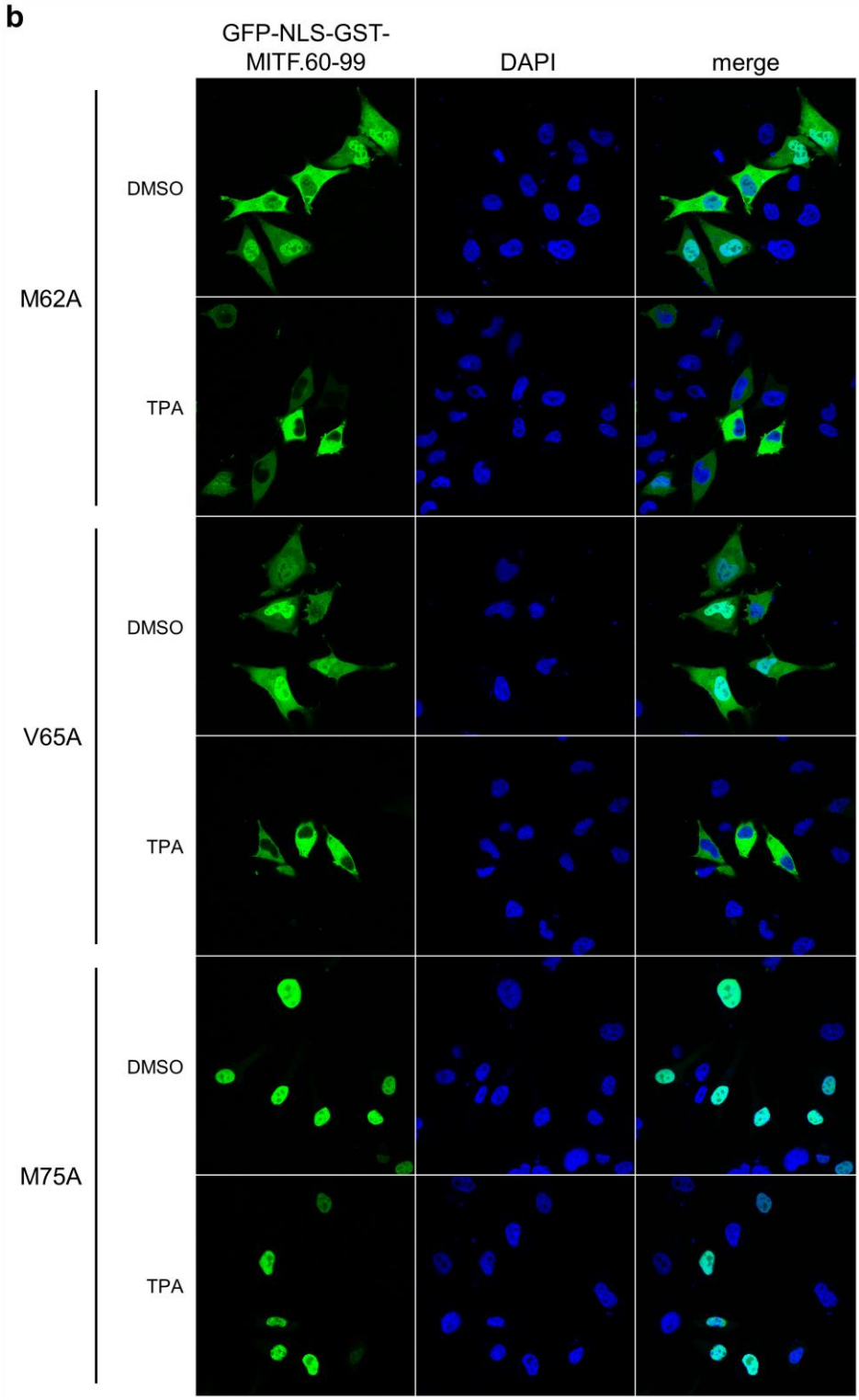

Figure 4.21 (b) Fluorescence images of 501mel cells ectopically expressing M62A, V65A, M75A, M77A, L78A and L80A mutants in GFP-NLS-GST-MITF.60-99 (green). Cells were grown on glass coverslips to 50% confluence before being transfected using Fugene 6. After 48 hours, cells were treated with 200 nM TPA or an equivalent volume of DMSO for 1 hour. Cells were then fixed before being stained with DAPI (blue). Images were acquired by confocal microscopy.

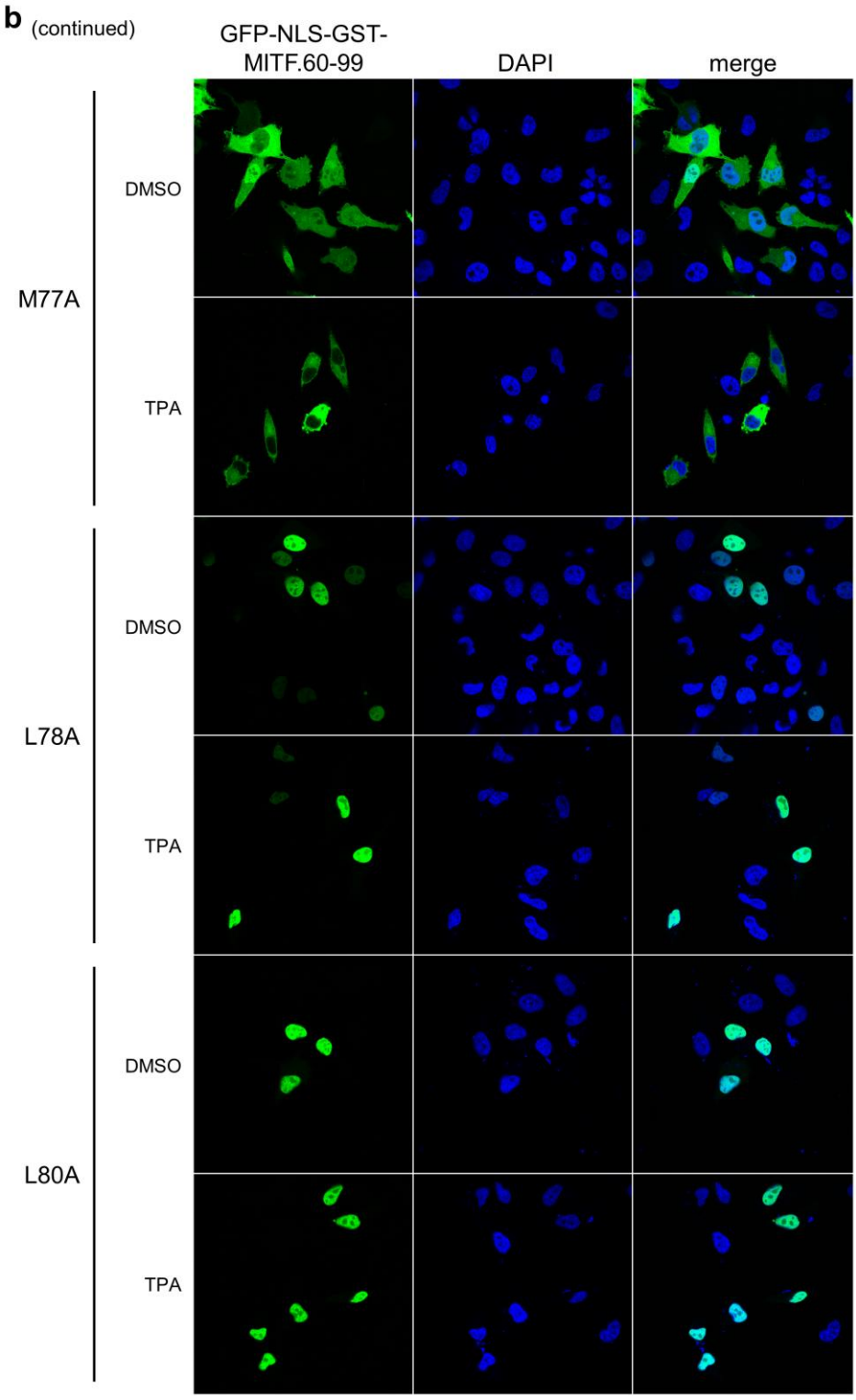
b (continued)
GFP-NLS-GST-MITF.60-99
DAPI
merge
M77A
DMSO
TPA
L78A
DMSO
TPA
L80A
DMSO
TPA

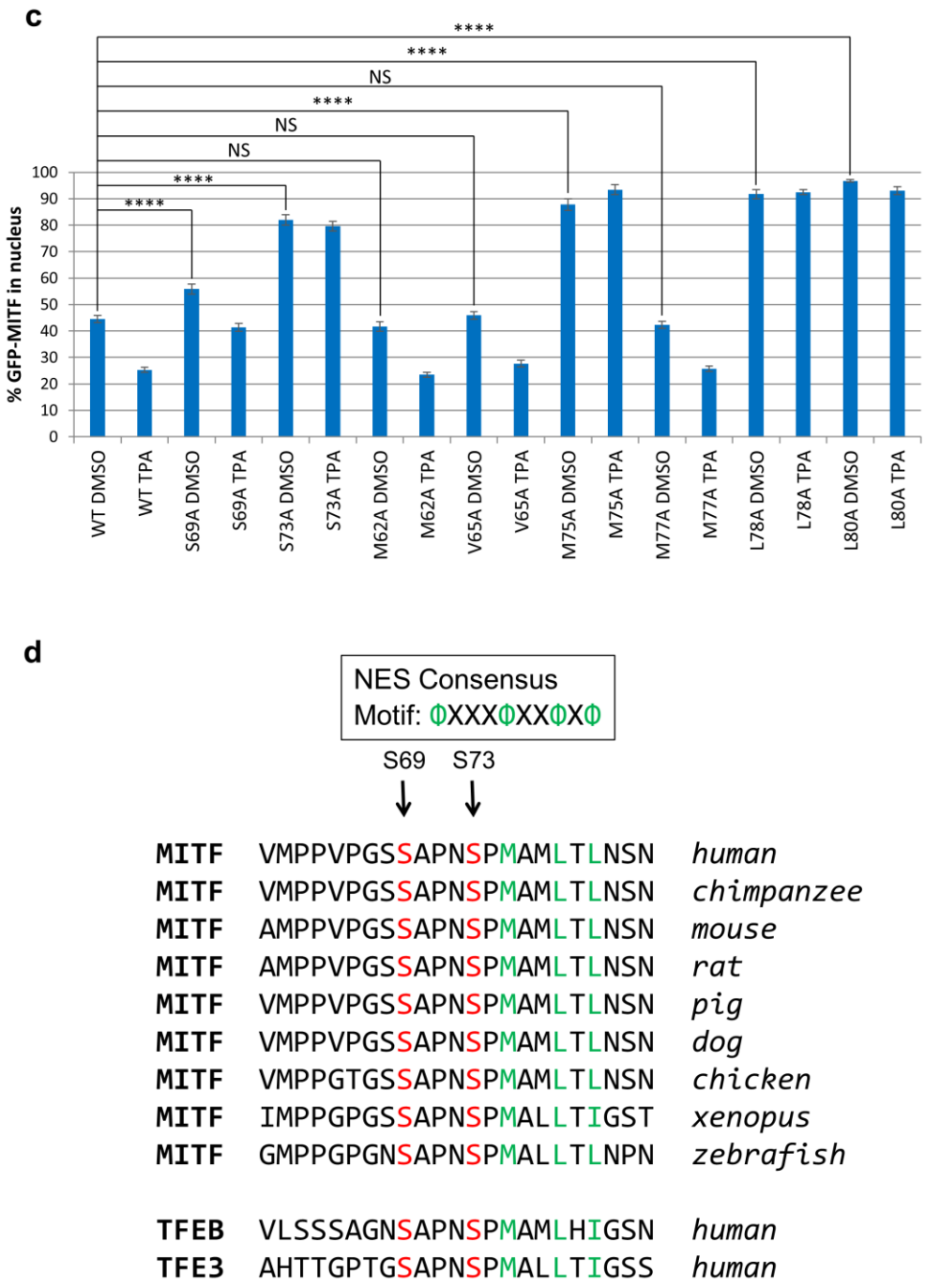

Figure 4.21 (c) Quantification of GFP-NLS-GST-MITF.60-99 sub-cellular localisation in 501mel cells. Cells were transfected and processed as in (a) and (b). A minimum of 40 cells were quantified per condition. Error bars represent SEM. 2-tailed t-test: **** *p<0.0001*, NS (not significant) *p>0.05*. **(d)** Summary of the key residues that make up the MITF NES. S69 and S73 in MITF highlighted in red, key hydrophobic residues of NES highlighted in green. Φ = L, M, I, V or F; X = any amino acid.

The results indicate that, similar to full-length MITF, the S69A mutant in GFP-NLS-GST-MITF.60-99 was significantly more nuclear than the wild-type variant (Figure 4.21a, c). The S73A mutant had an even greater degree of nuclear localisation than the S69A mutant, which was also the case with full-length MITF.

The S69A mutant translocated to the cytoplasm upon TPA stimulation, but to a lesser extent than the wild-type. The S73A mutant did not respond to TPA.

Among the six candidate hydrophobic residues tested, three of them failed to give a phenotype when mutated to alanine. There were no significant differences in the localisation of the M62A, V65A and M77A mutants compared to wild-type GFP-NLS-GST-MITF.60-99 (Figure 4.21b, c), and they responded to TPA-stimulation by translocating to the cytoplasm. On the other hand, the M75A, L78A and L80A mutants were significantly more nuclear compared to the wild-type variant. These three mutants also failed to translocate to the cytoplasm upon TPA stimulation.

As shown in Figure 4.21d, the M75, L78 and L80 residues are all evolutionarily conserved in MITF across multiple species, as well as in TFEB and TFE3. Importantly, these three residues appear to match 75% of the classical NES consensus motif, Φ-X-X-X-Φ-X-X-Φ-X-Φ (Φ = L, M, I, V or F; X = any amino acid), including the specific spacing intervals (Güttler et al., 2010; Kosugi et al., 2008; Kutay and Güttinger, 2005). Taken together, these observations suggested that M75, L78 and L80, together with S69 and S73, were important components of the MITF NES.

As a further verification step, we investigated if the M75, L78 and L80 residues were also implicated in the localisation of full-length MITF. We mutated these three residues to alanine in GFP-MITF, and expressed them in 501mel melanoma cells. We then treated the cells with TPA and examined the sub-cellular localisation of these mutants via immunofluorescence (Figure 4.22a, b).

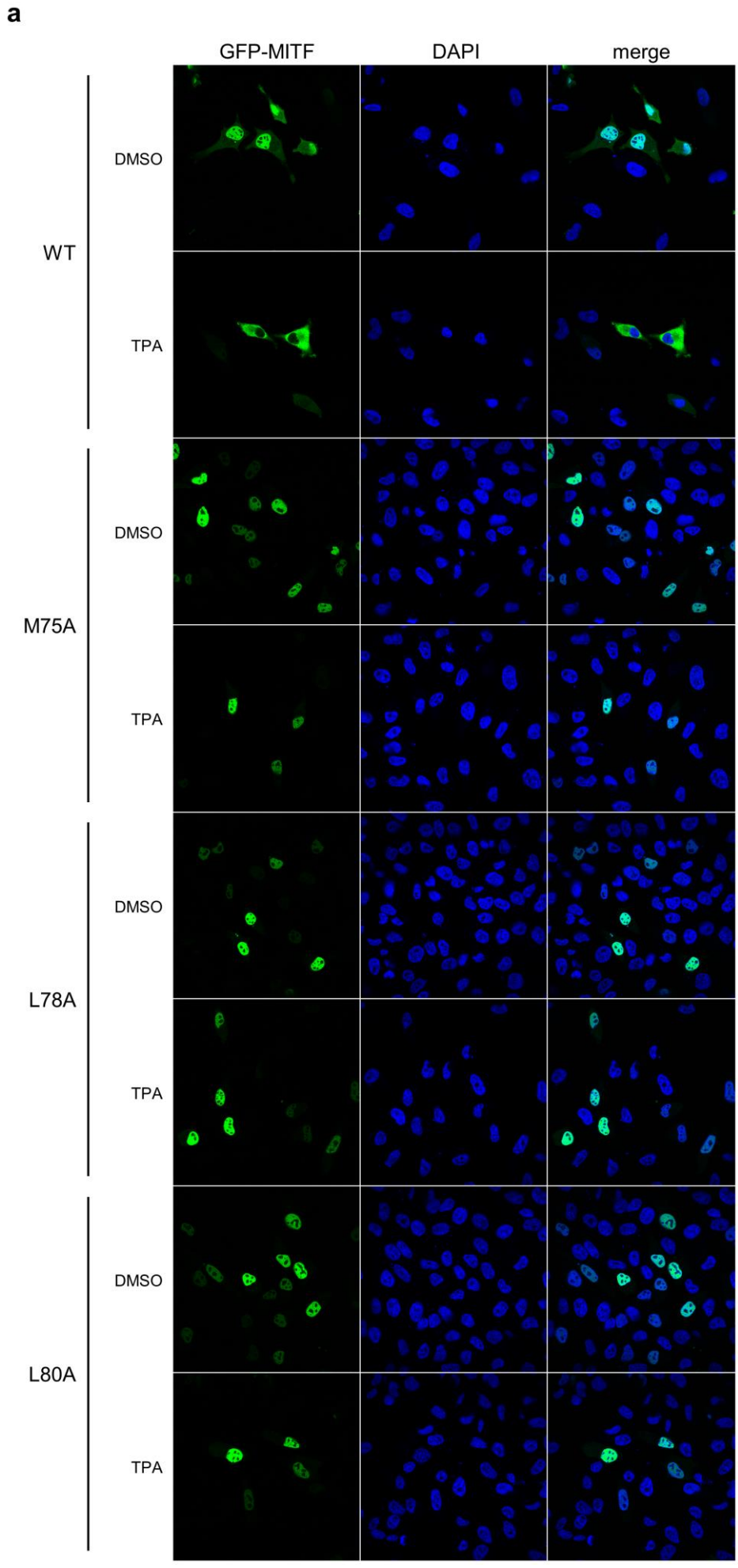
a
GFP-MITF
DAPI
merge
WT
DMSO
TPA
M75A
DMSO
TPA
L78A
DMSO
TPA
L80A
DMSO
TPA

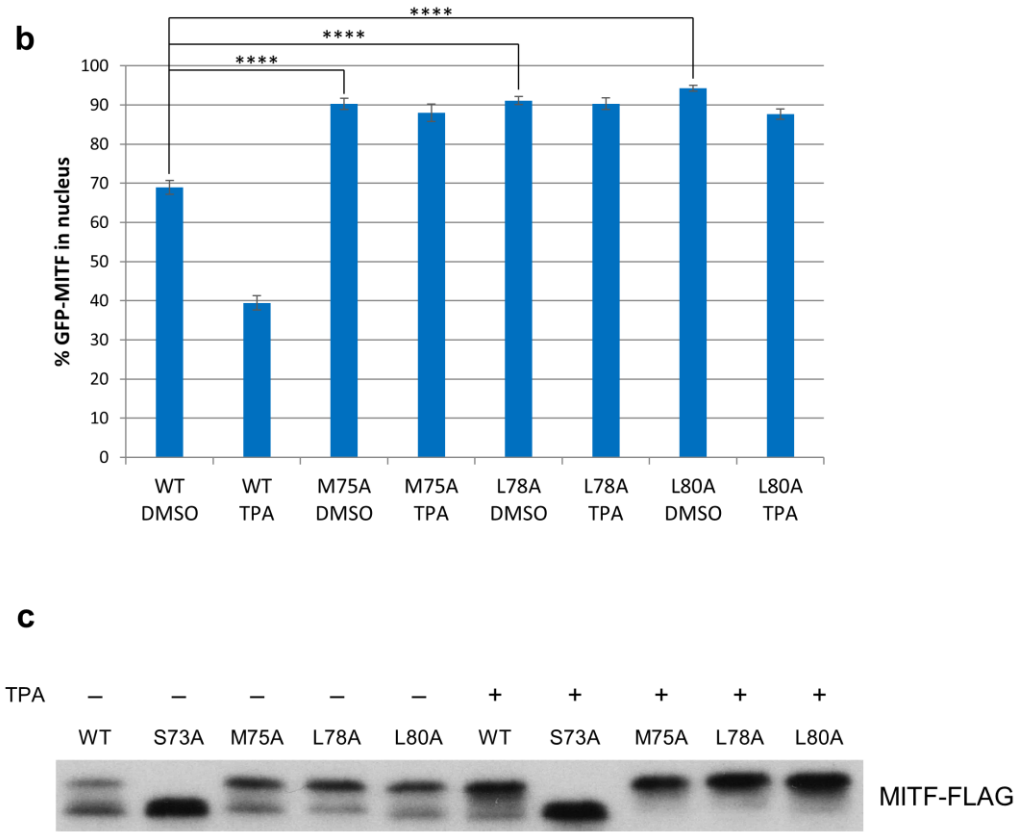

Figure 4.22 Mutations of the M75, L78 and L80 residues also affected the localisation of full-length MITF (a) Fluorescence images of 501mel cells ectopically expressing GFP-MITF mutants (green). Cells were grown on glass coverslips to 50% confluence before being transfected using Fugene 6. After 48 hours, cells were treated with 200 nM TPA or an equivalent amount of DMSO for 1 hour. Cells were then fixed before being stained with DAPI (blue). Images were acquired by confocal microscopy. **(b)** Quantification of GFP-MITF sub-cellular localisation in 501mel cells. Cells were transfected and processed as in (a). A minimum of 35 cells were quantified per condition. Error bars represent SEM. 2-tailed t-test: **** *p<0.0001*. **(c)** Western blot of 501mel cells expressing ectopic MITF-FLAG mutants, following treatment with SB-675259-M. Cells were grown to 50% confluence before being transfected using Fugene 6. After 48 hours, cells were treated with 200 nM TPA or an equivalent amount of DMSO for 1 hour, then lysed and immunoblotted with an antibody against FLAG.

In line with the results obtained with the MITF.60-99 fragment, the M75A, L78A and L80A mutants in full-length GFP-MITF all had significantly increased nuclear localisation relative to wild-type variant (Figure 4.22b). Importantly, all three mutants were resistant to TPA and failed to translocate to the cytoplasm upon TPA treatment.

Given the close proximity of M75, L78 and L80 to the S73 residue, we were concerned that localisation phenotypes we observed after mutating sites were a result

of altered ERK phosphorylation at S73. To investigate if the M75A, L78A and L80A mutants could still be phosphorylated at S73, we introduced these mutants into MITF-FLAG and expressed them in 501mel melanoma cells. We then treated the cells with TPA to induce MAPK activation, and did a western blot on the cell lysates (Figure 4.22c). Similar to wild-type MITF-FLAG, the M75A, L78A and L80A mutants all appeared as a doublet on western blot, indicating that they were being phosphorylated on S73. In contrast, the S73A mutant appeared as a single lower band that was not phosphorylated on S73. MAPK activation with TPA induced an electrophoretic mobility shift in the case of the wild-type, M75A, L78A and L80A variants, with an enrichment of the upper band observed in all the variants tested except for S73A. These results indicated that the mutagenesis at M75, L78 and L80 in MITF did not affect ERK phosphorylation at S73, which suggested that the increase in nuclear localisation of the M75A, L78A and L80A mutants was a bona fide effect of a change in nuclear export. As such, we concluded that S73, M75, L78, L80, and, to a lesser extent, S69 were the critical residues involved in mediating nuclear export of MITF.

4.2.10 In vivo and in vitro functional effects of S69 and S73 mutagenesis in MITF

We were interested to see if mutation of the S69 and S73 residues could affect the activity of MITF. To test this, we transfected HeLa cells with plasmids encoding the S69A and S73A mutants in MITF-FLAG, together with a firefly luciferase reporter whose expression was driven by the *TYR* promoter. The relative level of luciferase expression was determined by measuring the amount of luminescence following the addition of luciferase substrate, and used as a proxy for activation of the TYR promoter. The luminescence readings were then normalised against

expression levels of MITF-FLAG, as determined by western blot and quantified by densitometry.

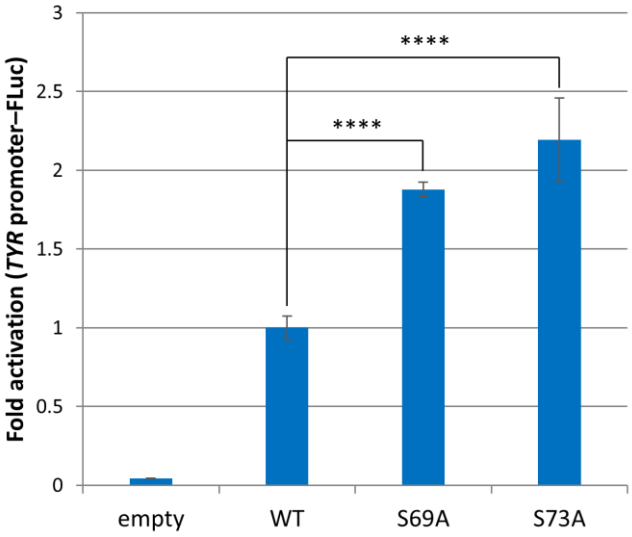

Figure 4.23 S69A and S73A mutants activated the *TYR* promoter significantly more than wild-type MITF-FLAG. Luciferase assay with MITF-FLAG mutants and *TYR* promoter-FLuc in HeLa cells. Cells were grown to 50% confluence before being transfected using Fugene 6. After 48 hours, cells were lysed and luminescence was measured with a luminometer. Readings were normalised to protein levels of MITF-FLAG, as determined by western blot. Error bars represent SEM. 2-tailed t-test: **** $p<0.0001$.

As Figure 4.23 indicates, both S69A and S73A mutants activated the *TYR* promoter significantly more than wild-type MITF-FLAG, with the S73A mutant having the highest amount of activity. The lack of *TYR* promoter activation in the absence of ectopic MITF-FLAG indicated that there was relatively little background endogenous MITF activity, as was expected with the non-melanocytic HeLa cells. Since MITF is a nuclear transcription factor, the increased activation of *TYR* promoter with the S69A and S73A mutants was consistent with these mutants having a higher proportion of nuclear localisation relative to the wild-type.

a

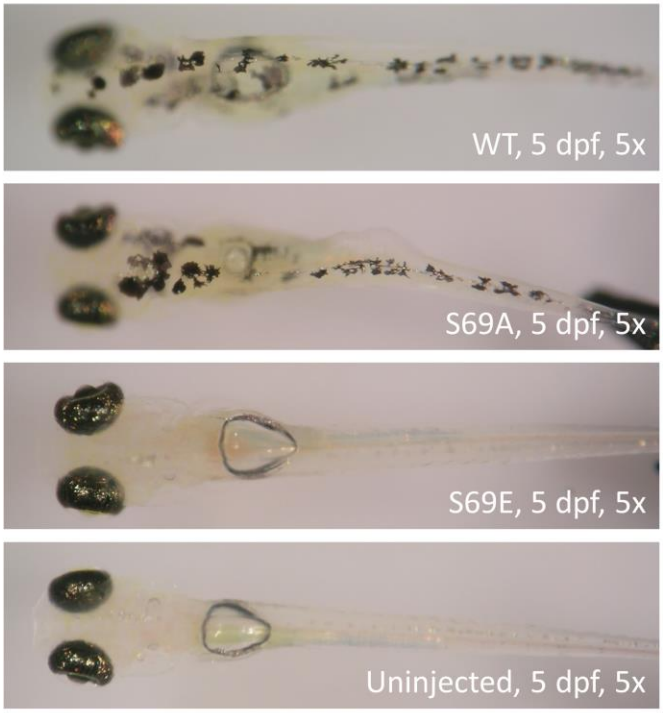

b

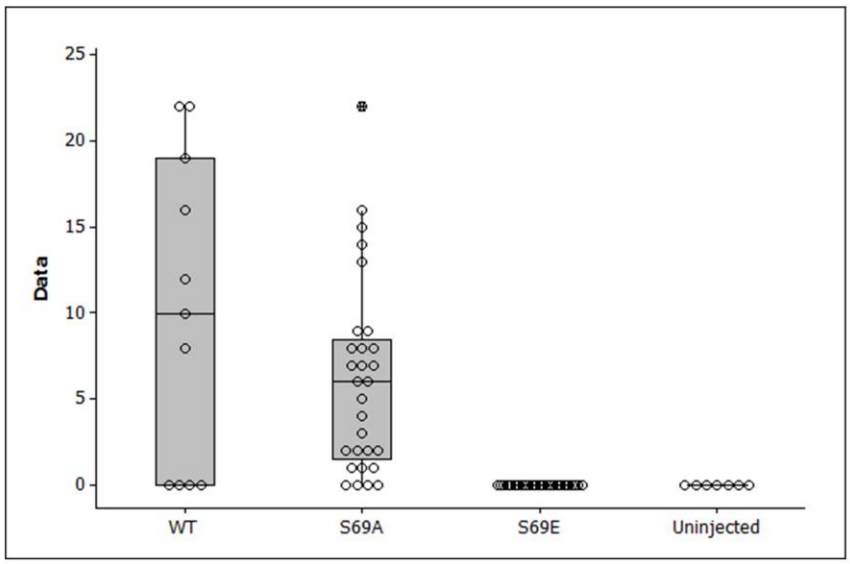

Figure 4.24 The S69A mutant was able to rescue melanophore development in *nacre* zebrafish embryos, while the S69E mutant failed to do so. (a) Representative images of *nacre* embryos injected with plasmids encoding Mitfa mutants, taken 5 days post fertilisation (dpf). **(b)** Quantification of the number of rescued melanophores per embryo. Data from Zhiqiang Zeng, University of Edinburgh, Edinburgh, UK.

We were also interested to know the effects of S69 mutagenesis on MITF activity *in vivo*. To investigate, we mutated the equivalent of the S69 residue in Mitfa to alanine, which mimics non-phosphorylation, as well as glutamic acid, which mimics constitutive phosphorylation. We then injected plasmids encoding these mutants into Mitfa-null *nacre* zebrafish embryos, and determined if the mutants could rescue melanophore development in these embryos (Figure 4.24a, b; data from Zhiqiang Zeng, University of Edinburgh, Edinburgh, UK).

The S69A mutant could rescue melanophore development (number of embryos = 29, mean number of melanophores per embryo = 6.1), as did wild-type Mitfa (n = 11, mean = 9.9). However, even though there were fewer melanophores per embryo with the S69A mutant compared to the wild-type, there were no significant differences between the two Mitfa variants as determined by one-way ANOVA test (95% confidence interval: [-0.876, 8.418]). On the other hand, the phospho-mimetic S69E mutant failed to rescue melanophore development in all injected embryos (n = 25, mean = 0). These results suggest that phosphorylation of the S69 residue in MITF might have an inhibitory effect on MITF activity during melanocyte generation.

4.3 Discussion

Our results describe a novel phosphorylation site in MITF, S69, which is implicated in the nuclear export of MITF together with the nearby S73 residue, also a phosphorylation site. We first observed that activation of the MAPK pathway resulted in significant relocalisation of MITF, a nuclear protein, to the cytoplasm. Conversely, inhibition of the MAPK pathway resulted in increased MITF nuclear localisation. This was also supported by other studies, which showed that MAPK inhibition in HeLa cells caused TFEB, a closely related member of the MiT family, to relocalise to the nucleus following dephosphorylation of S142 in TFEB, the equivalent residue to S73 in MITF (Settembre et al., 2011).

We also found increased nuclear localisation of MITF upon GSK3 inhibition. In line with our results, other studies have also noted that GSK3 inhibition caused an increase in nuclear localisation of MITF and stimulated melanogenesis (Bellei et al., 2008). Inhibition of GSK3 had an even greater effect on the localisation of TFEB, which was found to translocate from the cytoplasm to the nucleus following GSK3 inhibition (Marchand et al., 2015; Parr et al., 2012), again consistent with our observations.

We were aware that GSK3 inhibition would up-regulate MITF transcription via the accumulation of β-catenin in the nucleus (Takeda et al., 2000b; Widlund et al., 2002). However, an increase in MITF transcription would not account for the decrease in MITF cytoplasmic localisation upon GSK3 inhibition, suggesting that the observed effects of GSK3 inhibition on MITF were not mediated through β-catenin alone. We identified a novel phosphorylation site in MITF, S69, that is phosphorylated by GSK3. We showed that the increase in nuclear localisation and decrease in cytoplasmic localisation of MITF upon GSK3 inhibition was due to

dephosphorylation of the S69 residue, as opposed to other previously identified GSK3 phosphorylation sites in MITF.

As shown in our results, GSK3 phosphorylation of S69 in MITF required a priming phosphorylation at the nearby S73 residue, which is known to be phosphorylated by ERK (Hemesath et al., 1998). Our results showed that the increased cytoplasmic localisation of MITF following S69 and S73 phosphorylation was mediated by an up-regulation of MITF nuclear export. We also identified three other key residues that made up the NES, M75, L78 and L80. However, these three hydrophobic residues were only a partial 75% match for the classical NES consensus motif, Φ-X-X-X-Φ-X-X-Φ-X-Φ (Φ = L, M, I, V or F; X = any amino acid) (Güttler et al., 2010; Kosugi et al., 2008; Kutay and Güttinger, 2005). As for the role of S69 and S73 phosphorylation in the NES, we believe this is related to the fact that acidic amino acids are preferred in the spacers between the N-terminal hydrophobic residues in the NES (Güttler et al., 2010). We believe that following phosphorylation at S69 and S73, the negative charges of the additional phosphate groups confer an increase in acidity, thus enhancing the functionality of the NES.

Functionally, the increase in MITF nuclear localisation following dephosphorylation at S69 and S73 led to an increase in MITF activity, as indicated by luciferase assays measuring MITF transactivation of the *TYR* promoter. This is supported by other studies, which demonstrated that MITF activity is influenced by its localisation. MITF with mutations or deletions in its NLS became cytoplasmic and displayed reduced functionality in terms of its ability to transactivate downstream transcriptional targets such as the *TYR* promoter (Grill et al., 2013; Zhang et al., 2012).

In other studies, functional assays in cell culture indicate cooperativity between MITF and BRAF in oncogenesis, with melanocytes and neural crest progenitor cells being transformed by ectopic co-expression of MITF and activated $BRAF^{V600E}$ (Garraway et al., 2005; Kumar et al., 2014). In zebrafish models expressing a temperature-sensitive variant of *mitfa*, the zebrafish ortholog of *MITF*, low levels of Mitfa were found to promote tumorigenesis together with activated human $BRAF^{V600E}$ (Lister et al., 2014). Critically, the tumours regressed upon ablation of Mitfa activity following an increase in temperature, while $BRAF^{V600E}$ fish expressing wild-type Mitfa at normal levels did not develop any melanoma (Lister et al., 2014). These findings indicate an important role for MITF in $BRAF^{V600E}$-mediated oncogenesis and, more importantly, point to the existence of threshold levels of MITF activity which confer different outcomes in melanoma, in line with the rheostat model.

Our results demonstrate an additional way of regulating MITF activity by controlling its localisation. MITF nuclear export following MAPK activation can also provide a rational explanation for oncogene-induced senescence upon the acquisition of activating mutations in BRAF. As highlighted in Chapter 1, BRAF mutations are extremely common in both malignant melanoma as well as benign naevi. However, on their own, BRAF mutations are insufficient for tumorigenesis due to the onset of oncogene-induced senescence (Michaloglou et al., 2005, 2008). When the constitutively active $BRAF^{V600E}$ variant was expressed in primary human melanocytes, it was only able to induce a transient increase in proliferation before cell cycle arrest occurred (Michaloglou et al., 2005). In light of the complex effects exerted by different levels of MITF activity in determining melanoma sub-population identity, particularly with regards to cell cycle-arrested and senescent phenotypes, we

theorised that MITF could potentially play a crucial role in mediating oncogene-induced senescence following BRAF activation in melanocytes.

In the rheostat model outlined in Chapter 1, low MITF activity is associated with a growth-arrested and senescent phenotype, as evidenced by the fact that the siRNA-mediated silencing of MITF resulted in senescence (Giuliano et al., 2010) in melanoma cells due to the down-regulation of genes associated with mitosis, as well as DNA replication and repair (Strub et al., 2011).

In line with oncogene-induced senescence by BRAF being mediated via MITF, MITF expression was down-regulated following ectopic expression of $BRAF^{V600E}$ in melanocytes, as shown in numerous independent studies (Borgdorff et al., 2014; Garraway et al., 2005; Haq et al., 2013b; Wellbrock and Marais, 2005). As MITF plays an important role in regulating pigmentation genes, BRAF-mediated loss of MITF expression was also accompanied by a dramatic loss of pigmentation (Wellbrock and Marais, 2005). Conversely, MITF levels increased following siRNA-mediated depletion of $BRAF^{V600E}$ in melanoma cells, while the pigmentation enzymes TYR and TYRP1 downstream of MITF were also up-regulated (Rotolo et al., 2005). This occurred together with elevated production of melanin and melanosomes, which culminated in an increase in pigmentation (Rotolo et al., 2005). $BRAF^{V600E}$ inhibition with the small molecule inhibitor PLX4720 led to similar results as well, with an increase in mRNA levels of the melanocyte specific *MITF-M* isoform in melanoma cells accompanied by the induction of MITF target genes such as *TRPM1* and *DCT* (Haq et al., 2013b). An increase in pigmentation was also observed following $BRAF^{V600E}$ inhibition in melanoma cells (Haq et al., 2013b).

These various studies were all consistent with our theory that low MITF activity following BRAF activation could be mediating the oncogene-induced

senescence response in melanocytes. In addition to BRAF's effects on MITF mRNA and protein levels, the results in Chapter 4.2 describe an additional level of MITF regulation by BRAF via a reduction in MITF nuclear localisation.

In line with this, alterations in the *MITF* gene, the vast majority of which are amplifications, tend to co-occur with *BRAF* mutations ($p = 0.006$, Fisher's exact test) in patient-derived melanoma tumour samples (Akbani et al., 2015; Cerami et al., 2012). *MITF* amplification could potentially provide a mechanism for senescence bypass by increasing MITF activity to induce a proliferative phenotype according to the rheostat model.

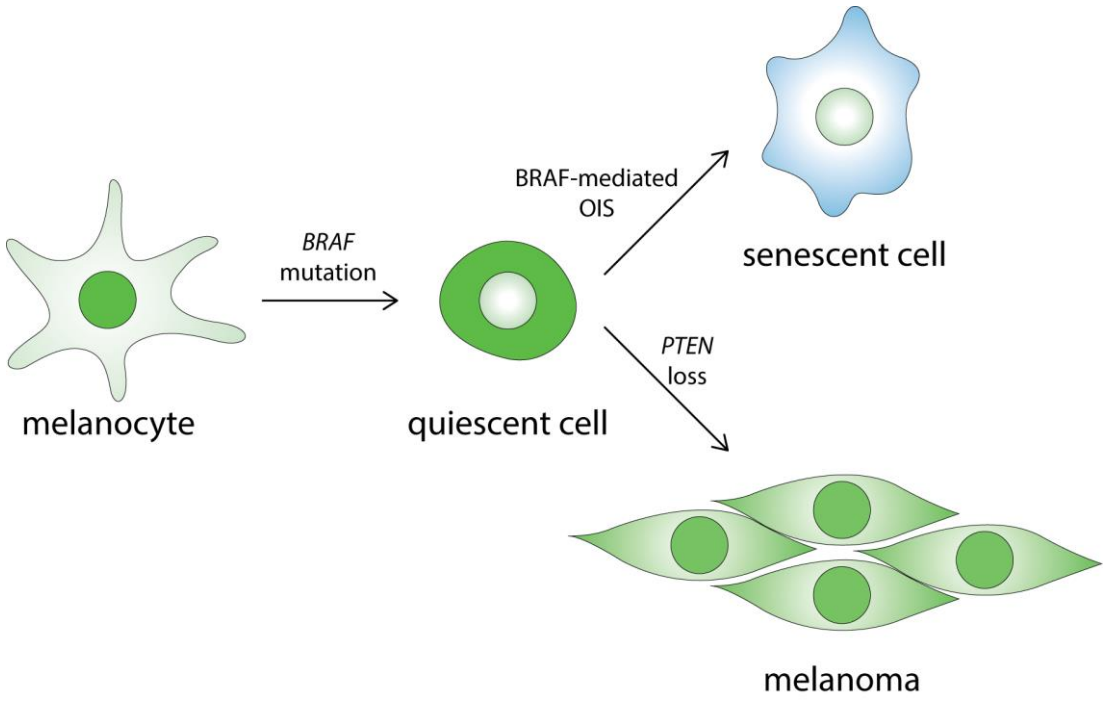

Figure 4.25 Model of how phosphorylation-dependent MITF nuclear export can potentially mediate oncogene-induced senescence (OIS) and senescence bypass. The acquisition of an activating *BRAF* mutation in a melanocyte causes nuclear export of MITF (indicated in green) to the cytoplasm following ERK-mediated phosphorylation of S73. This results in low MITF activity, which causes the cell to go into cell cycle arrest and eventually senescence. However, if the cell also acquires secondary mutations in *PTEN*, GSK3 activity will be inhibited, reducing phosphorylation at S69 in MITF. This decreases MITF nuclear export and increases MITF activity in the nucleus, thus inducing a proliferative phenotype which eventually manifests as melanoma.

Our results provide an additional mechanism for senescence bypass, whereby GSK3 inhibition leads to an increase in MITF nuclear localisation, thus increasing MITF activity towards its target genes and bypassing senescence (Figure 4.25). This is supported by the fact that BRAF mutations were insufficient for tumorigenesis in mice unless accompanied by secondary mutations in PTEN (Dankort et al., 2009). Since PTEN mutations inactivate GSK3, our model provides a novel explanation of how PTEN mutations lead to bypass of oncogene-induced senescence following BRAF activation – PTEN loss leading to GSK3 inactivation would prevent nuclear export of MITF upon BRAF activation, with nuclear retention of MITF providing a potential mechanism to bypass BRAF-induced senescence.

So far, our discussion has been limited to the implications of our findings for MITF function during melanoma oncogenesis. In the context of development, MITF is also known to play an important role in melanocyte stem cell maintenance (Nishimura et al., 2005) and differentiation (Lang et al., 2005), processes which are linked to MITF's regulation of the cell cycle (Carreira et al., 2005; Du et al., 2004; Loercher et al., 2005).

The Wnt signalling pathway plays a pivotal role in controlling stem cell maintenance and cell fate decisions during tissue regeneration and renewal (Clevers, 2006; Clevers et al., 2014; Nusse, 2008; Reya and Clevers, 2005). However, unlike most stem cells in which Wnt signalling leads to self-renewal and re-establishment of stemness, activation of the Wnt signalling pathway induces proliferation and differentiation of melanocyte stem cells into melanoblasts and melanocytes (Dorsky et al., 1998; Iyengar et al., 2015; Rabbani et al., 2011; Yamada et al., 2013).

Studies have also shown that MITF is a downstream target of the Wnt signalling pathway during development. For example, Wnt signalling results in the

transcriptional up-regulation of MITF, by promoting the recruitment of the Wnt (Dorsky et al., 2000; Takeda et al., 2000b; Widlund et al., 2002). Wnt signalling is also known to cooperate with MITF during melanocyte differentiation, via the interaction between β-catenin and PAX3 (Lang et al., 2005). In addition, MITF can also interact physically with β-catenin to redirect its transcriptional activity away from LEF1-regulated genes towards MITF downstream targets (Schepsky et al., 2006).

With regards to the interplay between Wnt signalling and MITF during development, our results provide a potential phosphorylation-dependent mechanism, involving nuclear export, for the regulation of MITF activity by Wnt signalling. We propose a model of melanocyte stem cell renewal and differentiation that involves this mechanism (Figure 4.26). In the bulge region of the hair follicle, Wnt ligands secreted by neighbouring epithelial stem cells can activate the Wnt signalling pathway in a melanocyte stem cell (Rabbani et al., 2011). Wnt pathway activation turns on MITF transcription via β-catenin. In addition, Wnt signalling also inhibits GSK3 phosphorylation of MITF S69, thus promoting increased nuclear localisation of MITF. This causes an increase in MITF activity, which relieves $p27^{Kip1}$-mediated G1 arrest (Carreira et al., 2006) and results in re-entry into the cell cycle. The Wnt signal also orients the plane of mitotic division, such that the stem cell undergoes asymmetric cell division (Habib et al., 2013), producing two daughter cells with distinct cell fates. The daughter cell close to the source of Wnt retains MITF in the nucleus since GSK3 remains inhibited, and will continue to proliferate and ultimately differentiate. On the other hand, due to the short, localised range of the Wnt signal, the distal daughter cell away from the Wnt source now has high GSK3 activity. This results in phosphorylation of MITF S69, which promotes nuclear export of MITF

into the cytoplasm. Consequently, MITF activity decreases in the distal daughter cell, which causes it to re-enter quiescence and regenerate the melanocyte stem cell. In support of this model, our results demonstrate that a phospho-mimetic glutamic acid substitution at S69, the site of GSK3 phosphorylation in MITF, resulted in significant abrogation of melanophore development in a zebrafish model.

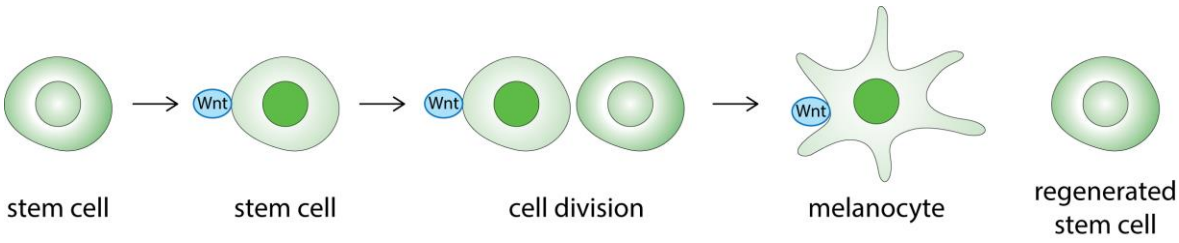

Figure 4.26 Model of how phosphorylation-dependent MITF localisation can potentially mediate melanocyte stem cell regeneration. Wnt pathway activation leads to transcriptional up-regulation and nuclear localisation of MITF (indicated in green), via GSK3 inhibition, in an MITF-low melanocyte stem cell. This causes the stem cell to re-enter the cell cycle and undergo asymmetric cell division, producing two daughter cells with different cell fates. The daughter cell closer to the Wnt source retains MITF in the nucleus, and continues to proliferate and ultimately differentiate. The distal daughter cell has GSK3 activity, which promotes MITF nuclear export and down-regulates MITF activity. Consequently, the distal daughter cell re-enters quiescence to regenerate the melanocyte stem cell.

In conclusion, our results describe a novel post-translational modification of MITF that is part of a previously undescribed NES located within the MITF N-terminus. We also show that this post-translational modification affects MITF activity and has potential implications in melanoma oncogenesis and melanocyte stem cell differentiation.

Chapter 5 – Cell cycle regulation of MITF phosphorylation

5.1 Introduction

MITF regulates cell cycle progression by affecting a number of different cyclin-dependent kinase (CDK) inhibitors. For example, MITF is known to inhibit the protein stability of the CDK inhibitor $p27^{Kip1}$ by up-regulating expression of the *DIAPH1* gene, which encodes the diaphanous-related formin-1 (DIAPH1) protein (Carreira et al., 2006). DIAPH1 regulates expression of S-phase kinase-associated protein 2 (SKP2) (Mammoto et al., 2004), which in turn promotes ubiquitination and degradation of $p27^{Kip1}$ (Carrano et al., 1999; Tsvetkov et al., 1999). Hence, siRNA-mediated depletion of MITF in melanoma cells results in decreased expression of DIAPH1 and SKP2, which causes stabilisation and accumulation of $p27^{Kip1}$ (Carreira et al., 2006). Since $p27^{Kip1}$ binds to and inhibits CDK2/cyclin E (Polyak et al., 1994), which plays a critical role in G1/S transition, accumulation of $p27^{Kip1}$ after knockdown of MITF results in cell cycle arrest in G1 (Carreira et al., 2006).

In addition to its indirect effects on degradation of $p27^{Kip1}$, MITF also activates transcription of the *CDKN1A* and *CDKN2A* genes, which encode the $p21^{Cip1}$ and $p16^{INK4a}$ CDK inhibitors respectively, by binding directly to their respective promoters (Carreira et al., 2005; Loercher et al., 2005). Like $p27^{Kip1}$, $p21^{Cip1}$ is an inhibitor of CDK2/cyclin E (Gu et al., 1993; Harper et al., 1993). In comparison, $p16^{INK4a}$ inhibits CDK4/cyclin D and CDK6/cyclin D (Serrano et al., 1993), thus preventing them from phosphorylating RB (Koh et al., 1995). This results in the accumulation of hypophosphorylated RB that inhibits cell cycle transition from G1 to S phase. Thus, overexpression of MITF in cells also led to cell cycle arrest in the G1 phase via up-regulation of $p21^{Cip1}$ and $p16^{INK4a}$ (Carreira et al., 2005; Loercher et al., 2005).

In addition to CDK inhibitors, MITF can also regulate cell-cycle progression by binding to the promoter of the *CDK2* gene to activate its transcription (Du et al., 2004). MITF regulation of CDK2 expression appears to be specific to cells of melanocytic origin, since MITF did not regulate *CDK2* transcription in non-melanocytes (Du et al., 2004). Functionally, expression of dominant-negative MITF resulted in repression of *CDK2* transcription and growth suppression in melanoma cells, which could be rescued by ectopic expression of CDK2 (Du et al., 2004).

Given MITF's role as a key regulator of the cell cycle, it was not inconceivable that cell cycle progression could regulate MITF in a feedback loop. In particular, we noted that there are several serine-proline (S-P) motifs within MITF, including the S73 residue. These can be potential phosphorylation targets of cyclin-dependent kinases (CDKs), which along with MAPKs are proline-directed kinases that phosphorylate serine or threonine residues preceding proline (Pinna and Ruzzene, 1996).

5.2 Results

5.2.1 MAPK inhibition does not completely abrogate MITF S73 phosphorylation

To get a better idea of whether the S73 residue in MITF could be phosphorylated by other kinases in addition to ERK, we treated 501mel melanoma cells, which contain an activating $BRAF^{V600E}$ mutation, with the small molecule inhibitors PLX4720 and U0126 for various periods of time up to 24 hours. As mentioned in Chapter 3, PLX4720 and U0126 are ATP-competitive small molecules that respectively inhibit activated $BRAF^{V600E}$ and MEK upstream of ERK in the MAPK pathway. We then examined the phosphorylation status of MITF at S73 by determining its electrophoretic mobility via western blot (Figure 5.1).

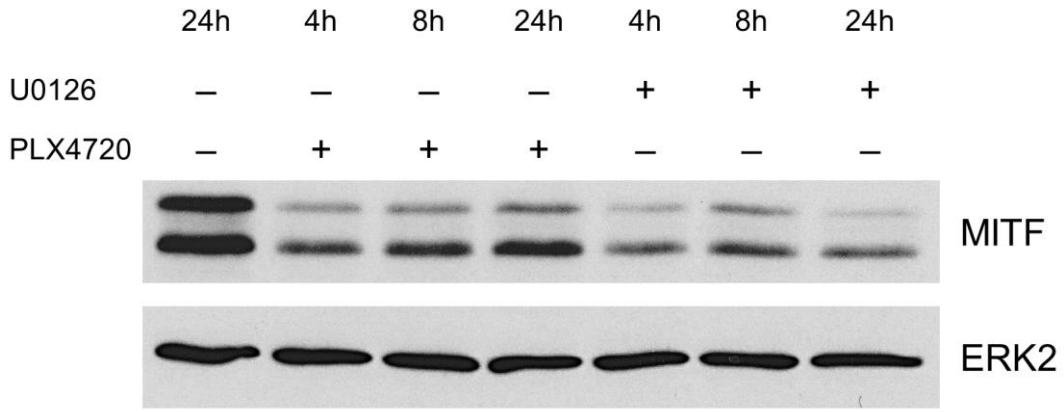

Figure 5.1 MITF retained some degree of S73 phosphorylation following MAPK inhibition. Western blot of 501mel cells following MAPK inhibition with PLX4720 or U0126. Cells were grown to 50% confluence and treated with 5 μM of PLX4720, 10 μM of U0126 or an equivalent volume of DMSO for the indicated period of time. Cells were then lysed and immunoblotted with an antibody against MITF.

MAPK inhibition with PLX4720 and U0126 for an extended period of 24 hours resulted in a sharp decrease in MITF protein levels relative to the DMSO-treated control, with a greater decrease observed with U0126 treatment (Figure 5.1). The decrease in MITF levels was not observed with previous experiments involving shorter periods of U0126 treatment (Figures 3.10, 4.2c).

As mentioned previously, MITF migrates as a doublet on western blots, with the upper band corresponding to a species that is phosphorylated on S73, while the lower band is not phosphorylated at that residue. In general, MEK inhibition with U0126 resulted in a stronger response on MITF S73 phosphorylation compared to BRAF inhibition with PLX4720, probably because MEK can also be activated by other isoforms of RAF in addition to BRAF. BRAF inhibition with PLX4720 proved to be ineffective in reducing phosphorylation of MITF at S73, as indicated by a slight decrease in the ratio of the upper to lower bands in the MITF western blot (Figure 5.1). U0126 elicited a stronger response, with a larger decrease in the upper MITF band relative to the lower MITF band.

It is possible that the remaining MITF S73 phospho-species were a result of basal ERK activity following incomplete inhibition of the MAPK pathway. However, both U0126 and PLX4720 proved to be very effective at inhibiting ERK phosphorylation in 501mel melanoma cells in previous experiments (Figures 3.10, 3.11 and 4.2c). Hence, we considered the possibility that there could be other kinases targeting the S73 residue in MITF, particularly CDKs. We reasoned that if CDKs were targeting MITF, then MITF phosphorylation patterns would vary over the course of the cell cycle.

5.2.2 MITF phosphorylation and protein levels vary throughout the cell cycle

To investigate, we synchronised 501mel melanoma cells at various stages of the cell cycle by treating them with thymidine or nocodazole (Figure 5.2a, b). High thymidine concentrations disrupt deoxynucleotide metabolism, thus blocking DNA synthesis and inducing cell cycle arrest in S-phase (Xeros, 1962). Nocodazole is a microtubule poison that interferes with microtubule polymerisation, thus arresting cells in prometaphase during mitosis (De Brabander et al., 1976).

As expected, a 24 hour-long treatment with thymidine resulted in an enrichment of cells in S phase, with 64% of the cells in S phase compared to 29% in the DMSO-treated control (Figure 5.2a). Treatment with nocodazole for 24 hours induced a G2/M phase block, with 52% of cells in G2/M versus 18% in the DMSO-treated control.

In terms of its effects on MITF, hyperphosphorylation of MITF at S73 was observed upon enrichment of G2/M cells with nocodazole treatment, as indicated by an increase in the ratio of the upper to lower MITF bands compared to the DMSO-treated control (Figure 5.2b). G2/M arrest with nocodazole also resulted in a decrease

in total MITF protein levels, despite equal protein loading as indicated by the actin loading control. On the other hand, S phase enrichment with thymidine did not result in any noticeable effects on MITF phosphorylation or total protein levels.

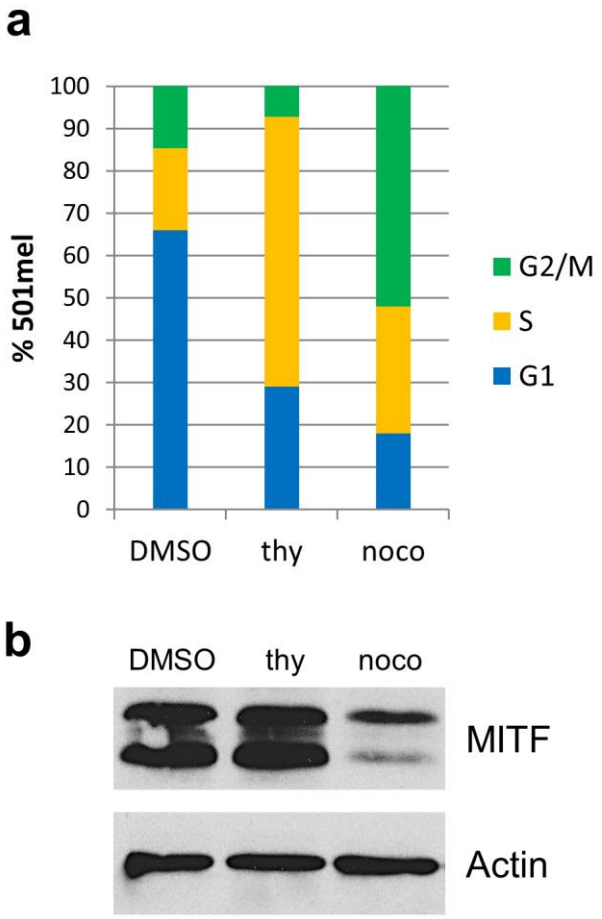

Figure 5.2 MITF was hyperphosphorylated at S73 during the G2/M phase. (a) Cell cycle profile of 501mel cells following cell cycle synchronisation with thymidine and nocodazole. Cells were grown to 50% confluence and treated with 2 mM thymidine (abbreviated as thy), 1 μM nocadazole (abbreviated as noco) or an equivalent volume of DMSO for 24 hours. Their cell cycle profiles were analysed by flow cytometry after fixation and staining with the nucleic acid stain propidium iodide (PI). **(b)** Western blot of 501mel cells following cell cycle synchronisation with thymidine and nocodazole. Cells were treated as in (a), then lysed and immunoblotted with an antibody against MITF.

We were aware that chemically-induced cell cycle synchrony had drawbacks in terms of cell toxicity, particularly in the case of nocodazole where a significant amount of cell death was observed (data not shown). These harsh and artificial methods of synchronising cells might produce artefacts and false positives in the data. To address this issue and minimise physiological perturbations, we made use of the mitotic shake-off method to synchronise cells (Jackman and O'Connor, 2001). First described in 1963 (Terasima and Tolmach, 1963), mitotic shake-off is a method of detaching mitotic cells from their growth surface via simple mechanical agitation. It makes use of the observation that adherent cells tend to round up thus attach less firmly to their culture vessel surface during mitosis.

To verify our results from the thymidine and nocodazole-induced cell cycle synchronisation, we synchronised adherent 501mel human melanoma cells via the mitotic shake-off method. Briefly, mitotic cells growing in T175 flasks were harvested by tapping the sides of the flasks, and collecting the floating cells that had detached. The mitotic cells were then spun down and plated out for fixed periods of time before being harvested for immunoblotting and cell cycle analysis via flow cytometry (Figure 5.3a, b, c, d).

Mitotic shake-off of 501mel cells resulted in an enriched population of cells in the G2/M phase of the cell cycle, with flow cytometry analysis revealing 41% of cells in G2/M at the point of shake-off compared to 21% in the unperturbed control (Figure 5.3a). Within 4 hours, 91% of cells had moved on to the G1 phase. They transitioned into S phase at approximately 12 hours (38% S phase), continuing into G2/M at around the 18-hour mark (46% G2/M phase).

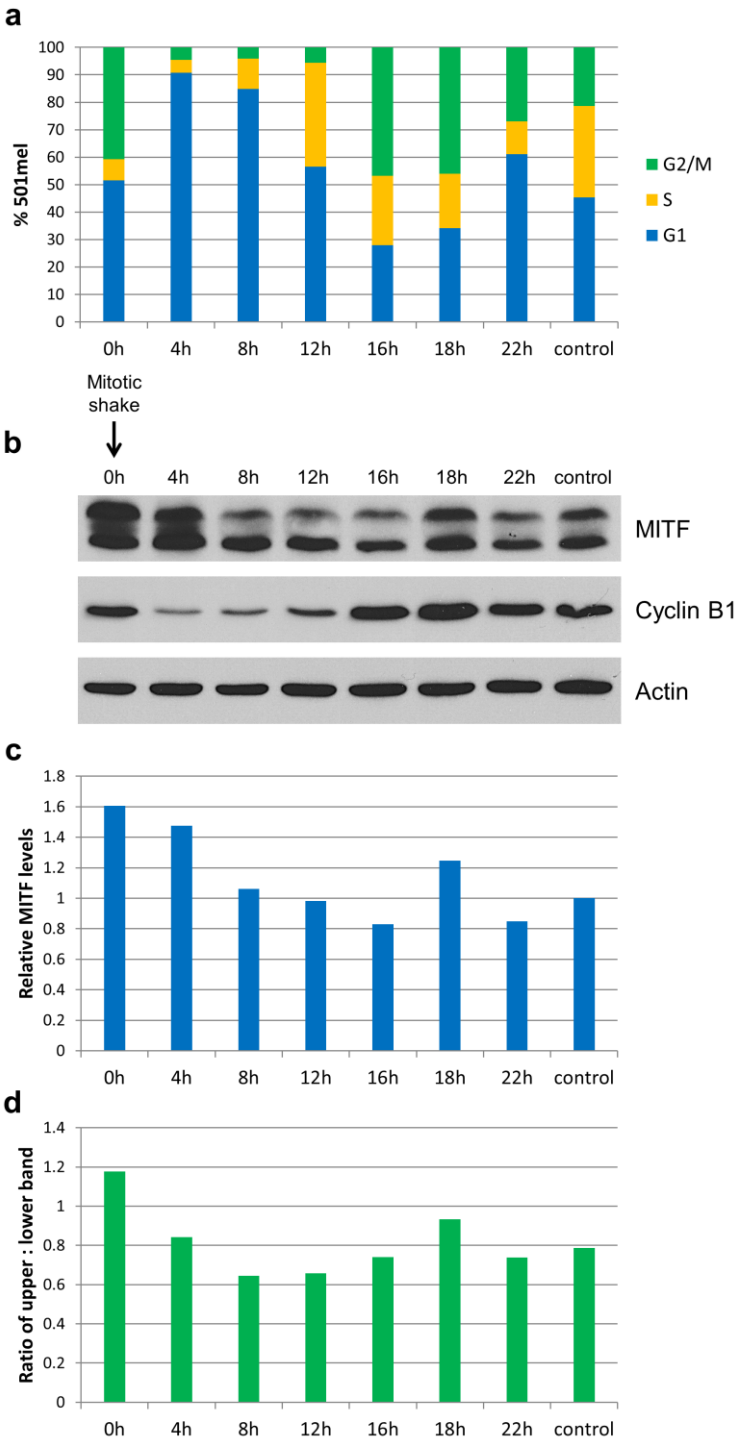

Figure 5.3 MITF phosphorylation and protein levels in 501mel cells varied throughout the cell cycle. (a) Cell cycle profile of 501mel cells at various stages of the cell cycle following mitotic shake. Cells were grown to 80% confluence, then subject to mitotic shake and re-plated for the indicated periods of time. Their cell cycle profiles were analysed by flow cytometry after fixation and staining with PI. **(b)** Western blot of 501mel cells various stages of the cell cycle following mitotic shake. Cells were grown as in (a), then lysed. Sample protein concentrations were normalised after measuring with BCA protein assay, then processed for western blotting. **(c)** Quantification of total MITF protein levels in (b) via densitometry. **(d)** Quantification of the upper MITF band : lower MITF band ratio in (b) via densitometry.

As a validation of the flow cytometry readings, the expression pattern of cyclin B1, which is up-regulated during mitosis, was consistent with the cell cycle profile of the cells obtained via flow cytometry analysis. Following mitotic shake-off at 0h, levels of cyclin B1 decreased and remained at a basal level throughout G1, before increasing again and reaching a maximum during the next round of the G2/M phase at 18 hours (Figure 5.3b). Actin was used as the loading control.

Western blots of MITF in 501mels revealed two distinct patterns throughout the cell cycle (Figure 5.3b). Firstly, total MITF protein levels were highest just after mitotic shake-off and in the early G1 phase (up to 4h after mitosis) (Figure 5.3c). MITF protein levels dropped back to basal levels during the late G1 and S phases before increasing again during the next round of mitosis at 18 hours. However, these observations were in contrast to results obtained with nocadazole-induced mitotic arrest, which showed down-regulation of MITF levels during the G2/M phase.

Secondly, the upper band of MITF also increased in intensity relative to the lower band during the G2/M phase, independent of the overall protein level (Figure 5.3d). This indicates an increase in MITF S73 phosphorylation during G2/M, reaffirming the observations made with nocadazole treatment.

To further confirm our results, we also carried out synchronisation of SK-MEL-28, another adherent human melanoma cell line, via the mitotic shake-off method (Figure 5.4a, b). Due to the fact that SK-MEL-28 cells were more adherent than 501mel cells, we were able to achieve better enrichment of cells in the G2/M phase, with 72% of SK-MEL-28 cells in G2/M at the point of shake-off versus 22% in the unperturbed control according to flow cytometry analysis (Figure 5.4a).

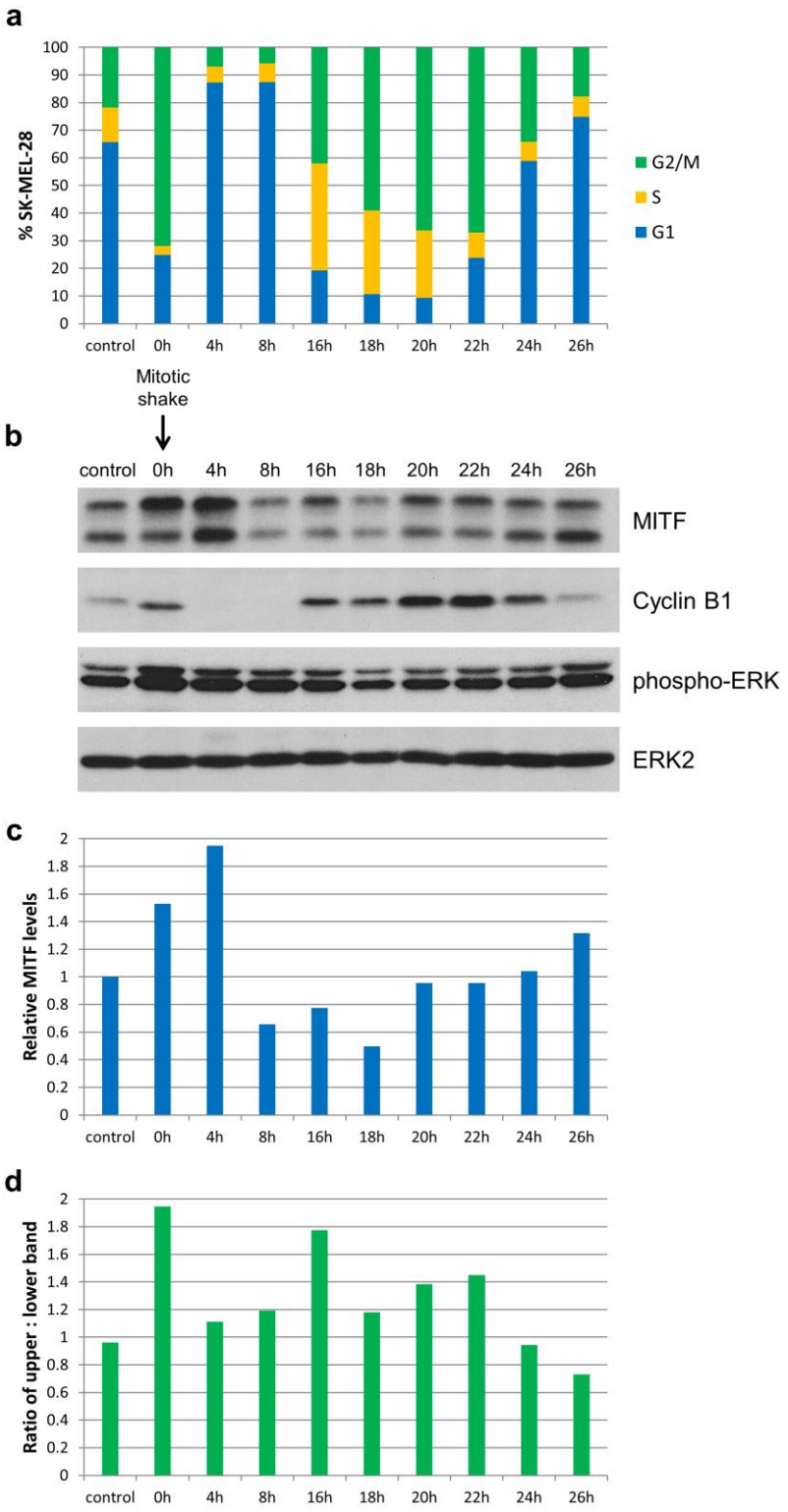

Figure 5.4 MITF phosphorylation and protein levels in SK-MEL-28 cells varied throughout the cell cycle. (a) Cell cycle profile of SK-MEL-28 cells at various stages of the cell cycle following mitotic shake. Cells were grown to 80% confluence, then subject to mitotic shake and re-plated for the indicated periods of time. Their cell cycle profiles were analysed by flow cytometry after fixation and staining with PI. **(b)** Western blot of SK-MEL-28 cells various stages of the cell cycle following mitotic shake. Cells were grown as in (a), then lysed. Sample protein concentrations were normalised after measuring with BCA protein assay, then processed for western blotting. **(c)** Quantification of total MITF protein levels in (b) via densitometry. **(d)** Quantification of the upper MITF band : lower MITF band ratio in (b) via densitometry.

Compared to 501mel cells, SK-MEL-28 cells were observed to have a longer cell cycle of around 22 hours (67% G2/M), with entry into S phase at around the 16-hour mark (39% S phase) (Figure 5.4a). As an additional verification step, cyclin B1 expression, as detected by western blot (Figure 5.4b), was consistent with the cell cycle profiles obtained by flow cytometry.

An examination of the western blot of SK-MEL-28 cells throughout the cell cycle revealed the same two patterns of MITF expression that we observed with 501mel cells (Figure 5.4b). As with the 501mel cells, MITF protein levels were up-regulated following mitotic shake-off and in early G1 (up to 4h after mitosis) (Figure 5.4c). This was followed by a decrease in MITF levels during late G1 at 8 hours, before increasing again in the lead-up to the next round of mitosis at 22 hours.

As was also the case with 501mel cells, an elevation in the ratio of the upper MITF band to lower MITF band was observed during the G2/M phase, independent of the overall protein level (Figure 5.4d). This suggests that MITF S73 was hyperphosphorylated during G2/M, again reconfirming the results obtained with nocadazole treatment. Importantly, the phosphorylation pattern of MITF did not appear to match phospho-ERK levels throughout the cell cycle. For example, relatively low amounts of MITF S73 phosphorylation were present at the 4-hour and 26-hour time points (Figure 5.4d) although phospho-ERK levels were relatively high (Figure 5.4b). In comparison, there was more S73 phosphorylation at 16 hours, despite having a lower amount of phospho-ERK. This suggests that MITF could be phosphorylated at S73 by a kinase other than ERK during the G2/M phase of the cell cycle.

Since nocodazole treatment and mitotic shake-off gave contrasting results with regards to the change in MITF levels during mitosis, we sought to examine this by other methods. We looked at MITF staining in SK-MEL-28 cells via immunofluorescence, paying particular attention to mitotic cells (Figure 5.5a). We also analysed both 501mel and SK-MEL-28 cells by flow cytometry, examining their MITF expression at various stages of the cell cycle (Figure 5.5b).

a

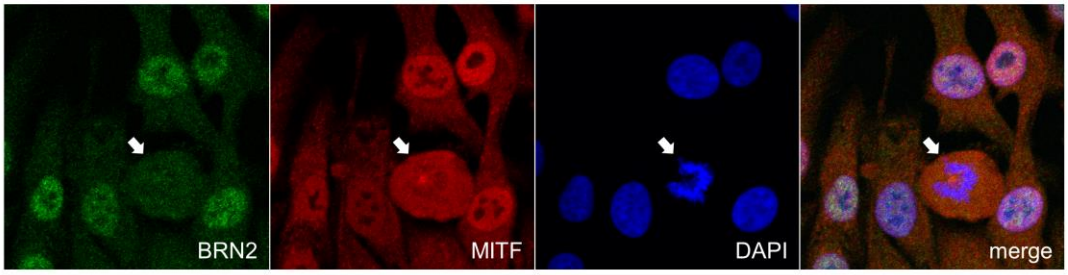

b

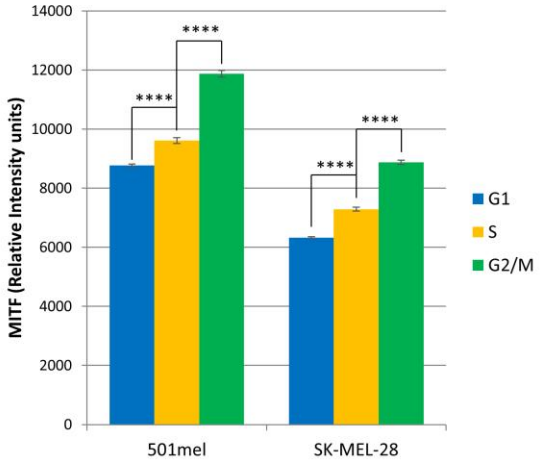

Figure 5.5 MITF levels were up-regulated during mitosis. (a) Immunofluorescence images of SK-MEL-28 cells. After fixation and permeabilisation, the cells were stained with DAPI (blue) and antibodies against BRN2 (green) and MITF (red). Images were acquired by confocal microscopy. Arrow indicates a mitotic cell. **(b)** Flow cytometry analysis of MITF expression in 501mel and SK-MEL-28 cells at different stages of the cell cycle. Cells were grown to 80% confluence, then fixed and stained with the nucleic acid stain TO-PRO-3 and an antibody against MITF. A minimum of 1600 cells were quantified per condition. Error bars represent standard error of the mean (SEM). 2-tailed t-test: **** $p<0.0001$.

MITF levels were up-regulated in the mitotic SK-MEL-28 cell that appeared to be in prometaphase, as shown in immunofluorescence images (Figure 5.5a). Interestingly, MITF appeared to be excluded from the DNA, as opposed to neighbouring non-mitotic cells where it co-localised with the DNA. We also stained for BRN2, another nuclear transcription factor. In contrast to MITF, expression of BRN2 was down-regulated during mitosis.

Up-regulation of MITF levels was also apparent in 501mel and SK-MEL-28 cells in the G2/M phase, as shown by flow cytometry (Figure 5.5b). Compared to 501mel cells in the G1 and S phases, 501mel cells in G2/M had significantly elevated expression of MITF. This was also true in the case of SK-MEL-28 cells. These results validate the increase in MITF levels of 501mel and SK-MEL-28 cells following mitotic shake-off.

5.2.3 MITF S73 phosphorylation is decreased following CDK inhibition

Since the variation of MITF S73 phosphorylation levels throughout the cell cycle did not correlate with phospho-ERK levels, we reasoned that CDKs might be involved in phosphorylating this residue. We were particularly interested in CDK1, whose activity is up-regulated during G2/M (Pines and Hunter, 1989), and CDK2, whose activity is elevated during the S and G2 phases (Rosenblatt et al., 1992).

To investigate, we treated 501mel melanoma cells with CVT-313 (Brooks et al., 1997), an ATP-competitive inhibitor of CDK2 (IC_{50} = 0.5 μM) and CDK1 (IC_{50} = 4.2 μM). We limited treatment time to a short period of 30 minutes since prolonged inhibition of CDKs with CVT-313 was known to induce cell cycle arrest. To verify that short-term treatment with CVT-313 did not cause any cell cycle-related effects, we analysed the cell cycle profile of the cells via flow cytometry

(Figure 5.6a). The results showed that the cell cycle profile of the CVT-313-treated cells was very similar to that of the DMSO-treated control.

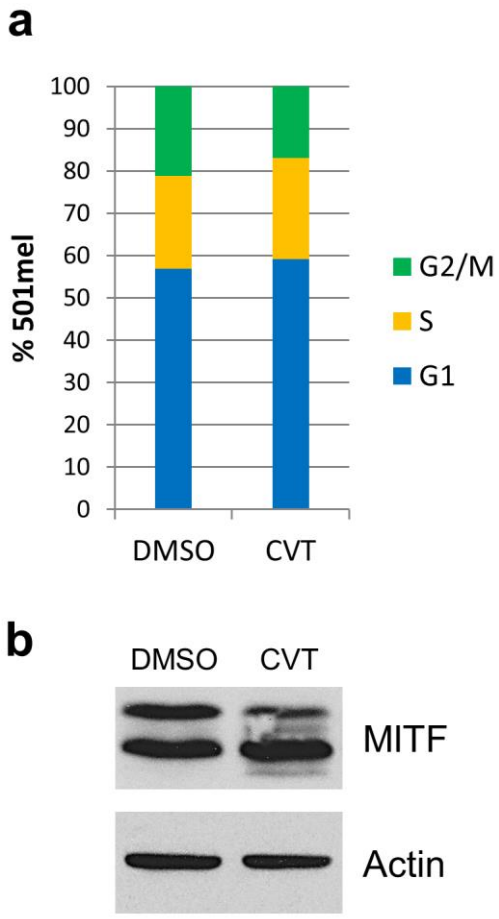

Figure 5.6 MITF S73 phosphorylation decreased following CDK inhibition. (a) Cell cycle profile of 501mel cells after treatment with CVT-313. Cells were grown to 80% confluence and treated with 1 μM CVT-313 (abbreviated as CVT) or an equivalent volume of DMSO for 30 minutes. Their cell cycle profiles were analysed by flow cytometry after fixation and staining with PI. **(b)** Western blot of 501mel cells following treatment with CVT-313. Cells were treated as in (a), then lysed and immunoblotted with an antibody against MITF.

Next, we analysed MITF expression in 501mel cells after CDK inhibition with CVT-313, as indicated by western blot (Figure 5.6b). A 30-minute treatment with CVT-313 was sufficient to induce a reduction in the upper band of MITF, while the lower band remained unchanged relative to the DMSO-treated control. The results indicate that CDK inhibition with CVT-313 caused a decrease in MITF S73

phosphorylation, which was consistent with MITF S73 being phosphorylated by CDK1 or CDK2.

5.2.4 Both CDK1 and CDK2 can phosphorylate MITF S73 in vitro

To ascertain whether MITF S73 could be phosphorylated by CDK1 or CDK2, we carried out an *in vitro* kinase assay. We generated a bacteria expression vector comprising of the first 203 amino acids of MITF and a GST tag. We also made an S73A mutant in this vector. Next, we expressed the mutant and wild-type proteins in BL21 *E. coli*, and pulled down the proteins with glutathione beads after lysing the cells. We then incubated the proteins on the beads with purified CDK1/cyclin B or CDK2/cyclin A in the presence of radioactive [γ-^{32}P]-ATP. Incorporation of ^{32}P was subsequently detected by X-ray film (Figure 5.7a, b).

As shown in Figure 5.7a, the wild-type GST-MITF.1-203 fragment was demonstrably phosphorylated by CDK1/cyclin B, as indicated by ^{32}P incorporation. On the other hand, there was only a very slight amount of CDK1/cyclin B-mediated phosphorylation detected with the S73A mutant, despite equal expression of both protein variants as detected by Coomassie staining of the SDS-PAGE gel.

The wild-type GST-MITF.1-203 fragment was also appreciably phosphorylated by CDK2/cyclin A (Figure 5.7b). In contrast, CDK2/cyclin A phosphorylation of the S73A mutant was virtually undetectable despite equal abundance of both protein variants as measured by Coomassie staining. The results indicate that both CDK1 and CDK2 are capable of phosphorylating the S73 residue in MITF, at least in the *in vitro* context.

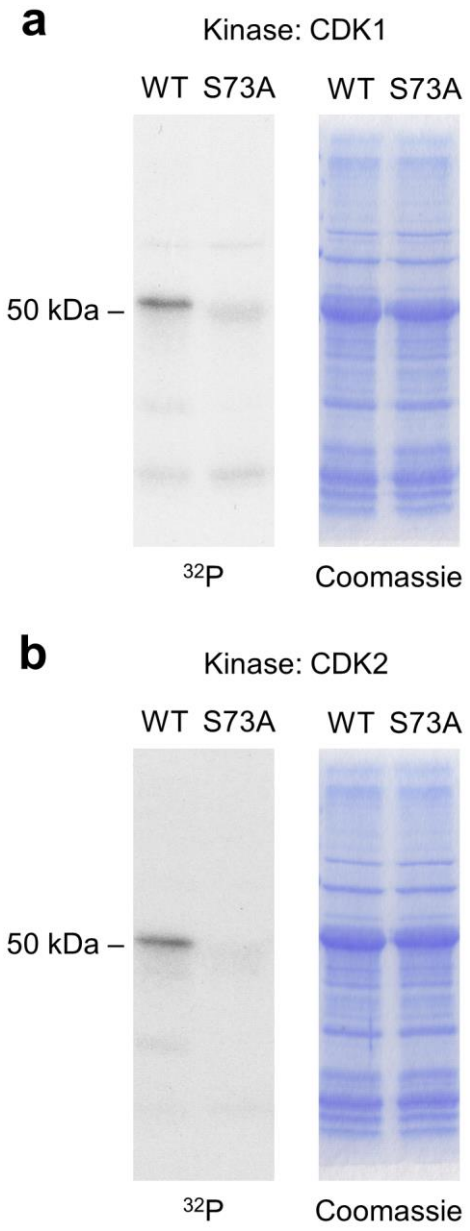

Figure 5.7 MITF S73 can be phosphorylated by both CDK1 and CDK2 *in vitro*. (a) An *in vitro* kinase assay demonstrating CDK1/cyclin B phosphorylation of MITF at S73. GST-MITF.1-203 mutants on glutathione beads were incubated with 50 ng of purified CDK1/cyclin B and 2.5 μCi [γ-^{32}P]-ATP at 30°C for 1 hour. After resolving the proteins by SDS-PAGE, the gel was stained with Coomassie to determine protein levels (right panel). Incorporation of ^{32}P was subsequently detected by X-ray film (left panel). **(b)** An *in vitro* kinase assay demonstrating CDK2/cyclin A phosphorylation of MITF at S73. Reaction conditions were similar to (a), with 50 ng of purified CDK2/cyclin A being used as the kinase instead.

5.3 Discussion

The results demonstrated that mitotic shake-off was a useful method of obtaining a synchronised population of the adherent melanoma cell lines 501mel and SK-MEL-28. The more commonly used chemical-based methods of inducing cell cycle arrest may introduce artifacts into the data since they often involve prolonged arrest of cells at a particular stage of the cell cycle. In contrast, mitotic shake-off is less disruptive as it relies on simple physical agitation to separate mitotic cells from non-mitotic ones (Jackman and O'Connor, 2001). However, the degree of synchrony is not a perfect 100%, which can be explained by the inherent deficiencies of the mitotic shake-off method. The floating cells that are collected during the shake-off is a heterogeneous population consisting of cells that are just entering mitosis and cells that have just completed mitosis, but have yet to reattach to the growth surface following cytokinesis. Hence, a sizeable proportion of the cells that were collected by mitotic shake-off were in the G1 phase of the cell cycle. We were able to obtain a higher degree of synchrony with SK-MEL-28 cells than with 501mel cells, possibly because SK-MEL-28 cells were more adherent and hence detached less easily and/or attached more readily compared to 501mel cells. Furthermore, as the duration of the G1 phase tends to be variable (Jackman and O'Connor, 2001), a further degree of synchrony is lost as the cells progress through the cell cycle after the shake-off.

Both 501mels and SK-MEL-28s exhibited similar profiles of increased MITF levels during and just after mitosis. Although MITF levels were down-regulated in mitotic 501mel cells following nocodazole treatment (Figure 5.2b), we believed this to be an artefact arising from prolonged cell cycle arrest, since the western blot data from mitotic shake-off of both 501mel and SK-MEL-28 cells indicated increased MITF expression during the G2/M phase of the cell cycle (Figure 5.3c, 5.4c).

Immunofluorescence and flow cytometry analysis of untreated 501mel and SK-MEL-28 cells also showed elevated MITF levels during G2/M. This is interesting because transcription is known to be globally repressed during mitosis (Gottesfeld and Forbes, 1997; Johnson and Holland, 1965), with the majority of transcription factors being displaced from the condensed mitotic chromatin (Egli et al., 2008; Martínez-Balbás et al., 1995). While MITF appeared to be displaced from the condensed chromatin during mitosis (Figure 5.5a), total MITF levels were elevated as compared to non-mitotic cells, with MITF levels remaining high throughout the G2/M phase to early G1 (Figure 5.3, 5.4). In contrast, some transcription factors, including BRN2 (Figure 5.5a), are down-regulated during mitosis (D'Annibale et al., 2014; Lindon et al., 1998). This suggests that MITF may be involved in mitosis itself, for example to regulate cyclin B, and/or play an important role in events that occur right after mitosis. Maintaining elevated levels of MITF during mitosis ensures that MITF is poised for reloading onto its transcriptional targets by mass action (Egli et al., 2008), which allows for rapid reestablishment and reactivation of the melanocyte-specific transcription programme upon exit from mitosis and re-entry into G1.

The results also demonstrated that hyperphosphorylation of MITF during the G2/M phase of the cell cycle, which was consistent with increased phosphorylation at the S73 residue, probably by a kinase other than ERK. Our results indicated that S73 phosphorylation in MITF was reduced upon treatment with CVT-313, a small molecule inhibitor whose primary target is CDK2 but also possesses activity against CDK1, suggesting that CDK1 and CDK2 could potentially be phosphorylating the MITF S73 residue. The consensus phosphorylation motif for CDKs has been biochemically determined to be **S/T**-P-X-R/K (Songyang et al., 1994), a requirement

which MITF S73 does not completely fulfill. However, some CDK targets can also be phosphorylated on a minimal motif containing only a serine or threonine residue followed by proline (**S/T**-P) (Errico et al., 2010; Rudner and Murray, 2000; Ubersax et al., 2003), which matches the S-P motif at the S73 residue in MITF. We were subsequently able to show that MITF could be phosphorylated at its S73 residue by both CDK1 and CDK2 *in vitro*. Given that the activity of CDK1 in complex with cyclin B at its highest during mitosis (Hochegger et al., 2008), we are inclined to believe that CDK1 is the main kinase responsible for the increased phosphorylation of S73 residue in MITF seen during the G2/M phase. However, we would not rule out CDK2 phosphorylation of MITF in other phases of the cell cycle, given that it would form a feedback loop in light of *CDK2* being a transcriptional target of MITF in melanocytes (Du et al., 2004).

In conclusion, our results describe regulation of MITF by the cell cycle, in terms of MITF protein levels as well as its phosphorylation status. MITF was found to have elevated expression in addition to being hyperphosphorylated at the S73 residue during G2/M phase of the cell cycle. We were also able to show phosphorylation of MITF S73 by both CDK1 and CDK2 *in vitro*, which was a novel discovery.

Chapter 6 – Concluding Discussion

In this study, we have identified novel sites of post-translational modifications in two oncogenic proteins that are known to play pivotal roles in driving tumorigenesis in melanoma.

6.1 Acetylation of BRAF at K473 and K475

We were able to detect acetylation in BRAF, the most commonly mutated oncoprotein in melanoma with approximately 50% of patients bearing activating genetic alterations in the *BRAF* gene. We showed that BRAF can be acetylated at two residues, K473 and K475, by the p300/CBP acetyltransferases. Treatment of melanoma cells with C646, an inhibitor of p300/CBP, resulted in dramatic activation of the MAPK pathway as shown by an increase in MEK and ERK phosphorylation. Mechanistically, p300/CBP-mediated acetylation of BRAF on K473 and K475 affected its interaction with MEK, hence blocking BRAF-mediated activation of MEK. Importantly, the inhibitory effect of BRAF acetylation appeared to be dominant over the activating V600E substitution, the most common mutation hotspot in BRAF. In addition, querying the COSMIC database revealed cases of colorectal cancer patients harbouring a $BRAF^{K475R}$ mutation. Since the K475R substitution mimics constitutive non-acetylation at the K475 residue in BRAF, it suggests that acetylation at this site may play an important physiological role in cancer.

Since MAPK signalling can also activate the p300 acetyltransferase activity of p300/CBP, BRAF acetylation provides a potential negative-feedback mechanism, which in non-cancer cells can potentially act as a rheostat that dictates the kinetics of MAPK signalling downstream from RTKs. In cancer, BRAF acetylation presents a new and promising target for therapeutic action, since it provides us with a novel way of manipulating MAPK activity that is effective on both V600 and non-V600

mutated BRAF. For example, inhibition of BRAF acetylation can potentially elevate MAPK signalling to levels poorly tolerated by cancer cells harbouring BRAF or NRAS mutations, but not in non-malignant cells where MAPK signalling is not driven by activating mutations in the pathway. On the other hand, up-regulating BRAF acetylation will conceivably lead to inhibition of MAPK signalling, thus providing an additional way of counteracting the constitutive MAPK activation seen in the majority of melanomas. Thus, drugs that target BRAF acetylation can potentially be used to augment treatment regimes, in conjunction with existing BRAF inhibitors such as vemurafenib, as well as newer "feedback buster" type MEK inhibitors that are able to mitigate rebound activation of the MAPK pathway in response to MAPK inhibition-induced relief of negative feedback mechanisms (Caunt et al., 2015).

Future work will be directed towards developing a zebrafish model of melanoma bearing mutations in the two BRAF acetylation sites in order to further investigate the functional significance of acetylation at these residues *in vivo* with regards to tumorigenesis. In addition, we will also like to find effective and specific ways of manipulating acetylation at the two BRAF residues without affecting global acetylation. This can potentially be achieved by developing specific antibodies against acetylated K473 and K475 in BRAF, and utilising these antibodies to carry out a small molecule library screen to identify active compounds with effects on acetylation at these two residues.

6.2 Phosphorylation of MITF at S69 and S73

We were able to identify a novel phosphorylation site, S69, in MITF, the master regulator of the melanocyte lineage that also plays an important role in melanoma tumorigenesis. We showed that phosphorylation at the S69 residue in MITF was mediated by the kinase GSK3. GSK3 phosphorylation of S69 was also demonstrated to cooperate with ERK phosphorylation of S73 in promoting nuclear export of MITF, with inhibition of GSK3 or MAPK signalling inducing an increase in MITF nuclear localisation. MITF nuclear export was mediated by a previously undescribed NES, which was found to comprise of the residues S69, S73, M75, L78 and L80. We also showed that MITF protein levels and phosphorylation status were varied throughout different stages of the cell cycle, with elevated MITF levels observed during the G2/M phase in conjunction with hyperphosphorylation at the S73 residue. Subsequently, we showed that S73 in MITF could also be phosphorylated by both CDK1 and CDK2 in addition to ERK.

Functionally, dephosphorylation at the S69 and S73 residues was associated with a significant increase in MITF activity *in vitro*. In addition, a phospho-mimetic glutamic acid substitution at S69 also disrupted melanophore development in zebrafish, suggesting that S69 phosphorylation had an inhibitory effect on MITF activity during development.

MITF nuclear export following GSK3 phosphorylation of S69 and ERK phosphorylation of S73 provides a framework and potential mechanism that explains oncogene-induced senescence in the context of BRAF activation. Following the acquisition of an activating BRAF mutation, MITF activity decreases due to increased ERK-mediated S73 phosphorylation resulting in nuclear export. Low MITF activity is associated with senescence and $p27^{Kip1}$-mediated cell cycle arrest in

G1. Acquisition of a PTEN mutation reduces GSK3 activity and causes dephosphorylation of S69 in MITF, thus inhibiting nuclear export and increasing MITF activity, which culminates in bypass of senescence.

GSK3 phosphorylation of S69 in MITF may also be important in melanocyte stem cell differentiation downstream of Wnt signalling. In our proposed model, the presence of Wnt inhibits GSK3 phosphorylation of S69, thus promoting increased MITF localisation in the nucleus via a decrease in nuclear export. This increases MITF activity, which induces melanocyte proliferation and ultimately differentiation by turning on genes involved in melanogenesis.

Future work will involve further investigations into oncogene-induced senescence and senescence bypass. We would like to know if oncogene-induced senescence in melanocytes is mediated via MITF. To investigate this, we will obtain a tetracycline-inducible human melanocyte cell line that expresses $BRAF^{V600E}$ in the presence of tetracycline. We will then ectopically express nuclear-export defective MITF in these melanocytes and measure the amount of senescence after inducing $BRAF^{V600E}$ expression. We are also in the process of generating zebrafish with a L80A mutation in Mitfa, which will allow us to further investigate the importance of MITF nuclear export in melanocyte stem cell differentiation and melanoma oncogenesis.

6.3 Conclusion

In conclusion, we have identified novel sites of post-translational modifications in BRAF and MITF and demonstrated their functional consequences in these two important drivers of tumorigenesis in melanoma. This information allows us to gain a better understanding of the mechanisms underlying melanoma tumorigenesis, which will potentially aid us in developing novel therapeutic options for melanoma treatment.

References

Agrawal, N., Akbani, R., Aksoy, B.A., Ally, A., Arachchi, H., Asa, S.L., Auman, J.T., Balasundaram, M., Balu, S., Baylin, S.B., et al. (2014). Integrated Genomic Characterization of Papillary Thyroid Carcinoma. Cell *159*, 676–690.

Ahmed, S., Grant, K.G., Edwards, L.E., Rahman, A., Cirit, M., Goshe, M.B., and Haugh, J.M. (2014). Data-driven modeling reconciles kinetics of ERK phosphorylation, localization, and activity states. Mol. Syst. Biol. *10*, 718–718.

Ait-Si-Ali, S., Carlisi, D., Ramirez, S., Upegui-Gonzalez, L.-C., Duquet, A., Robin, P., Rudkin, B., Harel-Bellan, A., and Trouche, D. (1999). Phosphorylation by p44 MAP Kinase/ERK1 Stimulates CBP Histone Acetyl Transferase Activity in Vitro. Biochem. Biophys. Res. Commun. *262*, 157–162.

Akbani, R., Akdemir, K.C., Aksoy, B.A., Albert, M., Ally, A., Amin, S.B., Arachchi, H., Arora, A., Auman, J.T., Ayala, B., et al. (2015). Genomic Classification of Cutaneous Melanoma. Cell *161*, 1681–1696.

Aksan, I., and Goding, C.R. (1998). Targeting the Microphthalmia Basic Helix-Loop-Helix–Leucine Zipper Transcription Factor to a Subset of E-Box Elements In Vitro and In Vivo. Mol. Cell. Biol. *18*, 6930–6938.

Alessil, D.R., Saito, Y., Campbell, D.G., Cohen, P., Sithanandam, G., Rapp, U., Ashworth, A., Marshall, C.J., and Cowley, S. (1994). Identification of the sites in MAP kinase kinase-1 phosphorylated by p74raf-1. EMBO J. *13*, 1610–1619.

Van Allen, E.M., Wagle, N., Sucker, A., Treacy, D.J., Johannessen, C.M., Goetz, E.M., Place, C.S., Taylor-Weiner, A., Whittaker, S., Kryukov, G. V., et al. (2014). The Genetic Landscape of Clinical Resistance to RAF Inhibition in Metastatic Melanoma. Cancer Discov. *4*, 94–109.

Allfrey, V.G., Faulkner, R., and Mirsky, A.E. (1964). Acetylation and methylation of histones and their possible role in the regulation of RNA synthesis. Proc. Natl. Acad. Sci. U. S. A. *51*, 786–794.

American Cancer Society (2015a). Global Cancer Facts & Figures 3rd Edition.

American Cancer Society (2015b). Cancer Facts & Figures. Cancer Facts Fig. 2015.

Amiel, J., Watkin, P.M., Tassabehji, M., Read, A.P., and Winter, R.M. (1998). Mutation of the MITF gene in albinism-deafness syndrome (Tietz syndrome). Clin. Dysmorphol. *7*, 17–20.

Amit, I., Citri, A., Shay, T., Lu, Y., Katz, M., Zhang, F., Tarcic, G., Siwak, D., Lahad, J., Jacob-Hirsch, J., et al. (2007). A module of negative feedback regulators defines growth factor signaling. Nat. Genet. *39*, 503–512.

Avraham, R., and Yarden, Y. (2011). Feedback regulation of EGFR signalling: decision making by early and delayed loops. Nat. Rev. Mol. Cell Biol. *12*, 104–117.

Balan, V., Leicht, D.T., Zhu, J., Balan, K., Kaplun, A., Singh-Gupta, V., Qin, J., Ruan, H., Comb, M.J., and Tzivion, G. (2005). Identification of Novel In Vivo Raf-1 Phosphorylation Sites Mediating Positive Feedback Raf-1 Regulation by Extracellular Signal-regulated Kinase. Mol. Biol. Cell *17*, 1141–1153.

Baljuls, A., Mueller, T., Drexler, H.C.A., Hekman, M., and Rapp, U.R. (2007). Unique N-region Determines Low Basal Activity and Limited Inducibility of A-RAF Kinase: The Role of N-region in the Evolutionary Divergence of RAF Kinase Function in Vertebrates. J. Biol. Chem. *282*, 26575–26590.

Baljuls, A., Schmitz, W., Mueller, T., Zahedi, R.P., Sickmann, A., Hekman, M., and Rapp, U.R. (2008). Positive Regulation of A-RAF by Phosphorylation of Isoform-specific Hinge Segment and Identification of Novel Phosphorylation Sites. J. Biol. Chem. *283*, 27239–27254.

Bannister, A.J., Miska, E.A., Görlich, D., and Kouzarides, T. (2000). Acetylation of importin-α nuclear import factors by CBP/p300. Curr. Biol. *10*, 467–470.

Bauer, G.L., Praetorius, C., Bergsteinsdottir, K., Hallsson, J.H., Gisladottir, B.K., Schepsky, A., Swing, D.A., O'Sullivan, T.N., Arnheiter, H., Bismuth, K., et al. (2009). The Role of MITF Phosphorylation Sites During Coat Color and Eye Development in Mice Analyzed by Bacterial Artificial Chromosome Transgene Rescue. Genetics *183*, 581–594.

Baxter, L.L., and Pavan, W.J. (2003). Pmel17 expression is Mitf-dependent and reveals cranial melanoblast migration during murine development. Gene Expr. Patterns *3*, 703–707.

Bellei, B., Flori, E., Izzo, E., Maresca, V., and Picardo, M. (2008). GSK3β inhibition promotes melanogenesis in mouse B16 melanoma cells and normal human melanocytes. Cell. Signal. *20*, 1750–1761.

Bennett, D.C. (2003). Human melanocyte senescence and melanoma susceptibility genes. Oncogene *22*, 3063–3069.

Bentley, N.J., Eisen, T., and Goding, C.R. (1994). Melanocyte-Specific Expression of the Human Tyrosinase Promoter: Activation by the Microphthalmia Gene Product and Role of the Initiator. Mol. Cell. Biol. *14*, 7996–8006.

Bertolotto, C., Buscà, R., Abbe, P., Bille, K., Aberdam, E., Ortonne, J.-P., and Ballotti, R. (1998a). Different cis-Acting Elements Are Involved in the Regulation of TRP1 and TRP2 Promoter Activities by Cyclic AMP: Pivotal Role of M Boxes (GTCATGTGCT) and of Microphthalmia. Mol. Cell. Biol. *18*, 694–702.

Bertolotto, C., Abbe, P., Hemesath, T.J., Bille, K., Fisher, D.E., Ortonne, J.P., and Ballotti, R. (1998b). Microphthalmia Gene Product as a Signal Transducer in cAMP-Induced Differentiation of Melanocytes. J. Cell Biol. *142*, 827–835.

Bertolotto, C., Lesueur, F., Giuliano, S., Strub, T., de Lichy, M., Bille, K., Dessen, P., D'Hayer, B., Mohamdi, H., Remenieras, A., et al. (2011). A SUMOylation-defective MITF germline mutation predisposes to melanoma and renal carcinoma. Nature *480*, 94–98.

Bhandaru, M., Ardekani, G., Zhang, G., Martinka, M., McElwee, K.J., Li, G., and Rotte, A. (2014). A combination of p300 and Braf expression in the diagnosis and prognosis of melanoma. BMC Cancer *14*, 398.

Bismuth, K., Skuntz, S., Hallsson, J.H., Pak, E., Dutra, A.S., Steingrimsson, E., and Arnheiter, H. (2008). An Unstable Targeted Allele of the Mouse Mitf Gene With a High Somatic and Germline Reversion Rate. Genetics *178*, 259–272.

Bleyer, A., O'Leary, M., Barr, R., and Ries, L.A.G. (2006). Cancer Epidemiology in Older Adolescents and Young Adults 15 to 29 Years of Age, Including SEER Incidence and Survival: 1975-2000. Natl. Cancer Institute, NIH Pub. No. 06-5767 5767.

Blüthgen, N., Legewie, S., Kielbasa, S.M., Schramme, A., Tchernitsa, O., Keil, J., Solf, A., Vingron, M., Schäfer, R., Herzel, H., et al. (2009). A systems biological approach suggests that transcriptional feedback regulation by dual-specificity phosphatase 6 shapes extracellular signal-related kinase activity in RAS-transformed fibroblasts. FEBS J. *276*, 1024–1035.

Bondurand, N., Pingault, V., Goerich, D.E., Lemort, N., Sock, E., Caignec, C. Le, Wegner, M., and Goossens, M. (2000). Interaction among SOX10, PAX3 and MITF, three genes altered in Waardenburg syndrome. Hum. Mol. Genet. *9*, 1907–1917.

Borgdorff, V., Rix, U., Winter, G.E., Gridling, M., Müller, A.C., Breitwieser, F.P., Wagner, C., Colinge, J., Bennett, K.L., Superti-Furga, G., et al. (2014). A chemical biology approach identifies AMPK as a modulator of melanoma oncogene MITF. Oncogene *33*, 2531–2539.

Boriack-Sjodin, P.A., Margarit, S.M., Bar-Sagi, D., and Kuriyan, J. (1998). The structural basis of the activation of Ras by Sos. Nature *394*, 337–343.

Bowers, E.M., Yan, G., Mukherjee, C., Orry, A., Wang, L., Holbert, M.A., Crump, N.T., Hazzalin, C.A., Liszczak, G., Yuan, H., et al. (2010). Virtual Ligand Screening of the p300/CBP Histone Acetyltransferase: Identification of a Selective Small Molecule Inhibitor. Chem. Biol. *17*, 471–482.

Boyle, G.M., Woods, S.L., Bonazzi, V.F., Stark, M.S., Hacker, E., Aoude, L.G., Dutton-Regester, K., Cook, A.L., Sturm, R.A., and Hayward, N.K. (2011). Melanoma cell invasiveness is regulated by miR-211 suppression of the BRN2 transcription factor. Pigment Cell Melanoma Res. *24*, 525–537.

De Brabander, M.J., Van de Veire, R.M., Aerts, F.E., Borgers, M., and Janssen, P.A. (1976). The Effects of Methyl [5-(2-Thienylcarbonyl)-1H-benzimidazol-2-yl]carbamate, (R 17934; NSC 238159), a New Synthetic Antitumoral Drug Interfering with Microtubules, on Mammalian Cells Cultured in Vitro. Cancer Res. *36*, 905–916.

Braeuer, R.R., Watson, I.R., Wu, C.-J., Mobley, A.K., Kamiya, T., Shoshan, E., and Bar-Eli, M. (2014). Why is melanoma so metastatic? Pigment Cell Melanoma Res. *27*, 19–36.

Brennan, D.F., Dar, A.C., Hertz, N.T., Chao, W.C.H., Burlingame, A.L., Shokat, K.M., and Barford, D. (2011). A Raf-induced allosteric transition of KSR stimulates phosphorylation of MEK. Nature *472*, 366–369.

Brondello, J.-M., Brunet, A., Pouyssegur, J., and McKenzie, F.R. (1997). The Dual Specificity Mitogen-activated Protein Kinase Phosphatase-1 and -2 Are Induced by the p42/p44MAPK Cascade. J. Biol. Chem. *272*, 1368–1376.

Brondello, J.-M., Pouysségur, J., and McKenzie, F.R. (1999). Reduced MAP Kinase Phosphatase-1 Degradation After p42/p44MAPK-Dependent Phosphorylation. Science (80-.). *286*, 2514–2517.

Bronisz, A., Sharma, S.M., Hu, R., Godlewski, J., Tzivion, G., Mansky, K.C., and Ostrowski, M.C. (2006). Microphthalmia-associated Transcription Factor Interactions with 14-3-3 Modulate Differentiation of Committed Myeloid Precursors. Mol. Biol. Cell *17*, 3897–3906.

Brooks, E.E., Gray, N.S., Joly, A., Kerwar, S.S., Lum, R., Mackman, R.L., Norman, T.C., Rosete, J., Rowe, M., Schow, S.R., et al. (1997). CVT-313, a Specific and Potent Inhibitor of CDK2 That Prevents Neointimal Proliferation. J. Biol. Chem. *272*, 29207–29211.

Brtva, T.R., Drugan, J.K., Ghosh, S., Terrell, R.S., Campbell-Burk, S., Bell, R.M., and Der, C.J. (1995). Two Distinct Raf Domains Mediate Interaction with Ras. J. Biol. Chem. *270*, 9809–9812.

Buhrman, G., Holzapfel, G., Fetics, S., and Mattos, C. (2010). Allosteric modulation of Ras positions Q61 for a direct role in catalysis. Proc. Natl. Acad. Sci. *107*, 4931–4936.

Burnet, N.G., Jefferies, S.J., Benson, R.J., Hunt, D.P., and Treasure, F.P. (2005). Years of life lost (YLL) from cancer is an important measure of population burden – and should be considered when allocating research funds. Br. J. Cancer *92*, 241–245.

Carpenter, A.E., Jones, T.R., Lamprecht, M.R., Clarke, C., Kang, I.H., Friman, O., Guertin, D.A., Chang, J.H., Lindquist, R.A., Moffat, J., et al. (2006). CellProfiler: image analysis software for identifying and quantifying cell phenotypes. Genome Biol. *7*, R100.

Carrano, A.C., Eytan, E., Hershko, A., and Pagano, M. (1999). SKP2 is required for ubiquitin-mediated degradation of the CDK inhibitor p27. Nat. Cell Biol. *1*, 193–199.

Carreira, S., Goodall, J., Aksan, I., La Rocca, S.A., Galibert, M.-D., Denat, L., Larue, L., and Goding, C.R. (2005). Mitf cooperates with Rb1 and activates p21Cip1 expression to regulate cell cycle progression. Nature *433*, 764–769.

Carreira, S., Goodall, J., Denat, L., Rodriguez, M., Nuciforo, P., Hoek, K.S., Testori, A., Larue, L., and Goding, C.R. (2006). Mitf regulation of Dia1 controls melanoma proliferation and invasiveness. Genes Dev. *20*, 3426–3439.

Caunt, C.J., Sale, M.J., Smith, P.D., and Cook, S.J. (2015). MEK1 and MEK2 inhibitors and cancer therapy: the long and winding road. Nat. Rev. Cancer *15*, 577–592.

Cerami, E., Gao, J., Dogrusoz, U., Gross, B.E., Sumer, S.O., Aksoy, B.A., Jacobsen, A., Byrne, C.J., Heuer, M.L., Larsson, E., et al. (2012). The cBio Cancer Genomics Portal: An Open Platform for Exploring Multidimensional Cancer Genomics Data. Cancer Discov. *2*, 401–404.

Chang, L., and Karin, M. (2001). Mammalian MAP kinase signalling cascades. Nature *410*, 37–40.

Chapman, P.B., Hauschild, A., Robert, C., Haanen, J.B., Ascierto, P., Larkin, J., Dummer, R., Garbe, C., Testori, A., Maio, M., et al. (2011). Improved Survival with Vemurafenib in Melanoma with BRAF V600E Mutation. N. Engl. J. Med. *364*, 2507–2516.

Chaudhary, A., King, W.G., Mattaliano, M.D., Frost, J.A., Diaz, B., Morrison, D.K.,

Cobb, M.H., Marshall, M.S., and Brugge, J.S. (2000). Phosphatidylinositol 3-kinase regulates Raf1 through Pak phosphorylation of serine 338. Curr. Biol. *10*, 551–554.

Cheli, Y., Ohanna, M., Ballotti, R., and Bertolotto, C. (2010). Fifteen-year quest for microphthalmia-associated transcription factor target genes. Pigment Cell Melanoma Res. *23*, 27–40.

Cheli, Y., Giuliano, S., Botton, T., Rocchi, S., Hofman, V., Hofman, P., Bahadoran, P., Bertolotto, C., and Ballotti, R. (2011). Mitf is the key molecular switch between mouse or human melanoma initiating cells and their differentiated progeny. Oncogene *30*, 2390–2390.

Cheli, Y., Giuliano, S., Fenouille, N., Allegra, M., Hofman, V., Hofman, P., Bahadoran, P., Lacour, J.-P., Tartare-Deckert, S., Bertolotto, C., et al. (2012). Hypoxia and MITF control metastatic behaviour in mouse and human melanoma cells. Oncogene *31*, 2461–2470.

Chen, D., Waters, S.B., Holt, K.H., and Pessin, J.E. (1996). SOS Phosphorylation and Disassociation of the Grb2-SOS Complex by the ERK and JNK Signaling Pathways. J. Biol. Chem. *271*, 6328–6332.

Chen, R.-H., Sarnecki, C., and Blenis, J. (1992). Nuclear Localization and Regulation of erk- and rsk-Encoded Protein Kinases. Mol. Cell. Biol. *12*, 915–927.

Chen, Y.J., Wang, Y.N., and Chang, W.C. (2007). ERK2-mediated C-terminal Serine Phosphorylation of p300 Is Vital to the Regulation of Epidermal Growth Factor-induced Keratin 16 Gene Expression. J. Biol. Chem. *282*, 27215–27228.

Chiaverini, C., Beuret, L., Flori, E., Busca, R., Abbe, P., Bille, K., Bahadoran, P., Ortonne, J.-P., Bertolotto, C., and Ballotti, R. (2008). Microphthalmia-associated Transcription Factor Regulates RAB27A Gene Expression and Controls Melanosome Transport. J. Biol. Chem. *283*, 12635–12642.

Chiloeches, A., Mason, C.S., and Marais, R. (2001). S338 Phosphorylation of Raf-1 Is Independent of Phosphatidylinositol 3-Kinase and Pak3. Mol. Cell. Biol. *21*, 2423–2434.

Chin, L., Pomerantz, J., Polsky, D., Jacobson, M., Cohen, C., Cordon-Cardo, C., Horner, J.W., and DePinho, R.A. (1997). Cooperative effects of INK4a and ras in melanoma susceptibility in vivo. Genes Dev. *11*, 2822–2834.

Chin, L., Garraway, L.A., and Fisher, D.E. (2006). Malignant melanoma: genetics and therapeutics in the genomic era. Genes Dev. *20*, 2149–2182.

Chong, H., Lee, J., and Guan, K. (2001). Positive and negative regulation of Raf kinase activity and function by phosphorylation. EMBO J. *20*, 3716–3727.

Choudhary, C., Kumar, C., Gnad, F., Nielsen, M.L., Rehman, M., Walther, T.C., Olsen, J. V, and Mann, M. (2009). Lysine Acetylation Targets Protein Complexes and Co-Regulates Major Cellular Functions. Science (80-.). *325*, 834–840.

Chuderland, D., Konson, A., and Seger, R. (2008). Identification and Characterization of a General Nuclear Translocation Signal in Signaling Proteins. Mol. Cell *31*, 850–861.

Clark, W.H., Elder, D.E., Guerry, D., Epstein, M.N., Greene, M.H., and Van Horn, M. (1984). A study of tumor progression: The precursor lesions of superficial spreading and nodular melanoma. Hum. Pathol. *15*, 1147–1165.

Clevers, H. (2006). Wnt/β-Catenin Signaling in Development and Disease. Cell *127*, 469–480.

Clevers, H., Loh, K.M., and Nusse, R. (2014). An integral program for tissue renewal and regeneration: Wnt signaling and stem cell control. Science (80-.). *346*, 1248012–1248012.

Cohen, P., and Frame, S. (2001). The renaissance of GSK3. Nat. Rev. Mol. Cell Biol. *2*, 769–776.

Colicelli, J. (2004). Human RAS Superfamily Proteins and Related GTPases. Sci. Signal. *2004*, re13–re13.

Corbalan-Garcia, S., Yang, S.S., Degenhardt, K.R., and Bar-Sagi, D. (1996). Identification of the Mitogen-Activated Protein Kinase Phosphorylation Sites on Human Sos1 That Regulate Interaction with Grb2. Mol. Cell. Biol. *16*, 5674–5682.

Coulombe, P., and Meloche, S. (2007). Atypical mitogen-activated protein kinases: Structure, regulation and functions. Biochim. Biophys. Acta - Mol. Cell Res. *1773*, 1376–1387.

Courtois-Cox, S., Jones, S.L., and Cichowski, K. (2008). Many roads lead to oncogene-induced senescence. Oncogene *27*, 2801–2809.

Cowley, S., Paterson, H., Kemp, P., and Marshall, C.J. (1994). Activation of MAP kinase kinase is necessary and sufficient for PC12 differentiation and for transformation of NIH 3T3 cells. Cell *77*, 841–852.

Cully, M., You, H., Levine, A.J., and Mak, T.W. (2006). Beyond PTEN mutations: the PI3K pathway as an integrator of multiple inputs during tumorigenesis. Nat. Rev. Cancer *6*, 184–192.

Curtin, J.A., Fridlyand, J., Kageshita, T., Patel, H.N., Busam, K.J., Kutzner, H., Cho, K.-H., Aiba, S., Bröcker, E.-B., LeBoit, P.E., et al. (2005). Distinct Sets of Genetic Alterations in Melanoma. N. Engl. J. Med. *353*, 2135–2147.

Cutler, R.E., Stephens, R.M., Saracino, M.R., and Morrison, D.K. (1998). Autoregulation of the Raf-1 serine/threonine kinase. Proc. Natl. Acad. Sci. *95*, 9214–9219.

D'Annibale, S., Kim, J., Magliozzi, R., Low, T.Y., Mohammed, S., Heck, A.J.R., and Guardavaccaro, D. (2014). Proteasome-dependent Degradation of Transcription Factor Activating Enhancer-binding Protein 4 (TFAP4) Controls Mitotic Division. J. Biol. Chem. *289*, 7730–7737.

Dankort, D., Curley, D.P., Cartlidge, R.A., Nelson, B., Karnezis, A.N., Damsky Jr, W.E., You, M.J., DePinho, R.A., McMahon, M., and Bosenberg, M. (2009). BrafV600E cooperates with Pten loss to induce metastatic melanoma. Nat. Genet. *41*, 544–552.

Datta, S.R., Dudek, H., Tao, X., Masters, S., Fu, H., Gotoh, Y., and Greenberg, M.E. (1997). Akt Phosphorylation of BAD Couples Survival Signals to the Cell-Intrinsic Death Machinery. Cell *91*, 231–241.

Davies, H., Bignell, G.R., Cox, C., Stephens, P., Edkins, S., Clegg, S., Teague, J., Woffendin, H., Garnett, M.J., Bottomley, W., et al. (2002). Mutations of the BRAF gene in human cancer. Nature *417*, 949–954.

Dean, M., Fojo, T., and Bates, S. (2005). Tumour stem cells and drug resistance. Nat. Rev. Cancer *5*, 275–284.

Debbache, J., Raza Zaidi, M., Davis, S., Guo, T., Bismuth, K., Wang, X., Skuntz, S., Maric, D., Pickel, J., Meltzer, P., et al. (2012). In Vivo Role of Alternative Splicing and Serine Phosphorylation of the Microphthalmia-Associated Transcription Factor. Genetics *191*, 133–144.

Der, C.J., Finkel, T., and Cooper, G.M. (1986). Biological and biochemical properties of human rasH genes mutated at codon 61. Cell *44*, 167–176.

Deuker, M.M., and McMahon, M. (2014). Oncogene Addiction and Overdose: Intermittent Treatment in Models of Drug-Resistant BRAF-Mutated Melanoma. Melanoma Lett. *32*.

Dhillon, A.S., Pollock, C., Steen, H., Shaw, P.E., Mischak, H., and Kolch, W. (2002). Cyclic AMP-Dependent Kinase Regulates Raf-1 Kinase Mainly by Phosphorylation of Serine 259. Mol. Cell. Biol. *22*, 3237–3246.

Dhillon, A.S., Hagan, S., Rath, O., and Kolch, W. (2007). MAP kinase signalling pathways in cancer. Oncogene *26*, 3279–3290.

Dhillon, A.S., Yip, Y.Y., Grindlay, G.J., Pakay, J.L., Dangers, M., Hillmann, M., Clark, W., Pitt, A., Mischak, H., and Kolch, W. (2009). The C-terminus of Raf-1 acts as a 14-3-3-dependent activation switch. Cell. Signal. *21*, 1645–1651.

Diaz, B., Barnard, D., Filson, A., MacDonald, S., King, A., and Marshall, M. (1997). Phosphorylation of Raf-1 Serine 338-Serine 339 Is an Essential Regulatory Event for Ras-Dependent Activation and Biological Signaling. Mol. Cell. Biol. *17*, 4509–4516.

Dorsky, R.I., Moon, R.T., and Raible, D.W. (1998). Control of neural crest cell fate by the Wnt signalling pathway. Nature *396*, 370–373.

Dorsky, R.I., Raible, D.W., and Moon, R.T. (2000). Direct regulation of nacre, a zebrafish MITF homolog required for pigment cell formation, by the Wnt pathway. Genes Dev. *14*, 158–162.

Dougherty, M.K., Müller, J., Ritt, D.A., Zhou, M., Zhou, X.Z., Copeland, T.D., Conrads, T.P., Veenstra, T.D., Lu, K.P., and Morrison, D.K. (2005). Regulation of Raf-1 by Direct Feedback Phosphorylation. Mol. Cell *17*, 215–224.

Douville, E., and Downward, J. (1997). EGF induced SOS phosphorylation in PC12 cells involves P90 RSK-2. Oncogene *15*, 373–383.

Drewry, D., Willson, T., and Zuercher, W. (2014). Seeding Collaborations to Advance Kinase Science with the GSK Published Kinase Inhibitor Set (PKIS). Curr. Top. Med. Chem. *14*, 340–342.

Du, J., Miller, A.J., Widlund, H.R., Horstmann, M.A., Ramaswamy, S., and Fisher, D.E. (2003). MLANA/MART1 and SILV/PMEL17/GP100 Are Transcriptionally Regulated by MITF in Melanocytes and Melanoma. Am. J. Pathol. *163*, 333–343.

Du, J., Widlund, H.R., Horstmann, M.A., Ramaswamy, S., Ross, K., Huber, W.E., Nishimura, E.K., Golub, T.R., and Fisher, D.E. (2004). Critical role of CDK2 for melanoma growth linked to its melanocyte-specific transcriptional regulation by MITF. Cancer Cell *6*, 565–576.

Dumaz, N., and Marais, R. (2003). Protein Kinase A Blocks Raf-1 Activity by Stimulating 14-3-3 Binding and Blocking Raf-1 Interaction with Ras. J. Biol. Chem. *278*, 29819–29823.

Dynek, J.N., Chan, S.M., Liu, J., Zha, J., Fairbrother, W.J., and Vucic, D. (2008). Microphthalmia-Associated Transcription Factor Is a Critical Transcriptional Regulator of Melanoma Inhibitor of Apoptosis in Melanomas. Cancer Res. *68*, 3124–3132.

Eggermont, A.M.M., and Robert, C. (2012). Melanoma in 2011: A new paradigm tumor for drug development. Nat. Rev. Clin. Oncol. *9*, 74–76.

Egli, D., Birkhoff, G., and Eggan, K. (2008). Mediators of reprogramming: transcription factors and transitions through mitosis. Nat. Rev. Mol. Cell Biol. *9*, 505–516.

Eisen, T., Ahmad, T., Flaherty, K.T., Gore, M., Kaye, S., Marais, R., Gibbens, I., Hackett, S., James, M., Schuchter, L.M., et al. (2006). Sorafenib in advanced melanoma: a Phase II randomised discontinuation trial analysis. Br. J. Cancer *95*, 581–586.

Elworthy, S., Lister, J.A., Carney, T.J., Raible, D.W., and Kelsh, R.N. (2003). Transcriptional regulation of mitfa accounts for the sox10 requirement in zebrafish melanophore development. Development *130*, 2809–2818.

Emery, C.M., Vijayendran, K.G., Zipser, M.C., Sawyer, A.M., Niu, L., Kim, J.J., Hatton, C., Chopra, R., Oberholzer, P.A., Karpova, M.B., et al. (2009). MEK1 mutations confer resistance to MEK and B-RAF inhibition. Proc. Natl. Acad. Sci. *106*, 20411–20416.

Emuss, V., Garnett, M., Mason, C., and Marais, R. (2005). Mutations of C-RAF Are Rare in Human Cancer because C-RAF Has a Low Basal Kinase Activity Compared with B-RAF. Cancer Res. *65*, 9719–9726.

Errico, A., Deshmukh, K., Tanaka, Y., Pozniakovsky, A., and Hunt, T. (2010). Identification of substrates for cyclin dependent kinases. Adv. Enzyme Regul. *50*, 375–399.

Fabian, J.R., Daar, I.O., and Morrison, D.K. (1993). Critical Tyrosine Residues Regulate the Enzymatic and Biological Activity of Raf-1 Kinase. Mol. Cell. Biol. *13*, 7170–7179.

Farrar, M.A., Alberola-lla, J., and Perlmutter, R.M. (1996). Activation of the Raf-1 kinase cascade by coumermycin-induced dimerization. Nature *383*, 178–181.

Favata, M.F., Horiuchi, K.Y., Manos, E.J., Daulerio, A.J., Stradley, D.A., Feeser, W.S., Van Dyk, D.E., Pitts, W.J., Earl, R.A., Hobbs, F., et al. (1998). Identification of a Novel Inhibitor of Mitogen-activated Protein Kinase Kinase. J. Biol. Chem. *273*, 18623–18632.

Feige, E., Yokoyama, S., Levy, C., Khaled, M., Igras, V., Lin, R.J., Lee, S., Widlund, H.R., Granter, S.R., Kung, A.L., et al. (2011). Hypoxia-induced transcriptional repression of the melanoma-associated oncogene MITF. Proc. Natl. Acad. Sci. *108*, E924–E933.

Feramisco, J.R., Gross, M., Kamata, T., Rosenberg, M., and Sweet, R.W. (1984). Microinjection of the oncogene form of the human H-ras (t-24) protein results in rapid proliferation of quiescent cells. Cell *38*, 109–117.

Ferlay, J., Soerjomataram, I., Ervik, M., Dikshit, R., Eser, S., Mathers, C., Rebelo, M., Parkin, D.M., Forman, D., and Bray, F. (2013). GLOBOCAN 2012 v1.0, Cancer Incidence and Mortality Worldwide: IARC CancerBase. No. 11.

Fiol, C.J., Mahrenholz, A.M., Wang, Y., Roeske, R.W., and Roach, P.J. (1987). Formation of Protein Kinase Recognition Sites by Covalent Modification of the Substrate. Molecular Mechanism for the Synergistic Action of Casein Kinase II and Glycogen Synthase Kinase 3. J. Biol. Chem. *262*, 14042–14048.

Fiol, C.J., Wang, A., Roeske, R.W., and Roach, P.J. (1990). Ordered multisite protein phosphorylation. Analysis of glycogen synthase kinase 3 action using model peptide substrates. J. Biol. Chem. *265*, 6061–6065.

Fischer, A., Hekman, M., Kuhlmann, J., Rubio, I., Wiese, S., and Rapp, U.R. (2007). B- and C-RAF Display Essential Differences in Their Binding to Ras: The Isotype-specific N terminus of B-RAF Facilitates Ras Binding. J. Biol. Chem. *282*, 26503–26516.

Fisher, J.C. (1958). Multiple-Mutation Theory of Carcinogenesis. Nature *181*, 651–652.

Flaherty, K.T., Infante, J.R., Daud, A., Gonzalez, R., Kefford, R.F., Sosman, J., Hamid, O., Schuchter, L., Cebon, J., Ibrahim, N., et al. (2012). Combined BRAF and MEK Inhibition in Melanoma with BRAF V600 Mutations. N. Engl. J. Med. *367*, 1694–1703.

Flaherty, K.T., Lee, S.J., Zhao, F., Schuchter, L.M., Flaherty, L., Kefford, R., Atkins, M.B., Leming, P., and Kirkwood, J.M. (2013). Phase III Trial of Carboplatin and Paclitaxel With or Without Sorafenib in Metastatic Melanoma. J. Clin. Oncol. *31*, 373–379.

Forbes, S.A., Beare, D., Gunasekaran, P., Leung, K., Bindal, N., Boutselakis, H., Ding, M., Bamford, S., Cole, C., Ward, S., et al. (2015). COSMIC: exploring the world's knowledge of somatic mutations in human cancer. Nucleic Acids Res. *43*, D805–D811.

Fornerod, M., Ohno, M., Yoshida, M., and Mattaj, I.W. (1997). CRM1 Is an Export Receptor for Leucine-Rich Nuclear Export Signals. Cell *90*, 1051–1060.

Frech, M., Darden, T.A., Pedersen, L.G., Foley, C.K., Charifson, P.S., Anderson, M.W., and Wittinghofer, A. (1994). Role of Glutamine-61 in the Hydrolysis of GTP by p21H-ras: An Experimental and Theoretical Study. Biochemistry *33*, 3237–3244.

Fu, J., Yoon, H.-G., Qin, J., and Wong, J. (2007). Regulation of P-TEFb Elongation Complex Activity by CDK9 Acetylation. Mol. Cell. Biol. *27*, 4641–4651.

Fuse, N., Yasumoto, K., Suzuki, H., Takahashi, K., and Shibahara, S. (1996). Identification of a Melanocyte-Type Promoter of the Microphthalmia-Associated Transcription Factor Gene. Biochem. Biophys. Res. Commun. *219*, 702–707.

Galibert, M.D., Carreira, S., and Goding, C.R. (2001). The Usf-1 transcription factor is a novel target for the stress-responsive p38 kinase and mediates UV-induced Tyrosinase expression. EMBO J. *20*, 5022–5031.

Gandini, S., Sera, F., Cattaruzza, M.S., Pasquini, P., Picconi, O., Boyle, P., and Melchi, C.F. (2005a). Meta-analysis of risk factors for cutaneous melanoma: II. Sun exposure. Eur. J. Cancer *41*, 45–60.

Gandini, S., Sera, F., Cattaruzza, M.S., Pasquini, P., Zanetti, R., Masini, C., Boyle, P., and Melchi, C.F. (2005b). Meta-analysis of risk factors for cutaneous melanoma: III. Family history, actinic damage and phenotypic factors. Eur. J. Cancer *41*, 2040–2059.

Garbe, C., and Leiter, U. (2009). Melanoma epidemiology and trends. Clin. Dermatol. *27*, 3–9.

Garnett, M.J., Rana, S., Paterson, H., Barford, D., and Marais, R. (2005). Wild-Type and Mutant B-RAF Activate C-RAF through Distinct Mechanisms Involving Heterodimerization. Mol. Cell *20*, 963–969.

Garraway, L.A., and Sellers, W.R. (2006). Lineage dependency and lineage-survival oncogenes in human cancer. Nat. Rev. Cancer *6*, 742–742.

Garraway, L.A., Widlund, H.R., Rubin, M.A., Getz, G., Berger, A.J., Ramaswamy, S., Beroukhim, R., Milner, D.A., Granter, S.R., Du, J., et al. (2005). Integrative genomic analyses identify MITF as a lineage survival oncogene amplified in malignant melanoma. Nature *436*, 117–122.

Geller, A.C., Clapp, R.W., Sober, A.J., Gonsalves, L., Mueller, L., Christiansen, C.L., Shaikh, W., and Miller, D.R. (2013). Melanoma Epidemic: An Analysis of Six Decades of Data From the Connecticut Tumor Registry. J. Clin. Oncol. *31*, 4172–4178.

Ghosh, S., Xie, W.Q., Quest, A.F.G., Mabrouk, G.M., Strum, J.C., and Bell, R.M. (1994). The Cysteine-rich Region of Raf-1 Kinase Contains Zinc, Translocates to Liposomes, and Is Adjacent to a Segment That Binds GTP-Ras. J. Biol. Chem. *269*, 10000–10007.

Gillies, R.J., Verduzco, D., and Gatenby, R.A. (2012). Evolutionary dynamics of carcinogenesis and why targeted therapy does not work. Nat. Rev. Cancer *12*, 487–493.

Giuliano, S., Cheli, Y., Ohanna, M., Bonet, C., Beuret, L., Bille, K., Loubat, A., Hofman, V., Hofman, P., Ponzio, G., et al. (2010). Microphthalmia-Associated Transcription Factor Controls the DNA Damage Response and a Lineage-Specific Senescence Program in Melanomas. Cancer Res. *70*, 3813–3822.

Glozak, M.A., Sengupta, N., Zhang, X., and Seto, E. (2005). Acetylation and deacetylation of non-histone proteins. Gene *363*, 15–23.

Goding, C.R. (2011). A picture of Mitf in melanoma immortality. Oncogene *30*, 2304–2306.

Goodall, J., Carreira, S., Denat, L., Kobi, D., Davidson, I., Nuciforo, P., Sturm, R.A.,

Larue, L., and Goding, C.R. (2008). Brn-2 Represses Microphthalmia-Associated Transcription Factor Expression and Marks a Distinct Subpopulation of Microphthalmia-Associated Transcription Factor-Negative Melanoma Cells. Cancer Res. *68*, 7788–7794.

Gottesfeld, J.M., and Forbes, D.J. (1997). Mitotic repression of the transcriptional machinery. Trends Biochem. Sci. *22*, 197–202.

Goueli, B.S., and Janknecht, R. (2004). Upregulation of the Catalytic Telomerase Subunit by the Transcription Factor ER81 and Oncogenic HER2/Neu, Ras, or Raf. Mol. Cell. Biol. *24*, 25–35.

Gray-Schopfer, V., Wellbrock, C., and Marais, R. (2007). Melanoma biology and new targeted therapy. Nature *445*, 851–857.

Grill, C., Bergsteinsdottir, K., Ogmundsdottir, M.H., Pogenberg, V., Schepsky, A., Wilmanns, M., Pingault, V., and Steingrimsson, E. (2013). MITF mutations associated with pigment deficiency syndromes and melanoma have different effects on protein function. Hum. Mol. Genet. *22*, 4357–4367.

Grunstein, M. (1997). Histone acetylation in chromatin structure and transcription. Nature *389*, 349–352.

Gu, W., and Roeder, R.G. (1997). Activation of p53 sequence-specific DNA binding by acetylation of the p53 C-terminal domain. Cell *90*, 595–606.

Gu, Y., Turck, C.W., and Morgan, D.O. (1993). Inhibition of CDK2 activity in vivo by an associated 20K regulatory subunit. Nature *366*, 707–710.

Guan, K.L., Figueroa, C., Brtva, T.R., Zhu, T., Taylor, J., Barber, T.D., and Vojtek, A.B. (2000). Negative regulation of the serine/threonine kinase B-Raf by Akt. J. Biol. Chem. *275*, 27354–27359.

Gupta, P.B., Kuperwasser, C., Brunet, J.-P., Ramaswamy, S., Kuo, W.-L., Gray, J.W., Naber, S.P., and Weinberg, R.A. (2005). The melanocyte differentiation program predisposes to metastasis after neoplastic transformation. Nat. Genet. *37*, 1047–1054.

Güttler, T., Madl, T., Neumann, P., Deichsel, D., Corsini, L., Monecke, T., Ficner, R., Sattler, M., and Görlich, D. (2010). NES consensus redefined by structures of PKI-type and Rev-type nuclear export signals bound to CRM1. Nat. Struct. Mol. Biol. *17*, 1367–1376.

ter Haar, E., Coll, J.T., Austen, D.A., Hsiao, H.-M., Swenson, L., and Jain, J. (2001). Structure of GSK3β reveals a primed phosphorylation mechanism. Nat. Struct. Biol. *8*, 593–596.

Habib, S.J., Chen, B.-C., Tsai, F.-C., Anastassiadis, K., Meyer, T., Betzig, E., and Nusse, R. (2013). A Localized Wnt Signal Orients Asymmetric Stem Cell Division in Vitro. Science (80-.). *339*, 1445–1448.

Haling, J.R., Sudhamsu, J., Yen, I., Sideris, S., Sandoval, W., Phung, W., Bravo, B.J., Giannetti, A.M., Peck, A., Masselot, A., et al. (2014). Structure of the BRAF-MEK Complex Reveals a Kinase Activity Independent Role for BRAF in MAPK Signaling. Cancer Cell *26*, 402–413.

Hanafusa, H., Torii, S., Yasunaga, T., and Nishida, E. (2002). Sprouty1 and Sprouty2 provide a control mechanism for the Ras/MAPK signalling pathway. Nat. Cell Biol.

4, 850–858.

Hanahan, D., and Weinberg, R. a (2000). The Hallmarks of Cancer. Cell *100*, 57–70.

Hanahan, D., and Weinberg, R.A. (2011). Hallmarks of Cancer: The Next Generation. Cell *144*, 646–674.

Haq, R., Yokoyama, S., Hawryluk, E.B., Jonsson, G.B., Frederick, D.T., McHenry, K., Porter, D., Tran, T.-N., Love, K.T., Langer, R., et al. (2013a). BCL2A1 is a lineage-specific antiapoptotic melanoma oncogene that confers resistance to BRAF inhibition. Proc. Natl. Acad. Sci. *110*, 4321–4326.

Haq, R., Shoag, J., Andreu-Perez, P., Yokoyama, S., Edelman, H., Rowe, G.C., Frederick, D.T., Hurley, A.D., Nellore, A., Kung, A.L., et al. (2013b). Oncogenic BRAF Regulates Oxidative Metabolism via PGC1α and MITF. Cancer Cell *23*, 302–315.

Hari, L., Brault, V., Kléber, M., Lee, H.Y., Ille, F., Leimeroth, R., Paratore, C., Suter, U., Kemler, R., and Sommer, L. (2002). Lineage-specific requirements of β-catenin in neural crest development. J. Cell Biol. *159*, 867–880.

Harper, J.W., Adami, G.R., Wei, N., Keyomarsi, K., and Elledge, S.J. (1993). The p21 Cdk-interacting protein Cip1 is a potent inhibitor of G1 cyclin-dependent kinases. Cell *75*, 805–816.

Harris, S.L., and Levine, A.J. (2005). The p53 pathway: positive and negative feedback loops. Oncogene *24*, 2899–2908.

Hatzivassiliou, G., Song, K., Yen, I., Brandhuber, B.J., Anderson, D.J., Alvarado, R., Ludlam, M.J.C., Stokoe, D., Gloor, S.L., Vigers, G., et al. (2010). RAF inhibitors prime wild-type RAF to activate the MAPK pathway and enhance growth. Nature *464*, 431–435.

Hausauer, A.K. (2011). Increases in Melanoma Among Adolescent Girls and Young Women in California. Arch. Dermatol. *147*, 783.

Hauschild, A., Agarwala, S.S., Trefzer, U., Hogg, D., Robert, C., Hersey, P., Eggermont, A., Grabbe, S., Gonzalez, R., Gille, J., et al. (2009). Results of a Phase III, Randomized, Placebo-Controlled Study of Sorafenib in Combination With Carboplatin and Paclitaxel As Second-Line Treatment in Patients With Unresectable Stage III or Stage IV Melanoma. J. Clin. Oncol. *27*, 2823–2830.

Hauschild, A., Grob, J.-J., Demidov, L. V., Jouary, T., Gutzmer, R., Millward, M., Rutkowski, P., Blank, C.U., Miller, W.H., Kaempgen, E., et al. (2012). Dabrafenib in BRAF-mutated metastatic melanoma: a multicentre, open-label, phase 3 randomised controlled trial. Lancet *380*, 358–365.

Hayward, N.K. (2003). Genetics of melanoma predisposition. Oncogene *22*, 3053–3062.

Heidecker, G., Huleihel, M., Cleveland, J.L., Kolch, W., Beck, T.W., Lloyd, P., Pawson, T., and Rapp, U.R. (1990). Mutational activation of c-raf-1 and definition of the minimal transforming sequence. Mol. Cell. Biol. *10*, 2503–2512.

Heidorn, S.J., Milagre, C., Whittaker, S., Nourry, A., Niculescu-Duvas, I., Dhomen,

N., Hussain, J., Reis-Filho, J.S., Springer, C.J., Pritchard, C., et al. (2010). Kinase-Dead BRAF and Oncogenic RAS Cooperate to Drive Tumor Progression through CRAF. Cell *140*, 209–221.

Hemesath, T.J., Steingrimsson, E., McGill, G., Hansen, M.J., Vaught, J., Hodgkinson, C.A., Arnheiter, H., Copeland, N.G., Jenkins, N.A., and Fisher, D.E. (1994). microphthalmia, a critical factor in melanocyte development, defines a discrete transcription factor family. Genes Dev. *8*, 2770–2780.

Hemesath, T.J., Price, E.R., Takemoto, C., Badalian, T., and Fisher, D.E. (1998). MAP kinase links the transcription factor Microphthalmia to c-Kit signalling in melanocytes. Nature *391*, 298–301.

Hershey, C.L., and Fisher, D.E. (2004). Mitf and Tfe3: members of a b-HLH-ZIP transcription factor family essential for osteoclast development and function. Bone *34*, 689–696.

Hochegger, H., Takeda, S., and Hunt, T. (2008). Cyclin-dependent kinases and cell-cycle transitions: does one fit all? Nat. Rev. Mol. Cell Biol. *9*, 910–916.

Hodgkinson, C.A., Moore, K.J., Nakayama, A., Steingrímsson, E., Copeland, N.G., Jenkins, N.A., and Arnheiter, H. (1993). Mutations at the mouse microphthalmia locus are associated with defects in a gene encoding a novel basic-helix-loop-helix-zipper protein. Cell *74*, 395–404.

Hodis, E., Watson, I.R., Kryukov, G. V., Arold, S.T., Imielinski, M., Theurillat, J.-P., Nickerson, E., Auclair, D., Li, L., Place, C., et al. (2012). A Landscape of Driver Mutations in Melanoma. Cell *150*, 251–263.

Hoeflich, K.P., Gray, D.C., Eby, M.T., Tien, J.Y., Wong, L., Bower, J., Gogineni, A., Zha, J., Cole, M.J., Stern, H.M., et al. (2006). Oncogenic BRAF Is Required for Tumor Growth and Maintenance in Melanoma Models. Cancer Res. *66*, 999–1006.

Hoek, K.S., and Goding, C.R. (2010). Cancer stem cells versus phenotype-switching in melanoma. Pigment Cell Melanoma Res. *23*, 746–759.

Hoek, K.S., Eichhoff, O.M., Schlegel, N.C., Dobbeling, U., Kobert, N., Schaerer, L., Hemmi, S., and Dummer, R. (2008). In vivo Switching of Human Melanoma Cells between Proliferative and Invasive States. Cancer Res. *68*, 650–656.

Holderfield, M., Merritt, H., Chan, J., Wallroth, M., Tandeske, L., Zhai, H., Tellew, J., Hardy, S., Hekmat-Nejad, M., Stuart, D., et al. (2013). RAF Inhibitors Activate the MAPK Pathway by Relieving Inhibitory Autophosphorylation. Cancer Cell *23*, 594–602.

Holderfield, M., Deuker, M.M., McCormick, F., and McMahon, M. (2014). Targeting RAF kinases for cancer therapy: BRAF-mutated melanoma and beyond. Nat. Rev. Cancer *14*, 455–467.

Honda, R., and Yasuda, H. (1999). Association of p19(ARF) with Mdm2 inhibits ubiquitin ligase activity of Mdm2 for tumor suppressor p53. EMBO J. *18*, 22–27.

Howlader, N., Noone, A.M., Krapcho, M., Garshell, J., Miller, D., Altekruse, S.F.,

Kosary, C.L., Yu, M., Ruhl, J., Tatalovich, Z., et al. (2015). SEER Cancer Statistics Review, 1975-2012. Natl. Cancer Institute. Bethesda, MD, http//seer.cancer.gov/csr/1975_2012/.

Hu, J., Stites, E.C., Yu, H., Germino, E.A., Meharena, H.S., Stork, P.J.S., Kornev, A.P., Taylor, S.S., and Shaw, A.S. (2013). Allosteric Activation of Functionally Asymmetric RAF Kinase Dimers. Cell *154*, 1036–1046.

Huber, W.E., Price, E.R., Widlund, H.R., Du, J., Davis, I.J., Wegner, M., and Fisher, D.E. (2003). A Tissue-restricted cAMP Transcriptional Response: SOX10 Modulates α-Melanocyte-Stimulating Hormone-Triggered Expression of Microphthalmia-Associated Transcription Factor in Melanocytes. J. Biol. Chem. *278*, 45224–45230.

Huff, K., End, D., and Guroff, G. (1981). Nerve growth factor-induced alteration in the response of PC12 pheochromocytoma cells to epidermal growth factor. J. Cell Biol. *88*, 189–198.

Hughes, A.E., Newton, V.E., Liu, X.Z., and Read, A.P. (1994). A gene for Waardenburg Syndrome type 2 maps close to the human homologue of the microphthalmia gene at chromosome 3p12–p14.1. Nat. Genet. *7*, 509–512.

Hwang, P.H., Yi, H. keun, Kim, D.S., Nam, S.Y., Kim, J.S., and Lee, D.Y. (2001). Suppression of tumorigenicity and metastasis in B16F10 cells by PTEN/MMAC1/TEP1 gene. Cancer Lett. *172*, 83–91.

Ikeya, M., Lee, S.M.K., Johnson, J.E., McMahon, A.P., and Takada, S. (1997). Wnt signalling required for expansion of neural crest and CNS progenitors. Nature *389*, 966–970.

Iyengar, S., Kasheta, M., and Ceol, C.J. (2015). Poised Regeneration of Zebrafish Melanocytes Involves Direct Differentiation and Concurrent Replenishment of Tissue-Resident Progenitor Cells. Dev. Cell *33*, 631–643.

Jackman, J., and O'Connor, P.M. (2001). Methods for Synchronizing Cells at Specific Stages of the Cell Cycle. In Current Protocols in Cell Biology, (Hoboken, NJ, USA: John Wiley & Sons, Inc.), p. Unit 8.3.

Jacquemin, P., Lannoy, V.J., O'Sullivan, J., Read, A., Lemaigre, F.P., and Rousseau, G.G. (2001). The Transcription Factor Onecut-2 Controls the Microphthalmia-Associated Transcription Factor Gene. Biochem. Biophys. Res. Commun. *285*, 1200–1205.

Janknecht, R. (1996). Analysis of the ERK-Stimulated ETS Transcription Factor ER81. Mol. Cell. Biol. *16*, 1550–1556.

Janknecht, R., and Nordheim, A. (1996). MAP Kinase-Dependent Transcriptional Coactivation by Elk-1 and Its Cofactor CBP. Biochem. Biophys. Res. Commun. *228*, 831–837.

Jaumot, M., and Hancock, J.F. (2001). Protein phosphatases 1 and 2A promote Raf-1 activation by regulating 14-3-3 interactions. Oncogene *20*, 3949–3958.

Javelaud, D., Alexaki, V.-I., Pierrat, M.-J., Hoek, K.S., Dennler, S., Van Kempen, L.,

Bertolotto, C., Ballotti, R., Saule, S., Delmas, V., et al. (2011). GLI2 and M-MITF transcription factors control exclusive gene expression programs and inversely regulate invasion in human melanoma cells. Pigment Cell Melanoma Res. *24*, 932–943.

Johannessen, C.M., Boehm, J.S., Kim, S.Y., Thomas, S.R., Wardwell, L., Johnson, L.A., Emery, C.M., Stransky, N., Cogdill, A.P., Barretina, J., et al. (2010). COT drives resistance to RAF inhibition through MAP kinase pathway reactivation. Nature *468*, 968–972.

Johannessen, C.M., Johnson, L. a, Piccioni, F., Townes, A., Frederick, D.T., Donahue, M.K., Narayan, R., Flaherty, K.T., Wargo, J. a, Root, D.E., et al. (2013). A melanocyte lineage program confers resistance to MAP kinase pathway inhibition. Nature *504*, 138–142.

Johnson, G.L., and Lapadat, R. (2002). Mitogen-Activated Protein Kinase Pathways Mediated by ERK, JNK, and p38 Protein Kinases. Science (80-.). *298*, 1911–1912.

Johnson, T.C., and Holland, J.J. (1965). Ribonucleic acid and protein synthesis in mitotic HeLa cells. J. Cell Biol. *27*, 565–574.

Joseph, E.W., Pratilas, C.A., Poulikakos, P.I., Tadi, M., Wang, W., Taylor, B.S., Halilovic, E., Persaud, Y., Xing, F., Viale, A., et al. (2010). The RAF inhibitor PLX4032 inhibits ERK signaling and tumor cell proliferation in a V600E BRAF-selective manner. Proc. Natl. Acad. Sci. *107*, 14903–14908.

Kalderon, D., Roberts, B.L., Richardson, W.D., and Smith, A.E. (1984). A short amino acid sequence able to specify nuclear location. Cell *39*, 499–509.

Kamentsky, L., Jones, T.R., Fraser, A., Bray, M.-A., Logan, D.J., Madden, K.L., Ljosa, V., Rueden, C., Eliceiri, K.W., and Carpenter, A.E. (2011). Improved structure, function and compatibility for CellProfiler: modular high-throughput image analysis software. Bioinformatics *27*, 1179–1180.

Karasarides, M., Chiloeches, A., Hayward, R., Niculescu-Duvaz, D., Scanlon, I., Friedlos, F., Ogilvie, L., Hedley, D., Martin, J., Marshall, C.J., et al. (2004). B-RAF is a therapeutic target in melanoma. Oncogene *23*, 6292–6298.

Kholodenko, B.N. (2006). Cell-signalling dynamics in time and space. Nat. Rev. Mol. Cell Biol. *7*, 165–176.

Kholodenko, B.N., Hancock, J.F., and Kolch, W. (2010). Signalling ballet in space and time. Nat. Rev. Mol. Cell Biol. *11*, 414–426.

Kido, K., Sumimoto, H., Asada, S., Okada, S.M., Yaguchi, T., Kawamura, N., Miyagishi, M., Saida, T., and Kawakami, Y. (2009). Simultaneous suppression of MITF and BRAF V600E enhanced inhibition of melanoma cell proliferation. Cancer Sci. *100*, 1863–1869.

Kim, H.J., and Bar-Sagi, D. (2004). Modulation of signalling by Sprouty: a developing story. Nat. Rev. Mol. Cell Biol. *5*, 441–450.

Kimelman, D., and Xu, W. (2006). β-Catenin destruction complex: insights and questions from a structural perspective. Oncogene *25*, 7482–7491.

King, A.J., Sun, H., Diaz, B., Barnard, D., Miao, W., Bagrodia, S., and Marshall, M.S. (1998). The protein kinase Pak3 positively regulates Raf-1 activity through phosphorylation of serine 338. Nature *396*, 180–183.

Koh, J., Enders, G.H., David, Dynlacht, B., and Harlow, E. (1995). Tumour-derived p16 alleles encoding proteins defective in cell-cycle inhibition. Nature *375*, 506–510.

Konieczkowski, D.J., Johannessen, C.M., Abudayyeh, O., Kim, J.W., Cooper, Z.A., Piris, A., Frederick, D.T., Barzily-Rokni, M., Straussman, R., Haq, R., et al. (2014). A Melanoma Cell State Distinction Influences Sensitivity to MAPK Pathway Inhibitors. Cancer Discov. *4*, 816–827.

Kopetz, S., Desai, J., Chan, E., Hecht, J.R., O'Dwyer, P.J., Lee, R.J., Nolop, K.B., and Saltz, L. (2010). PLX4032 in metastatic colorectal cancer patients with mutant BRAF tumors. J. Clin. Oncol. *28:15s*, (suppl;abstr 3534).

Kosugi, S., Hasebe, M., Tomita, M., and Yanagawa, H. (2008). Nuclear Export Signal Consensus Sequences Defined Using a Localization-Based Yeast Selection System. Traffic *9*, 2053–2062.

von Kriegsheim, A., Baiocchi, D., Birtwistle, M., Sumpton, D., Bienvenut, W., Morrice, N., Yamada, K., Lamond, A., Kalna, G., Orton, R., et al. (2009). Cell fate decisions are specified by the dynamic ERK interactome. Nat. Cell Biol. *11*, 1458–1464.

Krimpenfort, P., Quon, K.C., Mooi, W.J., Loonstra, A., and Berns, A. (2001). Loss of p16Ink4a confers susceptibility to metastatic melanoma in mice. Nature *413*, 83–86.

Kubicek, M., Pacher, M., Abraham, D., Podar, K., Eulitz, M., and Baccarini, M. (2002). Dephosphorylation of Ser-259 Regulates Raf-1 Membrane Association. J. Biol. Chem. *277*, 7913–7919.

Kumar, S.M., Dai, J., Li, S., Yang, R., Yu, H., Nathanson, K.L., Liu, S., Zhou, H., Guo, J., and Xu, X. (2014). Human skin neural crest progenitor cells are susceptible to BRAFV600E-induced transformation. Oncogene *33*, 832–841.

Kutay, U., and Güttinger, S. (2005). Leucine-rich nuclear-export signals: born to be weak. Trends Cell Biol. *15*, 121–124.

De La Serna, I.L., Ohkawa, Y., Higashi, C., Dutta, C., Osias, J., Kommajosyula, N., Tachibana, T., and Imbalzano, A.N. (2006). The Microphthalmia-associated Transcription Factor Requires SWI/SNF Enzymes to Activate Melanocyte-specific Genes. J. Biol. Chem. *281*, 20233–20241.

Lai, F., Guo, S.T., Jin, L., Jiang, C.C., Wang, C.Y., Croft, A., Chi, M.N., Tseng, H.-Y., Farrelly, M., Atmadibrata, B., et al. (2013). Cotargeting histone deacetylases and oncogenic BRAF synergistically kills human melanoma cells by necrosis independently of RIPK1 and RIPK3. Cell Death Dis. *4*, e655.

Lang, D., Lu, M.M., Huang, L., Engleka, K.A., Zhang, M., Chu, E.Y., Lipner, S., Skoultchi, A., Millar, S.E., and Epstein, J.A. (2005). Pax3 functions at a nodal point in melanocyte stem cell differentiation. Nature *433*, 884–887.

Larkin, J., Ascierto, P.A., Dréno, B., Atkinson, V., Liszkay, G., Maio, M., Mandalà, M., Demidov, L., Stroyakovskiy, D., Thomas, L., et al. (2014). Combined Vemurafenib and Cobimetinib in BRAF-Mutated Melanoma. N. Engl. J. Med. *371*, 1867–1876.

Larkin, J., Chiarion-Sileni, V., Gonzalez, R., Grob, J.J., Cowey, C.L., Lao, C.D., Schadendorf, D., Dummer, R., Smylie, M., Rutkowski, P., et al. (2015). Combined Nivolumab and Ipilimumab or Monotherapy in Untreated Melanoma. N. Engl. J. Med. *373*, 23–34.

Lavoie, H., and Therrien, M. (2015). Regulation of RAF protein kinases in ERK signalling. Nat. Rev. Mol. Cell Biol. *16*, 281–298.

Lavoie, H., Thevakumaran, N., Gavory, G., Li, J.J., Padeganeh, A., Guiral, S., Duchaine, J., Mao, D.Y.L., Bouvier, M., Sicheri, F., et al. (2013). Inhibitors that stabilize a closed RAF kinase domain conformation induce dimerization. Nat. Chem. Biol. *9*, 428–436.

Lee, H.-W., Ahn, D.-H., Crawley, S.C., Li, J.-D., Gum Jr., J.R., Basbaum, C.B., Fan, N.Q., Szymkowski, D.E., Han, S.-Y., Lee, B.H., et al. (2002). Phorbol 12-Myristate 13-Acetate Up-regulates the Transcription of MUC2 Intestinal Mucin via Ras, ERK, and NF-kappa B. J. Biol. Chem. *277*, 32624–32631.

Lee, M., Goodall, J., Verastegui, C., Ballotti, R., and Goding, C.R. (2000). Direct Regulation of the Microphthalmia Promoter by Sox10 Links Waardenburg-Shah Syndrome (WS4)-associated Hypopigmentation and Deafness to WS2. J. Biol. Chem. *275*, 37978–37983.

Levy, C., Sonnenblick, A., and Razin, E. (2003). Role Played by Microphthalmia Transcription Factor Phosphorylation and Its Zip Domain in Its Transcriptional Inhibition by PIAS3. Mol. Cell. Biol. *23*, 9073–9080.

Levy, C., Khaled, M., and Fisher, D.E. (2006). MITF: master regulator of melanocyte development and melanoma oncogene. Trends Mol. Med. *12*, 406–414.

Levy, C., Khaled, M., Iliopoulos, D., Janas, M.M., Schubert, S., Pinner, S., Chen, P.-H., Li, S., Fletcher, A.L., Yokoyama, S., et al. (2010). Intronic miR-211 Assumes the Tumor Suppressive Function of Its Host Gene in Melanoma. Mol. Cell *40*, 841–849.

Li, M., Luo, J., Brooks, C.L., and Gu, W. (2002). Acetylation of p53 Inhibits Its Ubiquitination by Mdm2. J. Biol. Chem. *277*, 50607–50611.

Li, X., Huang, Y., Jiang, J., and Frank, S.J. (2008). ERK-dependent threonine phosphorylation of EGF receptor modulates receptor downregulation and signaling. Cell. Signal. *20*, 2145–2155.

Li, X.-H., Kishore, A.H., Dao, D., Zheng, W., Roman, C.A., and Word, R.A. (2010). A Novel Isoform of Microphthalmia-Associated Transcription Factor Inhibits IL-8 Gene Expression in Human Cervical Stromal Cells. Mol. Endocrinol. *24*, 1512–1528.

Lin, Y.W., and Yang, J.L. (2006). Cooperation of ERK and SCFSkp2 for MKP-1 Destruction Provides a Positive Feedback Regulation of Proliferating Signaling. J. Biol. Chem. *281*, 915–926.

Lin, W.M., Luo, S., Muzikansky, A., Lobo, A.Z.C., Tanabe, K.K., Sober, A.J.,

Cosimi, A.B., Tsao, H., and Duncan, L.M. (2015). Outcome of patients with de novo versus nevus-associated melanoma. J. Am. Acad. Dermatol. *72*, 54–58.

Lin, Y.W., Chuang, S.M., and Yang, J.L. (2003). ERK1/2 Achieves Sustained Activation by Stimulating MAPK Phosphatase-1 Degradation via the Ubiquitin-Proteasome Pathway. J. Biol. Chem. *278*, 21534–21541.

Lindon, C., Montarras, D., and Pinset, C. (1998). Cell Cycle-regulated Expression of the Muscle Determination Factor Myf5 in Proliferating Myoblasts. J. Cell Biol. *140*, 111–118.

Lister, J.A., Robertson, C.P., Lepage, T., Johnson, S.L., and Raible, D.W. (1999). nacre encodes a zebrafish microphthalmia-related protein that regulates neural-crest-derived pigment cell fate. Development *126*, 3757–3767.

Lister, J.A., Capper, A., Zeng, Z., Mathers, M.E., Richardson, J., Paranthaman, K., Jackson, I.J., and Patton, E.E. (2014). A Conditional Zebrafish MITF Mutation Reveals MITF Levels Are Critical for Melanoma Promotion vs. Regression In Vivo. J. Invest. Dermatol. *134*, 133–140.

Lito, P., Pratilas, C.A., Joseph, E.W., Tadi, M., Halilovic, E., Zubrowski, M., Huang, A., Wong, W.L., Callahan, M.K., Merghoub, T., et al. (2012). Relief of Profound Feedback Inhibition of Mitogenic Signaling by RAF Inhibitors Attenuates Their Activity in BRAFV600E Melanomas. Cancer Cell *22*, 668–682.

Lito, P., Rosen, N., and Solit, D.B. (2013). Tumor adaptation and resistance to RAF inhibitors. Nat. Med. *19*, 1401–1409.

Liu, P., Cheng, H., Roberts, T.M., and Zhao, J.J. (2009). Targeting the phosphoinositide 3-kinase pathway in cancer. Nat. Rev. Drug Discov. *8*, 627–644.

Livak, K.J., and Schmittgen, T.D. (2001). Analysis of Relative Gene Expression Data Using Real-Time Quantitative PCR and the 2−ΔΔCT Method. Methods *25*, 402–408.

Lodish, H., Berk, A., Zipursky, S.L., Matsudaira, P., Baltimore, D., and Darnell, J. (2000). Molecular Cell Biology (W. H. Freeman).

Loercher, A.E., Tank, E.M.H., Delston, R.B., and Harbour, J.W. (2005). MITF links differentiation with cell cycle arrest in melanocytes by transcriptional activation of INK4A. J. Cell Biol. *168*, 35–40.

Long, G. V., Menzies, A.M., Nagrial, A.M., Haydu, L.E., Hamilton, A.L., Mann, G.J., Hughes, T.M., Thompson, J.F., Scolyer, R.A., and Kefford, R.F. (2011). Prognostic and Clinicopathologic Associations of Oncogenic BRAF in Metastatic Melanoma. J. Clin. Oncol. *29*, 1239–1246.

Long, G. V., Stroyakovskiy, D., Gogas, H., Levchenko, E., de Braud, F., Larkin, J., Garbe, C., Jouary, T., Hauschild, A., Grob, J.J., et al. (2014). Combined BRAF and MEK Inhibition versus BRAF Inhibition Alone in Melanoma. N. Engl. J. Med. *371*, 1877–1888.

Lu, K.K., Bazarov, A. V., Yoon, L.S., and Sedivy, J.M. (1998). Isolation of

Temperature-sensitive Mutations in the c-raf-1 Catalytic Domain and Expression of Conditionally Active and Dominant-defective Forms of Raf-1 in Cultured Mammalian Cells. Cell Growth Differ. *9*, 367–380.

Lu, S.-Y., Li, M., and Lin, Y.-L. (2010). Mitf Induction by RANKL Is Critical for Osteoclastogenesis. Mol. Biol. Cell *21*, 1763–1771.

Luo, Z., Tzivion, G., Belshaw, P.J., Vavvas, D., Marshall, M., and Avruch, J. (1996). Oligomerization activates c-Raf-1 through a Ras-dependent mechanism. Nature *383*, 181–185.

Luttrell, L.M. (2005). Composition and Function of G Protein-Coupled Receptor Signalsomes Controlling Mitogen-Activated Protein Kinase Activity. J. Mol. Neurosci. *26*, 253–264.

MacKie, R.M., Hauschild, A., and Eggermont, A.M.M. (2009). Epidemiology of invasive cutaneous melanoma. Ann. Oncol. *20*, vi1–vi7.

MacNicol, M.C., Muslin, A.J., and MacNicol, A.M. (2000). Disruption of the 14-3-3 Binding Site within the B-Raf Kinase Domain Uncouples Catalytic Activity from PC12 Cell Differentiation. J. Biol. Chem. *275*, 3803–3809.

Maehama, T., and Dixon, J.E. (1998). The Tumor Suppressor, PTEN/MMAC1, Dephosphorylates the Lipid Second Messenger, Phosphatidylinositol 3,4,5-Trisphosphate. J. Biol. Chem. *273*, 13375–13378.

Maertens, O., Johnson, B., Hollstein, P., Frederick, D.T., Cooper, Z.A., Messiaen, L., Bronson, R.T., McMahon, M., Granter, S., Flaherty, K., et al. (2013). Elucidating Distinct Roles for NF1 in Melanomagenesis. Cancer Discov. *3*, 338–349.

de Magalhães, J.P. (2013). How ageing processes influence cancer. Nat. Rev. Cancer *13*, 357–365.

Mahoney, K.M., Rennert, P.D., and Freeman, G.J. (2015). Combination cancer immunotherapy and new immunomodulatory targets. Nat. Rev. Drug Discov. *14*, 561–584.

Mammoto, A., Huang, S., Moore, K., Oh, P., and Ingber, D.E. (2004). Role of RhoA, mDia, and ROCK in Cell Shape-dependent Control of the Skp2-p27kip1 Pathway and the G1/S Transition. J. Biol. Chem. *279*, 26323–26330.

Mansky, K.C., Sankar, U., Han, J., and Ostrowski, M.C. (2002). Microphthalmia Transcription Factor Is a Target of the p38 MAPK Pathway in Response to Receptor Activator of NF-κB Ligand Signaling. J. Biol. Chem. *277*, 11077–11083.

Mansour, S.J., Matten, W.T., Hermann, A.S., Candia, J.M., Rong, S., Fukasawa, K., Vande Woude, G.F., and Ahn, N.G. (1994). Transformation of Mammalian Cells by Constitutively Active MAP Kinase Kinase. Science (80-.). *265*, 966–970.

Marais, R., Light, Y., Paterson, H.F., and Marshall, C.J. (1995). Ras recruits Raf-1 to the plasma membrane for activation by tyrosine phosphorylation. EMBO J. *14*, 3136–3145.

Marais, R., Light, Y., Paterson, H.F., Mason, C.S., and Marshall, C.J. (1997). Differential Regulation of Raf-1, A-Raf, and B-Raf by Oncogenic Ras and Tyrosine Kinases. J. Biol. Chem. *272*, 4378–4383.

Marchand, B., Arsenault, D., Raymond-Fleury, A., Boisvert, F.-M., and Boucher, M.-J. (2015). Glycogen Synthase Kinase-3 (GSK3) Inhibition Induces Prosurvival Autophagic Signals in Human Pancreatic Cancer Cells. J. Biol. Chem. *290*, 5592–5605.

Marin, O., Meggio, F., Marchiori, F., Borin, G., and Pinna, L.A. (1986). Site specificity of casein kinase-2 (TS) from rat liver cytosol. A study with model peptide substrates. Eur. J. Biochem. *160*, 239–244.

Marshall, C.. (1995). Specificity of receptor tyrosine kinase signaling: Transient versus sustained extracellular signal-regulated kinase activation. Cell *80*, 179–185.

Martínez-Balbás, M.A., Dey, A., Rabindran, S.K., Ozato, K., and Wu, C. (1995). Displacement of sequence-specific transcription factors from mitotic chromatin. Cell *83*, 29–38.

Marusyk, A., Almendro, V., and Polyak, K. (2012). Intra-tumour heterogeneity: a looking glass for cancer? Nat. Rev. Cancer *12*, 323–334.

Mason, C.S., Springer, C.J., Cooper, R.G., Superti-Furga, G., Marshall, C.J., and Marais, R. (1999). Serine and tyrosine phosphorylations cooperate in Raf-1, but not B-Raf activation. EMBO J. *18*, 2137–2148.

Matallanas, D., Birtwistle, M., Romano, D., Zebisch, A., Rauch, J., von Kriegsheim, A., and Kolch, W. (2011). Raf Family Kinases: Old Dogs Have Learned New Tricks. Genes Cancer *2*, 232–260.

Mazar, J., DeYoung, K., Khaitan, D., Meister, E., Almodovar, A., Goydos, J., Ray, A., and Perera, R.J. (2010). The Regulation of miRNA-211 Expression and Its Role in Melanoma Cell Invasiveness. PLoS One *5*, e13779.

McArthur, G.A., Chapman, P.B., Robert, C., Larkin, J., Haanen, J.B., Dummer, R., Ribas, A., Hogg, D., Hamid, O., Ascierto, P.A., et al. (2014). Safety and efficacy of vemurafenib in BRAFV600E and BRAFV600K mutation-positive melanoma (BRIM-3): extended follow-up of a phase 3, randomised, open-label study. Lancet Oncol. *15*, 323–332.

McGill, G.G., Horstmann, M., Widlund, H.R., Du, J., Motyckova, G., Nishimura, E.K., Lin, Y.-L., Ramaswamy, S., Avery, W., Ding, H.-F., et al. (2002). Bcl2 Regulation by the Melanocyte Master Regulator Mitf Modulates Lineage Survival and Melanoma Cell Viability. Cell *109*, 707–718.

McGill, G.G., Haq, R., Nishimura, E.K., and Fisher, D.E. (2006). c-Met Expression Is Regulated by Mitf in the Melanocyte Lineage. J. Biol. Chem. *281*, 10365–10373.

McKay, M.M., Ritt, D.A., and Morrison, D.K. (2009). Signaling dynamics of the KSR1 scaffold complex. Proc. Natl. Acad. Sci. *106*, 11022–11027.

Meacham, C.E., and Morrison, S.J. (2013). Tumour heterogeneity and cancer cell plasticity. Nature *501*, 328–337.

Meijer, L., Skaltsounis, A.-L., Magiatis, P., Polychronopoulos, P., Knockaert, M., Leost, M., Ryan, X.P., Vonica, C.A., Brivanlou, A., Dajani, R., et al. (2003). GSK-3-Selective Inhibitors Derived from Tyrian Purple Indirubins. Chem. Biol. *10*, 1255–1266.

Mhawech, P. (2005). 14-3-3 proteins—an update. Cell Res. *15*, 228–236.

Michaloglou, C., Vredeveld, L.C.W., Soengas, M.S., Denoyelle, C., Kuilman, T., van der Horst, C.M.A.M., Majoor, D.M., Shay, J.W., Mooi, W.J., and Peeper, D.S. (2005). BRAFE600-associated senescence-like cell cycle arrest of human naevi. Nature *436*, 720–724.

Michaloglou, C., Vredeveld, L.C.W., Mooi, W.J., and Peeper, D.S. (2008). BRAFE600 in benign and malignant human tumours. Oncogene *27*, 877–895.

Michaud, N.R., Fabian, J.R., Mathes, K.D., and Morrison, D.K. (1995). 14-3-3 Is Not Essential for Raf-1 Function: Identification of Raf-1 Proteins That Are Biologically Activated in a 14-3-3- and Ras-Independent Manner. Mol. Cell. Biol. *15*, 3390–3397.

Miller, A.J., and Mihm, M.C. (2006). Melanoma. N. Engl. J. Med. *355*, 51–65.

Miller, A.J., Levy, C., Davis, I.J., Razin, E., and Fisher, D.E. (2005). Sumoylation of MITF and Its Related Family Members TFE3 and TFEB. J. Biol. Chem. *280*, 146–155.

Mischak, H., Seitz, T., Janosch, P., Eulitz, M., Steen, H., Schellerer, M., Philipp, A., and Kolch, W. (1996). Negative Regulation of Raf-1 by Phosphorylation of Serine 621. Mol. Cell. Biol. *16*, 5409–5418.

Mittal, R., Peak-Chew, S.-Y., and McMahon, H.T. (2006). Acetylation of MEK2 and IκB kinase (IKK) activation loop residues by YopJ inhibits signaling. Proc. Natl. Acad. Sci. *103*, 18574–18579.

Montagut, C., Sharma, S. V., Shioda, T., McDermott, U., Ulman, M., Ulkus, L.E., Dias-Santagata, D., Stubbs, H., Lee, D.Y., Singh, A., et al. (2008). Elevated CRAF as a Potential Mechanism of Acquired Resistance to BRAF Inhibition in Melanoma. Cancer Res. *68*, 4853–4861.

Moore, K.J. (1995). Insight into the microphthalmia gene. Trends Genet. *11*, 442–448.

Morrison, D.K., Heidecker, G., Rapp, U.R., and Copeland, T.D. (1993). Identification of the major phosphorylation sites of the Raf-1 kinase. J. Biol. Chem. *268*, 17309–17316.

Mort, R.L., Jackson, I.J., and Patton, E.E. (2015). The melanocyte lineage in development and disease. Development *142*, 620–632.

Mukherjee, S., Keitany, G., Li, Y., Wang, Y., Ball, H.L., Goldsmith, E.J., and Orth, K. (2006). Yersinia YopJ Acetylates and Inhibits Kinase Activation by Blocking Phosphorylation. Science (80-.). *312*, 1211–1214.

Mukherjee, S., Hao, Y.-H., and Orth, K. (2007). A newly discovered post-translational modification – the acetylation of serine and threonine residues. Trends Biochem. Sci. *32*, 210–216.

Müller, J., Krijgsman, O., Tsoi, J., Robert, L., Hugo, W., Song, C., Kong, X., Possik, P.A., Cornelissen-Steijger, P.D.M., Foppen, M.H.G., et al. (2014). Low MITF/AXL ratio predicts early resistance to multiple targeted drugs in melanoma. Nat. Commun. *5*, 5712.

Murakami, H., and Arnheiter, H. (2005). Sumoylation modulates transcriptional activity of MITF in a promoter-specific manner. Pigment Cell Res. *18*, 265–277.

Muslin, A.J., Tanner, J.W., Allen, P.M., and Shaw, A.S. (1996). Interaction of 14-3-3 with Signaling Proteins Is Mediated by the Recognition of Phosphoserine. Cell *84*, 889–897.

Muzny, D.M., Bainbridge, M.N., Chang, K., Dinh, H.H., Drummond, J.A., Fowler, G., Kovar, C.L., Lewis, L.R., Morgan, M.B., Newsham, I.F., et al. (2012). Comprehensive molecular characterization of human colon and rectal cancer. Nature *487*, 330–337.

Nan, X., Collisson, E. a, Lewis, S., Huang, J., Tamguney, T.M., Liphardt, J.T., McCormick, F., Gray, J.W., and Chu, S. (2013). Single-molecule superresolution imaging allows quantitative analysis of RAF multimer formation and signaling. Proc. Natl. Acad. Sci. *110*, 18519–18524.

Nazarian, R., Shi, H., Wang, Q., Kong, X., Koya, R.C., Lee, H., Chen, Z., Lee, M.-K., Attar, N., Sazegar, H., et al. (2010). Melanomas acquire resistance to B-RAF(V600E) inhibition by RTK or N-RAS upregulation. Nature *468*, 973–977.

Nevins, J.R., Chellappan, S.P., Mudryj, M., Hiebert, S., Devoto, S., Horowitz, J., Hunter, T., and Pines, J. (1991). E2F Transcription Factor Is a Target for the RB Protein and the Cyclin A Protein. Cold Spring Harb. Symp. Quant. Biol. *56*, 157–162.

Nguyen, T.T., Scimecas, J.-C., Filloux, C., Peraldi, P., Carpentiern, J.-L., and Van Obberghen, E. (1993). Co-regulation of the Mitogen-activated Protein Kinase, Extracellular Signal-regulated Kinase 1, and the 90-kDa Ribosomal S6 Kinase in PC12 Cells. Distinct Effects of the Neurotrophic Factor, Nerve Growth Factor, and the Mitogenic Factor, Epidermal Growth. J. Biol. Chem. *268*, 9803–9810.

Nishimura, E.K., Granter, S.R., and Fisher, D.E. (2005). Mechanisms of Hair Graying: Incomplete Melanocyte Stem Cell Maintenance in the Niche. Science (80-.). *307*, 720–724.

Noble, C., Mercer, K., Hussain, J., Carragher, L., Giblett, S., Hayward, R., Patterson, C., Marais, R., and Pritchard, C.A. (2008). CRAF Autophosphorylation of Serine 621 Is Required to Prevent Its Proteasome-Mediated Degradation. Mol. Cell *31*, 862–872.

Norris, K.L., Lee, J.-Y., and Yao, T.-P. (2009). Acetylation Goes Global: The Emergence of Acetylation Biology. Sci. Signal. *2*, pe76–pe76.

Nusse, R. (2008). Wnt signaling and stem cell control. Cell Res. *18*, 523–527.

Oberholzer, P.A., Kee, D., Dziunycz, P., Sucker, A., Kamsukom, N., Jones, R., Roden, C., Chalk, C.J., Ardlie, K., Palescandolo, E., et al. (2012). RAS Mutations Are Associated With the Development of Cutaneous Squamous Cell Tumors in Patients Treated With RAF Inhibitors. J. Clin. Oncol. *30*, 316–321.

Ogryzko, V. V., Schiltz, R.L., Russanova, V., Howard, B.H., and Nakatani, Y. (1996). The Transcriptional Coactivators p300 and CBP Are Histone Acetyltransferases. Cell *87*, 953–959.

Olsen, J. V., Blagoev, B., Gnad, F., Macek, B., Kumar, C., Mortensen, P., and Mann,

M. (2006). Global, In Vivo, and Site-Specific Phosphorylation Dynamics in Signaling Networks. Cell *127*, 635–648.

Opdecamp, K., Nakayama, A., Nguyen, M.-T.T., Hodgkinson, C.A., Pavan, W.J., and Arnheiter1, and H. (1997). Melanocyte development in vivo and in neural crest cell cultures: crucial dependence on the Mitf basic-helix-loop-helix-zipper transcription factor. Development *124*, 2377–2386.

Ozaki, K., Kadomoto, R., Asato, K., Tanimura, S., Itoh, N., and Kohno, M. (2001). ERK Pathway Positively Regulates the Expression of Sprouty Genes. Biochem. Biophys. Res. Commun. *285*, 1084–1088.

Parr, C., Carzaniga, R., Gentleman, S.M., Van Leuven, F., Walter, J., and Sastre, M. (2012). Glycogen Synthase Kinase 3 Inhibition Promotes Lysosomal Biogenesis and Autophagic Degradation of the Amyloid- Precursor Protein. Mol. Cell. Biol. *32*, 4410–4418.

Patton, E.E., Widlund, H.R., Kutok, J.L., Kopani, K.R., Amatruda, J.F., Murphey, R.D., Berghmans, S., Mayhall, E.A., Traver, D., Fletcher, C.D.M., et al. (2005). BRAF Mutations Are Sufficient to Promote Nevi Formation and Cooperate with p53 in the Genesis of Melanoma. Curr. Biol. *15*, 249–254.

Payne, D.M., Rossomando, A.J., Martino, P., Erickson, A.K., Her, J.-H., Shabanowitz, J., Hunt, D.F., Weber, M.J., and Sturgill, T.W. (1991). Identification of the regulatory phosphorylation sites in pp42/mitogen-activated protein kinase (MAP kinase). EMBO J. *10*, 885–892.

del Peso, L., González-García, M., Page, C., Herrera, R., and Nuñez, G. (1997). Interleukin-3-Induced Phosphorylation of BAD Through the Protein Kinase Akt. Science (80-.). *278*, 687–689.

Petti, C., Molla, A., Vegetti, C., Ferrone, S., Anichini, A., and Sensi, M. (2006). Coexpression of NRASQ61R and BRAFV600E in Human Melanoma Cells Activates Senescence and Increases Susceptibility to Cell-Mediated Cytotoxicity. Cancer Res. *66*, 6503–6511.

Pierrat, M.J., Marsaud, V., Mauviel, A., and Javelaud, D. (2012). Expression of Microphthalmia-associated Transcription Factor (MITF), Which Is Critical for Melanoma Progression, Is Inhibited by Both Transcription Factor GLI2 and Transforming Growth Factor-β. J. Biol. Chem. *287*, 17996–18004.

Pines, J., and Hunter, T. (1989). Isolation of a human cyclin cDNA: Evidence for cyclin mRNA and protein regulation in the cell cycle and for interaction with p34cdc2. Cell *58*, 833–846.

Pinna, L.A., and Ruzzene, M. (1996). How do protein kinases recognize their substrates? Biochim. Biophys. Acta - Mol. Cell Res. *1314*, 191–225.

Platz, A., Egyhazi, S., Ringborg, U., and Hansson, J. (2008). Human cutaneous melanoma; a review of NRAS and BRAF mutation frequencies in relation to histogenetic subclass and body site. Mol. Oncol. *1*, 395–405.

Ploper, D., Taelman, V.F., Robert, L., Perez, B.S., Titz, B., Chen, H.-W., Graeber,

T.G., von Euw, E., Ribas, A., and De Robertis, E.M. (2015). MITF drives endolysosomal biogenesis and potentiates Wnt signaling in melanoma cells. Proc. Natl. Acad. Sci. *112*, E420–E429.

Pogenberg, V., Ögmundsdóttir, M.H., Bergsteinsdóttir, K., Schepsky, A., Phung, B., Deineko, V., Milewski, M., Steingrímsson, E., and Wilmanns, M. (2012). Restricted leucine zipper dimerization and specificity of DNA recognition of the melanocyte master regulator MITF. Genes Dev. *26*, 2647–2658.

Pollock, P.M., Harper, U.L., Hansen, K.S., Yudt, L.M., Stark, M., Robbins, C.M., Moses, T.Y., Hostetter, G., Wagner, U., Kakareka, J., et al. (2002). High frequency of BRAF mutations in nevi. Nat. Genet. *33*, 19–20.

Polyak, K., Kato, J., Solomon, M.J., Sherr, C.J., Massague, J., Roberts, J.M., and Koff, A. (1994). p27Kip1, a cyclin-Cdk inhibitor, links transforming growth factor-beta and contact inhibition to cell cycle arrest. Genes Dev. *8*, 9–22.

Pomerantz, J., Schreiber-Agus, N., Liégeois, N.J., Silverman, A., Alland, L., Chin, L., Potes, J., Chen, K., Orlow, I., Lee, H.-W., et al. (1998). The Ink4a Tumor Suppressor Gene Product, p19Arf, Interacts with MDM2 and Neutralizes MDM2's Inhibition of p53. Cell *92*, 713–723.

Postow, M.A., Chesney, J., Pavlick, A.C., Robert, C., Grossmann, K., McDermott, D., Linette, G.P., Meyer, N., Giguere, J.K., Agarwala, S.S., et al. (2015). Nivolumab and Ipilimumab versus Ipilimumab in Untreated Melanoma. N. Engl. J. Med. *372*, 2006–2017.

Potterf, S.B., Furumura, M., Dunn, K.J., Arnheiter, H., and Pavan, W.J. (2000). Transcription factor hierarchy in Waardenburg syndrome: regulation of MITF expression by SOX10 and PAX3. Hum. Genet. *107*, 1–6.

Poulikakos, P.I., Zhang, C., Bollag, G., Shokat, K.M., and Rosen, N. (2010). RAF inhibitors transactivate RAF dimers and ERK signalling in cells with wild-type BRAF. Nature *464*, 427–430.

Poulikakos, P.I., Persaud, Y., Janakiraman, M., Kong, X., Ng, C., Moriceau, G., Shi, H., Atefi, M., Titz, B., Gabay, M.T., et al. (2011). RAF inhibitor resistance is mediated by dimerization of aberrantly spliced BRAF(V600E). Nature *480*, 387–390.

Prahallad, A., Sun, C., Huang, S., Di Nicolantonio, F., Salazar, R., Zecchin, D., Beijersbergen, R.L., Bardelli, A., and Bernards, R. (2012). Unresponsiveness of colon cancer to BRAF(V600E) inhibition through feedback activation of EGFR. Nature *483*, 100–103.

Pratilas, C.A., Taylor, B.S., Ye, Q., Viale, A., Sander, C., Solit, D.B., and Rosen, N. (2009). V600EBRAF is associated with disabled feedback inhibition of RAF-MEK signaling and elevated transcriptional output of the pathway. Proc. Natl. Acad. Sci. *106*, 4519–4524.

Price, E.R., Horstmann, M.A., Wells, A.G., Weilbaecher, K.N., Takemoto, C.M., Landis, M.W., and Fisher, D.E. (1998). α-Melanocyte-stimulating Hormone Signaling Regulates Expression of microphthalmia, a Gene Deficient in Waardenburg Syndrome. J. Biol. Chem. *273*, 33042–33047.

Prior, I.A., Lewis, P.D., and Mattos, C. (2012). A Comprehensive Survey of Ras Mutations in Cancer. Cancer Res. *72*, 2457–2467.

Pylayeva-Gupta, Y., Grabocka, E., and Bar-Sagi, D. (2011). RAS oncogenes: weaving a tumorigenic web. Nat. Rev. Cancer *11*, 761–774.

Quintana, E., Shackleton, M., Foster, H.R., Fullen, D.R., Sabel, M.S., Johnson, T.M., and Morrison, S.J. (2010). Phenotypic Heterogeneity among Tumorigenic Melanoma Cells from Patients that Is Reversible and Not Hierarchically Organized. Cancer Cell *18*, 510–523.

Rabbani, P., Takeo, M., Chou, W., Myung, P., Bosenberg, M., Chin, L., Taketo, M.M., and Ito, M. (2011). Coordinated Activation of Wnt in Epithelial and Melanocyte Stem Cells Initiates Pigmented Hair Regeneration. Cell *145*, 941–955.

Rajakulendran, T., Sahmi, M., Lefrançois, M., Sicheri, F., and Therrien, M. (2009). A dimerization-dependent mechanism drives RAF catalytic activation. Nature *461*, 542–545.

Rebocho, A.P., and Marais, R. (2013). ARAF acts as a scaffold to stabilize BRAF:CRAF heterodimers. Oncogene *32*, 3207–3212.

Reya, T., and Clevers, H. (2005). Wnt signalling in stem cells and cancer. Nature *434*, 843–850.

Richon, V.M., Emiliani, S., Verdin, E., Webb, Y., Breslow, R., Rifkind, R.A., and Marks, P.A. (1998). A class of hybrid polar inducers of transformed cell differentiation inhibits histone deacetylases. Proc. Natl. Acad. Sci. *95*, 3003–3007.

Ritt, D.A., Zhou, M., Conrads, T.P., Veenstra, T.D., Copeland, T.D., and Morrison, D.K. (2007). CK2 Is a Component of the KSR1 Scaffold Complex that Contributes to Raf Kinase Activation. Curr. Biol. *17*, 179–184.

Robert, C., Thomas, L., Bondarenko, I., O'Day, S., Weber, J., Garbe, C., Lebbe, C., Baurain, J.-F., Testori, A., Grob, J.-J., et al. (2011). Ipilimumab plus Dacarbazine for Previously Untreated Metastatic Melanoma. N. Engl. J. Med. *364*, 2517–2526.

Robert, C., Karaszewska, B., Schachter, J., Rutkowski, P., Mackiewicz, A., Stroiakovski, D., Lichinitser, M., Dummer, R., Grange, F., Mortier, L., et al. (2015). Improved Overall Survival in Melanoma with Combined Dabrafenib and Trametinib. N. Engl. J. Med. *372*, 30–39.

Robertson, G.P., Furnari, F.B., Miele, M.E., Glendening, M.J., Welch, D.R., Fountain, J.W., Lugo, T.G., Huang, H.-J.S., and Cavenee, W.K. (1998). In vitro loss of heterozygosity targets the PTEN/MMAC1 gene in melanoma. Proc. Natl. Acad. Sci. *95*, 9418–9423.

Roesch, A. (2015). Tumor heterogeneity and plasticity as elusive drivers for resistance to MAPK pathway inhibition in melanoma. Oncogene *34*, 2951–2957.

Rogers, H.W., Weinstock, M.A., Harris, A.R., Hinckley, M.R., Feldman, S.R., Fleischer, A.B., and Coldiron, B.M. (2010). Incidence Estimate of Nonmelanoma Skin Cancer in the United States, 2006. Arch. Dermatol. *146*, 283–287.

Rommel, C., Radziwill, G., Lovrić, J., Noeldeke, J., Heinicke, T., Jones, D., Aitken, A., and Moelling, K. (1996). Activated Ras displaces 14-3-3 protein from the amino terminus of c-Raf-1. Oncogene *12*, 609–619.

Röring, M., Herr, R., Fiala, G.J., Heilmann, K., Braun, S., Eisenhardt, A.E., Halbach, S., Capper, D., von Deimling, A., Schamel, W.W., et al. (2012). Distinct requirement

for an intact dimer interface in wild-type, V600E and kinase-dead B-Raf signalling. EMBO J. *31*, 2629–2647.

Rosenblatt, J., Gu, Y., and Morgan, D.O. (1992). Human cyclin-dependent kinase 2 is activated during the S and G2 phases of the cell cycle and associates with cyclin A. Proc. Natl. Acad. Sci. *89*, 2824–2828.

Roskoski, R. (2010). RAF protein-serine/threonine kinases: Structure and regulation. Biochem. Biophys. Res. Commun. *399*, 313–317.

Rotolo, S., Diotti, R., Gordon, R.E., Qiao, R.F., Yao, Z., Phelps, R.G., and Dong, J. (2005). Effects on proliferation and melanogenesis by inhibition of mutantBRAF and expression of wild-typeINK4A in melanoma cells. Int. J. Cancer *115*, 164–169.

Roy, F., Laberge, G., Douziech, M., Ferland-McCollough, D., and Therrien, M. (2002). KSR is a scaffold required for activation of the ERK/MAPK module. Genes Dev. *16*, 427–438.

Rudner, A.D., and Murray, A.W. (2000). Phosphorylation by Cdc28 Activates the Cdc20-dependent Activity of the Anaphase-promoting Complex. J. Cell Biol. *149*, 1377–1390.

Rushworth, L.K., Hindley, A.D., O'Neill, E., and Kolch, W. (2006). Regulation and Role of Raf-1/B-Raf Heterodimerization. Mol. Cell. Biol. *26*, 2262–2272.

Sabo, A., Lusic, M., Cereseto, A., and Giacca, M. (2008). Acetylation of Conserved Lysines in the Catalytic Core of Cyclin-Dependent Kinase 9 Inhibits Kinase Activity and Regulates Transcription. Mol. Cell. Biol. *28*, 2201–2212.

Saha, B., Singh, S.K., Sarkar, C., Bera, R., Ratha, J., Tobin, D.J., and Bhadra, R. (2006). Activation of the Mitf promoter by lipid-stimulated activation of p38-stress signalling to CREB. Pigment Cell Res. *19*, 595–605.

Saito, H., Yasumoto, K.I., Takeda, K., Takahashi, K., Fukuzaki, A., Orikasa, S., and Shibahara, S. (2002). Melanocyte-specific Microphthalmia-associated Transcription Factor Isoform Activates Its Own Gene Promoter through Physical Interaction with Lymphoid-enhancing Factor 1. J. Biol. Chem. *277*, 28787–28794.

Sang, N., Stiehl, D.P., Bohensky, J., Leshchinsky, I., Srinivas, V., and Caro, J. (2003). MAPK Signaling Up-regulates the Activity of Hypoxia-inducible Factors by Its Effects on p300. J. Biol. Chem. *278*, 14013–14019.

Santos, S.D.M., Verveer, P.J., and Bastiaens, P.I.H. (2007). Growth factor-induced MAPK network topology shapes Erk response determining PC-12 cell fate. Nat. Cell Biol. *9*, 324–330.

Sasaki, A., Taketomi, T., Kato, R., Saeki, K., Nonami, A., Sasaki, M., Kuriyama, M., Saito, N., Shibuya, M., and Yoshimura, A. (2003). Mammalian Sprouty4 Suppresses Ras-Independent ERK Activation by Binding to Raf1. Cell Cycle *2*, 280–281.

Schadendorf, D., Fisher, D.E., Garbe, C., Gershenwald, J.E., Grob, J.-J., Halpern, A., Herlyn, M., Marchetti, M.A., McArthur, G., Ribas, A., et al. (2015). Melanoma. Nat. Rev. Dis. Prim. 15003.

Schepsky, A., Bruser, K., Gunnarsson, G.J., Goodall, J., Hallsson, J.H., Goding, C.R.,

Steingrimsson, E., and Hecht, A. (2006). The Microphthalmia-Associated Transcription Factor Mitf Interacts with β-Catenin To Determine Target Gene Expression. Mol. Cell. Biol. *26*, 8914–8927.

Selzer, E., Wacheck, V., Lucas, T., Heere-Ress, E., Wu, M., Weilbaecher, K.N., Schlegel, W., Valent, P., Wrba, F., Pehamberger, H., et al. (2002). The Melanocyte-specific Isoform of the Microphthalmia Transcription Factor Affects the Phenotype of Human Melanoma. Cancer Res. *62*, 2098–2103.

Serrano, M., Hannon, G.J., and Beach, D. (1993). A new regulatory motif in cell-cycle control causing specific inhibition of cyclin D/CDK4. Nature *366*, 704–707.

Settembre, C., Di Malta, C., Polito, V.A., Arencibia, M.G., Vetrini, F., Erdin, S., Erdin, S.U., Huynh, T., Medina, D., Colella, P., et al. (2011). TFEB Links Autophagy to Lysosomal Biogenesis. Science (80-.). *332*, 1429–1433.

Settembre, C., Zoncu, R., Medina, D.L., Vetrini, F., Erdin, S., Erdin, S., Huynh, T., Ferron, M., Karsenty, G., Vellard, M.C., et al. (2012). A lysosome-to-nucleus signalling mechanism senses and regulates the lysosome via mTOR and TFEB. EMBO J. *31*, 1095–1108.

Sharpless, N.E., Bardeesy, N., Lee, K.-H., Carrasco, D., Castrillon, D.H., Aguirre, A.J., Wu, E.A., Horner, J.W., and DePinho, R.A. (2001). Loss of p16Ink4a with retention of p19Arf predisposes mice to tumorigenesis. Nature *413*, 86–91.

She, Q.B., Wei-Ya, M., Zhong, S., and Dong, Z. (2002). Activation of JNK1, RSK2, and MSK1 Is Involved in Serine 112 Phosphorylation of Bad by Ultraviolet B Radiation. J. Biol. Chem. *277*, 24039–24048.

Shen, C.-H., Yuan, P., Perez-Lorenzo, R., Zhang, Y., Lee, S., Ou, Y., Asara, J.M., Cantley, L.C., and Zheng, B. (2013). Phosphorylation of BRAF by AMPK Impairs BRAF-KSR1 Association and Cell Proliferation. Mol. Cell *52*, 161–172.

Shi, H., Moriceau, G., Kong, X., Lee, M.-K., Lee, H., Koya, R.C., Ng, C., Chodon, T., Scolyer, R.A., Dahlman, K.B., et al. (2012). Melanoma whole-exome sequencing identifies V600EB-RAF amplification-mediated acquired B-RAF inhibitor resistance. Nat. Commun. *3*, 724.

Shi, H., Hugo, W., Kong, X., Hong, A., Koya, R.C., Moriceau, G., Chodon, T., Guo, R., Johnson, D.B., Dahlman, K.B., et al. (2014). Acquired Resistance and Clonal Evolution in Melanoma during BRAF Inhibitor Therapy. Cancer Discov. *4*, 80–93.

Shiohara, M., Shigemura, T., Suzuki, T., Tanaka, M., Morii, E., Ohtsu, H., Shibahara, S., and Koike, K. (2009). MITF-CM, a newly identified isoform of microphthalmia-associated transcription factor, is expressed in cultured mast cells. Int. J. Lab. Hematol. *31*, 215–226.

Shoag, J., Haq, R., Zhang, M., Liu, L., Rowe, G.C., Jiang, A., Koulisis, N., Farrel, C., Amos, C.I., Wei, Q., et al. (2013). PGC-1 Coactivators Regulate MITF and the Tanning Response. Mol. Cell *49*, 145–157.

Smalley, K.S.M., and Sondak, V.K. (2010). Melanoma — An Unlikely Poster Child for Personalized Cancer Therapy. N. Engl. J. Med. *363*, 876–878.

Smith, M.P., Ferguson, J., Arozarena, I., Hayward, R., Marais, R., Chapman, A.,

Hurlstone, A., and Wellbrock, C. (2013). Effect of SMURF2 Targeting on Susceptibility to MEK Inhibitors in Melanoma. J. Natl. Cancer Inst. *105*, 33–46.

Smith, S.D., Kelley, P.M., Kenyon, J.B., and Hoover, D. (2000). Tietz syndrome (hypopigmentation/deafness) caused by mutation of MITF. J. Med. Genet. *37*, 446–448.

Songyang, Z., Blechner, S., Hoagland, N., Hoekstra, M.F., Piwnica-Worms, H., and Cantley, L.C. (1994). Use of an oriented peptide library to determine the optimal substrates of protein kinases. Curr. Biol. *4*, 973–982.

Sosman, J.A., Kim, K.B., Schuchter, L., Gonzalez, R., Pavlick, A.C., Weber, J.S., McArthur, G.A., Hutson, T.E., Moschos, S.J., Flaherty, K.T., et al. (2012). Survival in BRAF V600–Mutant Advanced Melanoma Treated with Vemurafenib. N. Engl. J. Med. *366*, 707–714.

Sprenkle, A.B., Davies, S.P., Carling, D., Hardie, D.G., and Sturgill, T.W. (1997). Identification of Raf-1 Ser621 kinase activity from NIH3T3 cells as AMP-activated protein kinase. FEBS Lett. *403*, 254–258.

Stacey, D.W., and Kung, H.-F. (1984). Transformation of NIH 3T3 cells by microinjection of Ha-ras p21 protein. Nature *310*, 508–511.

Stahl, J.M., Cheung, M., Sharma, A., Trivedi, N.R., Shanmugam, S., and Robertson, G.P. (2003). Loss of PTEN Promotes Tumor Development in Malignant Melanoma. Cancer Res. *63*, 2881–2890.

Stambolic, V., Suzuki, A., de la Pompa, J.L., Brothers, G.M., Mirtsos, C., Sasaki, T., Ruland, J., Penninger, J.M., Siderovski, D.P., and Mak, T.W. (1998). Negative Regulation of PKB/Akt-Dependent Cell Survival by the Tumor Suppressor PTEN. Cell *95*, 29–39.

Stanton, V.P., and Cooper, G.M. (1987). Activation of Human raf Transforming Genes by Deletion of Normal Amino-Terminal Coding Sequences. Mol. Cell. Biol. *7*, 1171–1179.

Steingrímsson, E., Moore, K.J., Lamoreux, M.L., Ferré-D'Amaré, A.R., Burley, S.K., Sanders Zimring, D.C., Skow, L.C., Hodgkinson, C.A., Arnheiter, H., Copeland, N.G., et al. (1994). Molecular basis of mouse microphthalmia (mi) mutations helps explain their developmental and phenotypic consequences. Nat. Genet. *8*, 256–263.

Stewart, S., Sundaram, M., Zhang, Y., Lee, J., Han, M., and Guan, K.-L. (1999). Kinase Suppressor of Ras Forms a Multiprotein Signaling Complex and Modulates MEK Localization. Mol. Cell. Biol. *19*, 5523–5534.

Stowe, I.B., Mercado, E.L., Stowe, T.R., Bell, E.L., Oses-Prieto, J.A., Hernández, H., Burlingame, A.L., and McCormick, F. (2012). A shared molecular mechanism underlies the human rasopathies Legius syndrome and Neurofibromatosis-1. Genes Dev. *26*, 1421–1426.

Stratton, M.R., Campbell, P.J., and Futreal, P.A. (2009). The cancer genome. Nature *458*, 719–724.

Strub, T., Giuliano, S., Ye, T., Bonet, C., Keime, C., Kobi, D., Le Gras, S., Cormont, M., Ballotti, R., Bertolotto, C., et al. (2011). Essential role of microphthalmia

transcription factor for DNA replication, mitosis and genomic stability in melanoma. Oncogene *30*, 2319–2332.

Strum, J.C. (1996). Raf-1 Kinase Possesses Distinct Binding Domains for Phosphatidylserine and Phosphatidic Acid. J. Biol. Chem. *271*, 8472–8480.

Su, F., Bradley, W.D., Wang, Q., Yang, H., Xu, L., Higgins, B., Kolinsky, K., Packman, K., Kim, M.J., Trunzer, K., et al. (2012a). Resistance to Selective BRAF Inhibition Can Be Mediated by Modest Upstream Pathway Activation. Cancer Res. *72*, 969–978.

Su, F., Viros, A., Milagre, C., Trunzer, K., Bollag, G., Spleiss, O., Reis-Filho, J.S., Kong, X., Koya, R.C., Flaherty, K.T., et al. (2012b). RAS Mutations in Cutaneous Squamous-Cell Carcinomas in Patients Treated with BRAF Inhibitors. N. Engl. J. Med. *366*, 207–215.

Sun, H., Lesche, R., Li, D.-M., Liliental, J., Zhang, H., Gao, J., Gavrilova, N., Mueller, B., Liu, X., and Wu, H. (1999). PTEN modulates cell cycle progression and cell survival by regulating phosphatidylinositol 3,4,5,-trisphosphate and Akt/protein kinase B signaling pathway. Proc. Natl. Acad. Sci. *96*, 6199–6204.

Sundaram, M., and Han, M. (1995). The C. elegans ksr-1 gene encodes a novel raf-related kinase involved in Ras-mediated signal transduction. Cell *83*, 889–901.

Tachibana, M., Takeda, K., Nobukuni, Y., Urabe, K., Long, J.E., Meyers, K.A., Aaronson, S.A., and Miki, T. (1996). Ectopic expression of MITF, a gene for Waardenburg syndrome type 2, converts fibroblasts to cells with melanocyte characteristics. Nat. Genet. *14*, 50–54.

Takebayashi, K., Chida, K., Tsukamoto, I., Morii, E., Munakata, H., Arnheiter, H., Kuroki, T., Kitamura, Y., and Nomura, S. (1996). The Recessive Phenotype Displayed by a Dominant Negative Microphthalmia-Associated Transcription Factor Mutant Is a Result of Impaired Nuclear Localization Potential. Mol. Cell. Biol. *16*, 1203–1211.

Takeda, K., Takemoto, C., Kobayashi, I., Watanabe, A., Nobukuni, Y., Fisher, D.E., and Tachibana, M. (2000a). Ser298 of MITF, a mutation site in Waardenburg syndrome type 2, is a phosphorylation site with functional significance. Hum. Mol. Genet. *9*, 125–132.

Takeda, K., Yasumoto, K.I., Takada, R., Takada, S., Watanabe, K.I., Udono, T., Saito, H., Takahashi, K., and Shibahara, S. (2000b). Induction of Melanocyte-specific Microphthalmia-associated Transcription Factor by Wnt-3a. J. Biol. Chem. *275*, 14013–14016.

Takishima, K., Griswold-Prenner, I., Ingebritsen, T., and Rosner, M.R. (1991). Epidermal growth factor (EGF) receptor T669 peptide kinase from 3T3-L1 cells is an EGF-stimulated "MAP" kinase. Proc. Natl. Acad. Sci. *88*, 2520–2524.

Tang, Y., Zhao, W., Chen, Y., Zhao, Y., and Gu, W. (2008). Acetylation is indispensable for p53 activation. Cell *133*, 612–626.

Tassabehji, M., Newton, V.E., and Read, A.P. (1994). Waardenburg syndrome type 2 caused by mutations in the human microphthalmia (MITF) gene. Nat. Genet. *8*, 251–

255.

Taylor, S.S., and Kornev, A.P. (2011). Protein kinases: evolution of dynamic regulatory proteins. Trends Biochem. Sci. *36*, 65–77.

Terasima, T., and Tolmach, L.J. (1963). Growth and nucleic acid synthesis in synchronously dividing populations of HeLa cells. Exp. Cell Res. *30*, 344–362.

Das Thakur, M., Salangsang, F., Landman, A.S., Sellers, W.R., Pryer, N.K., Levesque, M.P., Dummer, R., McMahon, M., and Stuart, D.D. (2013). Modelling vemurafenib resistance in melanoma reveals a strategy to forestall drug resistance. Nature *494*, 251–255.

Therrien, M., Chang, H.C., Solomon, N.M., Karim, F.D., Wassarman, D.A., and Rubin, G.M. (1995). KSR, a novel protein kinase required for RAS signal transduction. Cell *83*, 879–888.

Thevakumaran, N., Lavoie, H., Critton, D.A., Tebben, A., Marinier, A., Sicheri, F., and Therrien, M. (2014). Crystal structure of a BRAF kinase domain monomer explains basis for allosteric regulation. Nat. Struct. Mol. Biol. *22*, 37–43.

Thoreen, C.C., Kang, S.A., Chang, J.W., Liu, Q., Zhang, J., Gao, Y., Reichling, L.J., Sim, T., Sabatini, D.M., and Gray, N.S. (2009). An ATP-competitive Mammalian Target of Rapamycin Inhibitor Reveals Rapamycin-resistant Functions of mTORC1. J. Biol. Chem. *284*, 8023–8032.

Thurber, A.E., Douglas, G., Sturm, E.C., Zabierowski, S.E., Smit, D.J., Ramakrishnan, S.N., Hacker, E., Leonard, J.H., Herlyn, M., and Sturm, R.A. (2011). Inverse expression states of the BRN2 and MITF transcription factors in melanoma spheres and tumour xenografts regulate the NOTCH pathway. Oncogene *30*, 3036–3048.

Tilbrook, P.A., Colley, S.M., McCarthy, D.J., Marais, R., and Klinken, S.P. (2001). Erythropoietin-Stimulated Raf-1 Tyrosine Phosphorylation Is Associated with the Tyrosine Kinase Lyn in J2E Erythroleukemic Cells. Arch. Biochem. Biophys. *396*, 128–132.

Tomasetti, C., Marchionni, L., Nowak, M.A., Parmigiani, G., and Vogelstein, B. (2015). Only three driver gene mutations are required for the development of lung and colorectal cancers. Proc. Natl. Acad. Sci. *112*, 118–123.

Tran, N.H., Wu, X., and Frost, J.A. (2005). B-Raf and Raf-1 Are Regulated by Distinct Autoregulatory Mechanisms. J. Biol. Chem. *280*, 16244–16253.

Traverse, S., Seedorf, K., Paterson, H., Marshall, C.J., Cohen, P., and Ullrich, A. (1994). EGF triggers neuronal differentiation of PC12 cells that overexpress the EGF receptor. Curr. Biol. *4*, 694–701.

Trosky, J.E., Li, Y., Mukherjee, S., Keitany, G., Ball, H., and Orth, K. (2007). VopA Inhibits ATP Binding by Acetylating the Catalytic Loop of MAPK Kinases. J. Biol. Chem. *282*, 34299–34305.

Tsai, J., Lee, J.T., Wang, W., Zhang, J., Cho, H., Mamo, S., Bremer, R., Gillette, S.,

Kong, J., Haass, N.K., et al. (2008). Discovery of a selective inhibitor of oncogenic B-Raf kinase with potent antimelanoma activity. Proc. Natl. Acad. Sci. *105*, 3041–3046.

Tsao, H., Zhang, X., Fowlkes, K., and Haluska, F.G. (2000). Relative Reciprocity of NRAS and PTEN/MMAC1 Alterations in Cutaneous Melanoma Cell Lines. Cancer Res. *60*, 1800–1804.

Tsao, H., Goel, V., Wu, H., Yang, G., and Haluska, F.G. (2004). Genetic Interaction Between NRAS and BRAF Mutations and PTEN/MMAC1 Inactivation in Melanoma. J. Invest. Dermatol. *122*, 337–341.

Tsao, H., Chin, L., Garraway, L.A., and Fisher, D.E. (2012). Melanoma: from mutations to medicine. Genes Dev. *26*, 1131–1155.

Tsvetkov, L.M., Yeh, K.-H., Lee, S.-J., Sun, H., and Zhang, H. (1999). p27Kip1 ubiquitination and degradation is regulated by the SCFSkp2 complex through phosphorylated Thr187 in p27. Curr. Biol. *9*, 661–S2.

Turner, N.C., and Reis-Filho, J.S. (2012). Genetic heterogeneity and cancer drug resistance. Lancet Oncol. *13*, e178–e185.

Tzivion, G., Luo, Z., and Avruch, J. (1998). A dimeric 14-3-3 protein is an essential cofactor for Raf kinase activity. Nature *394*, 88–92.

Ubersax, J.A., Woodbury, E.L., Quang, P.N., Paraz, M., Blethrow, J.D., Shah, K., Shokat, K.M., and Morgan, D.O. (2003). Targets of the cyclin-dependent kinase Cdk1. Nature *425*, 859–864.

Vachtenheim, J., and Novotná, H. (1999). Expression of genes for microphthalmia isoforms, Pax3 and MSG1, in human melanomas. Cell. Mol. Biol. *45*, 1075–1082.

VanBrocklin, M.W., Robinson, J.P., Lastwika, K.J., Khoury, J.D., and Holmen, S.L. (2010). Targeted delivery of NRASQ61R and Cre-recombinase to post-natal melanocytes induces melanoma in Ink4a/Arflox/lox mice. Pigment Cell Melanoma Res. *23*, 531–541.

Vazquez, F., Lim, J.-H., Chim, H., Bhalla, K., Girnun, G., Pierce, K., Clish, C.B., Granter, S.R., Widlund, H.R., Spiegelman, B.M., et al. (2013). PGC1α Expression Defines a Subset of Human Melanoma Tumors with Increased Mitochondrial Capacity and Resistance to Oxidative Stress. Cancer Cell *23*, 287–301.

Verastegui, C., Bille, K., Ortonne, J.-P., and Ballotti, R. (2000). Regulation of the Microphthalmia-associated Transcription Factor Gene by the Waardenburg Syndrome Type 4 Gene, SOX10. J. Biol. Chem. *275*, 30757–30760.

Villanueva, J., Vultur, A., Lee, J.T., Somasundaram, R., Fukunaga-Kalabis, M., Cipolla, A.K., Wubbenhorst, B., Xu, X., Gimotty, P.A., Kee, D., et al. (2010). Acquired Resistance to BRAF Inhibitors Mediated by a RAF Kinase Switch in Melanoma Can Be Overcome by Cotargeting MEK and IGF-1R/PI3K. Cancer Cell *18*, 683–695.

Vogelstein, B., Papadopoulos, N., Velculescu, V.E., Zhou, S., Diaz Jr., L.A., and Kinzler, K.W. (2013). Cancer Genome Landscapes. Science (80-.). *339*, 1546–1558.

Vojtek, A.B., Hollenberg, S.M., and Cooper, J.A. (1993). Mammalian Ras interacts directly with the serine/threonine kinase raf. Cell *74*, 205–214.

Wagle, N., Emery, C., Berger, M.F., Davis, M.J., Sawyer, A., Pochanard, P., Kehoe, S.M., Johannessen, C.M., MacConaill, L.E., Hahn, W.C., et al. (2011). Dissecting Therapeutic Resistance to RAF Inhibition in Melanoma by Tumor Genomic Profiling. J. Clin. Oncol. *29*, 3085–3096.

Wan, P.T.., Garnett, M.J., Roe, S.M., Lee, S., Niculescu-Duvaz, D., Good, V.M., Project, C.G., Jones, C.M., Marshall, C.J., Springer, C.J., et al. (2004). Mechanism of Activation of the RAF-ERK Signaling Pathway by Oncogenic Mutations of B-RAF. Cell *116*, 855–867.

Watanabe, A., Takeda, K., Ploplis, B., and Tachibana, M. (1998). Epistatic relationship between Waardenburg Syndrome genes MITF and PAX3. Nat. Genet. *18*, 283–286.

Watanabe, K.-I., Takeda, K., Yasumoto, K.-I., Udono, T., Saito, H., Ikeda, K., Takasaka, T., Takahashi, K., Kobayashi, T., Tachibana, M., et al. (2002). Identification of a Distal Enhancer for the Melanocyte-Specific Promoter of the MITF Gene. Pigment Cell Res. *15*, 201–211.

Weber, C.K., Slupsky, J.R., Herrmann, C., Schuler, M., Rapp, U.R., and Block, C. (2000). Mitogenic signaling of Ras is regulated by differential interaction with Raf isozymes. Oncogene *19*, 169–176.

Weber, C.K., Slupsky, J.R., Andreas Kalmes, H., and Rapp, U.R. (2001). Active Ras Induces Heterodimerization of cRaf and BRaf. Cancer Res. *61*, 3595–3598.

Weinhold, N., Jacobsen, A., Schultz, N., Sander, C., and Lee, W. (2014). Genome-wide analysis of noncoding regulatory mutations in cancer. Nat. Genet. *46*, 1160–1165.

Weis, K. (2003). Regulating Access to the Genome: Nucleocytoplasmic Transport throughout the Cell Cycle. Cell *112*, 441–451.

Wellbrock, C., and Marais, R. (2005). Elevated expression of MITF counteracts B-RAF-stimulated melanocyte and melanoma cell proliferation. J. Cell Biol. *170*, 703–708.

Wellbrock, C., Ogilvie, L., Hedley, D., Karasarides, M., Martin, J., Niculescu-Duvaz, D., Springer, C.J., and Marais, R. (2004). V599E B-RAF is an Oncogene in Melanocytes. Cancer Res. *64*, 2338–2342.

Wellbrock, C., Rana, S., Paterson, H., Pickersgill, H., Brummelkamp, T., and Marais, R. (2008). Oncogenic BRAF Regulates Melanoma Proliferation through the Lineage Specific Factor MITF. PLoS One *3*, e2734.

Wen, W., Meinkotht, J.L., Tsien, R.Y., and Taylor, S.S. (1995). Identification of a signal for rapid export of proteins from the nucleus. Cell *82*, 463–473.

Wetzker, R., and Böhmer, F.-D. (2003). Opinion: Transactivation joins multiple tracks to the ERK/MAPK cascade. Nat. Rev. Mol. Cell Biol. *4*, 651–657.

Whittaker, S.R., Theurillat, J.-P., Van Allen, E., Wagle, N., Hsiao, J., Cowley, G.S., Schadendorf, D., Root, D.E., and Garraway, L.A. (2013). A Genome-Scale RNA Interference Screen Implicates NF1 Loss in Resistance to RAF Inhibition. Cancer Discov. *3*, 350–362.

Widlund, H.R., Horstmann, M.A., Roydon Price, E., Cui, J., Lessnick, S.L., Wu, M., He, X., and Fisher, D.E. (2002). β-Catenin-induced melanoma growth requires the downstream target Microphthalmia-associated transcription factor. J. Cell Biol. *158*, 1079–1087.

Wilhelm, S.M., Carter, C., Tang, L., Wilkie, D., McNabola, A., Rong, H., Chen, C., Zhang, X., Vincent, P., McHugh, M., et al. (2004). BAY 43-9006 Exhibits Broad Spectrum Oral Antitumor Activity and Targets the RAF/MEK/ERK Pathway and Receptor Tyrosine Kinases Involved in Tumor Progression and Angiogenesis. Cancer Res. *64*, 7099–7109.

Williams, J.G., Drugan, J.K., Yi, G.-S., Clark, G.J., Der, C.J., and Campbell, S.L. (2000). Elucidation of Binding Determinants and Functional Consequences of Ras/Raf-Cysteine-rich Domain Interactions. J. Biol. Chem. *275*, 22172–22179.

Winkler, D.F.H., Hilpert, K., Brandt, O., and Hancock, R.E.W. (2009). Synthesis of Peptide Arrays Using SPOT-Technology and the CelluSpots-Method (Totowa, NJ: Humana Press).

Witherington, J., Bordas, V., Haigh, D., Hickey, D.M.., Ife, R.J., Rawlings, A.D., Slingsby, B.P., Smith, D.G., and Ward, R.W. (2003). 5-Aryl-pyrazolo[3,4-b]pyridazines: potent inhibitors of glycogen synthase kinase-3 (GSK-3). Bioorg. Med. Chem. Lett. *13*, 1581–1584.

Wu, D., and Pan, W. (2010). GSK3: a multifaceted kinase in Wnt signaling. Trends Biochem. Sci. *35*, 161–168.

Wu, M., Hemesath, T.J., Takemoto, C.M., Horstmann, M.A., Wells, A.G., Price, E.R., Fisher, D.Z., and Fisher, D.E. (2000). c-Kit triggers dual phosphorylations, which couple activation and degradation of the essential melanocyte factor Mi. Genes Dev. *14*, 301–312.

Xeros, N. (1962). Deoxyriboside Control and Synchronization of Mitosis. Nature *194*, 682–683.

Xu, W., Gong, L., Haddad, M.M., Bischof, O., Campisi, J., Yeh, E.T.H., and Medrano, E.E. (2000). Regulation of Microphthalmia-Associated Transcription Factor MITF Protein Levels by Association with the Ubiquitin-Conjugating Enzyme hUBC9. Exp. Cell Res. *255*, 135–143.

Yamada, T., Hasegawa, S., Inoue, Y., Date, Y., Yamamoto, N., Mizutani, H., Nakata, S., Matsunaga, K., and Akamatsu, H. (2013). Wnt/β-Catenin and Kit Signaling Sequentially Regulate Melanocyte Stem Cell Differentiation in UVB-Induced Epidermal Pigmentation. J. Invest. Dermatol. *133*, 2753–2762.

Yao, Z., Torres, N.M., Tao, A., Gao, Y., Luo, L., Li, Q., de Stanchina, E., Abdel-Wahab, O., Solit, D.B., Poulikakos, P.I., et al. (2015). BRAF Mutants Evade ERK-Dependent Feedback by Different Mechanisms that Determine Their Sensitivity to Pharmacologic Inhibition. Cancer Cell *28*, 370–383.

Yasumoto, K., Takeda, K., Saito, H., Watanab, K., Takahashi, K., and Shibahara, S. (2002). Microphthalmia-associated transcription factor interacts with LEF-1, a mediator of Wnt signaling. EMBO J. *21*, 2703–2714.

Yasumoto, K.-I., Amae, S., Udono, T., Fuse, N., Takeda, K., and Shibahara, S. (1998). A Big Gene Linked to Small Eyes Encodes Multiple Mitf Isoforms: Many Promoters Make Light Work. Pigment Cell Res. *11*, 329–336.

Yates, L.R., and Campbell, P.J. (2012). Evolution of the cancer genome. Nat. Rev. Genet. *13*, 795–806.

Yavuzer, U., Keenan, E., Lowings, P., Vachtenheim, J., Currie, G., and Goding, C.R. (1995). The Microphthalmia gene product interacts with the retinoblastoma protein in vitro and is a target for deregulation of melanocyte-specific transcription. Oncogene *10*, 123–134.

Yeung, F., Ramsey, C.S., Popko-Scibor, A.E., Allison, D.F., Gray, L.G., Shin, M., Kumar, M., Li, D., McCubrey, J.A., and Mayo, M.W. (2015). Regulation of the mitogen-activated protein kinase kinase (MEK)-1 by NAD+-dependent deacetylases. Oncogene *34*, 798–804.

Yip-Schneider, M.T., Wenyan, M., Lin, A., Barnard, D.S., Tzivion, G., and Marshall, M.S. (2000). Regulation of the Raf-1 kinase domain by phosphorylation and 14-3-3 association. Biochem. J. *351*, 151.

Yokoyama, S., Feige, E., Poling, L.L., Levy, C., Widlund, H.R., Khaled, M., Kung, A.L., and Fisher, D.E. (2008). Pharmacologic suppression of MITF expression via HDAC inhibitors in the melanocyte lineage. Pigment Cell Melanoma Res. *21*, 457–463.

Yokoyama, S., Woods, S.L., Boyle, G.M., Aoude, L.G., MacGregor, S., Zismann, V., Gartside, M., Cust, A.E., Haq, R., Harland, M., et al. (2011). A novel recurrent mutation in MITF predisposes to familial and sporadic melanoma. Nature *480*, 99–103.

Yoon, S., and Seger, R. (2006). The extracellular signal-regulated kinase: Multiple substrates regulate diverse cellular functions. Growth Factors *24*, 21–44.

Zha, J., Harada, H., Yang, E., Jockel, J., and Korsmeyer, S.J. (1996). Serine Phosphorylation of Death Agonist BAD in Response to Survival Factor Results in Binding to 14-3-3 Not BCL-XL. Cell *87*, 619–628.

Zhang, B., and Guan, K. (2000). Activation of B-Raf kinase requires phosphorylation of the conserved residues Thr598 and Ser601. EMBO J. *19*, 5429–5439.

Zhang, H., Luo, H., Chen, H., Mei, L., He, C., Jiang, L., Li, J.-D., and Feng, Y. (2012). Functional analysis of MITF gene mutations associated with Waardenburg syndrome type 2. FEBS Lett. *586*, 4126–4131.

Zhu, S., Wurdak, H., Wang, Y., Galkin, A., Tao, H., Li, J., Lyssiotis, C.A., Yan, F., Tu, B.P., Miraglia, L., et al. (2009). A genomic screen identifies TYRO3 as a MITF regulator in melanoma. Proc. Natl. Acad. Sci. *106*, 17025–17030.

Zimmermann, S., and Moelling, K. (1999). Phosphorylation and Regulation of Raf by Akt (Protein Kinase B). Science (80-.). *286*, 1741–1744.